

Selenium-Methionine Nanoparticles and Its Application in Chronic Inflammatory Arthritis

A THESIS
SUBMITTED
TO
SVKM's NMIMS (DEEMED-TO-BE) UNIVERSITY
FOR THE DEGREE OF
DOCTOR OF PHILOSOPHY
IN
BIOLOGICAL SCIENCES
BY
VRUNDALI SHINDE

UNDER THE SUPERVISION OF
Dr. KRUTIKA DESAI



SVKM'S
NMIMS
Deemed-to-be UNIVERSITY

**SUNANDAN DIVATIA
SCHOOL OF SCIENCE**

SVKM's Narsee Monjee Institute of Management Studies

(Deemed-to-be University)

V.L. Mehta Road, Vile Parle (W), Mumbai- 400056

1st October 2023

Selenium-Methionine Nanoparticles and Its Application in Chronic Inflammatory Arthritis

A THESIS
SUBMITTED
TO
SVKM's NMIMS (DEEMED-TO-BE) UNIVERSITY
FOR THE DEGREE OF
DOCTOR OF PHILOSOPHY
IN
BIOLOGICAL SCIENCES
BY
VRUNDALI SHINDE

Dr. Krutika Desai
(Project Mentor)

Dr. Purvi Bhatt
(I/C Dean)

Sunandan Divatia School of Science



SVKM'S
NMIMS
Deemed-to-be UNIVERSITY

**SUNANDAN DIVATIA
SCHOOL OF SCIENCE**

SVKM's Narsee Monjee Institute of Management Studies

(Deemed-to-be University)

V.L. Mehta Road, Vile Parle (W), Mumbai- 400056

1st October 2023

DECLARATION BY THE STUDENT

This is to certify that the work embodied in the thesis “**Selenium-Methionine Nanoparticles and Its Application in Chronic Inflammatory Arthritis**” for the award of the Degree of Doctor of Philosophy in Biological Sciences is my own contribution to the research work carried out under the supervision of Dr. Krutika Desai. The work has not been submitted for the award of any other degree/to any other University. Wherever a reference has been made to earlier reported findings, it has been cited in the thesis. The thesis fulfils the requirements of the ordinance relating to the award of the Ph.D. degree of the University.

Place: Mumbai

VRUNDALI SHINDE

Date: 1st October 2023

Forwarded by:

Dr. KRUTIKA DESAI

Principal

Mithibai College of Arts,

Chauhan Institute of Science & Amrutben Jivanlal

College of Commerce and Economics.

CERTIFICATE

This is to certify that the work described in this thesis entitled “**Selenium-Methionine Nanoparticles and Its Application in Chronic Inflammatory Arthritis**” has been carried out by Ms. Vrundali Shinde under my supervision. I certify that this is her bonafide work. The work described is original and has not been submitted for any degree to this or any other University.

Place: Mumbai

Date:

Dr. Purvi Bhatt

I/C Dean

Sunandan Divatia School of Science

Date:

Dr. Krutika Desai

Project Mentor

The Mithibai College of Arts, Chauhan Institute of Science & Amrutben Jivanlal College of Commerce and Economics

Date:



SVKM's Narsee Monjee Institute of Management Studies(Deemed-to-be
University)

V.L. Mehta Road, Vile Parle (W), Mumbai- 400056

*This Thesis is Dedicated to my
Loving Family*

Acknowledgement

“Our greatest weakness lies in giving up. The most certain way to succeed is always to try just one more time” - Thomas Edison.

I would like to express my deepest gratitude to all those who have contributed to the completion of this Ph.D. thesis. This research journey has been a challenging yet fulfilling endeavour, and I owe my heartfelt appreciation to the following individuals:

First and foremost, I am immensely grateful to my esteemed supervisor, **Dr. Krutika Desai**, for their unwavering guidance, invaluable expertise, and endless support throughout this entire research project. Their profound knowledge, critical insights, and constant encouragement have been instrumental in shaping the direction of my work and enhancing its quality. I am truly fortunate to have had the privilege of working under their supervision.

I would like to extend my sincere thanks to the members of my Ph.D. committee, **Dr. Sudeshna Chandra**, and **Dr. Mala Menon**, for their constructive feedback, valuable suggestions, and rigorous examination of my thesis. Their expertise and contributions have significantly strengthened this research and enriched its intellectual depth.

Dr. Purvi Bhatt, In charge- Dean, Sunandan Divatia School of Science, NMIMS. I extend my deepest gratitude for your invaluable support, guidance, and encouragement throughout my Ph.D. journey. Your unwavering commitment to the pursuit of knowledge, dedication to student success, and visionary leadership have left an indelible mark on my academic and personal development. I feel honored to have been a part of Sunandan Divatia School of Science under your esteemed leadership.

My heartfelt appreciation goes to **Dr. Aparna Khanna** and **Dr. Dhananjaya Sarnath**, for being my biggest motivators throughout my journey. My faculty members **Dr. Brijesh**, **Dr. Harinder**, **Dr. Mane** and staff at NMIMS **Madhuri Ma'am**, **Mansi Ma'am**, **Ms. Karuna**, **Ms. Nandini**, who have provided a stimulating academic environment and necessary resources for my research. Their commitment to excellence in education and research has been truly inspiring. **Dr. Shilpee Sachar**, University of Mumbai, for helping me through my characterization process.

I express my deepest gratitude to **“Women Graduates Union Scholarship”** for providing me with scholarships and supporting my PhD work. I am highly indebted to them for their contribution to my studies.

My gratitude to **Mithibai College** for allowing me to work in their central instrumentation laboratory and **OVI diagnostics** for animal work analysis.

My heartfelt gratitude to **Dr. Yogesh Kulkarni, Dr. Vaishali Londhe**, I am thankful to **Dr. Sailesh Khade, Manish Sir, Dr. Ankit Laddha, Dr. Vivek Sudam Kumawat** for their support during experiments involving animals.

I am indebted to my colleagues and fellow researchers **Dr. Ruchita Shelat, Dr. Yashika Mirchandani, Dr. Amruta Tambe, Dr. Maneeka Hoonjan, Dr. Nishant, Dr. Divya Desai, Ms. Neha Dubey, Mr. Mitesh Joshi, Ms. Aishwarya Shetty, Ms. Asmita Kamble** and **Ms. Zoya Peerzada**, for their friendship, intellectual exchanges, and collaborative efforts. Their diverse perspectives and insightful discussions have broadened my horizons and enriched my understanding of the subject matter.

Special thanks to my friends, **Ms. Amruta Parmar** and **Dr. Niloufer Dumasia**, who have always been there through thick and thin. Been my best cheerleaders and motivators. Thank you is a really small word to describe my gratitude towards them. I would like to express my gratitude to the participants of this study, whose voluntary involvement and cooperation have made this research possible. Their contributions are deeply appreciated, and I am grateful for their willingness to share their time and knowledge.

I would like to express my heartfelt gratitude to my family, who has been a constant source of support and encouragement throughout this journey. My parents, **Mr. Avinash Shinde** and **Mrs. Pragyna Shinde**, my sister **Mrs. Henali Sharma**, my brother-in-law **Mr. Rahul Sharma** and my niece **Ms. Ruhi Sharma** have always been my pillars of strength, providing unwavering love and understanding, as well as valuable insights into my work. My spouse, **Mr. Saurabh Kannothe**, has been my biggest cheerleader, offering encouragement and patience during the late nights and weekends dedicated to this project. My in-laws **Mr. Sugath Kumar** and **Mrs. Reena Sugath**, their belief in me and the sacrifices they made to create an environment conducive to my work are immeasurable. Lastly, I would like to acknowledge the countless individuals who have directly or indirectly contributed to this research but may not be mentioned explicitly. Your support, whether through insightful discussions, technical assistance, or emotional encouragement, has played a vital role in shaping the outcome of this thesis.

To all those who have been a part of this research endeavour, I offer my deepest gratitude. Your contributions have been invaluable, and I am honoured to have had the opportunity to work with each and every one of you.

THANK YOU.

TABLE OF CONTENTS

<i>List of Abbreviations</i>	8
<i>List of Figures</i>	11
<i>List of Table</i>	15
Chapter 1	16
Introduction and Literature Review	
1.1 Prologue	17
1.2 History of Nanotechnology	19
1.3 Nanomaterials Classification	21
1.3.1 Structural Classification	22
1.3.1.1 Organic Nanomaterials	22
1.3.1.2 Inorganic Nanomaterials	22
1.3.1.2.1 Metal-based Nanomaterials	22
1.3.1.2.2 Metal-oxide Nanomaterials	22
1.3.1.3 Ceramic Nanoparticles	22
1.3.1.4 Bio Nanoparticles	23
1.3.1.5 Carbon Nanomaterials	23
1.3.2 Classification based on Dimensions	23
1.3.2.1 Zero Dimensional Nanomaterials	24
1.3.2.2 One Dimensional Nanomaterials	24
1.3.2.3 Two Dimensional Nanomaterials	24
1.3.2.4 Three Dimensional Nanomaterials	25
1.4 Synthesis of Nanoparticles	26
1.4.1 Solvent Evaporation Method	27
1.4.2 Solvent Diffusion Method	28
1.4.3 Crystallization Method	29
1.4.4 The Ionic Gelation Method	30
1.4.5 Supercritical Fluid (SCF) Technology	31
1.4.6 Self-Assembly Method	32
1.4.7 Layer-by-Layer Deposition Method	32
1.4.8 Gas-phase Synthesis Method	33

1.4.9 Muffle Furnace Irradiated Synthesis Method	34
1.4.10 Flame Synthesis Method	35
1.4.11 Sputtering Process	36
1.4.12 Plasma Reactor Synthesis Method	37
1.4.13 Biological Synthesis (Green Synthesis)	38
1.4.14 Chemical Synthesis	40
1.5 Characterization of Nanoparticles	42
1.5.1 UV-Visible Spectrophotometer	42
1.5.2 X-Ray Diffraction (XRD)	42
1.5.3 Fourier Transform Infrared Spectroscopy (FTIR)	43
1.5.4 Zeta Potential	43
1.5.5 Inductive Coupled Plasma Atomic Emission Spectroscopy (ICP-AES)	43
1.5.6 Raman Spectroscopy	44
1.5.7 Transmission Spectroscopy (TEM)	44
1.6 Applications of Nanoparticles	45
1.6.1 Application in Electronics	45
1.6.2 Environmental Applications	45
1.6.3 Biomedical Applications	46
1.6.4 Multiple other Applications	47
1.7 Current Market of Nanotechnology in India	49
1.8 Probable Shortcomings of Nanotechnology	50
Chapter 2	51
Rational, Aim, and Objectives	
2.1 Rational	52
2.2 Aim	53
2.3 Objectives	54
Chapter 3	56
Synthesis, Coating, and characterization of Selenium-methionine-Folic acid Nanoparticles	

3.1 Introduction	57
3.1.1 Nano form of Selenium	62
3.2 Synthesis and Coating of Selenium NPs	64
3.2.1 Chemical Reduction Method	64
3.2.2 Hydrothermal Route	66
3.2.3 Microwave Assisted Synthesis	66
3.2.4 Biological Synthesis	67
3.2.5 Green Synthesis	68
3.2.6 Pulsed Laser Ablation Method	69
3.2.7 Electrodeposition Method	69
3.3 Stabilization of nanoparticles	70
3.4 Characterization of NPs	72
3.4.1 UV-Vis Spectrophotometer	72
3.4.2 Fourier transform infrared	72
3.4.3 Zeta Potential	73
3.4.4 ICP-AES	74
3.4.5 X-Ray diffraction	75
3.4.6 Raman Spectroscopy	76
3.4.7 Transmission electron microscopy	76
3.4.8 Differential scanning calorimeter	77
3.5 Materials	78
3.6 Methods and Experimental details	79
3.6.1 Synthesis and coating of selenium nanoparticles	79
3.6.2 Characterization of SeNP and Se-Met-Fa NPs	81
3.7 Results	81
3.7.1 Synthesis of SeNP and Se-Met-Fa NPs	81
3.7.2 Characterization techniques	81
3.8 Discussion	83
3.9 Conclusion	92

Chapter 4	93
<i>In Vitro</i> cyto-toxicity and Macromolecular Interaction studies	
4.1 Introduction	94
4.2 Cellular Uptake Mechanisms	96
4.2.1 Active transport	96
4.2.2 Passive uptake mechanisms	99
4.3 Interaction of nanoparticles with diverse macromolecules <i>in vitro</i>	100
4.3.1 Interaction of Nanoparticles with DNA	100
4.3.2 Interaction of Selenium NPs and DNA	102
4.3.3 Proteins and selenium nanoparticle Interactions	103
4.3.4 Characterization techniques for protein-Se NPs interaction	104
4.4 Anti-oxidant assay (DPPH)	106
4.5 <i>In vitro</i> cytotoxicity	108
4.6 Materials and methods	111
4.6.1 pBR322 plasmid- NPs interaction	111
4.6.2 BSA- NPs interaction	111
4.6.3 <i>In vitro</i> cytotoxicity assay	111
4.6.4 Antioxidant evaluation	112
4.6.5 Statistical Analysis	112
4.7 Results	113
4.7.1 pBR322 plasmid- NPs interaction	113
4.7.2 BSA- NPs interaction	114
4.7.3 <i>In vitro</i> cytotoxicity of NPs	117
4.7.4 Antioxidant assay	119
4.8 Discussion	121
4.9 Conclusion	124
Chapter 5	125
Bioavailability and <i>in Vivo</i> efficacy against chronic RA	
5.1 Introduction	126

5.1.1 Bioavailability	127
5.1.2 Intestinal permeability	129
5.1.2.1 Caco-2 cell chamber	129
5.1.2.2 Rat Gut sac method	130
5.1.2.3 Permeapad plate technique	132
5.1.3 Blood compatibility	133
5.1.3.1 Blood Haemolysis assay	133
5.1.4 Types of Arthritis	134
5.1.4.1 Gout	134
5.1.4.2 Reactive arthritis	134
5.1.4.3 Juvenile Idiopathic Arthritis	135
5.1.4.4 Fibromyalgia	136
5.1.4.5 Septic arthritis	136
5.1.4.6 Osteoarthritis	137
5.1.4.7 Rheumatoid arthritis (RA)	137
5.1.5 Evolving concepts of RA	138
5.1.6 Etiopathogenesis of RA	138
5.1.7 Potential role of reactive oxygen species (ROS) in RA	140
5.1.8 Antioxidant System	141
5.1.8.1 Enzymatically active antioxidants	141
5.1.8.2 Non-enzymatically active antioxidants	143
5.1.9 Biomarkers for Rheumatoid arthritis	144
5.1.10 Rheumatoid Factor	145
5.1.10.1 Anti-cyclic Citrullinated Peptide (ACCP)	145
5.1.10.2 Prostaglandin E2 (PGE2)	145
5.1.10.3 Tumor necrosis factor- α (TNF- α)	146
5.1.11 Arthritis-Related Therapeutic Agents	147
5.1.12 Animal Models for Chronic inflammatory arthritis	149
5.1.12.1 Adjuvant induced arthritis (AIA)	149
5.1.12.2 Collagen induced arthritis (CIA)	150
5.1.12.3 Cartilage oligometric matrix protein induced arthritis	150
5.1.12.4 Pristane induced arthritis	151
5.1.12.5 <i>Streptococcal</i> cell wall induced arthritis	151

5.2 Materials	152
5.3 Methodology	153
5.3.1 Blood compatibility of SeMetFa NPs	153
5.3.1.1 Hemolysis assay	153
5.3.2 Intestinal permeability assay	154
5.3.2.1 Sample preparation	154
5.3.2.2 Data analysis	154
5.3.3 Housing of animal models	155
5.3.4 Grouping of animals	155
5.3.5 Anti-arthritic study	156
5.3.5.1 Inflammatory marker study	156
5.3.5.2 Antioxidant enzyme assay	160
5.3.6 Histopathological findings	161
5.3.7 Radiographical findings	162
5.3.8 Statistical data analysis	162
5.4 Results	163
5.4.1 Blood Compatibility assay	163
5.4.2 Intestinal permeability	164
5.4.3 Arthritic rat model study	165
5.4.3.1 Assessment of rat paw edema and weight	165
5.4.3.2 Effect of SeMetFa NPs on antioxidant enzymes	167
5.4.3.3 Effect of SeMetFa NPs on inflammatory biomarkers	169
5.4.3.4 Histopathological and Radiological findings of rat paw	169
5.4.3.5 Histopathological findings of rat liver, spleen and kidney	176
5.5 Discussion	179
5.6 Conclusion	183
Chapter 6	184
Conclusion and Future prospects	
Bibliography	188
Synopsis	213

Appendix I	240
Statistical Analysis	
Appendix II	288
Preparation of reagents	
Appendix III	292
Ethics committee approvals	
Appendix IV	295
Certificates	
Appendix V	296
Conferences and Publications	

LIST OF ABBREVIATIONS

ACCP	Anti-cyclic Citrulline Protein
Ag	Silver
AIA	Adjuvant Induced Arthritis
ANOVA	Analysis of Variance
As	Arsenic
Au	Gold
BSA	Bovine Serum Albumin
CAT	Catalase
CFA	Complete Freund's Adjuvant
CIA	Collagen Induced Arthritis
COX	Cyclooxygenase
CPCSEA	Committee for the Purpose of Control and Supervision of Experiments on Animals
Cr	Chromium
CRP	C-Reactive Protein
Cu	Copper
DLS	Dynamic Light Scattering
DMARDs	Disease Modifying Anti-Rheumatic Drugs
DMEM	Dulbecco's Modified Eagle's Medium
DMSO	Dimethylsulphoxide
DPBS	Dulbecco's Phosphate Buffered Saline
EDTA	Ethylenediaminetetraacetic acid
ESR	Erythrocyte Sedimentation Rate
EtBr	Ethidium Bromide
FBS	Fetal Bovine Serum
FTIR	Fourier Transform Infrared Spectroscopy
GPx	Glutathione Peroxidase
GSH	Glutathione
H ₂ O ₂	Hydrogen Peroxide
HSA	Human Serum Albumin
ICP-AES	Inductively coupled plasma atomic emission spectroscopy

IgG	Immunoglobulin G
KBr	Potassium Bromide
MMPs	Matrix Metalloproteinases
Mn	Manganese
MnO	Manganese Oxide
MTT	3-(4, 5-Dimethylthiazol-2-yl)-2,5- Diphenyltetrazolium Bromide
NaBH ₄	Sodium Tetrahydridoborate
NAD	No Abnormality Detected
NADH	Nicotinamide Adenine Dinucleotide
NOEL	No Observable Effect Level
NSAIDS	Non-Steroidal Anti-Inflammatory Drugs
O.D.	Optical Density
OECD	Organization for Economic Cooperation and Development
PDGF	Platelet Derived Growth Factor
PDI	Polydispersity Index
PEG	Polyethylene Glycol
PGE ₂	Prostaglandin E ₂
PLGA	Poly (Lactic-Co-Glycolic) Acid
RA	Rheumatoid Arthritis
RF	Rheumatoid Factor
ROS	Reactive Oxygen Species
RPM	Rotations Per Minute
RT	Room Temperature
S.D.	Standard Deviation
SDS	Sodium Doceyl Sulphate
Se	Selenium
SEM	Scanning Electron Microscope
SeNP	Selenium Nanoparticles
SeMetFa NP	Selenium-Methionine-Folic acid Nanoparticles
SeO ₂	Selenium Dioxide
SLE	Systemic Lupus Erythematosus
SOD	Superoxide Dismutase

SPR	Surface Plasmon Resonance
TEM	Transmission Electron Microscope
TGF- β	Transforming Growth Factor Beta
TNF- α	Tumor Necrosis Factor Alpha
UV-Vis	Ultraviolet-Visible
WBC	White Blood Cell
XRD	X-Ray Diffraction

LIST OF FIGURES

Figure Number	Title	Page Number
Figure 1.1	Diagram nanoscale	18
Figure 1.2	Classification and application of nanomaterials	20
Figure 1.3	Different forms of nanomaterials	21
Figure 1.4	Different preparation methods for nanoparticles have been reported	27
Figure 1.5	Solvent evaporation method	28
Figure 1.6	Solvent Diffusion Method	29
Figure 1.7	Crystallization Method	30
Figure 1.8	Schematic representation of the ionic gelation method	30
Figure 1.9	The mechanism for the formation of tiny CeO ₂ particles in scH ₂ O	31
Figure 1.10	Schematic for Self-Assembly Method	32
Figure 1.11	Layer-by-layer Deposition Method	33
Figure 1.12	Schematic of the magnetron-sputter inert-gas condensation NP deposition system	34
Figure 1.13	Muffle furnace method for the synthesis of copper oxide nanoparticles	35
Figure 1.14	Flame assisted synthesis for Nanomaterials	36
Figure 1.15	A low-temperature magnetron sputtering system is shown schematically (not to scale), and is used to create nanoparticles and nanocrystalline thin films	37
Figure 1.16	Diagrammatic representation of the equipment for creating SiC nanoparticles in microwave plasma at low pressure	38
Figure 1.17	Schematic representation of various biological synthesis methods	40
Figure 1.18	Schematic of platinum nanoparticle synthesis using a chemical method	41
Figure 3.1	Black and red allotropic forms of selenium	58

Figure 3.2	Benefits of selenium nanoparticles	62
Figure 3.3 (A)	Complete selenite sodium reduction to selenium nanoparticles (Brick red)	86
Figure 3.3 (B)	UV spectrum: Se nanoparticles, Se-Met nanoparticles, methionine control, Se-Met-Fa nanoparticles, and folic acid control	86
Figure 3.3 (C)	FTIR spectra of Se nanoparticles, Se-Met nanoparticles, Se- Met-Fa nanoparticles, methionine control, and folic acid control	87
Figure 3.3 (D)	Functional group chart	87
Figure 3.3 (E)	Shows the values of pure selenium	87
Figure 3.3 (F)	Zeta potential plot of Se, Se-Met, and Se-Met-Fa nanoparticles	88
Figure 3.3 (G)	X-ray diffraction patterns of Se, Se-Met, and Se-Met-Fa NPs	88
Figure 3.3 (H)	Raman spectra of trigonal Se	89
Figure 3.3 (I)	Differential Scanning calorimetry thermograms of 1) Se NPs and 2) Se-Met-Fa NPs	89
Figure 3.4 (A)	Shows the TEM image of the Se NPs; the scale bar is 100 nm	90
Figure 3.4 (B)	Diffraction pattern of Se NPs as measured by TEM	90
Figure 3.4 (C)	Se-Met-Fa NPs TEM image	91
Figure 3.4 (D)	TEM-measured diffraction pattern of Se-Met-Fa nanoparticles	91
Figure 4.1	Different modes of active cellular internalization of nanoparticles	98

Figure 4.2	Active and passive cellular uptake of particles: (A) phagocytosis, (B) caveolin-mediated endocytosis, (C) clathrin-caveolin-independent endocytosis, (D) clathrin-mediated endocytosis, (E) macro-pinocytosis, (F) ion pumps, (G) exocytosis, (H) facilitated diffusion, and (I) simple diffusion	99
Figure 4.3	(A) Images of plasmid pBR322 after contact with controls on an agarose gel. (B) Varying doses of Se NPs and Se-Met-Fa NPs. Circular DNA nicked (red arrow) and intact supercoiled DNA (green arrow). Panels (C) and (D) indicate the percentage of nicked and supercoiled DNA.	113
Figure 4.4	(A) UV-visible spectroscopy of BSA protein and BSA binding to Se-MetFa NPs at various doses (10-100 g/ml) (B) Steady-state BSA fluorescence spectra with and without increasing amounts of Se-Met-Fa NPs. (C) Stern-Volmer plot of BSA protein fluorescence quenching by Se-Met-Fa NPs, plotted as F_0/F versus $[Q]$. (D) Circular dichroism spectra of BSA in the presence of Se, Se-Met, and Se-Met-Fa NPs	116
Figure 4.5	Images of AO/EB staining at 24, 48, and 72 h are shown in (1), (2), and (3), respectively.	118
Figure 4.6	<i>In vitro</i> cytotoxicity of Se NPs and Se-Met-Fa NPs (50-100 μ g) on NIH 3T3 and Raw 264.7 cells (A and B).	119
Figure 4.7	Radical scavenging assay showing the % suppression of DPPH by Se-Met-Fa NPs at various doses (10-60 μ g/ml)	120
Figure 5.1	Relationship between Selenium and human health	126
Figure 5.2	Multiple pathogenic mechanisms underlying RA	140
Figure 5.3	Preparations of PGE ₂ standards	158

Figure 5.4	(a) shows a graph of coated and uncoated objects. Compare the nanoparticles in nm was compared to their size. (b) Graph showing Se and SeMetFa NPs against percentage of hemolysis. (C and d) Illustrations of Se NPs and SeMetFa NPs at concentrations of 50, 100, and 200 g/ml, respectively.	163
Figure 5.5	Shows the permeability data. a) A graph was created for Se NPs against apparent permeability in the required pH range at three different time points (2,4 and 24 h). b) Graph with three different time points that compares the apparent permeability of SeMetFa NPs at each required pH (2,4 and 24 h). c) A bar graph is used to compare steps a) and b), d) Bar graph demonstrating the percentage of permeability of control samples, SeMetFa NPs, and Se NPs over a wide pH range (2,4,6,7,8 and 10).	165
Figure 5.6	A shows the average body weight of the rats used as an animal model and how it changed in each group from before CFA induction to day 21 of the experiment. B) Prednisolone and SeMetFaNPs (250, 500, and 750 g/kg b.w.) Effect on Paw Edema in CFA-induced Rats.	167
Figure 5.7	Shows the impact of SeMetFaNPs (250, 500, and 750 μ g/kg b.w.) and prednisolone on the levels of A) SOD, B) catalase, and C) Gpx in rats administered CFA.	168
Figure 5.8	Shows of prednisolone and SeMetFaNPs (250, 500, and 750 μ g/kg b.w.) on the levels of TNF alpha, CRP, and prostaglandins in rats administered CFA.	169
Figure 5.9	Images of the individual group's paws, histopathology of the tissue, and a radiographic image of the paw area.	170
Figure 5.10	Microphotographs of 1) Liver, 2) Spleen and 3) Kidney	177

LIST OF TABLES

Table Number	Title	Page Number
Table 3.1	Recommended amounts of selenium for different age groups	60
Table 3.2	Determination of pure selenium by ICP-AES	87
Table 4.1	Helicity variations when nanoparticles are present	117
Table 5.1	The effect of different concentrations of SeMetFa NPs on paw edema in adjuvant-induced arthritis.	166
Table 5.2	liver, spleen, kidney, and paw tissues were graded histopathologically, as well as the radiographic condition of the paws	171
Table 5.3 (a)	Histopathology report of liver	171
Table 5.3 (b)	Summary of the Histopathological Findings in Liver tissue	172
Table 5.4 (a)	Histopathology report of Kidney	173
Table 5.4 (b)	Summary of the Histopathological Findings in kidney tissue	174
Table 5.5 (a)	Histopathology report of Spleen	174
Table 5.5 (b)	Summary of the Histopathological Findings in Spleen tissue	175
Table 5.6	Microscopic Observations and Grades of Pathological Changes observed for paw Joints	175

Chapter 1:
Introduction and
Literature Review

1.1 Prologue

In the term "nanotechnology," the prefix nano refers to a billionth (1×10^9). Nanotechnology is troubled by different types of matter structures that have dimensions on the order of billionths of a meter (Figure 1.1). Although the term "nanotechnology" is fairly new, functional objects and structures with nanometer-scale dimensions have existed on Earth for as long as there has been life. Natural processes, such as complex protein folding or atomic arrangement in DNA, contain nanometer-sized structures (Maynard, 2007). Mollusks, such as abalone, organize calcium carbonate into sturdy nanostructured blocks that are composed of a glue made of a carbohydrate-protein mixture. These shells have iridescent inner surfaces. The nanostructured bricks prevented the cracks from passing through the shell. These shells serve as a natural example of the durability of an assembly made of nanoparticles. This discovery has generated interest in using the shell structure of the abalone as a model for creating stronger and more resilient materials. The replication and incorporation of these nanostructured bricks into a variety of applications, including the development of stronger building materials and more effective energy storage devices, are being investigated by researchers. Understanding and controlling these structures is the goal of nanotechnology, which has applications in industries such as electronics, energy, and medicine (Poole & Frank Owens, 2003).

Nanotechnology has recently emerged as one of the most noteworthy and captivating leading-edge disciplines in physics, engineering, chemistry, and biology. This validates the great potential for giving rise to several novelties that will modify the course of technical expansion in a variety of applications in the near future. It is crucial to have a comprehensive overview and commentary on a topic that is detailed enough to provide in-depth coverage and insight into the field and sufficiently readable and thorough to be accessible to a large audience of people who need to know the state of the field and its future prospects. This will help to accelerate the widespread adoption of this new technology.

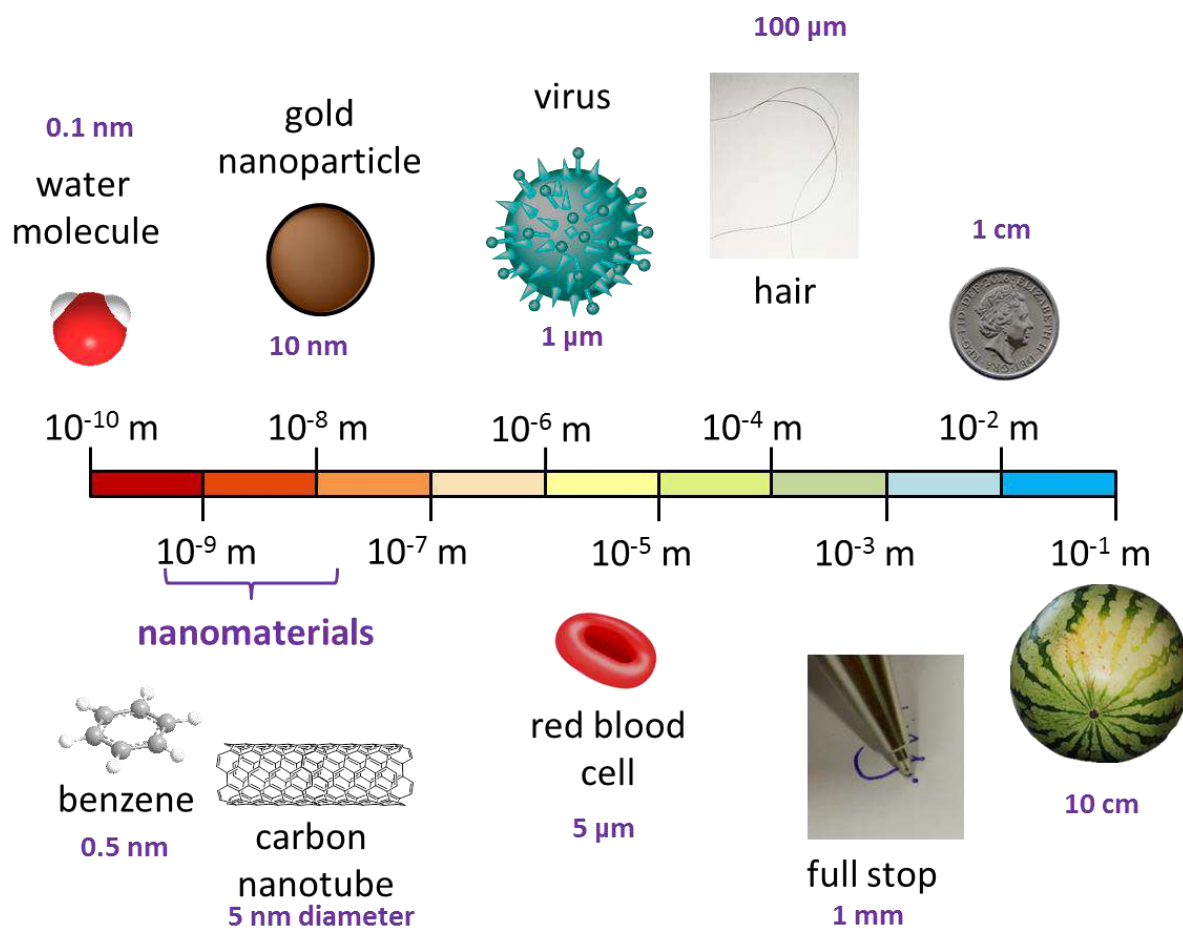


Figure 1.1 Diagram nanoscale(ChemBAM, n.d.) .

1.2 History of Nanotechnology

New science and technology are frequently the result of human dreams and imaginations. These aspirations have given rise to the 21st century frontier of nanotechnology. Understanding and manipulating matter with dimensions between 1 nm and 100 nm, where special phenomena allow for novel applications, is referred to as nanotechnology. Although nanoparticles have always been present, the industrial revolution saw a sharp rise in this exposure. Research on nanoparticles is not new. Richard Zsigmondy, the 1925 winner of the Nobel Prize in chemistry, was the one who first coined the term "nanometer." He was the first to use a microscope to measure the size of particles, such as gold colloids, and he also invented the term nanometer specifically to describe particle size (About the National Science and Technology Council About This Document, n.d.).

The inventor of contemporary nanotechnology was physicist Richard Feynman, who won the Nobel Prize in Physics in 1965. He presented the idea of manipulating matter at the atomic level in a lecture titled 'There's Plenty of Room at the Bottom' at the 1959 American Physical Society meeting held at Caltech. With this innovative concept, new ways of thinking were demonstrated and Feynman's theories were later found to be true. Due to these factors, he is regarded as the founding father of contemporary nanotechnology.

A Japanese scientist Norio Taniguchi was the first to use the term "nanotechnology" to describe semiconductor processes that took place on the order of a nanometer, almost 15 years after Feynman's lecture. He argued that processing, separating, consolidating, and deforming materials using a single atom or molecule constitutes nanotechnology. The golden age of nanotechnology began in the 1980s with the discovery of fullerenes by Kroto, Smalley, and Curl. Eric Drexler of the Massachusetts Institute of Technology (MIT) used concepts from Taniguchi's term "nanotechnology" and Feynman's "There is Plenty of Room at the Bottom" in his 1986 book, "Engines of Creation: The Coming Era of Nanotechnology." Drexler proposed the concept of a nanoscale "assembler" that can create duplicates of itself and other objects of any complexity. "Molecular nanotechnology" is a common name for Drexler's interpretation of nanotechnology. The creation of carbon nanotubes by Iijima, furthered the field of nanotechnology (Hulla et al., 2015; Saallah & Lenggoro, 2018).

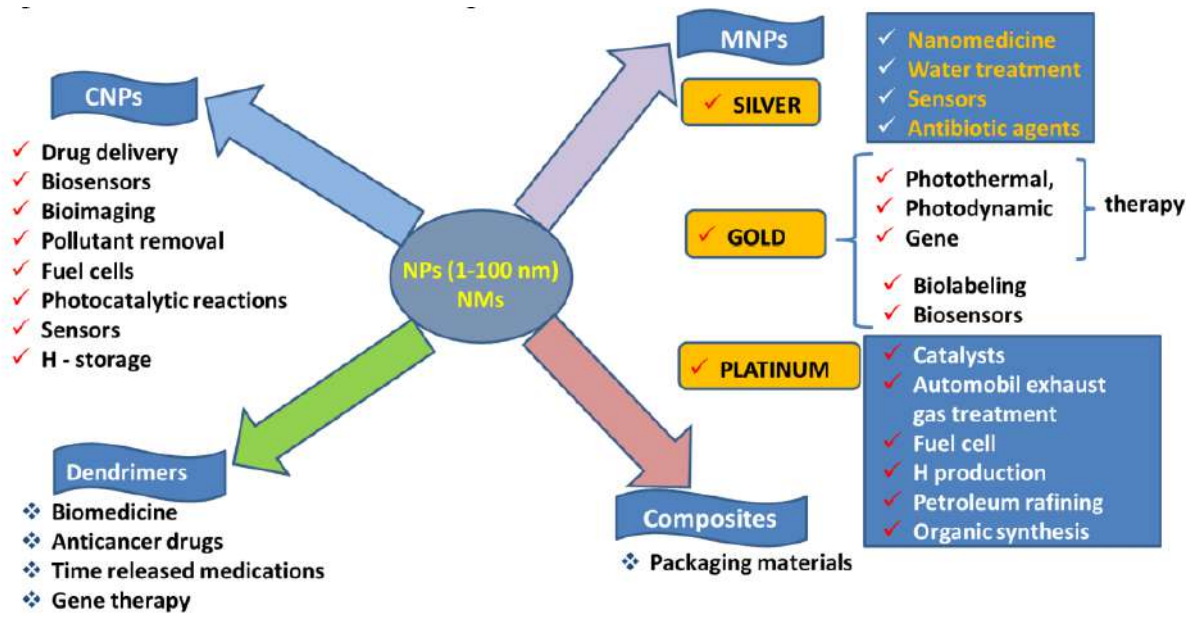


Figure 1.2 Classification and application of nanomaterials (Findik, 2021).

1.3 Nanomaterials classification

The major nanomaterial classifications are structural, in terms of their dimensions. (figure 1.3) Nanomaterials are classified as organic, nonorganic, or a combination of the two, and are classified as zero-dimensional, one-dimensional, two-dimensional, and three-dimensional. These classifications are essential for understanding the distinct properties and applications of nanomaterials. Organic nanomaterials are composed of carbon-based compounds, whereas inorganic nanomaterials are composed of metals, ceramics, and semiconductors. Dimensionality classification distinguishes between nanomaterials with a single dimension (such as nanowires) and those with complex three-dimensional structures (such as nanoparticles).

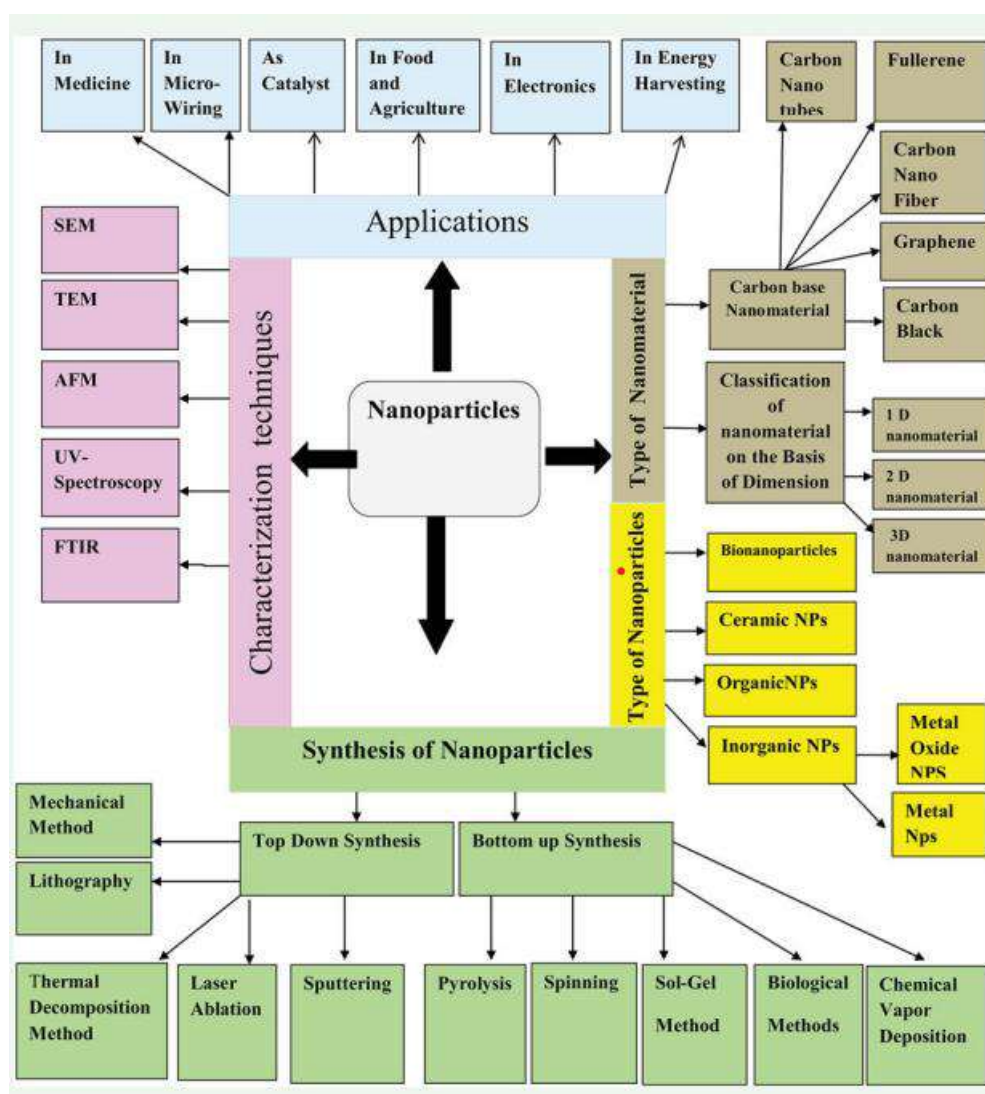


Figure 1.3 Different forms of nanomaterials (Ijaz et al., 2020).

1.3.1 Structural Classification

1.3.1.1 Organic Nanomaterials

Organic compounds are converted into organic nanomaterials at the nanoscale level. Liposomes, dendrimers, ferritin, and micelles are examples of organic nanoparticles. Non-toxic biodegradable nanomaterials with hollow interiors, such as nanocapsule micelles and liposomes, are sensitive to heat, electromagnetic radiation, and light. The surface of a dendrimer is covered with numerous chain ends that can accomplish specific chemical reactions. Dendrimers are used in molecular recognition, nanosensing, light-harvesting, and opt-electrochemical systems. Furthermore, three-dimensional (3D) dendrimers may be useful for drug administration because of internal holes that can hold additional molecules (Findik, 2021).

1.3.1.2 Inorganic Nanomaterials

Nanoparticles that don't comprise carbon atoms are referred to as inorganic nanomaterials. Nanomaterials made of metal- or metal-oxide-based nanomaterials are typically categorized as inorganic.

1.3.1.2.1 Metal-based Nanomaterials

There are two ways to create metal-based nanoparticles: destructive and constructive. Metal materials that are frequently used in the synthesis of nanoparticles include aluminum (Al), gold (Au), cadmium (Cd), copper (Cu), cobalt (Co), iron (Fe), lead (Pb), silver (Ag), and zinc (Zn). Metal nanoparticles have exceptional electrical, ultraviolet-visible sensitivity, and thermal, catalytic, and antibacterial properties owing to their quantum effects and high surface-to-volume ratio. Because of their exceptional optical qualities, metal nanomaterials have been used in a wide range of research fields (Schrand et al., 2010).

1.3.1.2.2 Metal-oxide Nanomaterials

Positive metallic ions and negative oxygen ions make up metal oxide nanoparticles, which are also referred to as metal oxide nanomaterials. Nanoparticles such as silicon dioxide (SiO₂), titanium oxide (TiO₂), zinc oxide (ZnO), and aluminum oxide (Al₂O₃) are frequently synthesized. These nanoparticles have remarkable properties compared to their metal analogs (Wahab et al., 2009).

1.3.1.3 Ceramic Nanoparticles

Non-metallic solids and ceramic nanoparticles are other names for them. Ceramic nanoparticles were created by heating or subsequent cooling. Nanoparticles of ceramic materials can be polycrystalline, amorphous, porous, dense, or hollow. Drug formulations containing ceramic nanoparticles are also possible. Nanomaterials have also received considerable attention from researchers owing to their applications in catalysis, photodegradation of dyes, photocatalysis, and imaging. Delivery systems, particularly those targeting tumors, glaucoma, and bacterial infections. Owing to their numerous applications in photocatalysis, catalysis, dye photodegradation, and imaging, researchers have focused on these nanoparticles (Z. Gao et al., 2022).

1.3.1.4 Bio Nanoparticles

An assembly of atoms or molecules created in a biological organization with at least one dimension between one and one hundred nanometers is referred to as a biological or bio-nanoparticle. The nanoparticles that originate in nature are all bio-nanoparticles. These nanoparticles were divided into two groups based on their extracellular and intracellular structures. Lipoproteins and viruses are examples of extracellular structures, while magnetosomes are examples of intracellular structures. Examples of bio-NPs include magnetosomes, exosomes, ferritin, lipoproteins, and viruses (Hasan, 2014).

1.3.1.5 Carbon Nanomaterials

There are five main types of carbon-based nanomaterials: carbon nanotubes, graphene, fullerenes, carbon nanofibers, and carbon black. Elliptical and spherical fullerenes, which are naturally configured carbon nanomaterials, are also known as buckyballs. Fullerenes are spherical structures made up of 28–1500 carbon atoms and have diameters of up to 8.2 nm for single layers and 4–36 nm for multilayered fullerenes. With a sheet thickness of approximately 1 nm, graphene is a hexagonal honeycomb lattice composed of carbon atoms on a two-dimensional (2D) planar surface. Cylindrical lattices are known as nanotubes. The same graphene nanofossils are used to make carbon nanofibers, and an amorphous form of carbon with diameters ranging from to 20-70 nm is known as carbon black. Hollow cylinders were formed to form nanotubes with diameters as low as 7×10^{-1} nm for a single layer and 100 nm for a multilayered carbon nanotube, and lengths varying from a few micrometers to several millimeters. Because carbon-based nanomaterials can occasionally outperform steel in terms of strength, they are primarily used for structural reinforcement. Nanomaterials made of carbon are thermally conductive down their length but not across the tube (K. D. Patel et al., 2019).

1.3.2 Classification based on Dimensions

1.3.2.1 Zero Dimensional Nanomaterials

These nanomaterials are either dimensionless outside the nanometric range (>10 nm) or all three dimensions (x, y, and z) within the nanoscale range. Examples of zero-dimensional (0D) nanomaterials include quantum dots, fullerenes, and nanoparticles. They can have different shapes and forms, such as metallic or ceramic, amorphous or crystalline, single-crystalline or polycrystalline, or any combination of these. The small volume, high surface-to-volume ratio, edge and quantum restraint effects, and respectable biocompatibility are characteristics of 0D nanomaterials. The use of 0D nanomaterials in the field of biosensing is growing rapidly because of their distinctive structures and properties (Z. Wang et al., 2020).

1.3.2.2 One Dimensional Nanomaterials

Two of the three dimensions (x, y) of the nanomaterials in this class are in the nanoscale range, but one of the three dimensions of the nanostructure is outside the nonmetric range (>10 nm). Its distinctive linear morphology, which has a large specific surface area, high electron-hole separation efficiency, strong light absorption capacity, a large number of exposed active sites, and other characteristics, has led to its extensive development and use in a variety of fields. Needle-shaped nanomaterials include 1D nanomaterials, such as nanofibers, nanotubes, nanohorns, nanorods, thin films, and nanowires. They can be standalone materials or embedded within another medium, such as metallic, ceramic, or polymeric materials. They can be amorphous, polycrystalline, crystalline, single crystalline, chemically pure, or impure. Ceramic, polymeric, or metallic 1D nanoparticles are all possible (T. Gao et al., 2021).

1.3.2.3 Two Dimensional Nanomaterials

A new class of nanomaterials, known as ultrathin two-dimensional (2D) nanomaterials, has sheet-like structures with transverse dimensions greater than 100 nm and a typical thickness of less than 5 nm. Two-dimensional (2D) nanomaterials have drawn increasing interest and attention in a variety of scientific fields, including functional electronics, catalysis, supercapacitors, batteries, and energy materials, owing to their high anisotropy and chemical functions. 2D nanomaterials have significantly advanced the field of nanomedicine in the biomedical industry, particularly in the areas of multimodal imaging, biosensing, antimicrobial agents, and tissue engineering. Due to their uniform structure, 2D nanomaterials with excellent physical, chemical, optical, and biological properties include graphene, graphene oxide (GO), reduced graphene oxide (rGO), silicate clays, layered double hydroxides (LDHs), transition metal dichalcogenides (TMDs), transition metal oxides (TMOs), black phosphorus

(BP), graphitic carbon nitride (g-C₃N₄), hexagonal boron nitride In a variety of fields, including energy storage, catalysis, sensing, and biomedical applications, these materials have garnered a lot of interest (Hu et al., 2019).

1.3.2.4 Three Dimensional Nanomaterials

Nanomaterials that are not restricted to nanoscale in any dimension or range are known as 3D nanomaterials or bulk materials. The bulk material is made up of individual blocks that are on the nanometer scale (1-100 nm); however, 3D nanomaterials have three arbitrary dimensions above 100 nm because all of their dimensions are outside the nanometer range or greater. 0D, 1D, and 2D structural elements are in close proximity to one another and form interfaces in multi-nanolayers, nanoparticle dispersions, and bundles of nanowires and nanotubes. Examples of 3D nanomaterials include colloids, free nanoparticles with different morphologies, and thin films with atomic-scale porosities. Owing to their nanoscale dimensions, 3D nanomaterials exhibit distinct characteristics and behaviors. Compared with their bulk counterparts, they have higher surface-to-volume ratios, are more reactive, and have better mechanical, electrical, and optical properties. Owing to these qualities, they are highly sought-after for a variety of applications in industries such as electronics, energy storage, catalysis, and biomedicine (Xiong et al., 2020).

1.4 Synthesis of Nanoparticles

Nanomaterials can be fabricated using various techniques. These approaches either take a "top down" or "bottom up" perspective (Figure 1.4). The transformation of bulk materials into nanomaterials is a component of the top-down approach (Camargo et al., 2009). Examples of this strategy include lasers, vaporization, and ultrafine grinding. The top-down approach has advantages in that bulk production can be achieved, which lowers manufacturing costs; however, there are also many drawbacks, including contamination, complexity, physical constraints, and heat dissipation.

Bottom-up approaches embrace the self-assembly or atom-by-atom construction of a material to form a stable structure in a specific category (Epple, n.d.; Gozhong Cao (university of washington, 2008; C. Zhang et al., 2015a). This method can be used to create nanoparticles from a variety of materials including proteins, polysaccharides, and synthetic polymers. There are various types of these methods. The size, properties, surface characteristics, biodegradability, biocompatibility, toxicity, antigenicity, drug release, and other factors are considered when selecting matrix materials. Bottom-up approaches have the advantage of being self-assembling processes with fewer product defects; however, the products formed are not very robust, and the process for forming nanoparticles is lengthy. Nanoparticles are synthesized using a variety of methods, including solvent evaporation, solvent diffusion, polymerization, ionic gelation, supercritical fluids, self-assembly, and layer-by-layer deposition.

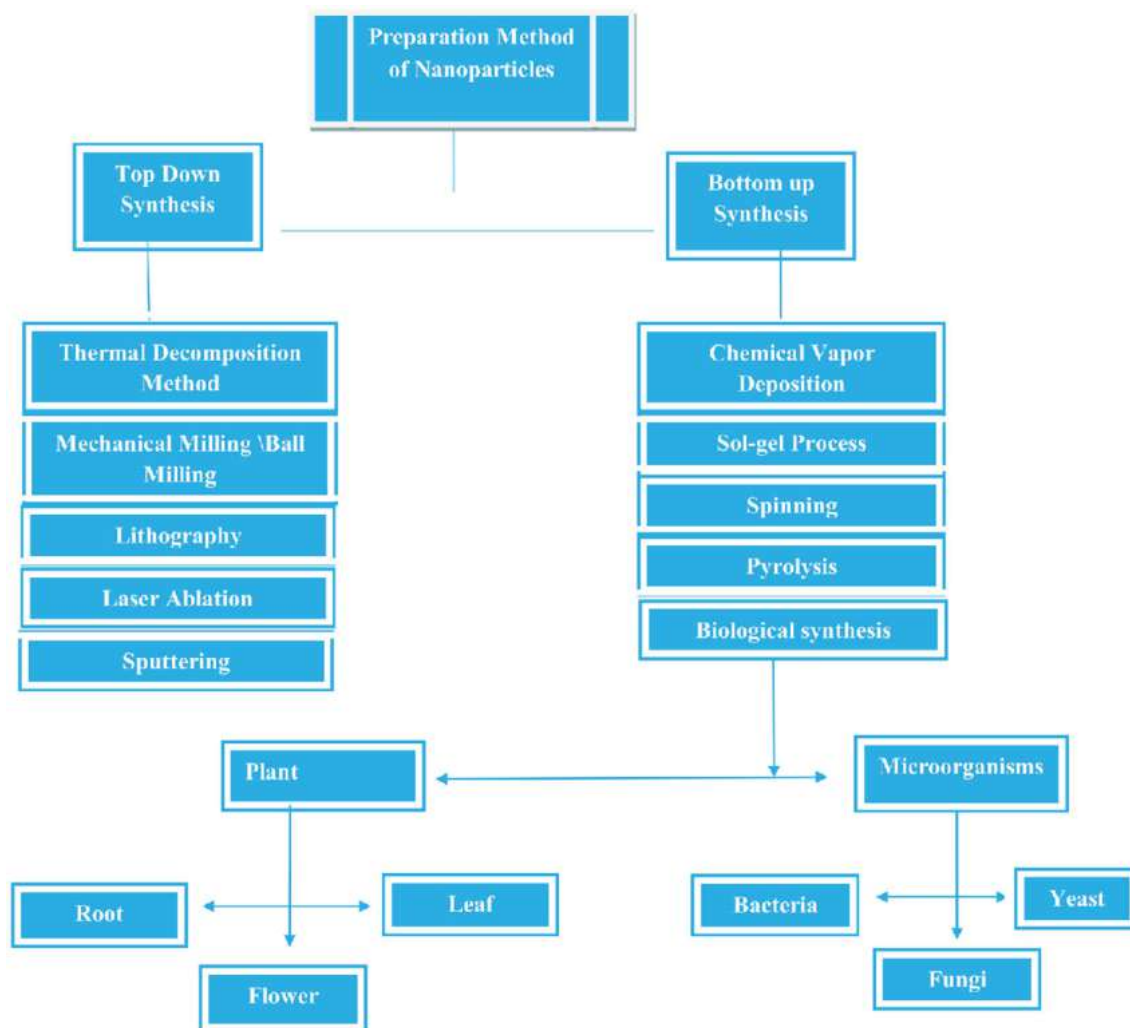


Figure 1.4 Different preparation methods for nanoparticles have been reported (Ijaz et al., 2020).

1.4.1 Solvent Evaporation Method

For the synthesis of all polymeric-based nanoparticles, the solvent evaporation method is typically used for the synthesis of polymeric-based nanoparticles. This entails emulsifying an organic solvent chosen to dissolve the polymer in an aqueous phase, followed by evaporation and the formation of nanomaterials (Figure 1.5). This synthesis method can also be used to encapsulate different drugs within polymeric nanoparticles. The solvent evaporation method has several advantages, including the ability to control the size and morphology of nanoparticles by adjusting the emulsification process parameters (Nam & Luong, 2019). They also enable the incorporation of hydrophobic drugs into the polymer matrix, which improves their stability and controlled-release properties. In a study conducted by Parikh and colleagues (Ughreja & Parikh, 2019), a multiparticulate system for colonic delivery of satranidazole was developed for better management of intestinal amoebiasis. It was proposed that the

fabrication of satranidazole microspheres by emulsion-solvent evaporation using ethyl cellulose as a polymer.

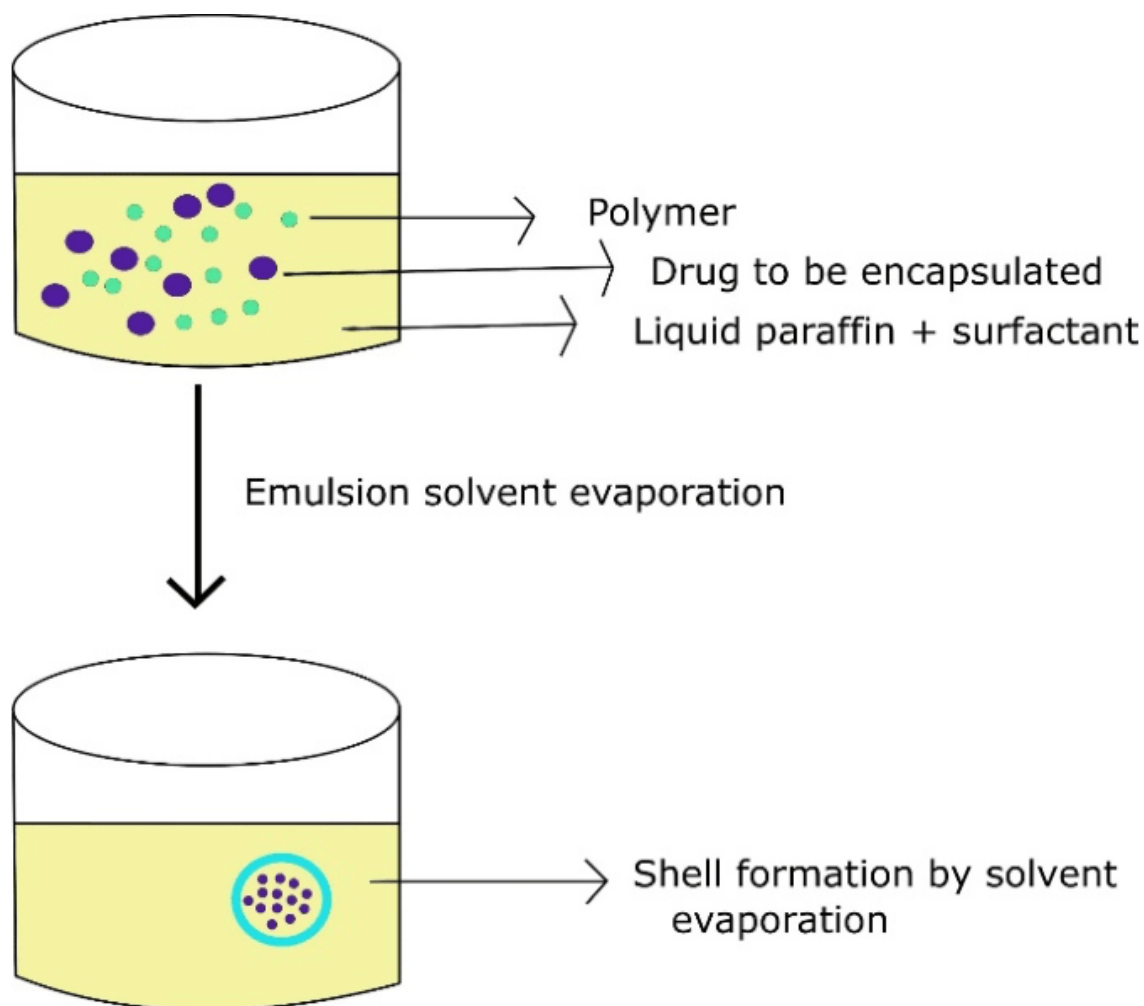


Figure 1.5 Solvent evaporation method (Maqbool & Noreen, 2019).

1.4.2 Solvent Diffusion Method

The solvent diffusion method is also commonly used to create polymeric nanoparticles. It consists of an oil phase containing both a water-miscible and a small amount of water-immiscible solvent, resulting in interfacial turbulence and spontaneous solvent diffusion, which leads to particle formation (Figure 1.6). As the concentration of the miscible solvent increases, the particle size decreases (Mohanraj & Chen, 2006). By adjusting the composition of the oil phase, this method allowed for control over particle size and morphology. Furthermore, the solvent diffusion method can be used to encapsulate hydrophobic drugs within polymeric nanoparticles, thereby increasing their solubility and bioavailability.

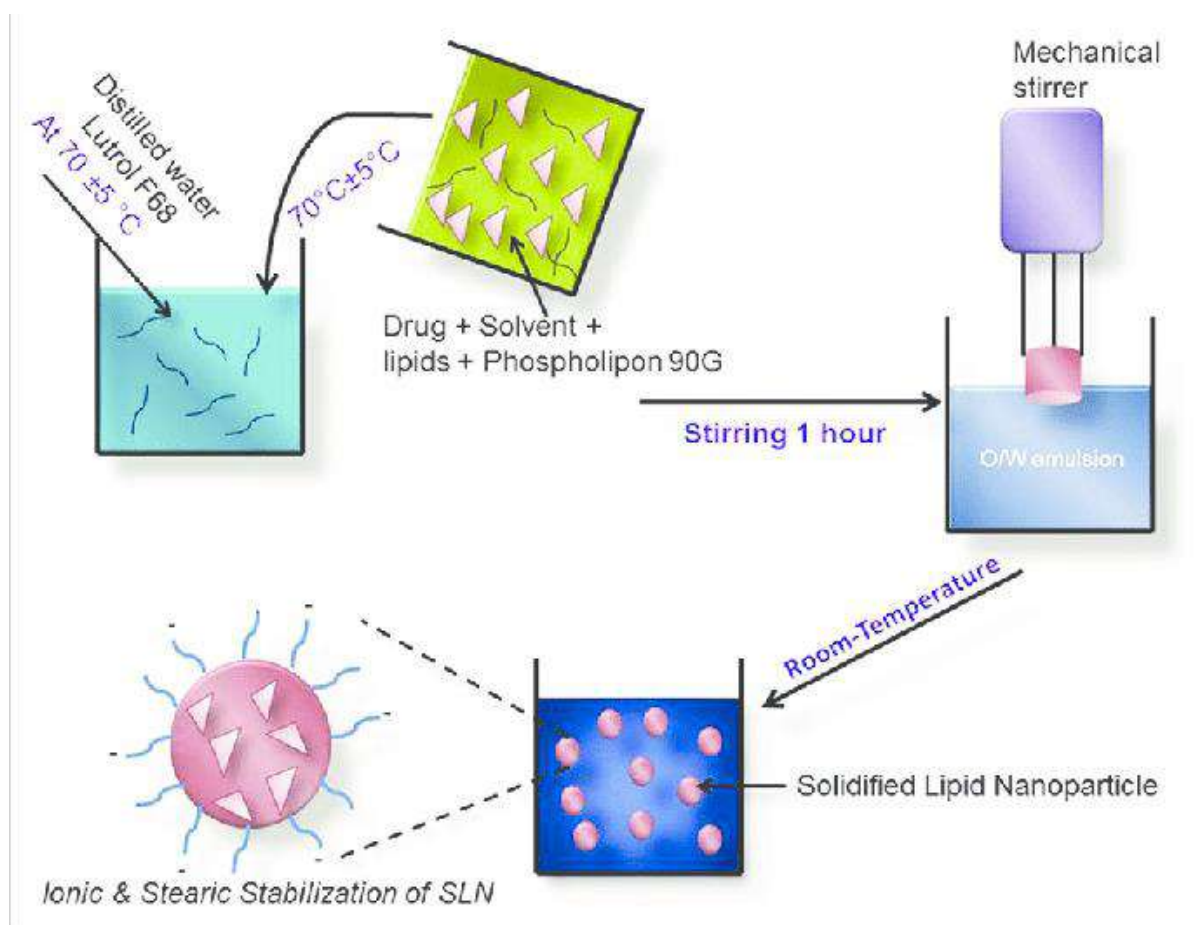


Figure 1.6 Solvent Diffusion Method (Shah et al., n.d.).

1.4.3 Crystallization Method

Polymerization of monomers results in the formation of nanoparticles (Fig 1.7). There are two types of polymerization: emulsion polymerization and interfacial polymerization. Emulsion polymerization can take place in either organic or aqueous continuous phases, which means that the monomer is either dispersed in an emulsion or dissolved in an aqueous solution. Interfacial polymerization uses two monomers dissolved in different phases, and the reaction occurs at the interface between the two liquids. These techniques can be used to load different drugs onto these polymers. Drugs can be adsorbed on particles or dissolved either during or after polymerization (Ijaz et al., 2020; Mohanraj & Chen, 2006). The preferred drug release profile and suitability of the drug for the polymerization process determine the loading method to be used. Adsorbing the drug onto particles can result in controlled release through surface interactions, whereas dissolving the drug during polymerization allows for homogeneous distribution of the drug within the polymer matrix.

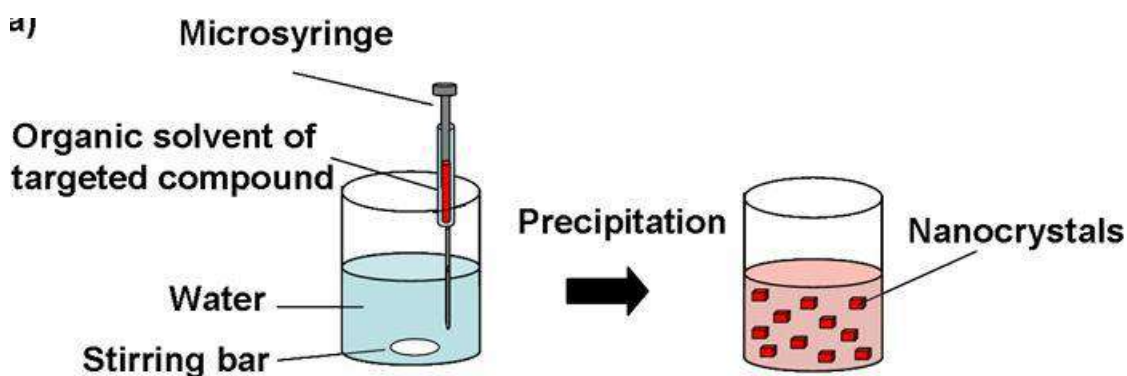


Figure 1.7 Crystallization Method (Baba et al., 2011).

1.4.4 The Ionic Gelation Method

The ionic gelation method can be performed easily, mildly, and quickly in typical laboratories because it requires expensive, simple, and readily available materials and equipment. In this procedure, a gel is created by reacting a crosslinking agent, such as calcium chloride or sodium alginate, with a polymer solution (Hoang et al., 2022). Drug delivery systems and scaffolds for tissue engineering are two uses of the resulting gels. Additionally, because the mechanism relies on electrostatic interactions rather than chemical reactions, organic solvents are not required, and potentially toxic chemicals or reagents are avoided. The drawbacks of this method include the difficulty in producing uniformly sized NPs and the paucity of research on polymers (other than CS).

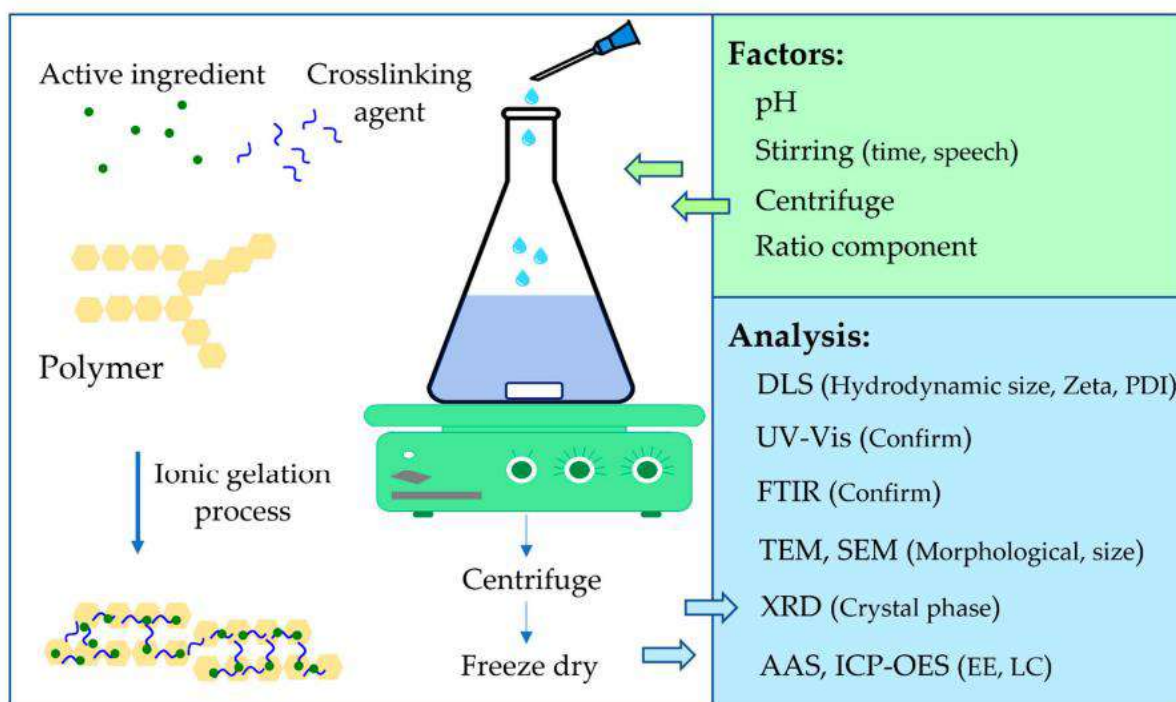


Figure 1.8 Schematic representation of the ionic gelation method (Hoang et al., 2022).

1.4.5 Supercritical Fluid (SCF) Technology

In the past 20 years, supercritical fluid (SCF) technology has grown in importance as a tool for processing materials. Supercritical fluids facilitate the precipitation of pure and encapsulated micro- to nanoscale particles. The most frequently used supercritical fluid is carbon dioxide. The carbon dioxide gas is subjected to pressure and heat during supercritical processes. It then enters a supercritical state, where it exhibits both liquid and gaseous characteristics. In this state, carbon dioxide effectively penetrates materials and dissolves solutes, making it a perfect solvent for a variety of industries, such as pharmaceuticals and food processing (Byrappa et al., 2008).

Compared to subcritical water, the hydrothermal reaction rate in scH₂O was higher, and the solubility of the metal oxides was significantly lower. This resulted in a higher degree of supersaturation. According to nucleation theory, the nucleation rate is predicted by the relationship between the degree of supersaturation and the surface energy. Consequently, under supercritical conditions, a very high nucleation rate can be anticipated, which results in the formation of nanoscale particles. The mechanism for the formation of tiny CeO₂ particles in scH₂O is shown in Figure 1.9 (Byrappa et al., 2008).

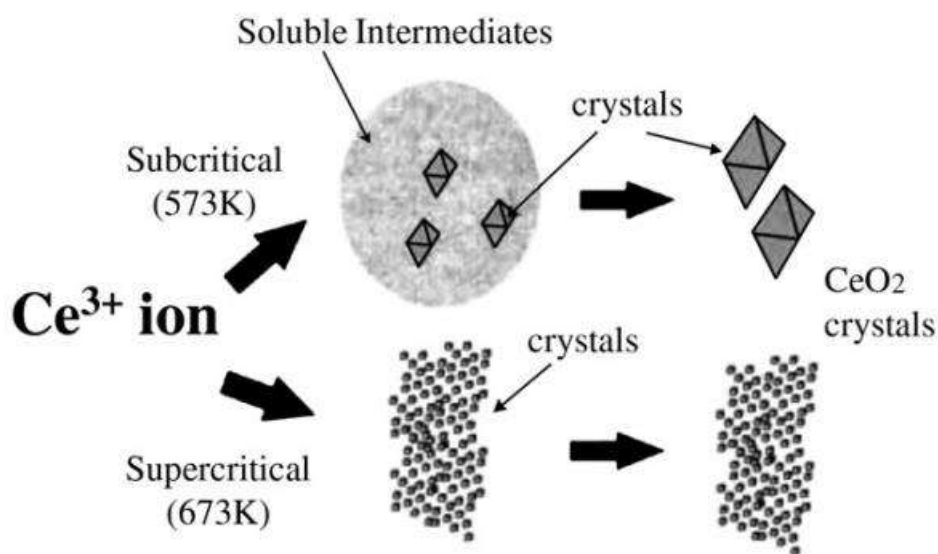


Figure 1.9 The mechanism for the formation of tiny CeO₂ particles in scH₂O (Byrappa et al., 2008).

1.4.6 Self-Assembly Method

Selective control of the noncovalent interactions between particles is the foundation for the self-assembly of nanoparticles. This is a crucial tool for developing molecular-scale structured systems. By adjusting chemical and physical parameters, such as pH, solute concentrations, and temperature, this technique can be used to synthesize fibrous nanostructures and monolayer-functionalized nanoparticles. Researchers can direct nanoparticles to form particular arrangements, such as chains, clusters, or lattices, by adjusting these parameters. As a result, the size, shape, and general structure of the resulting nanostructures can be precisely controlled, allowing their use in a variety of industries such as electronics, medicine, and materials science. Several groups (Vigderman et al., 2012) have used biorecognition-driven self-assembly of nanorods to detect antigens via antibody binding.

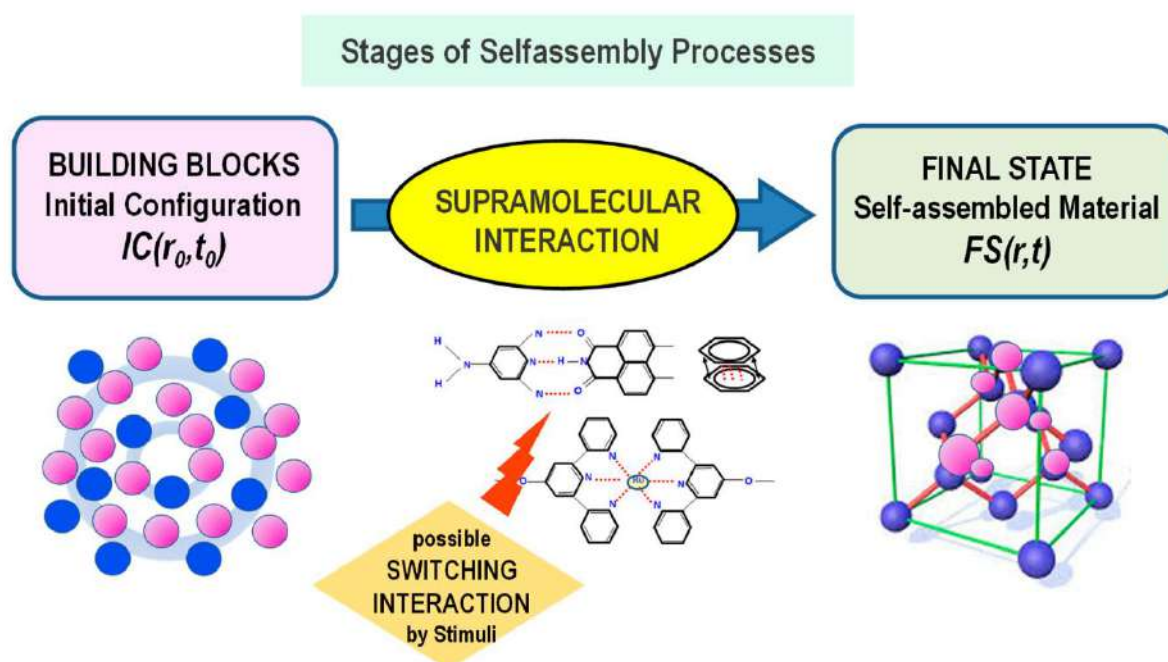


Figure 1.10 Schematic for Self-Assembly Method (Lombardo et al., 2020).

1.4.7 Layer-by-layer Deposition Method

Layer-by-layer deposition (figure 1.11) involves the use of polyelectrolytes with opposite charges assembled on a platform using bilayer membranes to form thin films with varying compositions, thicknesses, surface charges, permeabilities, and elasticities. *In vitro* studies revealed that the layer-by-layer technique reduced the undesirable initial burst release of DOX-loaded PLGA NPs (DOX-PLGA NPs) from 55.12% to 5.78%.

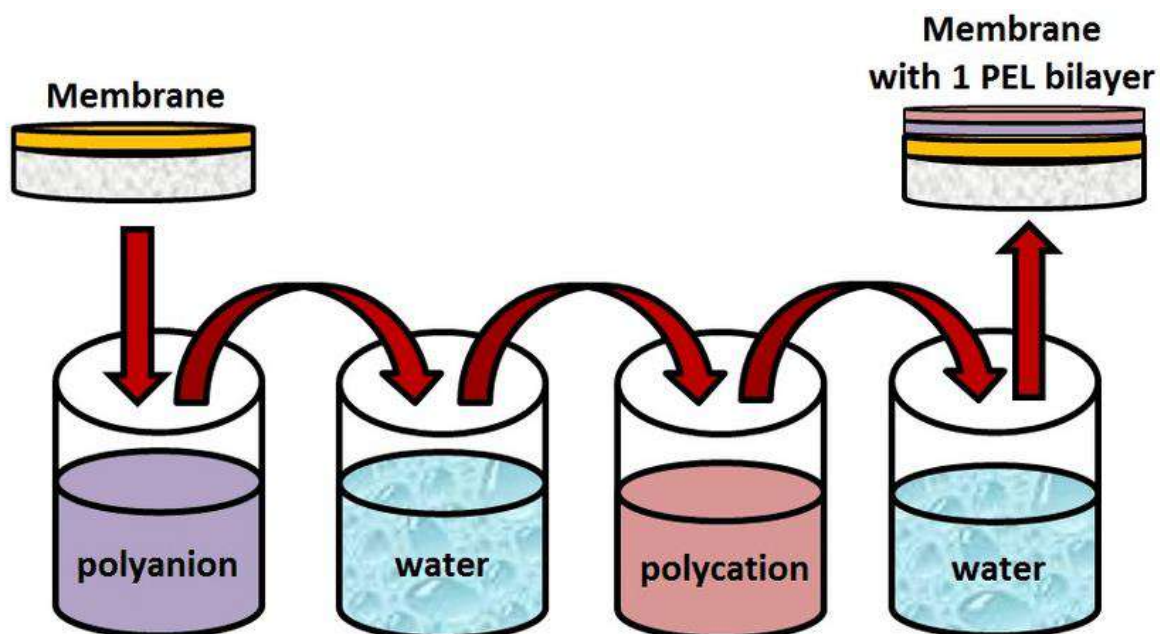


Figure 1.11 Layer-by-layer Deposition Method (Dmitrenko et al., 2021)

1.4.8 Gas-Phase Synthesis Method

The conditions created during gas-phase synthesis are such that the vapor-phase mixture is chemically supersaturated, causing the conditions to become thermodynamically unstable, where the vapor-phase molecules react chemically to form a condensed phase, converting the solid material into nanoparticles. The particles formed were homogeneous if the conditions were favorable and the level of supersaturation was sufficient. As soon as the particles are formed, the system is immediately quenched by removing the supersaturation source or by lowering the kinetics. This helps to maintain a constant particle size. The reaction was completed within seconds, and the size was continuously maintained. This technique is used to create nanocrystalline materials, which are frequently used in electronic applications. Through subsequent inert-gas cooling and gas-phase condensation of sputtered atomic vapor, magnetron sputtering (figure 1.12) has been extensively used to synthesize single- and multicomponent NPs (Grammatikopoulos et al., 2016).

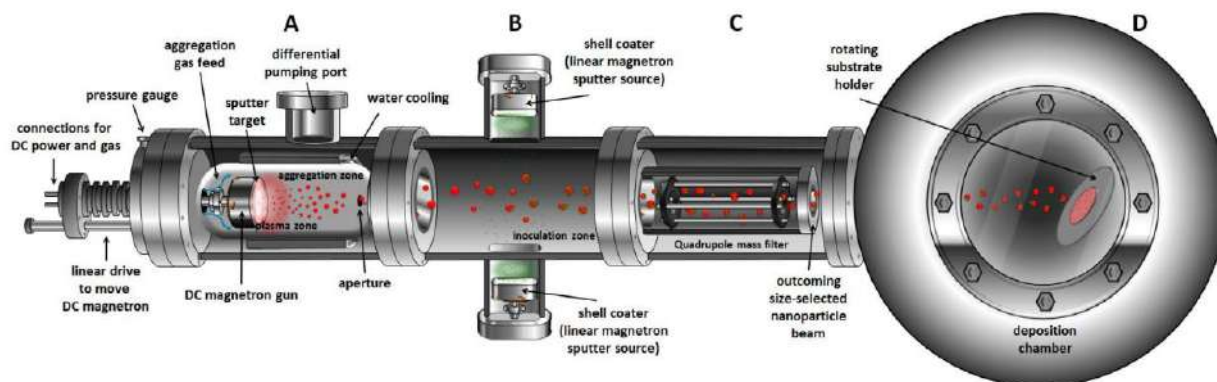


Figure 1.12 Schematic of the magnetron-sputter inert-gas condensation NP deposition system (Grammatikopoulos et al., 2016).

1.4.9 Muffle Furnace Irradiated Synthesis Method

The source material was placed in a vessel that could withstand high temperatures and was used in a furnace (Book, 2017). Using the heated flow of an inert carrier gas, the materials are heated to high temperatures. The furnace was used to prepare materials with high vapor pressure at intermediate temperatures of up to 1700°C. Materials that need to be transformed into nanoparticles are immediately cooled using dilution cooling or natural cooling techniques. Rapid cooling causes a significant change in the temperature, which leads to the formation of nanoparticles. Each vessel used in the furnace has its own operating temperature restrictions; therefore, the substance it transports may contain impurities from the vessel itself.

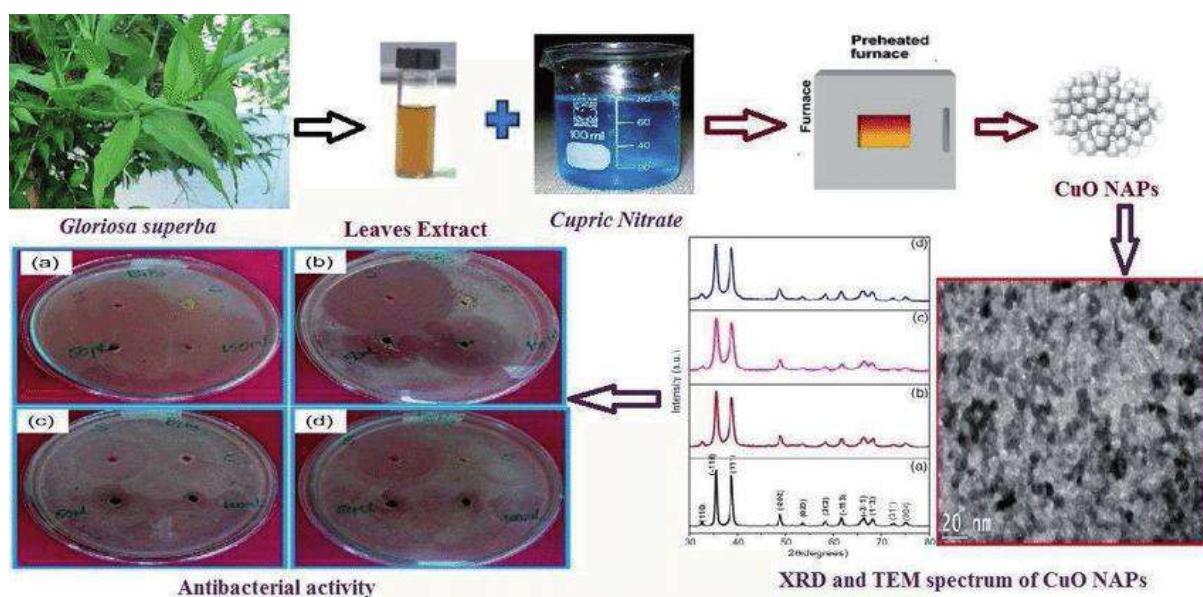


Figure 1.13 Muffle furnace method for the synthesis of copper oxide nanoparticles (Book 2017).

1.4.10 Flame Synthesis Method

A number of the first man-made nanomaterials and industrially produced nanoparticle goods, including carbon black, fumed silica, and pigmentary titania, were produced using the flame synthesis method, one of many nanofabrication techniques. Over the past two decades, the exploration of this technology for device applications has been driven by the adaptability of nanomaterials and the ease with which nanostructured films can be made using aerosol self-assembly. For the large-scale production of carbon black (CB), fumed silica, titania, alumina, and zinc oxide, which make up a significant portion of the production of commercial nanomaterials, flame synthesis (combustion), also known as the gas-liquid reaction, is used (John & Tricoli, 2022).

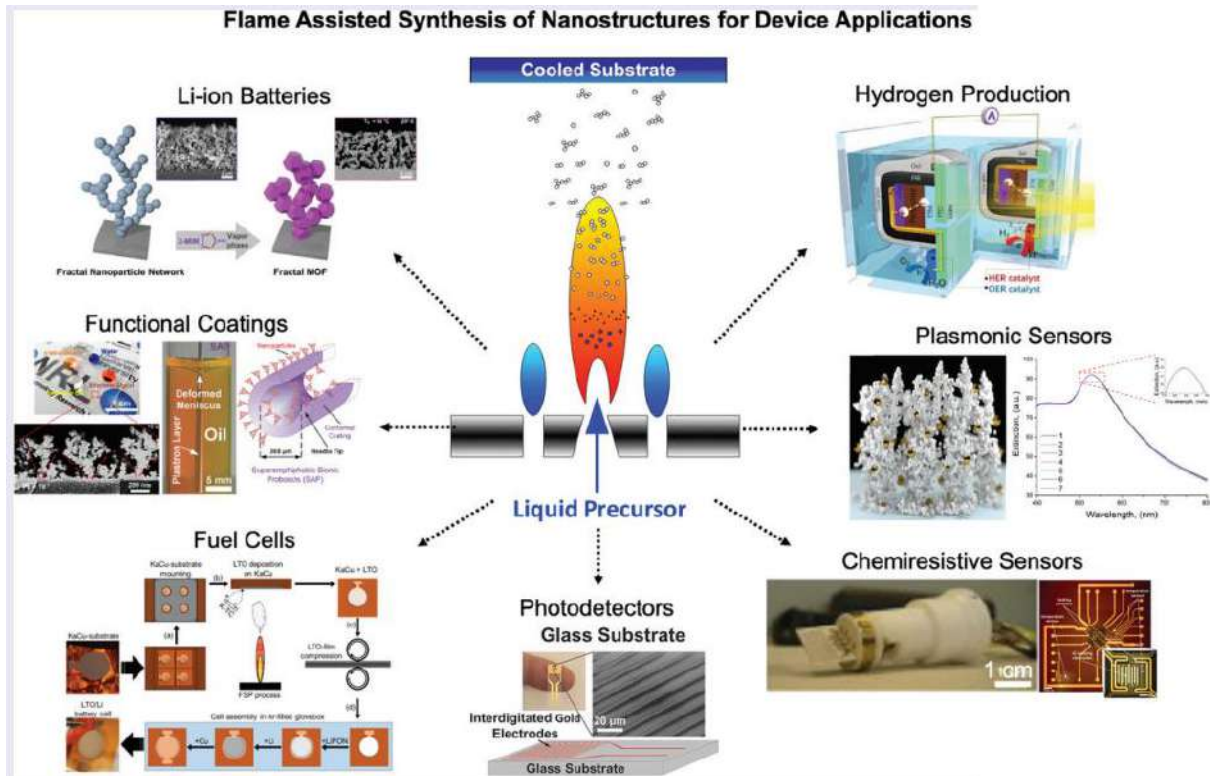


Figure 1.14 Flame assisted synthesis for Nanomaterials (John & Tricoli, 2022).

1.4.11 Sputtering Process

The sputtering process involves bombarding a target material with energetic gas or gaseous plasma ions, which cause microscopic particles of the target material to be ejected from its surface. Sputtering is caused by the atoms and ions of the elements exchanging momentum (Ayyub et al., 2001). There are many different sputtering techniques; however, magnetron, RF radio, and DC diode sputtering are the most well-known and frequently used techniques. The creation of fine thin films of materials is a common engineering practice. Microelectronics, including CPU processors, watches, batteries, cell phones, iPods, solar panels, medical, oxidation resistance, and antireflective coatings on automobiles, jewelry, and mirrors, among other applications, use thin films extensively. Sputtering was additionally employed for etching, analysis to determine the target material, and space weathering. Many different industries, including optical coatings, semiconductors, and microelectronics, can benefit greatly from sputtering processes.

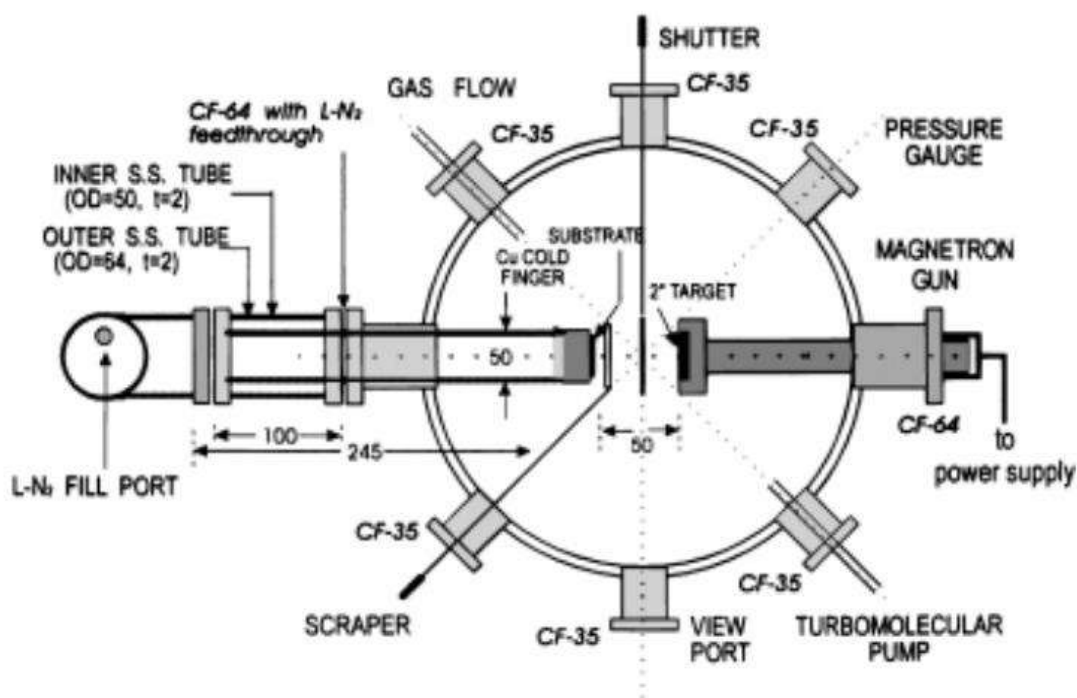


Figure 1.15 A low-temperature magnetron sputtering system is shown schematically (not to scale), and is used to create nanoparticles and nanocrystalline thin films (Ayyub et al., 2001).

1.4.12 Plasma Reactor Synthesis Method

Plasma synthesis methods have demonstrated the ability to produce a diverse range of nanopowders, including metal oxides, nitrides, and sulfides. A partially ionized gas, called plasma, which is regarded as the fourth state of matter, contains ions, electrons, atoms, and molecules. In cold plasma, an electronic system is selectively excited, resulting in extremely energetic electrons that, at much lower temperatures, are not in equilibrium with reactant molecules (H. Lin et al., 2008). Energetic electrons have the ability to partially ionize or dissociate reactant molecules, which then become highly activated. Additionally, the particles carry equal-sign electric charges during synthesis. Particle growth and agglomeration were both reduced by electrostatic repulsion. Consequently, in cold plasma, reactions that are kinetically delayed but thermodynamically advantageous are possible.

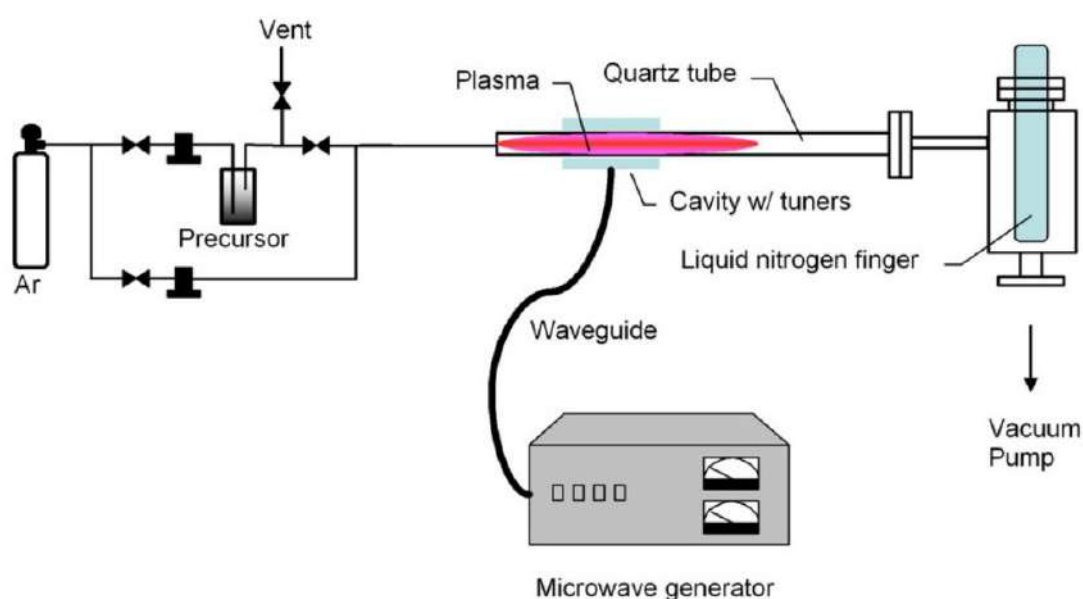


Figure 1.16 Diagrammatic representation of the equipment for creating SiC nanoparticles in microwave plasma at low pressure (H. Lin et al., 2008).

1.4.13 Biological Synthesis (Green Synthesis)

One of the most promising technologies currently used in all branches of science is nanotechnology. Metal nanoparticles created by nanotechnology have attracted attention on a global scale owing to their numerous applications in biomedical and physiochemical fields. In recent years, the production of metal nanoparticles using microorganisms and plants has been extensively studied and has been recognized as an environmentally friendly and effective method for utilizing microorganisms as practical nano-factories.

It has been demonstrated that microorganisms are significant nano-factories with enormous potential as environmentally friendly and economically advantageous tools, avoiding harsh, toxic chemicals, and the high energy demand necessary for physiochemical synthesis. Owing to a variety of reductase enzymes that can convert metal salts into metal nanoparticles with a narrow size distribution and low polydispersity, microorganisms have the capacity to accumulate and detoxify heavy metals. In recent years, extra- and intracellular studies of microorganisms such as bacteria (actinomycetes), fungi, and yeasts have been conducted to synthesize metal nanoparticles. Bacterial biomass, supernatants, and derived components have been used in a variety of biological protocols for nanoparticle synthesis (Mugesh et al., 2001). Extracellular synthesis has drawn the most attention among the different methodologies because it avoids the downstream processing steps needed for the recovery of nanoparticles in intracellular methodologies, such as sonication to break down the cell wall and several

centrifugation and washing steps required for nanoparticle purification. Furthermore, genes, proteins, peptides, enzymes, reducing cofactors, and organic materials play important roles by serving as reducing agents. Additionally, natural capping during the nanoparticle synthesis process aids in preventing nanoparticle aggregation and enhancing their long-term stability (Laslo et al., 2022; Martínez et al., 2020). For the synthesis of silver and gold nanoparticles, bacteria such as *Pseudomonas deceptionensis*, *Weissella oryzae*, (Singh, Kim, Wang, et al., 2016b; C. Wang et al., 2016) and *Bacillus methylotrophicus* have been investigated recently. Several *Bacillus* species, including *Bacillus licheniformis*, *Bacillus amyloliquefaciens*, *Rhodobacter sphaeroides*, and *Bacillus subtilis*, have demonstrated similar potentials for producing nanoparticles (Jo et al., 2016). Several genera of microorganisms, including *Bacillus*, *Pseudomonas*, *Klebsiella*, *Escherichia*, *Enterobacter*, *Aeromonas*, *Corynebacterium*, and *Lactobacillus*, have been implicated in the synthesis of metal nanoparticles (Singh, Kim, Wang, et al., 2016a).

Heavy metals have the potential to build up in different parts of plants in varying amounts. As a result, plant extract-based biosynthesis techniques have received more attention as excellent substitutes for traditional nanoparticle preparation techniques that are easy, efficient, affordable, and feasible. Many plants can be used in the "one-pot" synthesis process to reduce and stabilize metallic nanoparticles. To further investigate their many applications, many researchers have used green synthesis to create metal/metal oxide nanoparticles using plant leaf extracts. Biomolecules found in plants, such as proteins, coenzymes, and carbohydrates, have a remarkable capacity to transform metal salts into nanoparticles. Gold and silver metal nanoparticles were initially studied in plant extract-assisted synthesis, similar to other biosynthetic processes. Different plants, such as aloe vera (*Aloe barbadensis* Miller), oat (*Avena sativa*), alfalfa (*Medicago sativa*), tulsi (*Osimum sanctum*), lemon (*Citrus limon*), neem (*Azadirachta indica*), and mustard (*Brassica juncea*), have been used to produce silver and gold nanomaterials (Book, 2017; de Matos et al., 2013; Singh, Kim, Zhang, et al., 2016a). These nanoparticles have demonstrated positive antimicrobial effects against a variety of pathogens. In addition, compared to conventional chemical methods, the use of plant extracts as reducing agents in nanoparticle synthesis offers a more environmentally friendly and sustainable method (El-Ramady et al., 2015; Husen & Siddiqi, 2014; Megraj et al., 2011).

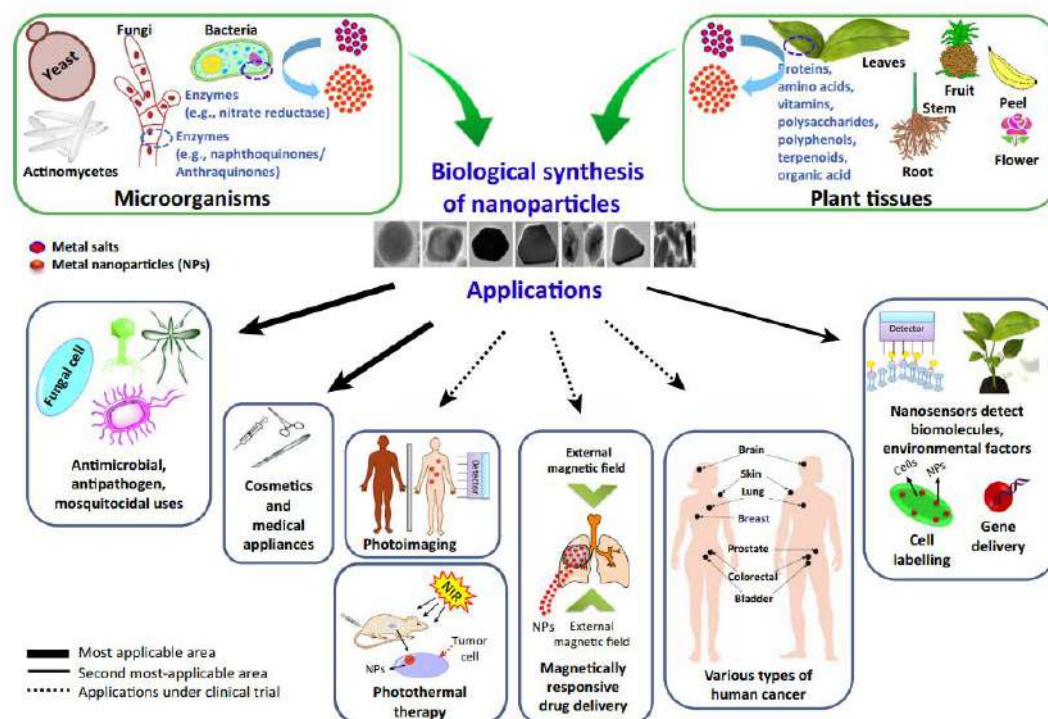


Figure 1.17 Schematic representation of various biological synthesis methods (Singh, Kim, Zhang, et al., 2016b).

1.4.14 Chemical Synthesis

Wet chemistry techniques are commonly used to create nanoparticles. These techniques start by creating particles in a solution, casting the wet particles onto a substrate, and then purging the particles of the solvent, surfactants, and other materials (Braun et al., 1951). This wet synthesis process requires considerable time and chemicals, and the final product may be contaminated with solution remnants. In particular, chemical synthesis routes have been used to create nanoparticles. Surface controlling agents (SCAs) were added during or soon after the formation of precipitates during precipitation from the liquid phase. To prevent agglomeration and regulate size, these disrupts the nucleation and growth of particles. Nanoparticles have been created from numerous systems. Numerous chemicals, such as sodium borohydrate, SDS, amino acids, reducing sugars, etc., (Benjamin, 1881; Shameli et al., 2011) are used to create nanoparticles with a variety of shapes and sizes (Figure 1.18) based on their compatibility and applications.

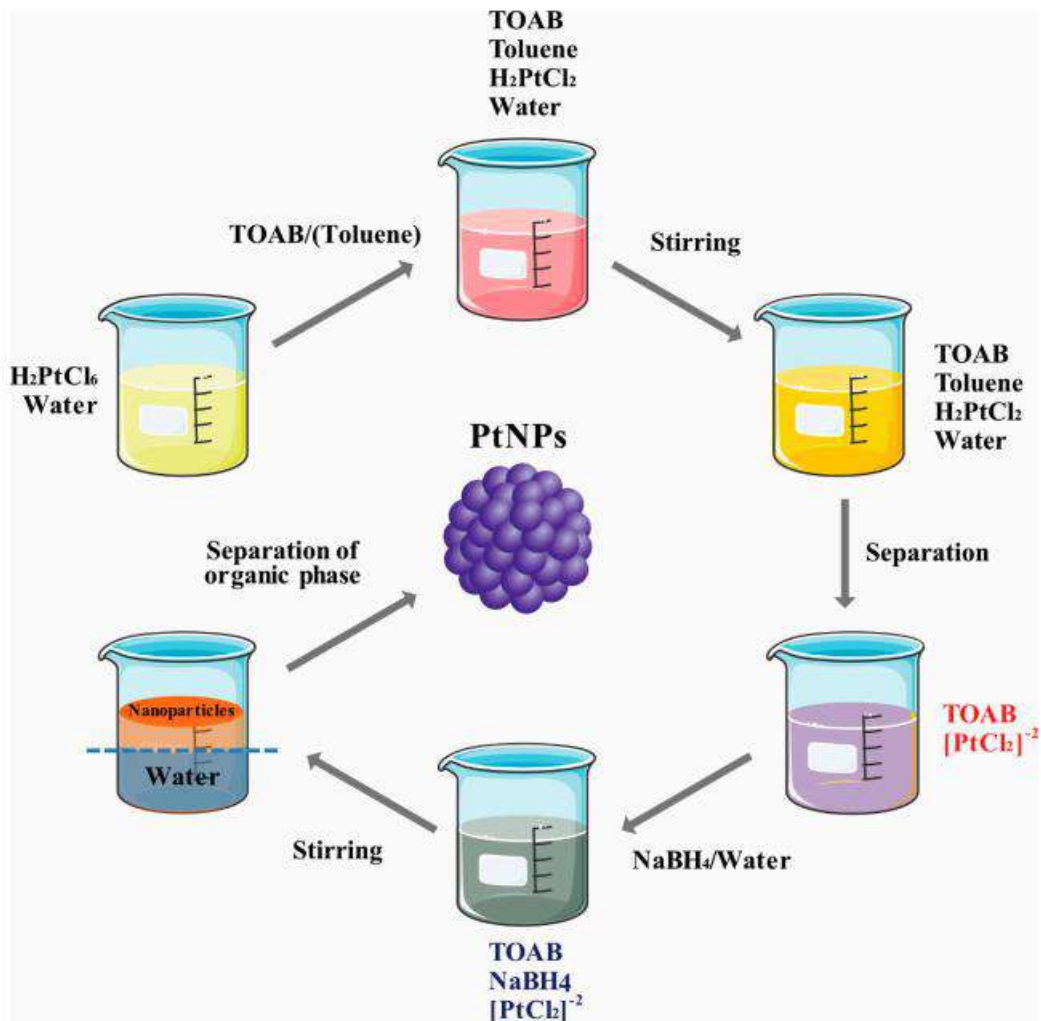


Figure 1.18 Schematic of platinum nanoparticle synthesis using a chemical method (Jeyaraj et al., 2019).

1.5 Characterization of Nanoparticles

Although traditional drug design, delivery, and medical diagnostics can benefit from nanotechnology, nanomedicines present significant preclinical challenges. Nanoparticle constructs intended for all applications often require modification of conventional characterization techniques because of their small size, distinctive physicochemical properties, and biological activity. Various analytical techniques have been used to characterize the size, shape, and composition of nanoparticles, which will help to illustrate their properties.

1.5.1 UV-Visible Spectrophotometer

The interactions between matter and electromagnetic radiation in the ultraviolet-visible range are the focus of ultraviolet-visible spectroscopy. The ultraviolet (UV) region of the electromagnetic spectrum spans the 10-380 nm range. It is typically divided into three main subregions: UVA in the 320–380 nm range, UVB in the 280–320 nm range, and UVC in the 100–280 nm range. Although it can only be studied if measurements are performed in vacuum, the 10-200 nm range is also known as vacuum ultraviolet (VUV). The 380–750 nm spectral range was covered by the visible (Vis) region. The term "electronic spectroscopy" is frequently used to describe UV-Vis spectroscopy because it is connected to the excitation of the outermost electrons of atoms, which play a role in the formation of molecules. Transmittance, reflectance, and photoluminescence (fluorescence and phosphorescence) modes are frequently used for UV-Vis measurements. Transmittance and reflectance measurements must be made in comparison to a standard, whereas photoluminescence acquisitions can be viewed as absolute measurements (Behzadi et al., 2015; K. S. Prasad et al., 2013).

1.5.2 X-Ray Diffraction (XRD)

X-ray diffraction (XRD) is a potent nondestructive method for characterizing crystalline materials. It offers details on crystal textures, preferred orientations for crystals, and other structural factors, such as average grain size, crystallinity, strain, and crystal defects. It also offers details on the structures and phases. X-ray diffraction peaks can be created by constructively interfering with a monochromatic beam of X-rays scattered at particular angles from each set of lattice planes in a sample. The distribution of atoms within the lattice controls the peak intensities. As a result, the X-ray diffraction pattern is a material's unique signature of periodic atomic arrangements (Bunaciu et al., 2015; Speakman, 1902).

1.5.3 Fourier Transform Infrared Spectroscopy (FTIR)

The vibrational characteristics of amino acids and cofactors, which are sensitive to minute structural changes, are investigated using Fourier transform infrared (FTIR) spectroscopy. The lack of specificity of this technique enables us to directly examine the vibrational characteristics of almost all the cofactors, amino acid side chains, and water molecules. However, we can choose vibrations corresponding to individual chemical groups involved in a particular reaction using reaction-induced FTIR difference spectroscopy. The resulting reaction-induced FTIR difference spectra were used to determine the IR signatures of each relevant residue using various methods. (Specific) Chemical groups are frequently identified using hydrogen/deuterium exchange, site-directed mutagenesis, and isotope labelling. We were able to translate the IR frequencies into specific structural traits of the chemical group or target molecule based on studies on model compounds and the growing application of theoretical chemistry to normal mode calculations (Laurent et al., 2008; Mekuye & Abera, 2023; Tugarova et al., 2018).

1.5.4 Zeta Potential

An approach for calculating the electrostatic potential at the electrical double-layer encircling a nanoparticle is to dissolve it in a solution. The zeta potential was used to describe this phenomenon. When the zeta potential of a nanoparticle is between 10 mV and +10 mV, it is said to be roughly neutral, whereas when it is greater than +30 mV or lower than 30 mV, it is said to be strongly cationic or anionic. The zeta potential can influence a nanoparticle's propensity to penetrate membranes because the majority of cellular membranes have a negative charge. Cationic particles typically exhibit greater toxicity owing to disruption of cell walls. Colloidal gold (strongly anionic) and amine-terminated PAMAM dendrimers, two types of nanoparticles frequently used in biological applications, have been used to demonstrate this technique (strongly cationic) (Biriukov et al., 2020; Walker, 1974).

1.5.5 Inductive Coupled Plasma Atomic Emission Spectroscopy (ICP-AES)

ICP-AES is an emission spectroscopy technique that uses a plasma to excite atoms and ions, which causes the plasma to emit electromagnetic radiation at wavelengths specific to a particular element. Although the limit is as low as 0.2 g/l with the most recent axial plasma instruments with ultrasonic nebulization, inductively coupled plasma atomic emission spectrometry (ICPAES) (Fig. 3) is significantly more sensitive than F-AAS. Calibration using standard addition is crucial. This method offers sufficient sensitivity for the acid digestion of biological samples, soil, sediment, or water

contaminated with metals. ICP-AES has a sizable advantage due to its multi-element capability (Crosland et al., 2008; Vonderheide et al., 2002).

1.5.6 Raman Spectroscopy

In the analytical process of Raman spectroscopy, the vibrational energy modes of a sample are determined by measuring the scattered light. It is named after Indian physicist C. V. Raman, who first observed Raman scattering in 1928 along with his research partner K. S. Krishnan. Raman spectroscopy is one of the best methods for analyzing two-dimensional (2D) materials. This quick, nonintrusive, and sensitive technique can capture the spectra of many 2D materials, even from a single flake. The best example is graphene, which, when illuminated by a green laser, exhibits distinct Raman features at wavenumbers of 1355 (D peak) and 1600 cm^{-1} (G peak), as well as a 2D peak at higher wavenumbers (Pandiarajan et al., 2004; Shipp et al., 2017).

1.5.7 Transmission Spectroscopy (TEM)

The smallest structures in matter can be seen using the analytic approach known as transmission electron microscopy (TEM). Unlike optical microscopes, which rely on light in the visible spectrum, TEM can enlarge nanometer structures by up to 50 million times to reveal stunning details at the atomic scale. The crystal and surface structures of the nanophase materials determine their physical and chemical characteristics. A powerful and distinctive transmission electron microscopy (TEM) method was used to characterize the structures. Real-space imaging of nanoparticles at atomic resolution is the most significant use of TEM. In this method, a sample is in contact with a beam of negatively charged electrons during transmission. This interaction produces an image on the screen that is sharpened even more to capture the particle's outward appearance precisely. A higher molecular weight will result in less transmission and a light color image, which is how the capacity of transmission varies with the sample thickness. Colloidal suspensions are typically applied to carbon tape (Fultz & Howe, 2013; Lin et al., 2008; Mondal & Srivastava, 2010).

1.6 Applications of Nanoparticles

Owing to their small size, nanomaterials have modified properties that distinguish them from bulk materials. A good example of this is a material with a very high surface area to volume ratio, which creates a lot of surface or interfacial atoms and more "surface" dependent material properties. Other alterations include improvements in the mechanical strength, diamagnetism, or optical properties. Scientists have developed new uses for these materials because of their ability to vividly alter their properties at the nanoscale. Overview of various fields impacted by nanomaterials. Nanomaterials have revolutionized the development of smaller and more effective devices in a number of industries, including electronics, medicine, drug delivery systems, and diagnostic equipment. Furthermore, nanomaterials have been used in energy storage, environmental cleanup, and the development of stronger and lighter materials for aerospace engineering. The distinctive qualities of nanomaterials continue to spur innovation in a variety of sectors.

1.6.1 Application in Electronics

The extensive use of electronic devices in modern society has necessitated numerous revolutionary changes in the electronics industry. Small, lightweight, portable, and less power-consuming equipment have gradually replaced bulky, expensive, and energy-intensive equipment. As a result of this evolution, electronic devices have become more affordable and space friendly. The demand for these electronics has increased along with the demand for their improvement, which has aided in the fabrication of the device's large circuits as well as its size. e.g. In computers, the power increases with the number of transistors; however, if the size of each transistor is reduced, the power increases. Therefore, computers have become more powerful as transistor size has decreased. Until recently, the most advanced commercial technology available was computer chips with transistors with 45-nanometer features, such as graphene transistors (Matsui, 2005).

1.6.2 Environmental Applications

The global degradation of water, soil, and the atmosphere caused by the release of hazardous chemicals from ongoing human activities is becoming a serious issue. This presents several ecological and health-related problems that make it more difficult to apply conventional treatment technologies. Recent advancements in nanotechnology and their critical role in meeting the urgent need to monitor and treat emerging hazardous waste affordably, efficiently, and with minimal energy use. One of the key uses of nanoparticles is the treatment of wastewater, which will help save money, time, and energy, while significantly increasing productivity and lowering environmental risks (Ibrahim et al., 2016). The

remediation of groundwater is one of the most significant uses of nanotechnology. Titanium dioxide is used for this purpose. Recently, water desalination and purification processes have been applied in nanotechnology. Solid-phase extraction is the most frequently used method for removing and separating toxic substances from water. Recently, nanoparticles, such as TiO_2 , Al_2O_3 , ZrO_2 , MnO , and CeO_2 , have been used as solid-phase extractants to separate trace elements and organic compounds. The method for purifying water was greatly enhanced by the use of nanoparticles. NPs can assist in the removal or monitoring of environmental pollutants. It can substitute environmentally friendly energy systems such as fuel cells, lithium-ion batteries, and solar cells for hazardous chemicals used in batteries (Y. Wang et al., 2015).

With the aid of a microfluidic device, nanoparticles can also be helpful for the detection of viruses in aqueous systems. Owing to their fluorescence, quantum dots are well known. In the form of fluorescent labels, it was discovered that this property can be used in the detection of microbial loads (Y. Wang et al., 2011). Researchers have experimented with nanoscale sensors and carbon nanotube-based membranes for desalinating water and identifying contaminants in water systems (Ibrahim et al., 2016; C. Peng et al., 2017; Wu et al., 2020).

1.6.3 Biomedical Applications

The search for materials with exceptional properties for use in medicine has increased owing to their ability to examine substances at the molecular level. The use of these novel materials has given rise to the new scientific field of nanobiotechnology, which is crucial for the diagnosis of diseases, development of drugs, and delivery of implants. Carbon nanotubes, liposomes, metallic and metal oxide nanoparticles, and nanopatterned flat surfaces have particular biomedical uses. These materials can be used for diagnosis, biosensing, bioimaging devices, drug delivery systems, and bone substitute implants owing to the chemical and physical characteristics of their surfaces. Numerous researchers have created nanorobots and nanodevices for specialized applications. Prior to researching nanotechnology in medicine and biology, biocompatibility was the primary area of concern. The application of nanotechnology in various therapeutic fields has completely changed the practice of medicine. Nanotechnology has been applied in biomedical research and diagnostics (Madaan et al. 2014). Nanotechnology can be used to develop drugs with higher levels of cell specificity and sensitivity as well as to diagnose a number of diseases, assist in early detection, and improve prognosis. With the aid of nanotechnological tools, therapy at the molecular level is now possible, helping to treat the illness and control its pathogenesis. The adverse effects that result from non-specific drug action and lack of efficacy as a result of improper or ineffective dose formulations severely limit the use of

many conventional drugs. Consequently, targeted therapy has made extensive use of nanotechnology. Chemically functionalized dendrimers, used as molecular building blocks for gene therapy or imaging, are highly porous, self-assembling bilayer tubule systems.

Nanoparticles may be employed as fluorescent potential biomarkers, as markers for detecting proteins, probing DNA structures, and separating and purifying biological molecules and cells. They can also be heated to kill tumors, be used in tissue engineering, and separate and purify biological molecules and cells. Due to their small size, they are not recognized by the immune system of the human body; they can cross the blood-brain barrier and pierce cell membranes smaller than a critical size. The development of nanoscale ferries that deliver high-potential pharmaceuticals precisely to their destination makes use of these characteristics. Different types of nanoparticles, including liposomes, polymer nanoparticles (Nano-spheres and Nano-capsules), solid lipid nanoparticles, nanocrystals, polymer therapeutics such as dendrimers, fullerenes (most commonly C60 or buckyball, similar in size to hormones and peptide -helices), and inorganic nanoparticles, are suitable for use in drug and gene delivery, probing DNA (e.g., gold and magnetic nanoparticles) (Sandhiya & Chandra Pradhan, 2009).

Gene therapy is used to treat a variety of inherited and acquired diseases, including cystic fibrosis, diabetes mellitus (Callejas et al., 2013), and others. Gene therapies primarily depend on drug efficacy, safe delivery, and efficient monitoring (Evans et al., 2009). However, the safety of viral vectors used for gene delivery has several drawbacks. A method of delivery is crucial for gene transfer because DNA encounters delivery issues inside the cell due to its negative charge, which interferes with the cell membrane. Accordingly, liposomes smaller than 100 nm can be a substitute for other gene delivery methods. For instance, liposomes combined with polyethylene glycol and galactose target liver cells and are useful for the treatment of a variety of liver diseases, including hereditary hemochromatosis. Chitosan nanoparticles can be used to transfect the human insulin gene. Magnetofection and theragnostic are two terms used to describe the use of nanoparticles in the delivery of viral vectors and nucleic acids (Scheller & Krebsbach, 2009).

1.6.4 Multiple other Applications

Thin films can be constructed from different nanoscale materials to make them impermeable to water, anti-reflective, self-cleaning, resistant to ultraviolet or infrared light, anti-fog, anti-microbial, scratch-resistant, or electrically conductive. Nanoparticles such as titanium dioxide, zinc oxide, and silver are added to thin films to produce these effects. Because the properties of the film can be precisely

controlled using nanoscale materials, they are extremely versatile in a variety of applications ranging from optics to electronics. Nanofilms are currently used to treat or protect surfaces on cameras, computer displays, and eyewear. To increase functionality without degrading the surface's appearance or performance, these nanoscale materials are applied in thin layers, usually less than 100 nm thick. The application of nanofilms has transformed a number of industries by offering robust and adaptable coatings that raise the general calibration and longevity of products (Findik, 2021; Matsui, 2005; Nam & Luong, 2019; Z. Wang et al., 2020).

1.7 Current Market of Nanotechnology in India

The Department of Science and Technology (DST)-led Nanoscience and Technology Mission (NSTM), which had an initial budget of \$ 12 million, helped lay the groundwork for nanotechnology in India during the 10th planning period (2002–2007). With a predicted CAGR of 19.1% over the next ten years, the nanotechnology market in India is anticipated to experience significant growth in the years to come. The demand for nanotechnology-based products in the healthcare and energy sectors is fueling this growth. To meet the country's expanding needs in several sectors, including electronics, medicine, clean food and water, and high-quality textiles, nanotechnology is intended to make use of India's diverse natural resources (Ali, 2023).

The companies and innovative start-ups below are some of those active in India's nanotechnology market.

- NoPo Nanotechnologies

Advanced nanomaterials, specifically single-walled carbon nanotubes, are produced by NoPo Nanotechnologies. The company created single-walled carbon nanotubes using a modified HiPCO method. It is asserted that these nanotubes can be used in solar cells and as thermal conductors, and are 1000 times more conductive than copper and 100 times stronger than steel (Ali, 2023).

- Amnivor Medicare

A healthcare company, Amnivor Medicare, uses nanotechnology to separate collagen from fish scales. According to the company, this resource is inexpensive and plentiful. Burns, diabetes, and chronic wounds are just a few conditions that collagen and collagen-based products can treat (Ali, 2023).

1.8 Probable Shortcomings of Nanotechnology

With the development of nanotechnology, researchers have continued to focus more on its negative effects than on its potential benefits. It is an expensive technology because it requires a significant investment for a small return. The main characteristic of nanomaterials is that their properties change as the size of the material decreases, but there is a risk involved because as the size decreases, the surface area to volume ratio increases, and with it, the reactivity of the molecule, which, if unchecked, could result in a high level of chemical reaction. As the size decreases, there is a chance that it can cross the blood–brain barrier, which could be dangerous. Because of its characteristics, it can be used to create potent weapons that have the potential to cause destruction. Retaining the size of nanoparticles after they are created in a solution is one of the issues with nanomaterials (Manam et al., n.d.).

Nanomaterials are highly reactive and can interact with the environment very easily because they are smaller, which can lead to contamination. Additionally, nanoparticle encapsulation is necessary to prevent particle aggregation. The synthesis of pure nanoparticles is extremely challenging because the stabilization of nanoparticles with other materials is a component of the synthesized nanoparticles (Hosnedlova et al., 2018; Nam & Luong, 2019). Owing to their small size and free form, nanoparticles can be released into the air, water, and soil, where they can accumulate and negatively impact plant life. As nonbiodegradable pollutants, they may present a threat to the environment. People involved in the production of these nanomaterials may be exposed to occupational health risks from nanoparticles. There are no strict guidelines for the safe disposal of nanomaterials. Their toxicity is still a subject of debate, and exposure experimental results are not yet available. Therefore, it is necessary to evaluate the uncertainty surrounding the effects of nanomaterials before developing policies for their disposal (Genwa et al., 2019).

Chapter 2:
Rational, Aim, and
Objectives

2.1 RATIONAL

Selenium an essential trace element is used in this study. It acts as an indirect antioxidant, but at a higher dosage (400 μ g/kg b.w./day), it causes toxicity (National Research Council, 2000). Selenium is available in different forms such as organic (selenomethionine and selenocysteine) and inorganic (selenite and selenate). The inorganic form has reduced bioavailability, whereas the organic form has better bioavailability, with high toxicity at higher doses. Selenomethionine at 1000 μ g/kg b.w./day shows no observed adverse effect level (NOAEL), and approximately 90% of it can also be incorporated into proteins (EFSA, 2009)(Baines et al., 2002). Methionine is an essential amino acid required by the body and can increase the bioavailability of selenium nanoparticles. Folate is known for its anti-inflammatory properties, and its tolerable upper intake level (UL) for adults is 1000 μ g/day (TAURINE: Uses, Side Effects, Interactions and Warnings-WebMD, 2009)(Butterworth & Tamura, 1989). Folate receptor beta is activated in macrophages under conditions such as rheumatoid arthritis and chronic inflammatory diseases. Selenium nanoparticles coated with low concentrations of methionine and folic acid may provide better uptake of selenium and help in the management of RA. Hence, selenium-methionine-folate nanoparticles may show better bioavailability and reduced toxicity compared to selenium nanoparticles and commercially available drugs.

2.2 AIM

Synthesis of selenium-methionine nanoparticles and to study its effects in the treatment of experimentally induced chronic inflammatory arthritis in rats

2.3 OBJECTIVES

- a) To carry out the chemical synthesis of selenium-methionine-folic acid nanoparticles (SeMetFa NPs) and characterization using various analytical techniques.
- Chemical precipitation method for synthesis of Se NPs
 - *In situ* coating of biomaterials: Methionine and Folic acid
 - Characterization of the nanoparticles carried out using UV-Vis spectrophotometer, FT-IR, Zeta potential, X-Ray Diffraction, Raman Spectroscopy, DSC, TEM
- b) To check the *in-vitro* and *in-vivo* cytotoxicity effects of Se-Met-Fa NPs synthesized using chemical methods.
- *In-vitro* cytotoxicity was examined using two techniques: MTT assay and AO/EB staining method
 - *In-vivo* toxicity was examined by tissue histopathology of spleen, kidney and liver of dissected animals from each group
- c) To check intestinal permeability and bioavailability
- Intestinal permeability and bioavailability was carried out using Permeapad plate, which has a synthetic coating mimicking intestinal membrane
 - Blood compatibility was also observed using haemolysis assay
- d) Establishment of arthritis model in rats using Freund's complete adjuvant
- Freund's complete adjuvant was injected in the paw region of each rat except the rats in normal control group
 - Inflammation was developed at day 1, and up till day 21 the study was conducted
- e) To investigate the treatment of experimentally induced Rheumatoid Arthritis (RA)

in rats using Se-Met-Fa NPs

- Paw inflammation was examined using digital vernier calliper
 - Radiography technique was carried out to check the bone tissue of paw region for detecting degradation or deformation
 - Inflammatory markers like CRP protein, TNF alpha and PGE2 was studied
 - Antioxidant enzymes CAT, SOD and GPx were studied for organs such as; spleen, kidney and liver
 - Histopathology of spleen, kidney, liver and paw region were thoroughly studied
- f) To compare Se-Met-Fa NPs with commercially available RA drugs
- Results were compared with prednisolone drug

Chapter 3:
Synthesis, Coating, and
characterization of
Selenium-methionine-
Folic acid Nanoparticles

3.1 Introduction

Selenium originates from the ore sulfide, which is amorphous, brick red in color, and powdered form, which has properties similar to those of sulfur. It is acknowledged as one of the most abundant elements present in the Earth's crust, with a rank of 67 (USEPA 2014). Selenium is a trace element, which possesses atomic number 34 and symbol Se in the periodic table. It was discovered in 1817 by Swedish chemist Jons Jacob Berzelius. It was named after the ancient Greek word 'Selene, which means Moon. It belongs to the category of non-metal or metalloid, which is located in the P block, Group 16, and Period IV of Mendeleev's Periodic table (Tinggi, 2008a). Se has six isotopes, which are also called nuclear isomers (Langsdorf et al., n.d.). Three well-defined allotropic forms of Se have been identified. These allotropic forms are crystalline monoclinic forms that are red in color and have eight rings, a red powdered form, and a black vitreous form, which has trigonal chemistry of compounds. Elemental selenium is nontoxic in nature, whereas hydrogen selenide and other relevant compounds are highly toxic. The intolerable limit for humans is 1.5 ppm concentration (*Selenium Elemental Selenium*, n.d.). Se has been identified as a non-metal element with several allotropes, such as black, irregular vitreous form, red colored form (3), and hexagonal crystal structure, which is grey in color and is also known as the most dense and stable form. The crystalline allotropes of Se, which are primarily known, are alpha-monoclinic and trigonal, of which trigonal is the most stable form at RT. There are two types of crystalline arrangements in Se: hexagonal and monoclinic forms (α and β) (C. Liu et al., 2019).



Figure 3.1: Black and red allotropic forms of selenium (*Selenium Elemental Selenium*, n.d.).

There are multiple applications of selenium; its biggest use is in the glass and steel industries, where it is used as an additive. Se is used to decolorize the glass, and for some, it is used to produce a deep red color. In architectural glass, it is used to reduce the transmission effect and give it a brown coloration. It is also used in other major industries such as paint, ceramics, and plastics to produce pigments. Owing to its multiple properties, it is known for its photovoltaic and photoconductive properties, and is used in industries that manufacture photocells, solar cells, and photocopiers. It is utilized as an important component in electric rectifiers, as it can convert AC current to DC current (*“Chemistry-It’s Elemental!” EResources for K-12 National Chemistry Week-A Periodic Table of the Elements : A Resource for Elementary, Middle School, and High School Students (E,I,HS)*, n.d.).

Selenium is known as a nutrient that is contradictory in nature; therefore, it is also known as an essential poison. A higher quantity in the diet leads to toxicity, and a minimal quantity leads to a chronic, fatal deficiency (El-Ramady et al., 2015). A study on selenium-treated *Brassica* plants showed a 43% increase in seed production, respiratory activity of leaves and flowers, and overall improvement in plant health. The obtained results were compared with those of the low-selenium controls. This study strengthens the notion of the beneficial role and scope of

selenium in agriculture (Lyons et al., 2009). Along with selenium-treated plants showing improvement in seed production, studies have shown that selenium deficiency leads to poor plant health. One such important study was conducted by Gissel-Nielsen and Gupta (1984) (Brady, 1984); selenium content in field crops was increased with the help of different means, and its bioavailability to animals was studied with respect to different livestock. It was observed that 10 g of selenium content in soil fertilizers or 3 g as foliar application would be effective, economical, and safe for plants, as well as help overcome selenium deficiency.

Se naturally exists in two different forms: organic and inorganic. Organic forms of selenium, namely, Selenocysteine and Selenomethionine, are present in humans. Inorganic forms such as selenite and selenate are available. Selenium is available as a dietary element and is present in many naturally available foods such as grains, meat, poultry, and fish. Selenium is a nutritionally essential component required by humans. It is an integral component of 25 selenoproteins that play critical roles in DNA synthesis, reproduction, thyroid hormone metabolism, protection from oxidative damage, and infection (*Selenium-HealthProfessional.Pdf*, n.d.). The Recommended Dietary Allowance (RDA) for adult men and women aged > 19 years was 55 µg/day. For pregnant and lactating women, the need is approximately 60 – 70 µg/day respectively. A detailed list of RDA for selenium is provided in Table 3.1. To maintain toxicity, The National Institute of Health Office of Dietary Supplements determines the tolerable upper intake Level (UL) level. UL is the highest quantity of a substance that can be ingested without any harm. The Selenium UL for all adults above 19 years of age is 400 µg/day (*Selenium - Health Professional Fact Sheet*, n.d.).

Selenium is mostly famous for being an important part of selenoproteins and seleno-enzymes. The most vital function of these proteins and enzymes is to break down harsh peroxides, which are known for their tissue-and DNA damage activity. Breaking down these peroxides protects organs from damage and prevents complex inflammation and other related problems (Hariharan & Dharmaraj, 2020).

Table 3.1: Recommended amounts of selenium for different age groups (*Selenium - Health Professional Fact Sheet*, n.d.).

Age	Male ($\mu\text{g}/\text{day}$)	Female ($\mu\text{g}/\text{day}$)	Pregnancy ($\mu\text{g}/\text{day}$)	Lactation ($\mu\text{g}/\text{day}$)
Birth to 6 months	15	15		
7-12 months	20	20		
1- 3 years	20	20		
4- 8 years	30	30		
9- 13 years	40	40		
14- 18 years	55	55	60	70
19- 50 years	55	55	60	70
51 + years	55	55		

Selenium in recent years have gained popularity in the field of medicine for its efficiency in managing multiple disorders. Se is an essential trace element that has been studied for its potential role in cancer prevention and treatment. Studies have suggested that individuals with higher blood levels of selenium have a lower risk of developing certain types of cancers, such as prostate, lung, and colon cancer. An interesting study on HBV-infected liver cancer suggested the use of selenium nanoparticles to improve targeted delivery of baicalin. Fang et al. (Fang et al., 2017) designed and synthesized multifunctional selenium nanoparticles with baicalin and folic acid (B-SeNP-FA) to overcome the issues of poor targeting and bioavailability of baicalin. These combinations in nanoforms could increase the stability and cellular uptake by tumor cells compared with normal cells. The primary target of B-SeNP-FA was the lysosomes in HepG2215 cells through endocytosis. This strategy of combining selenium with baicalin and folic acid has proven to be a promising nanomaterial for the treatment of HBV-infected liver cancer. One proposed mechanism underlying the cancer-preventative effects of selenium is its antioxidant properties. Selenium is a key component of selenoproteins, which act as antioxidants by neutralising harmful free radicals. These free radicals can damage cells and contribute to the development of cancer. By neutralising free

radicals, selenium may help protect cells from damage and prevent cancer growth (Maiyo & Singh, 2017). Se has also been studied for its potential role in cancer treatment. Some studies have suggested that selenium supplementation may improve the effectiveness of chemotherapy and radiotherapy. Additionally, selenium has been found to exert antitumor effects by inducing apoptosis in cancer cells and inhibiting angiogenesis. It is important to note that more research is needed to fully understand the effects of selenium on cancer, and that selenium should be taken under medical supervision. High selenium levels can cause toxicity and other health issues.

Selenium nanoparticles (NPs) have been studied for their potential use in the treatment of diabetes. These nanoparticles have antioxidant properties, which may help protect cells from damage caused by high blood sugar levels. In addition, selenium has been found to improve insulin sensitivity and glucose metabolism in animal models of diabetes. A previous study (Ahmed et al., 2017) provided evidence of the potency of elemental selenium nanoparticles for the treatment of type II diabetes mellitus. L-selenium nanoparticles in a 21 days long animal study showed an improvement in insulin levels, which in turn reduced blood glucose, reduced pancreatic inflammation, and repressed oxidative stress in the pancreas. These nanoparticles have the potential for use in anti-ageing treatments owing to their antioxidant properties. Selenium can neutralise harmful free radicals, which can cause damage to cells, leading to ageing and various diseases. Studies have shown that selenium nanoparticles can be effectively delivered to the skin where they can protect against UV-induced damage and improve skin elasticity (Bjørklund et al., 2022).

Some of the health benefits associated with selenium include (Tinggi, 2008b):

1. Supporting the immune system: Selenium plays a role in the production of white blood cells, which helps fight infections and diseases.
2. Protecting against oxidative stress: Selenium is an important component of antioxidant enzymes that protects the body against damage from harmful molecules called free radicals.
3. Improving heart health: Selenium may help lower the risk of heart disease by reducing inflammation and improving blood vessel function.

4. Preventing certain cancers: Some studies have suggested that selenium may help reduce the risk of certain types of cancer, such as prostate and lung cancer.
5. Supporting thyroid function: Selenium plays a role in the production of thyroid hormones, which help regulate metabolism.

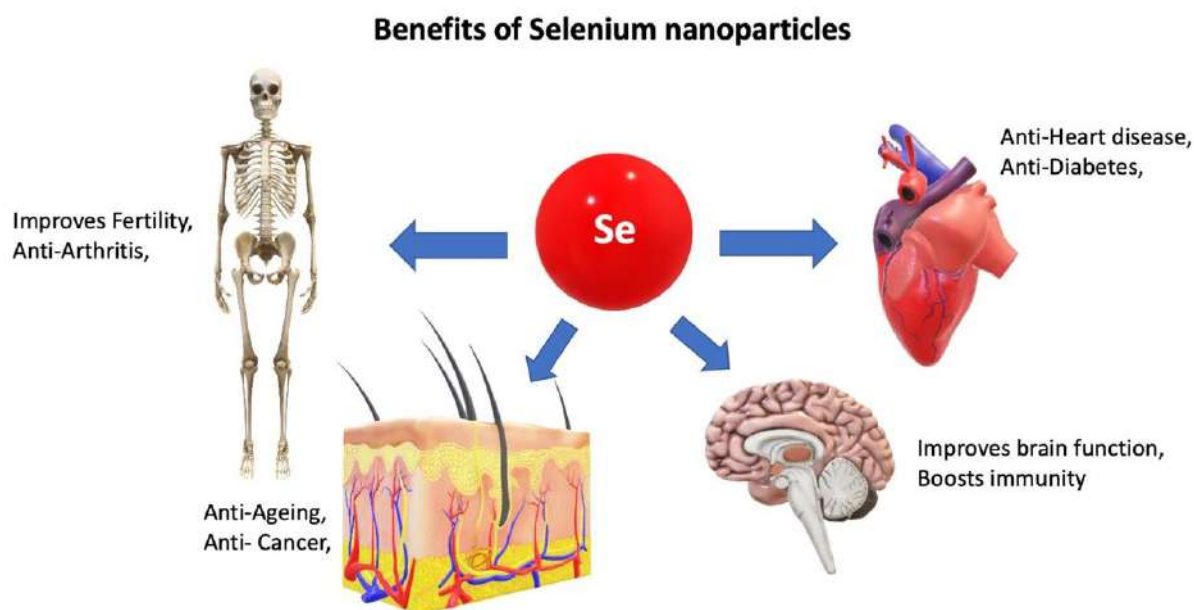


Figure 3.2: Benefits of Selenium nanoparticles

3.1.1 Nano form of Selenium

Selenium nanoparticles, also known as nano-selenium, have unique properties that make them useful in a variety of applications. This improvement in application is mainly due to changes in properties and surface area. Biomedical applications of nano-selenium have been studied for its potential use as an antioxidant, anti-inflammatory agent, and anticancer agent. It has also been investigated for its ability to improve the effectiveness of chemotherapeutic drugs. Selenium nanoparticles have potential biomedical applications in cancer therapy, imaging, and wound healing. They can act as antioxidants and have been shown to possess anticancer properties, potentially making them useful in cancer therapy (Chaudhary et al., 2014; Ferro et al., 2021; Menon, Agarwal, et al., 2019). Selenium nanoparticles can also be used as contrast agents in imaging techniques such as computed tomography and magnetic resonance imaging.

Additionally, selenium nanoparticles have been shown to have wound-healing properties and may be useful in the treatment of skin wounds.

Nano Se is an effective alternative to traditional chemical methods for removing heavy metals from contaminated water. Major health issues have arisen to humans and their surroundings owing to the release of textile dyes from industries. Menon et al. focused on the production of selenium nanoparticles using *Mucuna pruriens* seed powder and applying this in optimum concentration of $250 \mu\text{g}/\text{ml}^{-1}$ for degradation of dyes and removal of bacterial pathogenic culture from lake water. The optimum time was identified to be 60 min (Menon et al., 2021). Nanoscale selenium can help remediate soil contaminated with heavy metals and other toxic substances. Research conducted by Wang et al. at the Chinese Academy of Sciences (X. Wang et al., 2017), claims aerobic and anaerobically biosynthesized selenium nanoparticles could reduce from 57% to 48% mercury contamination from soil. The presence of nano-Se reacts with mercury contaminants and forms an insoluble mercuric selenide that can be easily removed from the surface and subsurface soils. Like mercury, cadmium is a heavy metal that is toxic to organisms, as well as an environmental pollutant. Lactic acid bacteria and selenium nanoparticles are useful tools for removing heavy metals from different environmental ecosystems. The efficiency of cadmium biosorption was approximately 50% with a 1:2 ratio of lactic acid bacteria: selenium nanoparticles (Laslo et al., 2022).

Nano selenium has been used as an alternative to traditional silicon in the production of thin-film solar cells, due to its ability to absorb a wider range of light. Selenium nanoparticles were synthesized using selenium tetrachloride as the starting reagent. The synthesized nano-Se was capped with sodium dodecyl sulfate (SDS), polyethylene glycol (PEG) 600, and CTAB. A preliminary study focused on the possibility of developing cost-effective solar cells. This solar cell comprises FTO/TiO₂/Se/Pt-FTO and FTO/Se/CdS/Pt-FTO (Panahi-Kalamuei et al., 2014). Selenium nanoparticles have been used in sunscreens to protect the skin from ultraviolet (UV) radiation. A study investigated the photoprotective potential of selenium nanoparticles and *L. rhamnosus*. This study focused on the formulation of probiotic and prebiotic mixtures. The results indicated optimized skin care formulation in Wistar rats, which exhibited an SPF of 29.77 and an IC₅₀ of 61.63 $\mu\text{g}/\text{ml}$. It was also inferred that this combination would work

topically to feature selenium and probiotic mass of lactobacilli, which can offer an effective alternative for the treatment of complications that arise from sunburn (Kaur & Rath, 2019). As concluded by these studies, nano-selenium in organic or inorganic forms can be beneficial in various fields at appropriate concentrations.

3.2 Synthesis and Coating of Selenium NPs

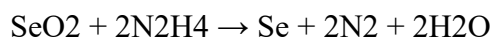
Se nanoparticles can be synthesized using a variety of methods, including chemical reduction, photochemical reduction, and electrochemical reduction. During chemical reduction, selenium ions are reduced to selenium nanoparticles in the presence of a reducing agent. For example, selenium dioxide can be reduced to selenium nanoparticles using hydrazine as the reducing agent. During photochemical reduction, selenium ions are exposed to light, leading to their reduction to selenium nanoparticles. During electrochemical reduction, selenium ions are reduced to selenium nanoparticles by passing an electric current through an electrolyte solution containing selenium ions. Other methods that can be utilized for synthesis are biological synthesis, solvothermal route, hydrothermal route, microwave-assisted synthesis, pulsed laser ablation, and green synthesis.

Regardless of the method used, the size and shape of the resulting selenium nanoparticles can be controlled by adjusting the synthesis conditions such as the concentration of the reactants, reaction temperature, and reaction time. Synthesized selenium nanoparticles have potential applications in solar cells, electronics, and biomedicine owing to their unique electronic and optical properties.

3.2.1 Chemical Reduction Method

Chemical reduction is one of the most commonly used methods for the synthesis of selenium nanoparticles. In this method, selenium ions are reduced to selenium nanoparticles by using a reducing agent in solution. The reducing agent acts as an electron donor, providing electrons to selenium ions and causing them to be reduced to selenium nanoparticles. Hydrazine is one of the most commonly used reducing agents for the synthesis of selenium nanoparticles (Shameli et al., 2010). When hydrazine was added to a solution containing selenium ions, it

acted as a reducing agent, reducing selenium ions to selenium nanoparticles. The reactions can be summarized as follows:



The size and shape of the resulting selenium nanoparticles can be controlled by adjusting the synthesis conditions such as the concentration of the reactants, reaction temperature, and reaction time. For example, increasing the concentration of hydrazine or the reaction temperature can result in smaller and more uniform selenium nanoparticles. Such reactions can involve multiple reducing agents such as potassium borohydride, thioglycolic acid, and hydrazine. Furthermore, Se nanoparticles were created and deposited as a thin film on the surface of the TiO₂ layer and FTO, and used in light-harvesting applications (Panahi-Kalamuei et al., 2015).

In addition to hydrazine, other reducing agents such as sodium borohydride, sodium citrate, and ascorbic acid have also been used to synthesize selenium nanoparticles. The choice of reducing agent depends on the desired properties of the selenium nanoparticles, as well as the desired size and shape. The chemical reduction method for the synthesis of selenium nanoparticles is a simple and cost-effective method that can produce selenium nanoparticles with a high yield and reproducibility. The synthesized selenium nanoparticles have potential applications in various fields, including solar cells, electronics, and biomedicine, owing to their unique electronic and optical properties. Ascorbic acid was used as a reducing agent to form the nanohybrid selenium nanoparticles. This combination was used to determine the synergistic antibacterial properties of lysozymes and selenium nanoparticles (Vahdati & Tohidi Moghadam, 2020a). Different concentrations of selenium nanoparticles were precipitated using glutathione (100 M) and NaOH (1 M) onto the surface of PVC and showed no cytotoxic effects on fibroblast cells (Ramos & Webster, 2012).

3.2.2 Hydrothermal Route

The hydrothermal synthesis of Se nanoparticles involves the use of a solvent under a high-pressure, high-temperature reaction in an aqueous solution (Fardsadegh & Jafarizadeh-Malmiri, 2019). In this process, selenium precursor compounds are dissolved in water and subjected to high temperatures (typically approximately 200°C) and pressures (typically approximately 10-20 atmospheres). The reaction conditions caused the precursor compounds to undergo chemical reduction and form selenium nanoparticles. (Zeng et al., 2013) In this research, they synthesized selenium nanoparticles using this method. Selenium was dissolved in ethylenediamine and incubated in a Teflon coating, which was maintained at 160 °C for 2 hours and then kept static until it attained RT to form a homogenous solution. To this, chilled acetone was added to make it amorphous SeNP, which was further transformed into a hexagonal rod-shaped structure. The size, shape, and purity of the nanoparticles can be controlled by adjusting reaction parameters such as temperature, pressure, reactant concentration, and reaction time. A research article by Farsadegh and Malmiri utilized Aloe vera extract to hydrothermally reduce Na_2SeO_3 to selenium nanoparticles. A polydispersity of 0.344 was obtained. This colloidal mixture was studied for its antibacterial activity against *Staphylococcus aureus*, *Escherichia coli*, *Staphylococcus aureus* (PTCC 1112), and *E. coli* (PPTCC 1270), and antifungal activity against *Colletotrichum coccodes* and *Penicillium digitatum* (Fardsadegh & Jafarizadeh-Malmiri, 2019). The hydrothermal synthesis route is relatively simple and cost-effective, making it a popular method for the synthesis of Se nanoparticles.

3.2.3 Microwave Assisted Synthesis

The microwave-assisted synthesis of selenium nanoparticles (Se NPs) involves the use of microwave radiation to generate heat and synthesize selenium nanoparticles in a short amount of time. This method has been shown to be a fast and efficient way of producing selenium nanoparticles and has been widely studied in recent years owing to its potential applications in various fields such as catalysis, solar cells, and biomedical imaging. In a typical microwave-assisted synthesis process, a precursor solution containing selenium ions is subjected to microwave radiation. Intense electromagnetic radiation leads to rapid generation of heat, which results in the reduction and subsequent formation of selenium nanoparticles (Y. Wang et al.,

2015). Microwave energy can also aid in controlling the size and shape of selenium nanoparticles. Several studies have investigated the effects of different parameters, such as the reaction time, precursor concentration, and microwave power, on the synthesis of selenium nanoparticles using this method. For example, a study by Mellinas et al. found that increasing the reaction time and precursor concentration led to an increase in the size of selenium nanoparticles, while increasing the microwave power resulted in a decrease in particle size. Selenium nanoparticles were successfully synthesized through a microwave heating method using *Theobroma cacao* L. bean shell extract, with potential applications in the food, medicine, and pharmaceutical sectors. Approx 0.14 g of Sodium selenite was used as the precursor to react with 50 ml of the bean shell extract. The obtained colloidal NPs were stable for up to 55 days at 4 °C (Mellinas et al., 2019).

The microwave-assisted synthesis of selenium nanoparticles is a fast and efficient method for producing selenium nanoparticles with controlled sizes and shapes. Further research is needed to optimize the synthesis process and explore the potential applications of these nanoparticles in various fields.

3.2.4 Biological Synthesis

Biological synthesis of selenium nanoparticles (Se NPs) is a green and sustainable method for producing these materials using microorganisms, such as bacteria, fungi, and yeast. This process involves the reduction of selenite or selenate ions to elemental selenium by the metabolic activities of these microorganisms.

The biological synthesis of Se NPs can be summarized as follows:

1. Selection of microorganisms: The first step is to select microorganisms that can reduce selenite or selenate ions to elemental selenium. This can be achieved by screening different microorganisms or by using known selenium-reducing microorganisms.
2. Preparation of growth medium: A suitable growth medium was prepared with the necessary nutrients and pH conditions for the growth of the selected microorganisms.
3. Incubation: The microorganisms were incubated in a growth medium containing selenite or selenate ions. During this process, the metabolic activities of microorganisms reduce selenium ions to elemental selenium, which forms Se NPs.

4. Characterization of Se NPs: The size, shape, and composition of Se NPs were characterized using various analytical techniques, such as transmission electron microscopy (TEM), energy-dispersive X-ray spectroscopy (EDS), and X-ray diffraction (XRD).

The biological synthesis of Se NPs has several advantages over conventional chemical methods, such as lower cost, reduced waste generation, and milder conditions. Additionally, the use of microorganisms in the synthesis process can result in the formation of Se NPs with different shapes, sizes, and surface charges that can be tailored for specific applications. Several studies have reported the biological synthesis of Se NPs using different microorganisms and their potential applications in the fields of medicine and biotechnology, including anticancer activity, antioxidant activity, and heavy metal removal. A study by Pouri et al. aimed to synthesize selenium nanoparticles using *Bacillus cereus*. The process included incubation at 30 °C, for 24 hours followed by purification and washing with 0.9% NaCl, Tris-HCl, SDS, and final isolation with water-octanol systems. These particles suggested no environmental contamination and increased bioavailability, which could be applicable in medicine and veterinary medicine (Pouri et al., 2017). One article suggested antiproliferative and anti-angiogenic activity against cancer cells by synthesizing selenium nanoparticles using *Pseudomonas stutzeri*. The method also involves biowaste with 6% banana peel extract enriched with tryptophan (0.25 mM) (Rajkumar et al., 2020). Selenium nanoparticles were biologically synthesized using *Aspergillus flavus* and *Candida albicans* and exhibited favorable inhibitory activity against the growth of fungal strains (Bafghi et al., 2021).

3.2.5 Green Synthesis

The green synthesis of selenium nanoparticles refers to the process of synthesizing selenium nanoparticles using environmentally friendly and non-toxic materials. This method typically involves the use of natural substances such as plants, bacteria, and fungi to reduce selenium salts to selenium nanoparticles. The process is considered "green" because it eliminates the use of harmful chemicals and reduces the production of toxic by-products. The synthesis of selenium nanoparticles using green methods, such as *Abelmoschus esculentus* extract as the capping and reducing agent, and the antimycobacterial effect was tested against

Mycobacterium tuberculosis (H37RV) and *Mycobacterium simiae* isolates (Ghaderi et al., 2022). Other synthesis methods can be performed using a variety of techniques, including biological reduction, plant-mediated synthesis, and microbial reduction. In biological reduction, selenium ions are reduced to selenium nanoparticles by bacteria or fungi, whereas in plant-mediated synthesis, plant extracts are used as the reducing agents. Microbial reduction involves the use of microorganisms to reduce selenium ions in nanoparticles.

Advantages of the green synthesis of selenium nanoparticles include the elimination of harmful chemicals, reduced cost, and improved biocompatibility. The use of environment-friendly methods can also make the synthesis process more sustainable. Biodegradation of methylene blue dye in the presence of sunlight was achieved using selenium nanoparticles, which were synthesized using *Withania somnifera* leaf extract and selenious acid solution (Alagesan & Venugopal, 2019). Green synthesis of selenium nanoparticles is a promising approach that provides a safe and sustainable alternative to traditional methods for the synthesis of selenium nanoparticles.

3.2.6 Pulsed Laser Ablation Method

Pulse laser ablation and YAG laser were used to create selenium nanoparticles with a diameter of 532 nm. The nanoparticles were deposited on three different substrates: metallic gold films, glass, and silicon wafers. Nanoparticles on the substrate surface were created using five laser pulses. The nanoparticles were characterized using the atomic motive force method. All significant nanoparticle properties were highly dependent on the experimental settings used during the ablation process. characteristics of selenium nanoparticles, including size, shape, and population (Quintana et al., n.d.).

3.2.7 Electrodeposition Method

The synthesis of Se nanowires was performed using electrodeposition. The synthesis of Se nanowires was based on an anodic alumina membrane with a 100 nm pore size (Whatman, commercially available). Analytical grade chemical reagents were used directly from the package. The electrolyte was an aqueous solution of 40 g LiH_3BO_3 and 80 g LiSeO_2 . The electrolyte had a 2.5 pH value. A constant potential (1.5 V) and room-temperature (301C)

electrodeposition procedure was performed for 30 min. Immediately following electrodeposition, the color of the sample became dark blackish orange; however, after 20 h, it changed to a dark, metallic black color. A PANalytical X'pert X-ray diffractometer outfitted with Cu-K α radiation was used to examine the crystallography of the nanowires made using a template. In 1M NaOH, a small portion of the deposition sample was dissolved which helped in the morphological studies. The absorbance of the nanowires was observed in the range–300-700 nm (S. Kumar, 2009).

3.3 Stabilization of nanoparticles

Given their propensity to aggregate or precipitate, maintaining nanoparticle stability is a fundamental requirement for further applications of these nanoparticles. Coating the particle is crucial to protect it from any reaction, because as the particle size decreases, its reactivity increases. The simplest way to stabilize the particles is to coat them with a single layer of a dense matrix such as a polymer or surfactant. As a result, there will be fewer interactions between the processes of selenium nanoparticle synthesis, coating, characterization, and stability. The nanoparticles prevented these particles from expanding further. The coating assists in functionalizing the particles with particular substances, such as drugs, functional groups, and available binding sites, in addition to protecting the particles.

Bare SeNPs have high surface energy because they quickly aggregate, and surface coating is frequently required to increase the stability of SeNPs. However, it is also anticipated that coating with NPs will affect both their ecotoxicological and physicochemical characteristics. Dextrin coated selenium nanoparticles increased the stability of Se NPs and could be used in the application of Rheumatoid arthritis in rats (Malhotra et.al). Polysaccharides have frequently been used as common coating polymers to create stable and uniformly dispersed SeNPs with low toxicity and biocompatibility. In contrast to chitosan (CS), which is made up of glucosamine and N-acetyl glucosamine, sodium carboxymethyl cellulose (CMC) is made up of D-glucose molecules with their hydroxyl groups replaced with carboxymethyl groups. The preparation of SeNPs with the popular polysaccharides CMC and CS has been investigated for the treatment of cancer, bacterial infections, and aquaculture (Wu et al., 2020; C. Zhang et al., 2015). Using Lake Geneva water and a Waris-H cell culture medium, it is thought that chitosan (CS) and sodium carboxymethyl cellulose (CMC) coated SeNPs was used to examine SeNPs and its efficiency with respect to the toxicity of the common mixotrophic flagellate *Poteroochromonas malhamensis*. The surface coating of selenium nanoparticles with CMC

showed better stability than the CS coating. Algal toxicity is also reduced with improved zeta potential and reduced aggregation (Chen et al., 2022).

The most prevalent neurodegenerative disease, Alzheimer's disease (AD), is caused by the accumulation of amyloid- (A) plaque deposits in the brain. Epigallocatechin-3-gallate (EGCG) may partially shield cells from A-mediated neurotoxicity by preventing A aggregation, according to mounting evidence. EGCG was attached to the surface of selenium nanoparticles (EGCG@Se) to better understand the process of aggregation and amyloid fibril disaggregation and to reduce the cytotoxicity of EGCG at high doses. EGCG-stabilized selenium nanoparticles coated with Tet-1 peptide (Tet-1-EGCG@Se, a synthetic selenoprotein analog) were created, taking into account the affinity of Tet-1 for the targeted cells and the low delivery efficiency of EGCG@Se to the targeted cells, as well as the involvement of selenoprotein in antioxidation and neuroprotection, which are the key factors for preventing the onset and progression of AD (Zhang et al., 2014).

3.4 Characterization of NPs

To improve the quality of the development and synthesis process, the nanoparticles were characterized. Various advanced analytical methods are used for this purpose, including UV-Visible spectrophotometry, FTIR, Zeta Potential, ICP-AES, X-Ray Diffraction, Raman spectroscopy, TEM, DSC.

3.4.1 UV-Vis spectrophotometer

The most noticeable characteristic of nanoparticles is their color change with size. Therefore, as the size changes, the color of the newly formed particles will also change, absorbing light in the visible spectrum. For example, all metal nanoparticles, including Cu, Au, Ag, and Se, absorb light in the visible spectrum. Hence, UV-Vis spectroscopy is the most fundamental and crucial method for identifying and characterizing the spectrum. It is quick, time-saving, sensitive to nanoparticles, simple to use, and requires few sample preparation steps. This technique has a number of benefits, but it also has some drawbacks, such as the need for clear solutions for analysis, tendency to use colored solutions for detection, and inability to determine the morphology of the particle (Rajeshkumar et al., 2018).

3.4.2 Fourier transform infrared

Fourier transform infrared (FTIR) spectroscopy can be used to determine changes in functional groups in biomolecules to determine variations in the overall composition of microorganisms. FTIR analyses the vibration and rotation of molecules that are affected by an infrared wavelength. This method enables the detection of structural alterations in the molecular interactions between organisms and metal atoms, which can shed light on the types of interactions they have (Faghihzadeh et al., 2016).

To prevent artifacts and variations in the spectra caused by surrounding environmental conditions and sample heterogeneity, restrictions such as multiple background scans and sample scans are required. The FTIR spectra of a sample, for instance, can be affected by measuring it in culture media at various temperatures. It may be necessary to purify the samples beforehand to avoid peak overlap in the spectra. For instance, the large absorption of water molecules at 1637 cm^{-1} can cause water from bacterial samples in liquids to overlap with the

band of amide compounds, resulting in a loss of information. By creating a dried solid sample, this can occasionally be avoided (Cadet et al., 2012).

3.4.3 Zeta Potential

In the study of nanoparticles, Zeta Potential (ZP) is a significant macroscopic parameter of great interest from both scientific and practical standpoints (NPs). According to the traditional interpretation, the ZP is connected to the electrostatic potential that forms at an ill-defined boundary between an NP and the surrounding fluid, including an immobile layer containing strongly adsorbed species that move along with the NP (usually an aqueous solution). The counterions in the solution balance the surface charge created when a solid surface is exposed to an aqueous solution or another liquid (Biriukov et al., 2020). The importance of the potential is related to the stability of the colloidal dispersion, which also represents the strength of attraction between nearby particles with similar charges. The colloidal dispersion was more stable at high potentials. In the study mentioned, it was discovered that SeNPs had a potential of -16.2 mV while Chitosan-SeNPs had a value of +29.1 mV, indicating that SeNPs' highly positive-charged NH_3^+ groups were exposed on the outside surface (Yu et al., 2012).

It is important to note that zeta potential is a crucial sign of how stable colloidal suspensions are. Untreated SeNPs had a zeta potential of approximately 30.2 mV, which increased to approximately 3.3 mV by the adsorption of positively charged lysozyme molecules onto the SeNP matrix. This suggests that the formation of protein-loaded nanoparticles is significantly influenced by electrostatic interactions. The fact that the protein-loaded nanoparticles had a negative charge demonstrates that the system as a whole was stable. With an increase in the concentration of biomolecules, the nanoparticle absorption intensity at their characteristic wavelength (265 nm) decreased. However, the characteristic band retained its typical shape, demonstrating that the nanoparticles did not aggregate upon contact with the positively charged biomolecules. The appearance of the samples further supports this claim (Vahdati and Tohidi Moghadam, 2020).

3.4.4 ICP-AES

In ICP-AES, the optical spectrometer is used to observe the photons produced by electronically excited or ionised atoms. The 'atom' and 'ion' lines are used, respectively, for qualitative and quantitative measurements. In addition to the relatively high continuum emission produced by the Ar + - e- recombination processes, spectral lines are observed. Within the resolution (0.005-0.03 nm), spectral overlaps are frequent, and several elements, including Ni, Fe, and W, produce complex, line-rich spectra. Rowland Circle "simultaneous" polychromators with fixed wavelength detector channels, versatile but slow Czerny-Turner monochromator-based instruments that measure one line at a time, and two-dimensional imaging spectrometers that simultaneously measure entire spectra or selected spectral windows using a planar charge-coupled device detector are three types of optical spectrometers that have been widely used in commercial instruments (Ketterer, n.d.). The high continuum emission background is the main drawback of ICP-AES; it limits the detection limits to low microgram-per-litre values for the majority of elements, although some elements produce sub-microgram-per-liter detection limits. Because of the high continuum background in ICP-AES, background correction measurements must be taken immediately next to each spectral line, because the background level can be elevated or suppressed by the matrix. However, ICP-AES can be viewed as a much more "robust" technique than ICPMS in the absence of interfering spectral lines because matrix effects are generally tolerable, and simple external calibration (without internal standards) is acceptable. Even though ICP-AES has a fairly wide range of elements, including nonmetals, its detection limits are inadequate for specific elements such as Th or U. Generally, ICP-AES systems are simpler (Jarvis & Jarvis, 1992).

The Se concentrations in HeLa cells after 24-h exposure were determined using ICP-AES method in order to investigate the cellular uptake of Se-NPs. Compared to the group of Se-NPs without sialic acid (SA) decoration (0.58 µg/10⁷ cells), treatments with sialic acid-Se-NPs significantly increased the Se concentrations from 0.045 (control) to 2.54 µg/10⁷ cells, which was 338% higher. These findings demonstrate the usefulness of SAs for the uptake of Se NPs by cancer cells (Zheng et al., 2011). ICP-AES analysis was used to look at the cellular uptake of chitosan (CS) -SeNPs in HK-2 cells and A375 cells after treatment for 24 hours. Se concentrations in A375 cells treated with 10 and 20 µM chitosan-SeNPs increased noticeably from 0.0046 (control) to 0.69 and 2.95 µg/10⁷ cells, respectively. There was a significant increase in the concentration of SeNPs without CS decoration (0.16 µg/10⁷ cells).

Unexpectedly, it was discovered that treatments with 10 and 20 μM CS-SeNPs only raised the Se concentrations in HK-2 cells from 0.0040 (control) to 0.39 and 0.46 $\mu\text{g}/10^7$ cells, which was much less than what was observed in A375 cancer cells. Together, these findings imply that the enhanced cellular uptake of CS-SeNPs compared to SeNPs in cancer cells is caused by their smaller size and positive surface charge (Yu et al., 2012).

3.4.5 X-Ray diffraction

XRD is frequently used in the field of nanotechnology to characterize and gather precise data on the composition, crystal structure, and crystalline grain size of nanoparticles, the versatile technique of X-ray diffraction (XRD) is frequently used in the field of nanotechnology (Fultz & Howe, 2013). The scattering of X-rays caused by the rotation of electrons in the atom's nucleus when the rays hit the nanoparticles is the basis for the operation of the XRD method. Interference patterns result from scattered X-rays that are reflected in different ways. Only scattered X-rays that interact constructively with other scattered X-rays cause diffraction regardless of whether these patterns are destructive or constructive. When two waves move in phase with one another, constructive interference occurs in the nanoparticle; when they move out of phase, destructive interference occurs. Atoms with shorter periodic arrangements exhibit greater diffraction angles and vice versa. The atomic-scale arrangement and diffraction are strongly and inversely correlated (Fultz & Howe, 2013).

XRD was used to determine the crystal structure of selenium nanoparticles. Typical XRD patterns of the synthetic sample after heating at 130°C for six hours and those of selenium that are readily available in the market. Without heat treatment, the XRD pattern of the synthesized selenium nanoparticles was much noisier, with broader peaks, indicating the amorphous nature of the particles. The selenium sol presented further evidence that amorphous selenium is red in color. The lattice constants for all the diffraction pattern peaks, $a = 4.362 \text{ \AA}$ and $c = 4.958 \text{ \AA}$, are in excellent agreement with the reported values (JCPDS file no. 06-362) (M. Kumar et al., 2011).

3.4.6 Raman Spectroscopy

Raman spectroscopy is a method that is becoming more and more common in a variety of fields, including biology and medicine. It is based on a phenomenon called Raman scattering, in which incident photons interact with vibrating molecules in a sample to gain or lose energy. The molecular makeup of the sample can be determined using these energy shifts with a high degree of accuracy. Raman spectroscopy has been used in life sciences to characterize nanoparticles and to quantify biomolecules in cells and tissues using hyperspectral molecular imaging (Shipp et al., 2017).

Raman spectroscopy is known to be sensitive to variations in selenium's crystallinity and various allotropic modifications, making it useful for studying Se nanomaterials. The Raman spectrum of Se NPs made by the bacterium *Azospirillum thiophilum* (strain VKM B-2513) revealed a single, very strong band with a maximum at 250 cm⁻¹, which corresponds to the A₁ stretching Se-Se mode and, in accordance with its increased half-width (ca. 30 cm⁻¹), can be attributed to amorphous Se. For comparison, it should be noted that the Raman spectra for the Se NPs created by *A. brasilense* Sp7 were similar (Tugarova et al., 2018).

3.4.7 Transmission electron microscopy

Most histograms produced by transmission electron microscopy have been used by researchers (. K. Liu, 2009) to characterise the size distributions of solution-grown NPs (TEM). Although TEM-based analyses are extremely accurate and reliable, they have the drawbacks of being performed ex situ (i.e., monitoring NPs during a reaction is challenging), requiring expensive equipment, and additional sample preparation steps. In addition, it may be challenging to determine the ensemble-averaged region. Properties such as the average diameter or shape because a typical TEM analysis only looks at a small portion of the sample. A non-representative sample of NPs may be obtained because of size segregation effects that may occur during the drying process and human subjectivity when choosing which areas of the grid to image and photograph.

3.4.8 Differential scanning calorimeter

The only way to determine the enthalpy directly associated with the process of interest is through calorimetry, which is the primary technique for measuring the thermal properties of materials. This technique establishes a relationship between the temperature and physical properties of substances. Differential scanning calorimetry (DSC) is one of the many varieties of calorimeters. A thermal analysis tool, called DSC, measures how a sample's physical characteristics change over time along with its temperature. The apparatus is a tool for thermal analysis that calculates the temperature and heat flow related to material transitions as a function of temperature and time. DSC measures the heat quantity that is excessively radiated or absorbed by the sample during a temperature change based on the temperature difference between the sample and the reference material (Gill et al., 2010).

The DSC thermograms of the synthesized selenium nanoparticles and a standard commercial selenium sample had their DSC thermograms taken between 50 and 250 C. The DSC thermogram reveals an exothermic transition at 90°C and an endothermic melting peak at 217°C. The transition's enthalpy was discovered to be 45.2 J/g. The repeated DSC thermogram of the same selenium sample, which was taken after it reached room temperature, failed to capture an exothermic peak at the specified temperature. As a result, the transition could be attributed to an increase in the crystallinity of selenium nanoparticles. This clearly shows that the selenium particles lost their nanocrystalline nature in the first thermal run (M. Kumar et al., 2011).

3.5 Materials

Folic acid was acquired from Sigma-Aldrich (product number: F8758). The following items were purchased from Molychem: analytical grade sodium selenite (product code 18770), L-methionine (product code 15900), analytical grade ascorbic acid (product code 12480), and HPLC (de-ionized water). All plastics were of cell culture grade.

3.6 Methods and Experimental details

3.6.1 Synthesis and coating of selenium nanoparticles

Se-Met-Fa NPs were synthesized by reducing 100 mM sodium selenite in a 1:4 ratio using 100 mM ascorbic acid as the reducing agent. After addition of ascorbic acid, the pH of the mixture was 2.5. The biomaterial coating of Se NPs was accomplished *in situ*, with methionine (Met) used at a 1:5 ratio to the precursor volume. The pH ranged from 5. to 5.5. The second coating material, 1 mM folic acid (Fa), was introduced and had a 1:10 ratio to the precursor. Before addition, Fa was activated (activation was performed using 1 N NaOH, pH 9, for 2 h). The entire reaction was maintained overnight at room temperature using a magnetic stirrer at 1200 rpm.

3.6.2 Characterization of SeNP and Se-Met-Fa NPs

To create a colloidal mixture for UV-visible spectroscopy, 100 µg/ml of Se-Met-Fa NPs were dissolved in 10 ml of D/W and sonicated for 5 min. The UV to visible spectrum of the colloidal mixture was measured using three millilitres of the mixture (200–700 nm). Infrared (FTIR) spectroscopy was performed between 4000 and 400 cm⁻¹ wavenumbers. We examined KBr pellets and 1 mg Se-Met-FaNPs. The actual selenium content of each nanomaterial was ascertained using atomic emission spectroscopy. The nanostructures were liquefied in 1:2 ratios of hydrochloric acid and nitric acid as part of the sample preparation for ICP-AES. ICP-AES was used to analyse the mixture after it was incubated at room temperature. A 1:10 dilution of the Zetapotential samples in distilled water. Nanoparticle samples were developed in a pH range of 2–12, sonicated twice for five minutes each, and then examined using the zeta potential method. Raman spectra were captured using Renishaw microscope software using an argon lamp with a range of 200–300 cm⁻¹. The samples used for X-ray diffraction and Raman spectroscopy were powdered. The NPs sample was diluted using D/W at a ratio of 1:10 in preparation for the TEM. This was subjected to two 15-minute sonication cycles, dried on a copper grid for an hour, and subjected to TEM analysis. Differential scanning calorimetry (DSC; DSC 1 Stare Mettler Toledo, OH, USA) was used to analyse the thermal properties of uncoated Se and SeMetFa nanoparticles. Each sample was weighed in the range of 2–4 mg in an aluminum crucible. The pans were then set up one by one with a reference pan for each analysis (empty aluminum pan). The temperature range used for heating the samples was 30–

400 °C. An inert nitrogen stream was continuously maintained at a flow rate of 40 ml/min, and the samples were analyzed at a rate of 10 °C/min.

3.7 Results

3.7.1 Synthesis of SeNP and Se-Met-Fa NPs

The transition of the color of Figure 3.3 A from transparent to pale orange to brick red enables us to visually observe the formation of Se nanoparticles. Sodium selenite was reduced to selenium nanoparticles in ratios of 1:1 (a), 1:2 (b), and 1:4. (c) (Figure 3.3).

3.7.2 Characterization techniques

The absorbance was measured across a broad spectrum (figure 3.3 B). The spectrum of the Se nanoparticles had a noticeable peak at 266 nm. Se-Met nanoparticles showed methionine with a redshift (bathochromic shift) peak at 267 nm and another peak at 230–190 nm. The methionine control had a similar peak, ranging from 240 to 190 nm. It can be said that Se NPs are coated with methionine because a shift can be seen in both the spectra of Se (redshift) and methionine control (blueshift). The most significant peak for selenium in the Se-Met-Fa NPs spectrum, at 266 nm, demonstrated a hypsochromic shift (blueshift); other peaks at 286 and 369 nm coincided with peaks from folic acid control at 280 and 352 nm, indicating a hypsochromic shift. This peak, which is approximately 200 nm in wavelength, can be used to detect the presence of methionine.

The Se-Met-Fa NPs and FTIR images of the other biomaterials are shown in Figure 3.3 C. The identified peaks were attributed to OH stretching at 1316, 940, and 3366 cm^{-1} OH stretching. The folic acid amide peak at 1698 cm^{-1} , the 1606 cm^{-1} C=C alkene group, 2938 cm^{-1} C - H stretching, and 3415 cm^{-1} NH stretching were compared to the significant peaks observed for the Se-Met-Fa NPs. The observed shifts can affirm weak hydrogen bond formation.

The percentage of pure metal in all compounds was determined using ICP-AES. SeMet-Fa NPs contain 55% pure Se, compared to 99.6% in Se nanoparticles. This can be inferred from the fact that the remaining 45% may be the organic material used as the coating material (Figure 3.3 E and Table 3.2). All three types of nanoparticles, Se, Se-Met, and Se-Met-Fa NPs, have zeta potential plots in the pH range of 2 to 12. Figure 3.3 F shows a similar trend for the zeta plot.

The XRD pattern is shown in Figure 3.3 G. Peaks that have been observed with 2θ values are 23.5, 29.8, 41.5, 43.5, 45.71, 48.2, 51.8, 55.8, 62, and 65.2. These numbers represent the diffraction from the (100), (101), (110), (102), (111), (200), (201), (003), (103), and (210)

planes, respectively. All the two-peak structures are consistent with the information on JCPDS card number 06-03620 and also correspond to Se's trigonal structure, which has lattice constants of 4.35 and 4.93. Scherrer's equation, which takes D as the grain size, K as a constant value of 0.94, as the X-ray radiation wavelength, as the full width at half maximum, and as the angle of diffraction, was used to determine the crystalline size of Se-Met-Fa NPs. The calculated average crystallite size was 32 nm.

Raman spectroscopy was used to confirm the nanoparticles' allotropic form and purity (Figure 3.3 H). A single trigonal Se peak was observed at 235 Raman shifts/cm⁻¹. Because of the absence of other peaks, such as those belonging to monoclinic Se and alpha-Se, respectively, at 256 and 264 Raman shifts per cm⁻¹ region, respectively. This indicates that Se exists only in its trigonal form.

The Se NPs are depicted in a TEM image, with a spherical morphology with an average size of 50 nm (Figure 3.4 A). Figure 3.4 C shows that they have a cloud-like appearance while maintaining the spherical morphology of the Se NPs. The methionine and folic acid coatings are represented by clouds. Se-Met-Fa NPs typically range in size from 50 nm to 52 nm. Image 3.4 C. The diffraction patterns of the Se-Met-Fa NPs in Figures 3.4 B and D demonstrate their crystallinities.

The thermal characteristics of the Se and Se-Met-Fa NPs were investigated using DSC. Both Se NPs and Se-Met-Fa NPs showed a sharp endothermic peak at 217 °C and a small peak at 55 °C in their DSC thermograms (figure 3.3 I). At 103 °C, the Se NPs underwent an exothermic transition, whereas the SeMetFa NPs did so at 93 °C.

3.8 Discussion

Every step is crucial in the bio-nano interaction process, including nanostructured material constituents, synthesis, coating materials, and microscopic and spectroscopic characterization methods (Faria et al., 2018). Nanoparticles with the potential to develop into therapeutic agents are produced by the interaction of bio-nanotechnology with the stability and therapeutic properties of nanostructures. Selenium nanoparticles have been created and coated with a variety of materials including dextrin, chitosan, polyethylene glycol, baicalin, and folic acid (Malhotra et al., 2016; Plano et al., 2010; Rocourt & Cheng, 2013; Saptarshi et al., 2013). With a few drawbacks such as cytotoxicity and bioavailability, selenium in nano form has many benefits, including its potential as an antioxidant, anticancer, and antimicrobial agent (Malhotra et al., 2014; Menon, Shrudhi, et al., 2019).

Se-Met-Fa nanoparticles were synthesized by the simple three-step chemical precipitation reaction used to create Se NPs, using ascorbic acid as a reducing agent and sodium selenite as a precursor. The primary sign that the reaction had completed and that Se NPs had been formed was the color change of the mixture from colorless to brick-red (Figure 3.3 A). This method has been modified and used with modifications of alteration in pH which increased its efficiency of accepting the bio coating materials (Malhotra et al., 2014). FTIR and UV-Vis spectroscopy along with their zeta potential were investigated, as shown in Figures 3.3 B, C, and F, to ensure that methionine and folic acid interacted with Se NPs. Figure 3.3 B shows the three main peaks in the UV-visible spectrum of Se-Met-Fa NPs, which correspond to SeNPs at 250 nm, methionine at 190 nm, and folic acid at 286 and 369 nm. The presence of selenium peak shifts implies a decrease in wavelength, which also indicates a decrease in nanoparticle size (Stobiecka & Hepel, 2011). In a study by S. Muthu, who synthesized selenium nanoparticles using selenium dioxide as the precursor, egg white lysozyme as a stabilizing agent, and ascorbic acid as a reducing agent, UV absorbance of 250 nm, spherical shape, and size of 40–60 nm were observed. Although the reaction precursor was different from the precursor used in the current study, the results of the study's measurements of nanoparticle size, shape, and absorbance were consistent (Figure 3.3 A, Band, and Figure 3.4 A)(Muthu et al., 2019).

The bond formation between the Se NPs and dextrin polymer was investigated using FTIR characterization of dextrin-coated Se NPs (Malhotra et al., 2014). The results showed that selenium was not absorbed as a single element in the infrared region. Its presence is indicated by the peaks of the OH bonds. Therefore, no obvious peak of selenium in the infrared region

has been reported in the literature (Battin et al., 2006; Kolb et al., 1986). In the present study, FTIR was used to investigate the peak intensity, vibrations, and shifting caused by interactions between methionine and folic acid in the infrared region. A strong hydrogen bond, represented by the 3415 cm⁻¹ NH stretching in Figure 3.3 C, did not change significantly in intensity, but there were shifts that could confirm the formation of weak hydrogen bonds. The intensity of the amide peak at 1686 cm⁻¹ region has significantly decreased, indicating the formation of an amide linkage. The FTIR spectra of baicalin and folic acid-coated selenium nanoparticles were depicted in a similar manner. The peaks at 1640 cm⁻¹ and 3368 cm⁻¹ were found to be similar (Fang et al., 2017). Positive and negative charges exist because the coating materials have NH and amide bonds, respectively. Amide bond 1686 cm⁻¹ grows in comparison to Se-met 1588 cm⁻¹ as Se-Met-Fa NPs concentration rises, indicating a rise in the negative charge of SeMet-FaNPs. Similarly, NPs' negative charge of NPs was observed in the zeta potential. All three sets of NPs showed a similar trend in the plots, demonstrating the unfavorable nature of the nanoparticles even after dual coating (Figure 3.3 F). The same pattern then appeared, showing a positive charge at pH 2, before moving towards a negative charge at pH 4. The trend of a positive to negative shift in zeta potential is justified by the correlation between the charge of nanoparticles determined by zeta potential and the functional groups from the FTIR results.

Recognizing the functional groups of both coating agents. Se nanoparticles are negatively charged, so when methionine bonds with Se at the amino end and later forms a bond with the amino end of folic acid, the surface of the SeMet-Fa NPs displays the negative side of folic acid. Se-Met-Fa NPs have a charge of 60 mV at alkaline pH, making them stable. Controlled selenium nanoparticles stabilized with chitosan (Zhang et al., 2015) exhibit a high stability of selenium nanoparticle charge between +100 and 100 mV.

This can be justified in light of the current study, which suggests that coating agents stabilize the charge of the Se NPs. The selenium rod structure and selenium nanoparticle X-ray diffraction values from various planes were observed (C. Zhang et al., 2015; J. Zhang et al., 2008), and they are comparable to the planar values found in Figure 1G. The trigonal peak seen in Figure 3.3 H is also supported by our previous research (Malhotra et al., 2014), which points to a peak resembling that of dextran-coated selenium nanoparticles.

Selenium nanoparticles (NPs) created with GSH and BSA protein in an earlier study by (J. S. Zhang et al., 2001) displayed an aggregation pattern as a result of their cumulative negative charge, which was demonstrated by zetapotential and TEM techniques. Figure 3.4 C, a TEM

image of Se-Met-Fa NPs, also demonstrates the aggregation pattern brought on by their negative charge as well as the blue peak shift in UV absorbance. Se-MetFa NPs are 200 nm in size, whereas selenium nanoparticles coated with folic acid and baicalin compound (Fang et al., 2017) have a comparatively larger size.

The thermal behavior of the dual-coated Se NPs compared with that of the uncoated Se NPs was characterized using DSC analysis (Figure 3.3 I). Exothermic transitions and endothermic melting peaks were visible in the DSC thermograms of the Se and SeMetFa NPs at 103 °C and 93 °C, respectively. The melting peak for the selenium powder sample was obtained at 217° C when these results were compared with it, confirming the presence of selenium (M. Kumar et al., 2011). Exothermic transitions may have changed, which may be related to the crystal structure and/or broken molecular chains (Jana, 2019). Thus, the crystalline structure of SeMetFa NPs was maintained, which is supported by the XRD results (Shinde, 2022). These findings could also be the cause of the more robust intermolecular bonds and enhanced crystal structure, which, when compared to the Se NPs, also results in improved thermal stability.

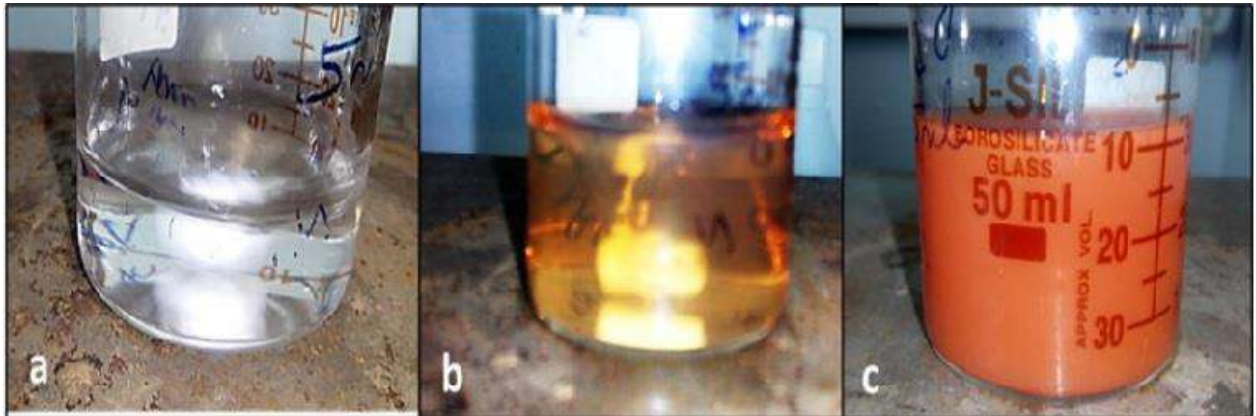


Figure 3.3 (A): Complete selenite sodium reduction to selenium nanoparticles (Brick red)

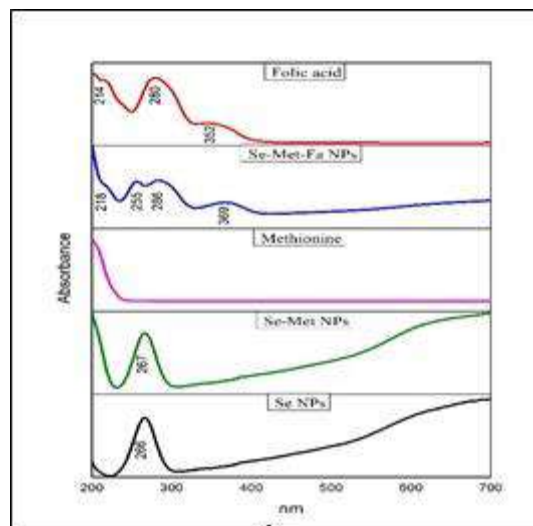


Figure 3.3 (B): UV spectrum: Se nanoparticles, Se-Met nanoparticles, methionine control, Se-Met-Fa nanoparticles, and folic acid control

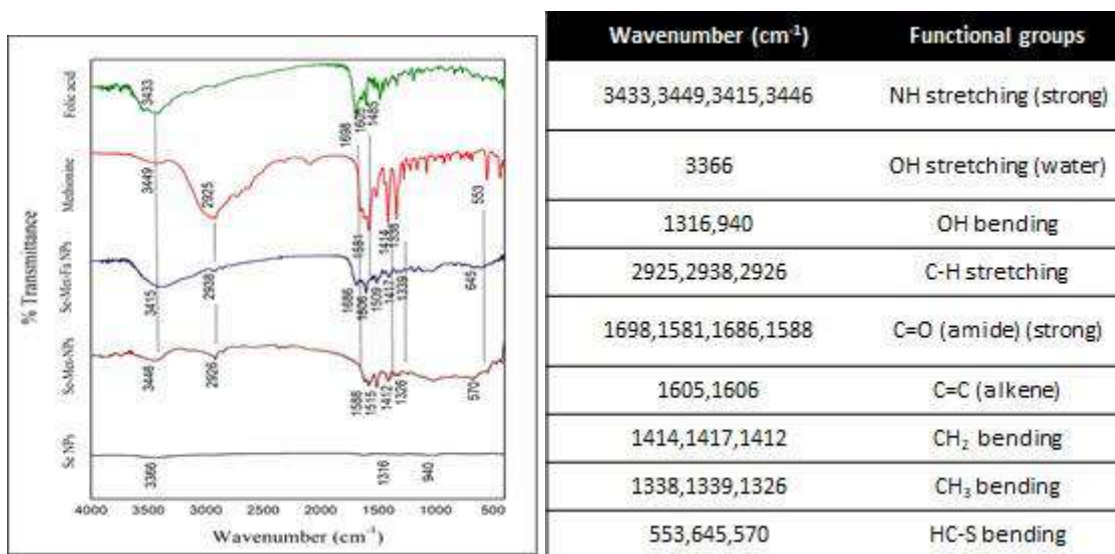


Figure 3.3 (C): FTIR spectra of Se nanoparticles, Se-Met nanoparticles, Se-Met-Fa nanoparticles, methionine control, and folic acid control. (D) Functional group chart.

Table 3.2: Determination of pure selenium by ICP-AES.

Samples	Selenium in 50ppm sample	% Selenium present
Selenium standard	50	100
Se NPs	49.8	99.6
Se Met NPs	42.1	84.2
Se Met Fa NPs	27.5	55

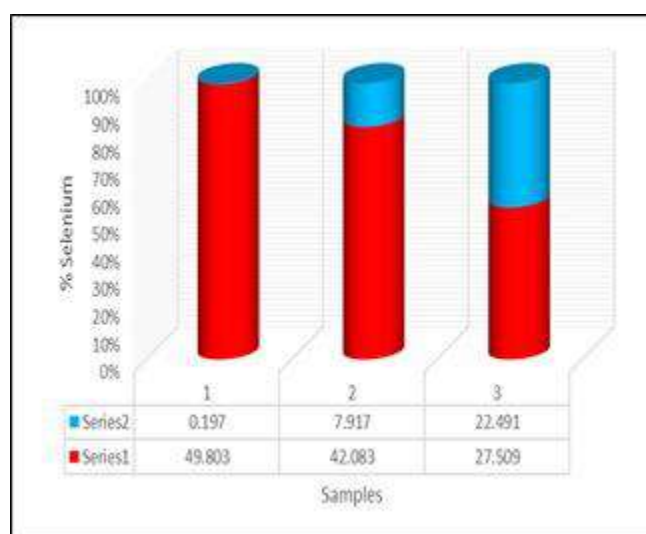


Figure 3.3 (E) Shows the values of pure selenium.

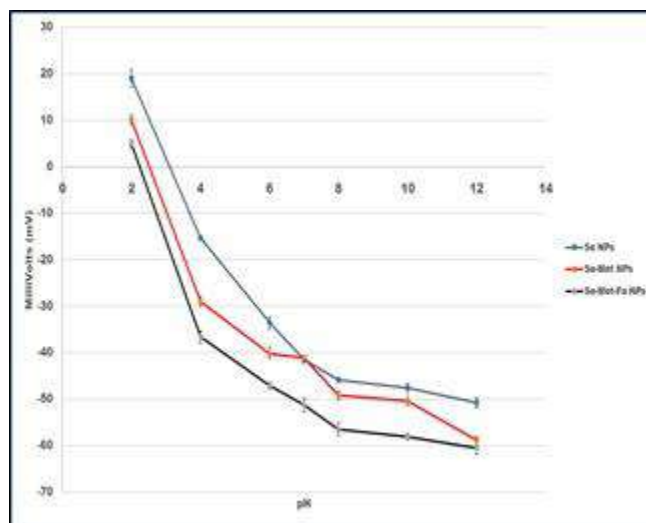


Figure 3.3 (F): Zeta potential plot of Se, Se-Met, and Se-Met-Fa nanoparticles, where n = 3.

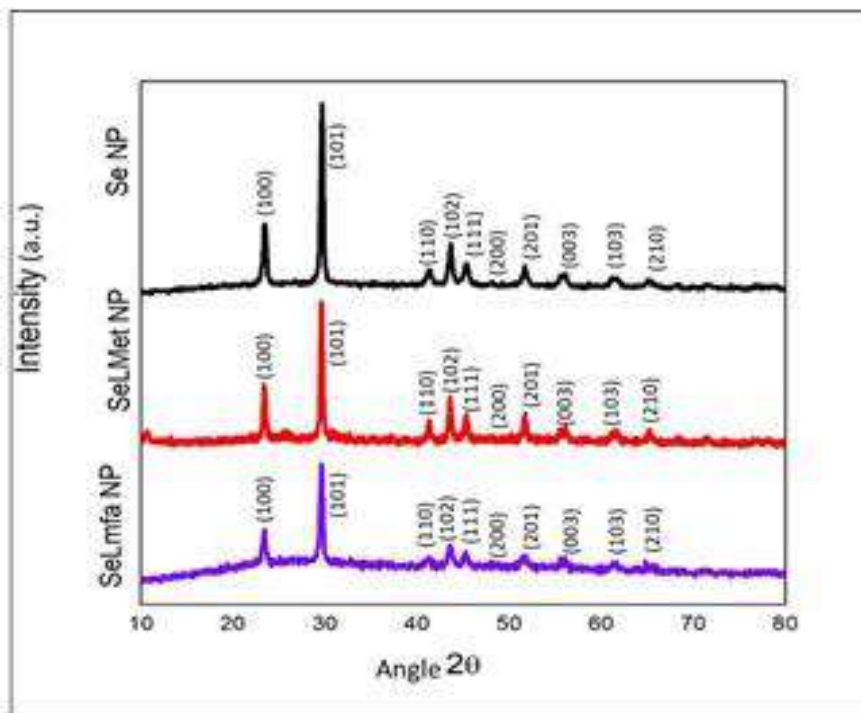


Figure 3.3 (G): X-ray diffraction patterns of Se, Se-Met, and Se-Met-Fa NPs.

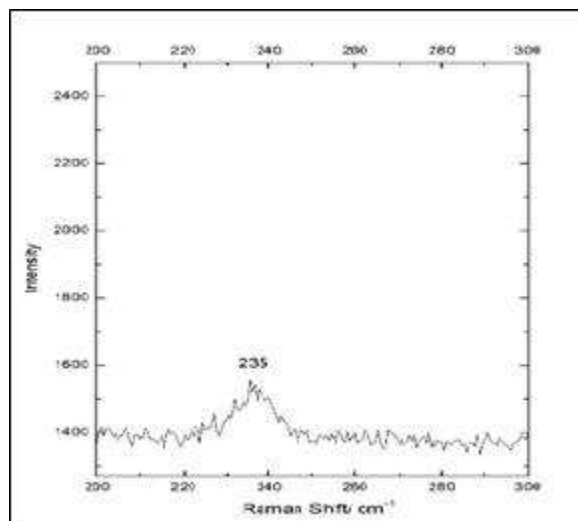


Figure 3.3 (H): Raman spectra of trigonal Se

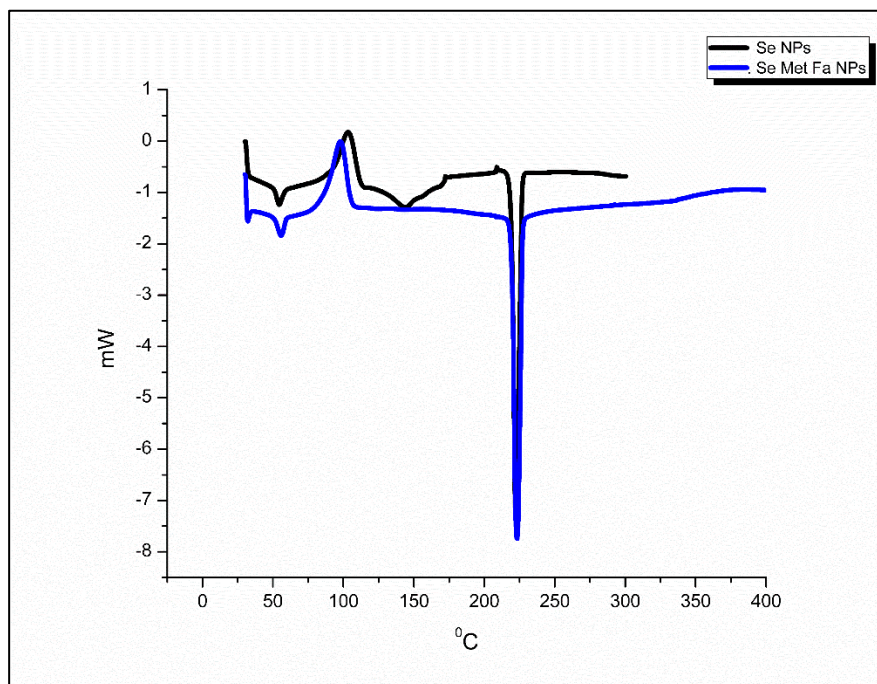


Figure 3.3 (I): Differential Scanning calorimetry thermograms of 1) Se NPs and 2) Se-Met-Fa NPs.

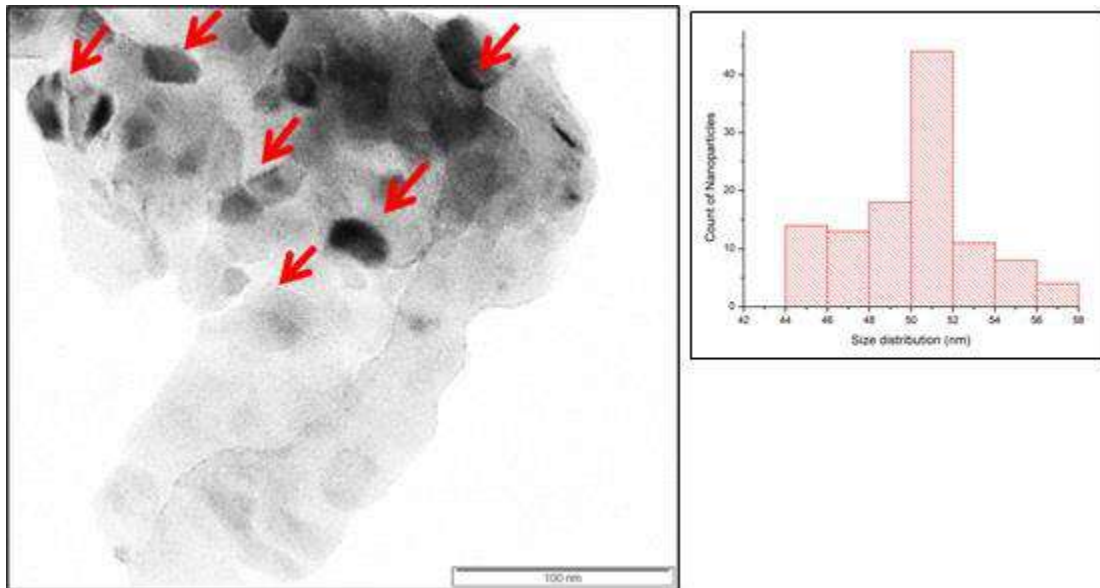


Figure 3.4 (A) Shows the TEM image of the Se NPs; the scale bar is 100 nm.

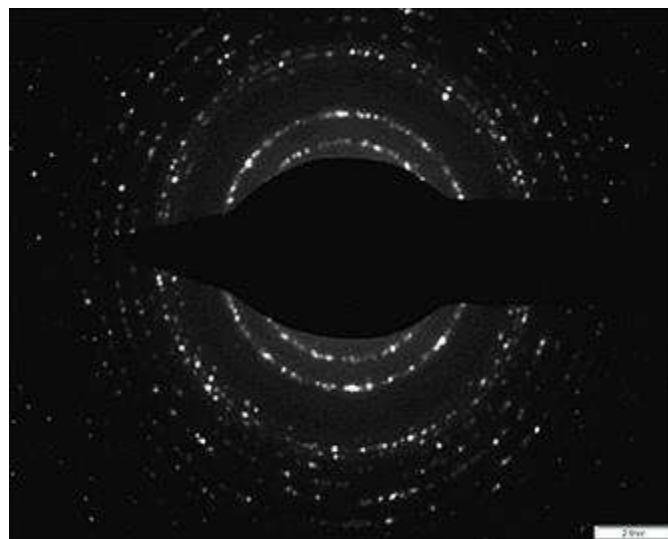


Figure 3.4 (B) Diffraction pattern of Se NPs as measured by TEM.

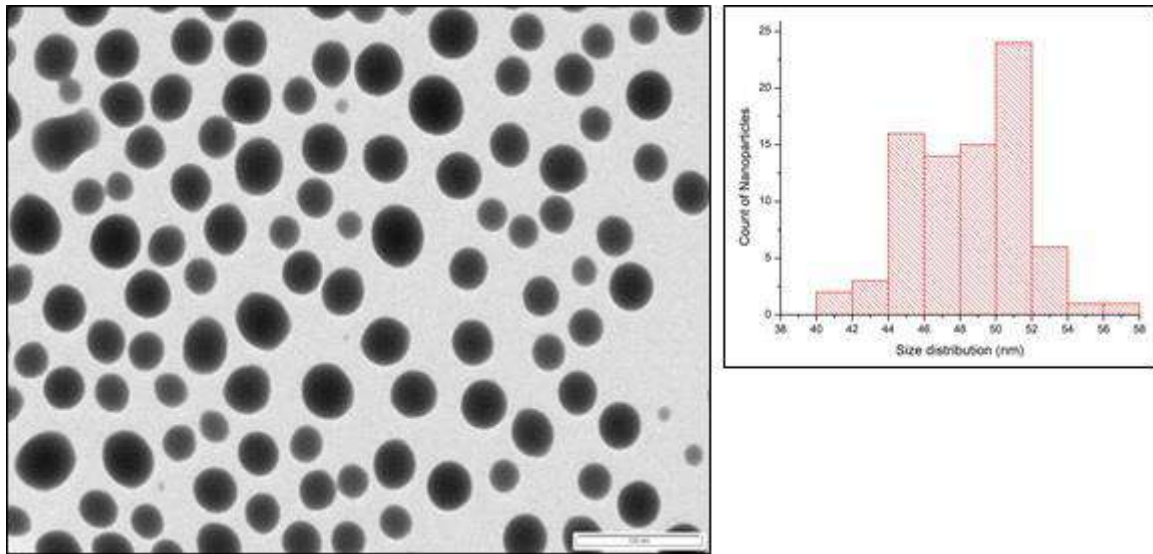


Figure 3.4 (C) Se-Met-Fa NPs TEM image (scale bar = 100 nm).

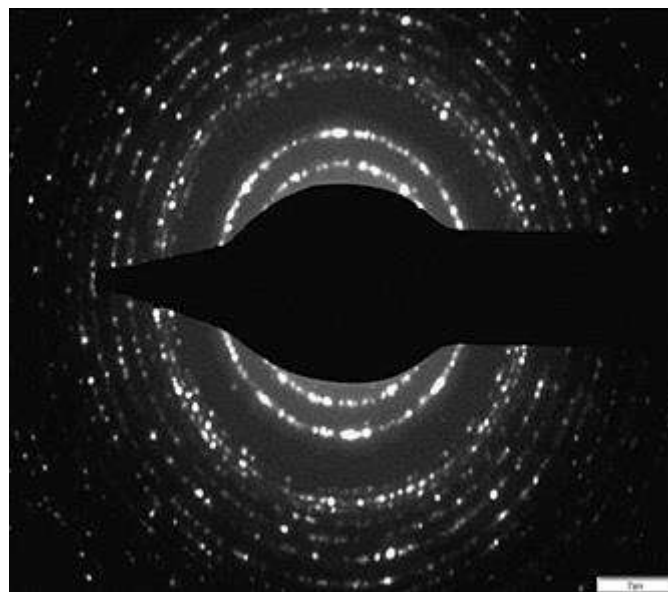


Figure 3.4 (D) TEM-measured diffraction pattern of Se-Met-Fa nanoparticles.

3.9 Conclusion

A straightforward but effective three-step chemical precipitation method was used to successfully synthesize Se-Met-Fa NPs and dual-coat them. Numerous microscopic and spectroscopic characterizations confirm the effectiveness of this method. The spherical morphology of the nanoparticles, which were maintained under 100 nm in size, and their ability to do so were confirmed by TEM analysis. DSC thermal analysis by DSC enunciated the stability of the dual-coated NPs. These nanoparticles have been further utilized in various macromolecular and toxicity studies.

Chapter 4:
In Vitro cyto-toxicity and
Macromolecular
Interaction studies

4.1 Introduction

Nanotoxicology research is currently gaining attention because human exposure to nanoparticles is unavoidable as nanoparticles become more widely used. Although the types and uses of nanoparticles are expanding, comparatively few studies have characterized their post-exposure effects and addressed their potential toxicity. Nanoparticles are used as diagnostic and therapeutic tools to better understand, detect, and treat human diseases, particularly in the medical field. Prior to clinical use, it is essential to comprehend the characteristics of nanoparticles and how they interact with the body because exposure to nanoparticles for medical purposes involves intentional contact or administration (Lewinski et al., 2008).

Bioconjugates, such as DNA, proteins, and monoclonal antibodies, are frequently purposefully coated on nanoparticles for imaging and drug delivery to target particular cells. It is critical to ensure that these enhancements do not have any negative effects, because these nanoparticles are designed specifically to interact with cells. What matters more is how biodegradable nanoparticles interact with cells and what reactions they cause, whether they are coated or uncoated, in the cellular environment. For instance, biodegraded nanoparticles may build up inside cells and cause intracellular changes such as gene alterations or disruption of organelle integrity (Maynard, 2007; Ramos & Webster, 2012).

Additionally, it is important to consider the potential long-term effects of nanoparticle exposure on human health and the environment. Studies have shown that certain nanoparticles can accumulate in the body and cause damage to organs, such as the liver, lungs, and brain. Furthermore, these particles can enter the food chain and affect ecosystems. To mitigate these risks, researchers are exploring various strategies for reducing nanoparticle toxicity, such as using biocompatible coatings or designing particles with specific shapes and sizes that minimize their harmful effects. Ultimately, a better understanding of how nanoparticles interact with biological systems will be crucial for developing safe and effective nanotechnology applications in medicine, energy production, and other fields.

Poly (D,L-lactide-co-glycolide) nanoparticles were abundant in the intermediate layer of primary cultured rabbit conjunctival epithelial cells (RCECs), distributed in a punctate manner around the cell membrane, perinuclear area, below the cell surface, and in distinct compartments, but were not found in the nuclear region (Qaddoumi et al., 2004).

4.2 Cellular Uptake Mechanisms

Any biological membrane can be traversed using one of two primary methods. These modes of transportation are passive and active. Passive transport occurs most frequently by diffusion along a concentration gradient from high to low concentrations. The energy required for this mode of transportation is zero. Molecules moving against a concentration or an electrochemical gradient require energy for active transport.

4.2.1 Active transport

Membrane proteins move molecules across cells via an energy-driven process known as active transport (Foroozandeh & Aziz, 2018; Geck & Heinz, 1989; Hü Bner & Jentsch, n.d.; Salatin & Yari Khosroushahi, 2017). These mechanisms are primarily classified as primary or secondary based on how energy is coupled to power them. With sodium/potassium-ATPase and hydrogen-ATPase pumps, the former acts as a mechanism by which a chemical reaction, such as ATP hydrolysis, powers the direct transport of molecules to establish particular concentration gradients (Geck & Heinz, 1989). The latter method uses built-in gradients to transport additional molecules. These gradients are essential for the preservation of cellular and bodily homeostasis, because they support the functions of other membrane proteins and other cellular processes. Consequently, it is easy to see the significance of active transport when considering various defects throughout the body that can appear in a variety of diseases, such as cystic fibrosis and cholera, all as a result of a deficiency in some aspects of active transport (Hü Bner & Jentsch, n.d.). Because the phospholipid bilayer or electrochemical gradient prevents certain substances from transferring through cell membranes, transmembrane proteins are required. One way in which cells move is through active transport, which involves working against the formation of equilibrium, and typically involves concentrating molecules based on the specific requirements of the cell, such as ions, sugars, and amino acids (Foroozandeh & Aziz, 2018; Salatin & Yari Khosroushahi, 2017).

Metal ions such as sodium, potassium, magnesium, and calcium are frequently transported by primary or direct active transport, which primarily uses transmembrane ATPases and ion pumps/channels. The energy stored in the electrochemical gradients created by direct active transport, which is primarily produced by sodium ions via sodium-potassium ATPase, is used

by secondary active (coupled) transport to move other molecules against their respective gradients, notably without direct coupling to ATP. This procedure is essential for both the removal of waste materials, such as urea, and absorption of crucial nutrients, such as glucose, amino acids, and vitamins. The sodium-glucose cotransporter (SGLT), found in the kidneys and small intestine, is an illustration of secondary active transport. To transport glucose into cells against its concentration gradient, SGLT use energy from the sodium gradient. Another example is the sodium-calcium exchanger (NCX) present in the cardiac muscle cells. Calcium ions must be removed from the cells by NCX for muscle contraction and relaxation. This was accomplished using energy from the sodium gradient. Secondary active transport is essential for cellular homeostasis and physiological function (Sano et al., 2020).

Endocytosis can be divided into different categories according to the cell type, proteins, lipids, and other substances involved in the procedure. Phagocytosis, clathrin-mediated endocytosis, caveolin-mediated endocytosis, clathrin/caveolae-independent endocytosis, and macropinocytosis are the five main endocytic mechanisms (Kumari et al., 2010). Professional phagocytes, which are responsible for host defense and uptake of dead cells and cell debris such as macrophages, monocytes, neutrophils, and dendritic cells, are the main types of phagocytes that engage in phagocytosis. However, several other cell types, such as fibroblasts and epithelial and endothelial cells, also exhibit phagocytic activity, albeit to a lesser degree, and are known as phagocytes (Swanson, 2008). The primary method by which cells acquire nutrients and components of the plasma membrane, such as cholesterol via low-density lipoproteins (LDLs) and iron via transferrin carriers, is clathrin-mediated endocytosis. This process occurs inside the cell. CME can occur either by uptake of a molecule by a specific receptor or by non-specific adsorptive mechanisms, which is also known as receptor-independent CME. In receptor-independent CME, uptake occurs without direct binding to membrane constituents; instead, non-specific hydrophobic or electrostatic interactions eventually begin uptake. This is because receptors are not present in this type of CME (N. Chaudhary et al., 2014).

Caveolae-dependent endocytosis is essential for a wide variety of biological functions, including cell signalling, transcytosis, and the regulation of lipids, fatty acids, membrane proteins, and membrane tension. Caveolae also play a role in membrane protein transport. Caveolae-mediated endocytosis is thought to play a role in a wide range of disorders including cancer, diabetes, and viral infections. Endocytosis can occur in cells that lack both clathrin and

caveolae; this process is called clathrin- and caveolae-independent endocytosis. These cells take in a variety of cargoes, including cellular fluids, interleukin-2, and growth hormones, via alternative pathways. This requires a particular lipid composition (mainly cholesterol), as well as the absence of clathrin and caveolae in the cell membrane. The method of pinocytosis, known as macropinocytosis, is distinct from other types of pinocytosis, because it does not require the use of lipid rafts or pit-forming proteins. As a result of cytoskeleton reorganization, huge membrane extensions or ruffles are created. These membrane extensions or ruffles then fuse back onto the plasma membrane, which results in the formation of a large vesicle (0.2–5 μ m) that captures a big "gulp" of extracellular fluid. Macropinocytosis is a form of nonspecific bulk fluid uptake; therefore, all particles and dissolved compounds in the extracellular fluid are absorbed into the endocytic vesicle regardless of the presence of specialized receptors. Macropinocytosis occurs in the absence of specific receptors (Behzadi et al., 2017; N. Chaudhary et al., 2014; Kumari et al., 2010).

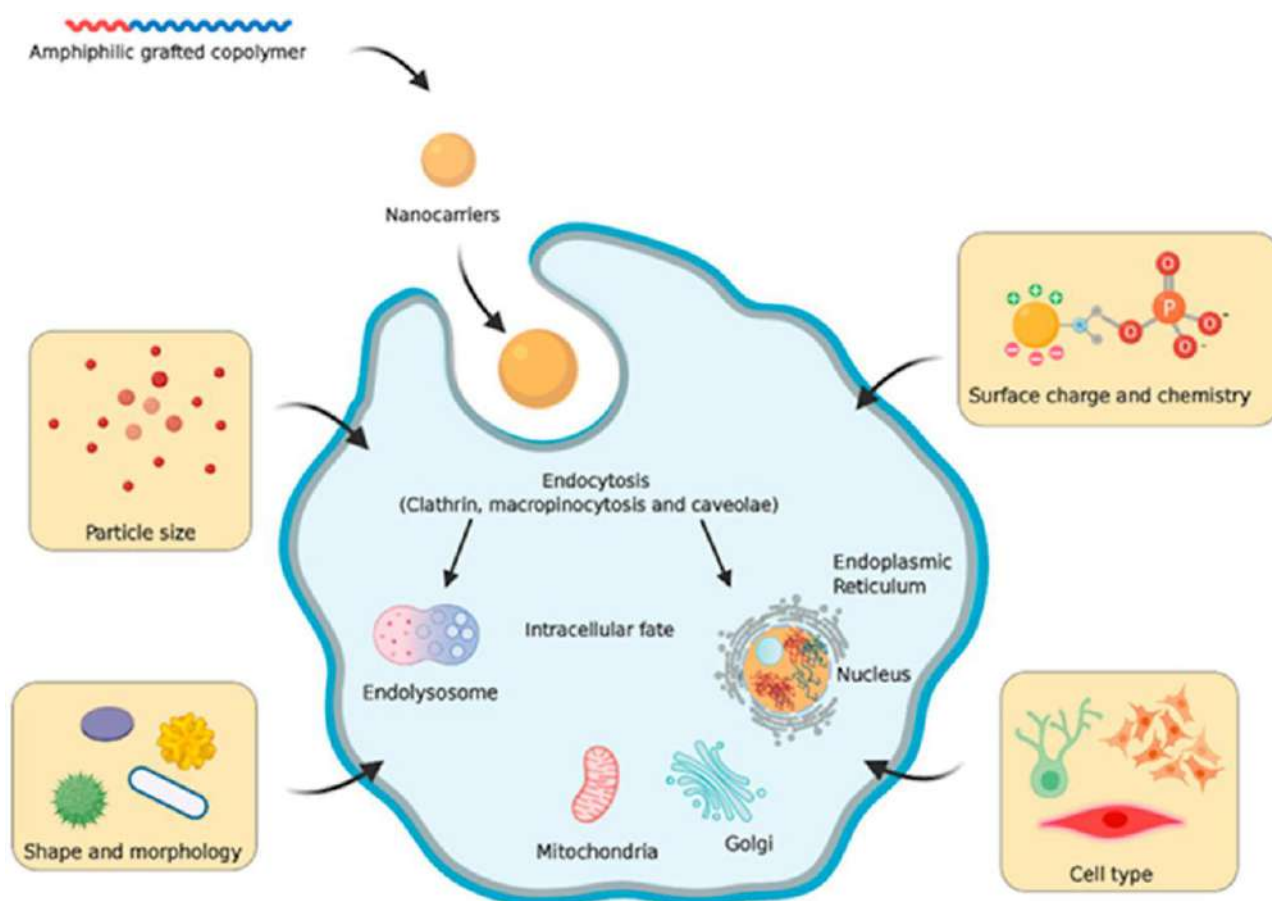


Figure 4.1: Different modes of active cellular internalization of nanoparticles (Mazumdar et al., 2021).

4.2.2 Passive uptake mechanism

The uncompetitive movement of molecules and NPs through membrane phospholipids, or in conjunction with membrane proteins, is known as passive transport or diffusion. Because diffusion occurs in the direction of the concentration gradient, it does not consume energy. There are two types of passive uptake: simple and assistive. In the process of simple diffusion, molecules or NPs enter the cell by moving through intramolecular gaps present in protein channels or membranes. Lipophilic substances can directly pass through the lipid bilayer, whereas hydrophilic compounds require protein channels for internalization. For both routes, the rate of substance internalization was proportional to the concentration of the diffusing substance. Facilitated diffusion is the second passive pathway that requires the presence of specific protein carriers. When a higher concentration of the chemical diffuses, the rate of internalization via the facilitated pathway is at its highest point (Attia et al., 2019; Sabourian et al., 2020).

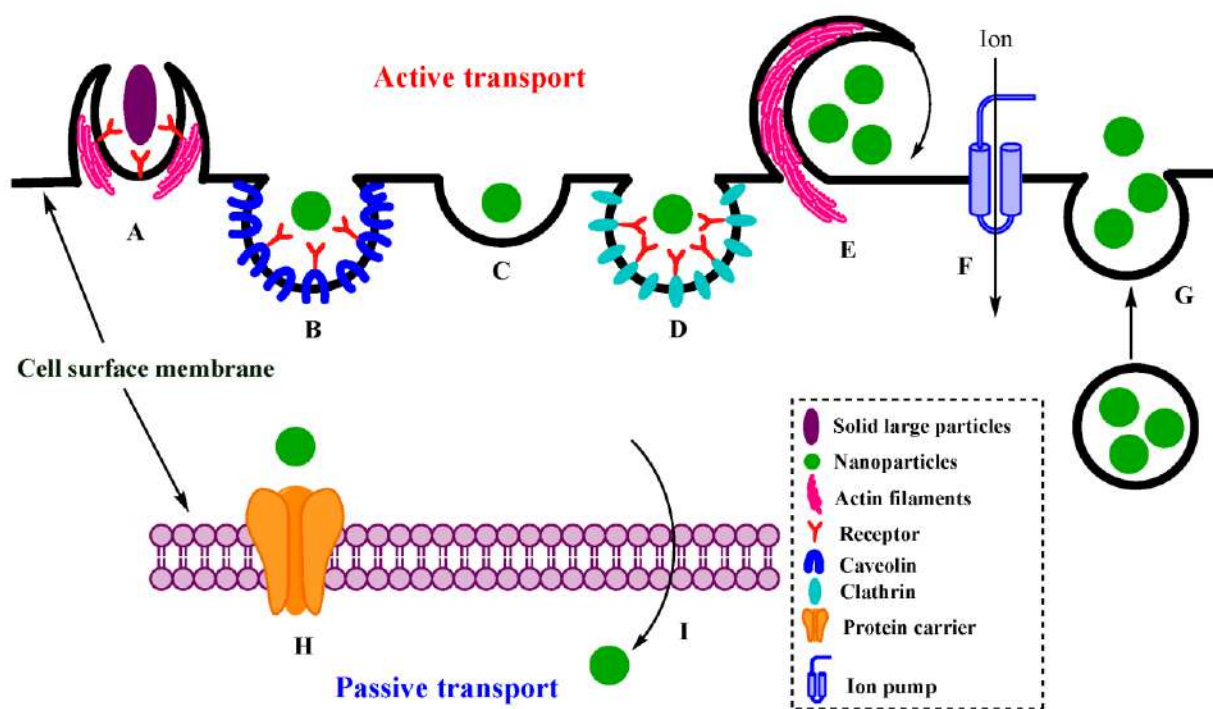


Figure 4.2: Active and passive cellular uptake of particles: (A) phagocytosis, (B) caveolin-mediated endocytosis, (C) clathrin-caveolin-independent endocytosis, (D) clathrin-mediated

endocytosis, (E) macro-pinocytosis, (F) ion pumps, (G) exocytosis, (H) facilitated diffusion, and (I) simple diffusion (Sabourian et al., 2020).

4.3 Interaction of nanoparticles with diverse macromolecules *in vitro*

4.3.1 Interaction of Nanoparticles with DNA

Nanoparticles (NPs) made of metal oxide are the designed NPs that find the most widespread application in consumer goods. In addition, metal oxide nanomaterials, also known as mineral NPs, are widespread and can be found in a variety of habitats, including the soil, atmosphere, and seas. These nanoparticles (NPs) display outstanding antibacterial activity, cytotoxicity, and genotoxicity in various organisms. The binding of metal oxide NPs to genetic materials (such as DNA and RNA), indirect damage from NP-generated reactive oxygen species (ROS), and toxic ions released from soluble NPs are some of the postulated processes that contribute to the toxicity of metal oxide NPs. Compared to the relevance of oxidative stress generated by NPs, less attention has been paid to the direct binding of NPs to DNA. However, previous studies have demonstrated that the usual shape of DNA molecules can be altered when quantum dots or Au NPs are bound to the molecule. NPs that bind to DNA with high affinity could limit the normal operation of some essential DNA-binding proteins, such as RNA or DNA polymerases, by occupying protein-binding sites and hindering the passage of proteins along DNA. This could result in the competitive inhibition of genetic functions. NPs that bind to DNA with a low affinity may have the opposite effect. Therefore, the interaction between metal oxide NPs and DNA might play a significant role in NP toxicity. Hence, a comprehensive explanation or definition of the mechanisms at play is required (C. H. Gao et al., 2019; Peng et al., 2017).

The kinetics of the interaction between gold nanoparticles capped with N-(2-mercaptopropionyl) glycine and double-stranded DNA was investigated in both water and salt (NaCl) solutions. The AuNPs were suspended in the solution and allowed to interact with the DNA. The biexponential nature of the kinetic curves demonstrates the existence of three distinct kinetic stages. The dependence of the reciprocal fast and slow relaxation times on DNA concentration is a curve that tends to plateau at high DNA concentrations. This plateau occurs when the DNA concentration is sufficiently high. The simplest mechanism, which is consistent with the kinetic data, involves a straightforward reaction scheme that takes place over the course of three steps. The first step is a very rapid step related to the diffusion-controlled

formation of an external precursor complex (DNA, AuNPs), and the second step involves the formation of a (DNA/AuNPs)I complex, which occurs as a result of the binding affinity between the hydrophilic groups of tiopronin and the DNA grooves. Finally, the third step was interpreted as a consequence of the conformational shift that occurred in the (DNA/AuNPs)I complex created in the second step to a more compressed version known as (DNA/AuNPs)II. This change occurred in the third step. As the NaCl concentration increased, the rate constant values for each step decreased (Prado-Gotor & Grueso, 2011). Dynamic light scattering and cryogenic transmission electron microscopy were used to directly monitor and visualize changes in particle size and appearance during the functionalization of AuNPs with thiol-ssDNA and non-thiolated dsDNA. Both thiol-ssDNA and dsDNA stabilize gold nanoparticle dispersions, although nonspecific interactions between the hydrophobic DNA bases and the gold surface increase interparticle contact and produce aggregation in a relatively short amount of time (Cárdenas et al., 2006).

ZnO nanoparticles at various concentrations (0.5-5 mg/ml conc.) were treated with 100 bp DNA at different electrophoretic times (20, 30, and 40 min). Slab-gel electrophoresis measurements confirmed the visualization of DNA, whereas UV-vis and AFM spectroscopy revealed the interaction of zinc oxide nanoparticles with DNA. Furthermore, the surface-bonded states of zinc $Zn_{2p1/2}$, $Zn_{2p3/2}$, and N1s peaks clearly indicate the attachment of Zn. X-ray photoelectron spectroscopy was used to examine DNA (Wahab et al., 2009). The Cu-based NPs caused significant ds-CT-DNA degradation, as well as dose-dependent pDNA degradation. The lowest IC₅₀ values (2.13 g/mL and 3.7 g/mL) against *B. cereus* and *B. subtilis*, respectively, are shown by Cu₂O NPs of 16 nm and 12 nm. Cu₂O NPs-treated ds CT-DNA electrophoretically separated on an agarose gel revealed deterioration at high concentrations. Viscosity measurements have revealed groove binding at lower doses (Giannousi et al., 2014). Chromodulin, also known as glucose tolerance factor or Cr (III), is thought to be a crucial component of chromodulin and is therefore necessary for appropriate glucose metabolism in the body. It increases insulin sensitivity by activating insulin receptor kinase to become active. If surpassed, it can lead to oxidative stress, which harms DNA by generating Cr-DNA bonds, DNA-protein linkages, and DNA-DNA breaks. In *in vitro* settings, Cr (VI) has no impact on DNA; however, when it enters the body, it interacts with DNA and causes damage. It produces superoxide radicals when it interacts with thiol molecules, which subsequently converts Cr (VI) to Cr (V), breaks down H₂O₂, and damages the DNA. As participates in the formation of superoxide, singlet oxygen, nitric oxide, hydrogen peroxide,

and peroxy radicals. As (III) is oxidized to As (V), resulting in the formation of hydrogen peroxide, which damages cellular DNA (Valko et al., 2006).

4.3.2 Interaction of Selenium NPs and DNA

Deoxyribonucleic acid (DNA) is one of the final biomolecular targets for several anticancer treatments such as nano-selenium. To determine whether the anticancer function of Nano-Se is connected to its contact with DNA, the interaction of Nano-Se with ct-DNA was assessed using a multispectroscopic technique at pH = 7.40 (simulative physiological circumstances) to validate the binding impact between them. The interaction between ct-DNA and SeNPs revealed that SeNPs might bind to ct-DNA via a partial intercalation binding mechanism. Therefore, the anticancer activities of SeNPs could be linked to their interaction with DNA (Shahabadi et al., 2021).

Another study described the use of *A. sativum* aqueous extract (AqEAS) for the formation of selenium nanoparticles. Many spectroscopic and cyclic voltammetry tests have been conducted to investigate many aspects of the interaction between SeNPs and CT-DNA. These findings indicate the intercalation and groove-binding modes of the interaction of SeNPs with CT-DNA stacked base pairs. The Stern-Volmer quenching constant (KSV) was determined to be $7.02 \times 10^6 \text{ M}^{-1}$ (ethidium bromide), $4.22 \times 10^6 \text{ M}^{-1}$ (acridine orange), and $7.6 \times 10^6 \text{ M}^{-1}$ (Hoechst), showing that SeNPs bind to CT-DNA strongly. AFM was used to directly visualize the SeNP-CT-DNA interactions, which revealed an increase in height range compared to free DNA molecules, which was measured to be 52.24 nm, as well as the morphology of bound nanoparticles with DNA, obtaining further direct evidence of nanoparticle binding with DNA (Ezhuthupurakkal et al., 2017).

The ecologically friendly synthesis and characterization of selenium nanoparticles, as well as their protective effect against UV-induced DNA damage. An aqueous leaf extract of lemon plant was used as a precursor for the creation of colloidal selenium nanoparticles. The results revealed that when lymphocytes were exposed to UVB, their viability was reduced, implying that cell death was increased. When the cells were infused with biologically synthesized Se nanoparticles, minimal cell death was observed. This clearly demonstrates that the inclusion of selenium nanoparticles prevents lymphocyte cell death (Prasad et al., 2013). Toxicological investigation (S. Chaudhary et al., 2018), 0.8% agarose gel was placed in wells-biolab gel

electrophoresis to evaluate the effect of SeNPs on human DNA. For the analysis, ethidium bromide (10 mg/ml) and bromophenol blue (0.25%) dyes were used. Because ethidium bromide is a monovalent cationic dye, it can interact with nanoparticles and the base pair of a DNA helix. Using the gel doc equipment, the respective bands of the nanoparticles and control were observed. In the instance of Brij-58 coated SeNPs, the intensity of the band was comparable to that of the control, indicating that the SeNps had no effect on human DNA.

4.3.3 Proteins and selenium nanoparticle Interactions

The interaction of proteins with metal (e.g., gold), oxide (e.g., silica and titana), and chemically fabricated (e.g., polystyrene) NPs has attracted considerable attention because of their interesting basic features. Various potential applications of NPs, including targeted drug delivery (Zhdanov & Cho, 2016), hyperthermia therapy, contrast imaging, fabrication of virus-like particles, and resolution of the potential threat of adsorption of specific proteins to such NPs in biological fluids, results in the formation of the so-called protein corona, which has a significant impact on the function of NPs in biological systems (Chakraborty et al., 2018). A protein corona is a biomolecule coating that forms around nanoparticles when in contact with biological fluids. Van der Waals interactions, hydrogen bonds, hydrophobic interactions, electrostatic interactions, and π - π -stacking are the binding forces responsible for these interactions (Wolfram et al., 2014). A dynamic interchange between biomolecules with lower and greater affinities on a nanosurface results in the formation of a protein corona, which could have major *in vivo* effects that could be either favorable or negative. NPs are assigned a new biological identity as a result of this occurrence, which may have an impact on their biodistribution, immunological recognition, adoption, toxicity, and efficacy. Therefore, it is crucial to understand how proteins interact with NPs to fully understand their biological effects (Zhdanov & Cho, 2016).

Human serum albumin (HSA) is one of the most significant proteins in human blood plasma, and it contains many binding sites that allow both endogenous and external ligands and medicines to adhere to it. It regulates various crucial physiological processes, including feeding across the entire human body. HHb, as a drug carrier, plays a significant role in the delivery of various chemicals to the necessary physiological areas during the treatment of numerous diseases. Despite the complicated forms of nano-selenium, the native secondary structure of

HSA does not change significantly. Such interactions can alter the spectroscopic characteristics of HSA. However, for other proteins, interactions with drugs or nanoparticles can result in structural alterations and loss of function. Based on these findings, it can be concluded that denaturation of HSA did not occur when exposed to nano-selenium and that this protein maintains its normal secondary structure and biological function (Shahabadi et al., 2021).

Isocitrate lyase, isocitrate dehydrogenase [NADP], outer membrane protein C precursor (Porin ompC), alcohol dehydrogenase, and propanol-preferring were found to be uniquely and entirely related to SeNPs. The size (36-48 kDa), function (enzyme or structural protein), and isoelectric point (4.58-5.94) of these four proteins differed. Furthermore, there was no clear amino acid sequence similarity between the four proteins. The identification of these significantly connected proteins revealed that none of them were linked to NP production or metal reduction. These proteins are mostly involved in energy, carbohydrate, or fatty acid metabolism, although they do not share chemical features, such as isoelectric point, cofactor, or size. It can be concluded that the binding capacity of proteins is determined by either the spatial structure or physicochemical qualities of their amino acids (Dobias et al., 2011).

Amino acid-modified selenium nanoparticles (SeNPs@AAs) were synthesized using a simple redox system. To decorate the SeNPs, neutral (valine), acidic (aspartic acid), and basic (lysine) amino acids were utilized, and the nanoparticles were characterized using zeta potential and transmission electron microscopy. X-ray photoelectron spectroscopy (XPS) revealed that the interaction of amino acid-NH₃⁺ groups with negatively charged SeNPs could be a driving mechanism for nanoparticle dispersion. Screening of *in vitro* anticancer activity revealed that SeNPs@AAs had varied growth inhibitory effects on diverse human cancer cell lines. SeNPs with Lys outperformed those with valine and aspartic acid in terms of anticancer effectiveness. *In vitro* cellular uptake processes experiments demonstrated that SeNPs@AAs were internalized by cancer cells via endocytosis (Feng et al., 2014).

4.3.4 Characterization techniques for protein-Se NPs interaction

Various analytical methods can be used to characterize the development of biocorona on NP surfaces. These techniques include surface plasmon resonance (SPR), transmission electron microscopy (TEM), mass spectrometry-based (MS) based proteomics, chromatography, fluorescence spectroscopy, CD spectroscopy, electrophoresis (gel, capillary, and 2D

electrophoresis), dynamic light scattering (DLS), isothermal titration calorimetry (ITC), infrared spectroscopy (FTIR), and nuclear magnetic resonance spectroscopy (NMR). These methods have been used to detect the structural and conformational changes in proteins on NP surfaces (Li et al. 2010).

Various approaches have been applied to characterize the type of interaction between BSA protein and dual-coated selenium nanoparticles, including UV-visible spectroscopy, fluorescence spectroscopy, and circular dichroism spectroscopy.

- UV-Visible Spectroscopy

The localized surface plasmon resonance (LSPR) phenomenon has been employed in UV-visible (UV-Vis) spectroscopy to characterize metallic nanoparticles (AuNPs) and their conjugates. The absorbance spectra of the NP–protein complex were altered and broadened depending on the bioconjugate size, aggregation stage, and local dielectric environment. UV-Vis is commonly used to quantify metallic NPs and qualitatively measure conjugate binding because of this phenomenon. UV-Vis is a non-invasive technology that does not affect sample integrity and is a low-cost technique that requires minimum sample preparation. The UV-Vis adsorption spectrum is heavily impacted by the solvent, pH, temperature, and high electrolyte concentration. Furthermore, UV-Vis spectroscopy alone can reveal very little about biomolecular structures (Li et al., 2010).

- Fluorescence Spectroscopy

Proteins are polymeric amino acid complexes that contain fluorophores such as tyrosine, tryptophan, and phenylalanine. Fluorescence spectroscopy is sensitive to protein dynamics because the excited fluorescent state lasts for nanoseconds, which is the time scale of many important biological processes such as protein side chain rotation, molecular binding, and protein conformational changes (Palomar et al., 2020). Fluorescence emission from NPs can be observed when they are naturally luminous or labelled with fluorescence probes³⁶. Fluorescence spectroscopy, fluorescence resonance energy transfer (FRET), and stepwise single-molecule photobleaching can all be used to study NP-protein binding (Randika Perera et al., 2019). The interaction of NPs with proteins changes the local chemical environment of the fluorophores and reduces protein fluorescence. As a result, the decrease in fluorescence intensity and shift in the emission peak maximum suggested NP-protein interactions. If fluorescence quenching is caused by the collision effect, the lifetime of the

fluorophore is likewise reduced. The Stern-Volmer equation governs the relationship between the fluorescence intensity, lifetime, and quencher concentration:

$$F_0/F = 1 + K_{sv}[Q]$$

where F_0 , F , τ_0 , and τ denote the initial or modified fluorescence intensity or lifetime, respectively. The Stern-Volmer constant is denoted by K_{sv} , and the quencher concentration is denoted by $[Q]$ (Htun, 2004).

- Circular Dichroism (CD) Spectroscopy

Although neither fluorescence nor Raman spectroscopy can detect changes in the secondary or tertiary structures of proteins, CD is often employed to determine the secondary structure and how these structures change when proteins bind to NP surfaces. A molecule must be chiral to display a CD signal; however, NP surfaces are not often chiral and do not generally interfere with signal and data interpretation. Poly (acrylic acid)-coated gold nanoparticles (PAA-AuNPs) with fibrinogen, a large protein with both α -helices and β -sheets, and far-ultraviolet circular dichroism (UV-CD) were used to monitor protein structural changes upon NP interaction. The progressive increase in ellipticity indicates that the fibrinogen secondary structure was lost with the addition of PAA-AuNPs. They concluded that PAA-AuNPs caused structural alterations and revealed their C-terminus. Because the unbound (native) protein is generally left in the cuvette when the NP-bound protein is measured and the unbound protein frequently dominates the detected signal, UV-CD offers only an approximate estimate of conformational changes. Separating NP-bound proteins by centrifugation or measuring differences is a possible option, although the signal originating purely from NP-bound proteins is sometimes quite faint (Slocik et al., 2011).

4.4 Anti-oxidant assay (DPPH)

The ability of the NPs to scavenge free radicals was evaluated using the DPPH radical scavenging assay. The ability of selenium to donate hydrogen atoms was tested by decolorizing a methanol solution of 2,2-diphenyl-1-picrylhydrazyl (DPPH). In the presence of antioxidants, DPPH generates a violet/purple color in methanol solution and fades yellow (Rahman et al., 2015). The synthesized Se NPs was chemically reduced using ascorbic acid (Vitamin C) as a catalyst and polyvinyl alcohol (PVA) or chitosan (CS) as

stabilizers. A radical scavenging (DPPH) assay was used to assess the antioxidant capability of the synthesized Se nanoparticles *in vitro*. The IC₅₀ values were 26.56 and 530 ppm for PVA coated SeNPs (PVASeNPs) and CS-coated SeNPs (CS-SeNPs), respectively (Boroumand et al., 2019).

4.5 *In vitro* cytotoxicity

To overcome the side effects of chemo-and anti-inflammatory therapies, a variety of medications such as increased white blood cell drugs, pain relievers, and antiemetics are used clinically to improve patients' quality of life. However, with increased administration of adjuvant medications that cannot fundamentally improve cachexia, additional side effects will emerge. The concurrent use of adjuvant medicines, which can reduce drug toxicity without sacrificing efficacy, is a prospective therapeutic option for solving this problem. However, the major difficulty is that while medications lower chemotherapy toxicity, anti-inflammatory toxicity treatments necessarily diminish therapeutic efficacy. Given the limitations of therapeutic agents, there is an urgent need to develop novel treatment regimens that lower the toxicity of important medications, while reversing drug resistance and improving therapeutic selectivity (Y. Chen et al., 2022; F. Gao et al., 2014; Khurana et al., 2019; Menon et al., 2018).

Selenium (Se) has recently sparked widespread interest owing to its numerous health benefits, notably those connected to the immune response and cancer prevention. Se has been proven in epidemiological, preclinical, and clinical research to reduce the incidence of a variety of malignancies, including breast, prostate, lung, colon, and liver cancers. According to these findings, both the dose and Se form are important for anticancer action. At high doses, some molecular Se compounds, such as selenomethionine (SeMet), sodium selenite, and methylselenocysteine, exhibit more effective anticancer activity (Khurana et al., 2019). However, high doses of selenite raise serious concerns regarding toxicity. In this regard, nanoparticles of elemental selenium (Nano Se) appear to be more effective than other Se sources for inducing selenoproteins, scavenging free radicals, and preventing oxidative DNA damage via potent antioxidant activity with low toxicity and acceptable bioavailability. Furthermore, Che-SeNP can be administered via numerous routes, such as p.o. or i.v. routes, and is simple to administer. These benefits make Che-SeNP an excellent adjuvant drug for tumor treatment. Irinotecan and Che-SeNP alone reduced HCT-8 cell viability to 62% and 80%, respectively, but the two reduced viability to 46%. Additionally, when compared to IEC6 cells, Che-SeNP and the combination of Che-SeNP and irinotecan had greater cytotoxic effects on HCT-8 cells (F. Gao et al., 2014).

Biogenic Se NPs produced by *Bacillus* sp. MSh-1 exhibited significant cytotoxicity in intracellular amastigotes after 24, 48, and 72 h of exposure. After 72 hours, the IC₅₀ for Se NPs against this parasite strain of *L. major* was $4.4 \pm 0.6 \mu\text{g ml}^{-1}$. A low concentration of

biogenic Se NPs ($2.5 \mu\text{g ml}^{-1}$) dramatically reduces the viability of intramacrophage amastigotes after 72 h of incubation (Beheshti et al., 2013). The MTT assay was used to investigate the cytotoxicity of nanoparticles on HepG2 cells. Cytotoxicity was assessed using Graph Pad Prim5 programme. SeNPs exhibited cytotoxic effects against HepG2 cells, with 77%, 63%, and 33.7% cell viability at concentrations of 2, 4, and 30 $\mu\text{g/ml}$, respectively. Biogenic SeNPs displayed cytotoxic action against the HepG2 cell line, warranting further investigation into their biosafety and potential as oral antimicrobial drugs (Indumathy et al., 2020).

In another study (Pillay et al., 2020), an apoptosis assay was used to determine whether the putative harmful effects of the nanocomplexes at the reported optimal ratios were attributable to toxicity or planned cell death. In this acridine orange/ethidium bromide (AO/EB) dual staining system, AO can perfuse all cells, emitting bright green fluorescence indicative of healthy cell nuclei, whereas the dominant EB dye only pervades cells with compromised cytoplasmic membranes, resulting in yellow to red fluorescence. The fluorescence images and estimated apoptotic indices revealed that the investigated nanocomplexes, particularly the targeting NPs, caused negligible apoptotic activity in the cell lines, indicating that the cytotoxic nature of the dendrimer was greatly reduced after functionalization with SeNP or FA.

In the current investigation, methionine and folic acid coatings were compared with dual-coated and uncoated SeNPs for their *in vitro* toxicity using the MTT assay on the NIH/3T3 cell line and Raw 264.7. SeNPs coated with methionine and folic acid interacted with DNA, and proteins were further evaluated. Protein interactions were investigated using BSA, a homolog of human serum albumin (HSA) (Topală et al., 2014). The single polypeptide chain was 66.4 kDa in size. The net charge was negative at physiological pH values. The 60 positively charged surface lysine residues on BSA may interact electrostatically with the negatively charged SeNPs, even though BSA is negatively charged at physiological pH and can therefore still attach to them. The conjugation of BSA and SeNPs could be caused by hydrophobic interactions.

The interaction between BSA and SeNPs was investigated using UV-Vis spectroscopy, fluorescence spectroscopy, and CD spectroscopy. The DNA interaction study used plasmid DNA pBR322, and its *in vitro* toxicity and antioxidant impact were assessed using the MTT assay, AO/EB staining method, and DPPH assay, respectively.

4.6 Materials and methods

4.6.1 pBR322 plasmid- NPs interaction

Using modified techniques developed by (Malhotra et al., 2016), (Battin et al., 2006) (Acharya & Ghaskadbi, 2013), pBR322 plasmid DNA was exposed to Se NPs and Se-Met-Fa NPs at increasing concentrations (250, 500, and 750 µg/ml) and subjected to oxidative stress. After 5 min, the plasmid was added to the reaction mixture. The cells were treated with 50 µM H₂O₂ and shaken for 30 min at room temperature. EDTA (50 mM) was then added, and the mixture was shaken for 20 min at room temperature. For 1.5 hours at 50 mV, the samples were placed onto a 1% agarose gel.

4.6.2 BSA- NPs interaction

Interaction of BSA and SeMetFa NP was observed using UV-Vis spectrophotometer (Shimadzu UV 1900) and Spectro fluorometer (Shimadzu RF 6000). Nanoparticles were incubated with BSA in concentration ratio ratios (1:10, 1:12.5, 1:16.6, 1:25, and 1:50) and time points such as (30, 60, and 240 min). Following incubation, absorption was measured ranging from 200 to 500 nm. Further fluorescence was excited at 296 nm and scanned in the Far UV range between 250 and 190 nm.

4.6.3 *In vitro* cytotoxicity assay

- MTT assay

MTT assay was used to assess the cytotoxicity of Se NPs and Se-Met-Fa NPs *in vitro*. Raw 264.7 and NIH-3T3 murine fibroblast cell lines. At 37 °C humidified with 5% CO₂, macrophages were cultivated and maintained in DMEM with 10% FBS and 1% antibiotics (100 U/ml penicillin and 100 mg/ml streptomycin). In a 96-well plate, 10,000 cells per well were seeded and incubated for 24 h at 37 °C with 5% CO₂. After 24 h, the wells were replaced with serum-free DMEM containing varying concentrations of Se NPs and Se-Met-Fa NPs ranging from to 50-100 µg/ml and incubated for another 24 h. The wells were filled with 100 µL of 5 mg/ml MTT reagent in DPBS and incubated at 37°C for 4 h in the dark. In the evening, 100 µL of DMSO was added and shaken at room temperature for 20 min before measuring solubilized formazan at 570 nm and 655 nm on an ELISA plate reader.

- AO/EB staining test

An acridine orange/ethidium bromide (AO/EB) assay was performed on primary (NIH-3T3) cell lines to determine the percentage of living and dead cells. A total of 10,000 cells were sown in each 35 mm Petri plate with DMEM containing 10% FBS and 1% antibiotics and cultured for 24 h at 37°C with 5% CO₂. Following incubation, the medium was changed in a 1:1 ratio with acridine orange and ethidium bromide, with a total volume of 100 µL in each plate. Subsequently, the FITC filter was viewed using a fluorescent lamp.

4.6.4 Antioxidant evaluation

The ability of Se-Met-Fa NPs to scavenge free radicals was investigated using the DPPH assay, using modification of methods of (Menon, Agarwal, et al., 2019; Menon, Shrudhi, et al., 2019). 0.1mM of DPPH was prepared in methanol. Various concentrations of SeMetFa nanoparticles ranging from 10-100 µg/ml were prepared at an interval of 10 µg/ml. 1 ml of DPPH was added in each concentration mentioned and were incubated in the dark for 1 hour. At the end of 1 hr, absorbance was measured at 517 nm using ELISA plate reader (Bio-rad).

4.6.5 Statistical Analysis

All assays were performed in triplicate at various times. PRISM software was used to represent the data as the mean standard deviation.

The ORIGIN Software was used to plot the spectra. To detect statistical significance across different groups of nanoparticles and controls, MTT results were analyzed using two-way ANOVA with the Bonferroni test of multiple comparisons. A p-value of .05 was considered significant. A Stern-Volmer graph was created using the regression value and line equation for varying nanoparticle concentrations.

4.7 Results

4.7.1 pBR322 plasmid- NPs interaction

The concentration of 250 $\mu\text{g/ml}$ Se NPs, H₂O₂-induced oxidative damage was avoided. The prevention was significantly better in the case of 250 μg of Se-Met-Fa NPs, with 10% supercoiled DNA intensity equivalent to the activity of 750 μg of Se NPs (Figure 5B). The effective concentration of Se is 0.25 μg per 250 $\mu\text{g/ml}$ and 0.75 μg per 750 μg of Se NPs. This demonstrates that even at 0.25 μg concentration, Se NPs was protective against oxidative damage. Figure 4.3 A shows that the coating materials had antioxidative properties when compared to the controls. The intensity of the gel images was calculated using ImageJ software to determine the percentage of supercoiled undamaged DNA and the percentage of nicked circular DNA (Figure 4.3 C, D). Treatment groups with increasing concentrations of Se-Met-Fa NPs demonstrated remarkable scavenging efficacy against oxidative stress. As with the control pBR322 plasmid, the supercoiled DNA remained intact for up to 15% of the time.

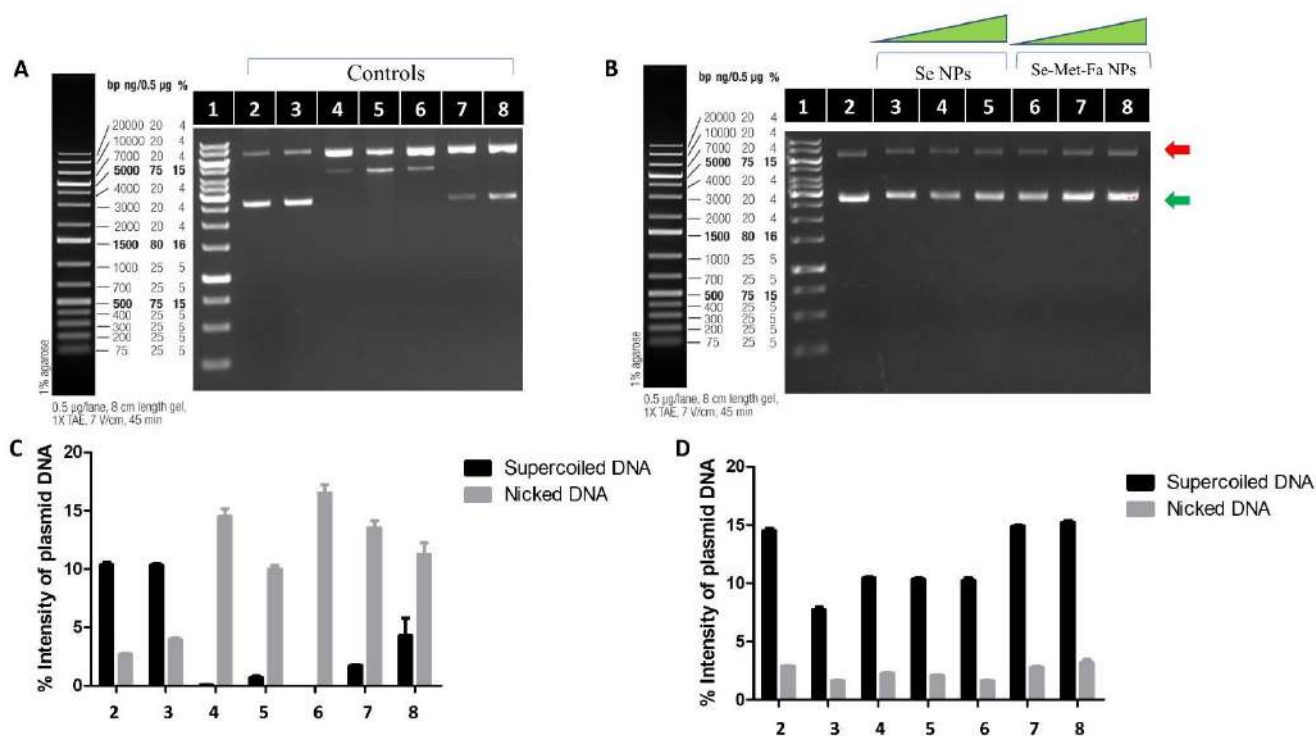


Figure 4.3 (A) Images of plasmid pBR322 after contact with controls on an agarose gel. (B) Varying doses of Se NPs and Se-Met-Fa NPs. Circular DNA nicked (red arrow) and intact supercoiled DNA (green arrow). Panels (C) and (D) indicate the percentage of nicked and supercoiled DNA. (A) and (C): (1) a 1 kb DNA ladder, (2) pBR322 plasmid control, (3)

pBR322 + H₂O₂, (4) pBR322 + H₂O₂ + Cu⁺, (5) pBR322 + H₂O₂ + Cu⁺ + EDTA, (6) pBR322 + H₂O₂ + Cu⁺ + EDTA + 1% sodium selenite, (7) pBR322 + H₂O₂ + Cu⁺ + EDTA + 1% methionine, and (8) pBR322 + H₂O₂ + Cu⁺ + EDTA + 0.1% folic acid. (1) 1 kb DNA ladder, (2) pBR322 plasmid control, (3–5) Se NPs (250, 500, and 750 μg), and (6–8) Se-Met-Fa NPs (250, 500, and 750 μg).

4.7.2 BSA- NPs interaction

As shown in Figure 4.4 A, BSA had a maximum absorbance at 278 nm, and no peak shift was observed as the concentration of BSA + Se-Met-Fa NPs increased. The wavelength of 278 nm, which was observed as the common max, approximated the $\pi-\pi^*$ transition of the aromatic amino acid residues tryptophan and tyrosine. From to 10-100 g/ml, there was a progressive increase. This increase in BSA intensity indicated the formation of a ground-state complex containing Se-Met-Fa NPs.

Figure 4.4 B shows the fluorescence emission spectra of BSA and BSA with varying amounts of Se-Met-Fa NPs. The excitation wavelength was maintained at 286 nm to preferentially excite the tryptophan amino acid residue. Although there was a progressive drop in the emission intensity, there was no shift in the emission wavelength.

The Stern-Volmer Equation was used to calculate the fluorescence quenching constant of BSA in the absence and presence of Se-Met-Fa NPs (Goodpaster & McGuffin, 1999).

$$F_0/F = 1 + K_{sv}[Q]$$

where F_0 and F represent the intensities of BSA fluorescence in the absence and presence of Se-Met-Fa NPs (quencher), respectively. The Stern-Volmer constant, commonly known as the quenching constant, is denoted by K_{sv} .

where, Q is the quencher concentration. Figure 4.4 C depicts the Stern-Volmer plot, which is a straight-line plotting F_0/F against the quencher concentration $[Q]$. The slope yielded a K_{sv} of $0.12 \times 10^4 \text{ M}^{-1}$. There are two types of fluorescence-quenching chemical phenomena: dynamic and static. The quenching rate constant was determined to establish the quenching mechanism responsible for the interaction of BSA.

The following equation can be used to calculate the quenching rate constant, K_q (Praktikum & Quenching, 2016):

$$K_q = \frac{K_{SV}}{\tau}$$

K_q is also known as the quenching rate constant, K_{SV} , and is the average lifetime of BSA in the absence of a quencher (10^{-8}). As a result, the value of K_q is $1.2 \times 10^{11} \text{M}^{-1}\text{s}^{-1}$, which is greater than the maximum diffusion collision rate for a biological molecule ($2.0 \times 10^{10} \text{M}^{-1}\text{s}^{-1}$). This suggests that the interaction between BSA and Se-Met-Fa NPs involves a static quenching process.

The far-UV CD spectra of BSA were recorded in the presence of Se, Se-Met, and Se-Met-Fa NPs to investigate how the secondary structure of BSA changes when it interacts with all three nanoparticles. In the ultraviolet range, the CD spectra in Figure 4.4 D show two negative peaks: the first at 209 nm and the second at 222 nm. These negative peaks are typical of the helical shape of BSA. The first peak at 209 nm was caused by π - π^* peptide bond transfer, and the second peak at 222 nm was caused by n - π^* peptide bond transfer at the α -helix. The ellipticity of BSA was reduced when conjugated with Se NPs, Se-Met NPs, and Se-Met-Fa NPs, but there was no substantial shift in the peak. BSA's α -helicity is calculated using the following equation (A. S. Patel et al., 2016; Vaughns, 2007):

$$\alpha\text{Helix \%} = \frac{-\text{MRE}_{209} - 4000}{33000 - 4000}$$

The ellipticity of BSA was reduced when conjugated with Se NPs, Se-Met NPs, and Se-Met-Fa NPs, but there was no substantial shift in the peak. BSA's α -helicity is calculated using the following equation (Htun, 2004):

$$\text{MRE}_{BSA} = \frac{\text{observed CD (mdeg)}}{C_p n l \times 10}$$

where C_p is the BSA molar concentration, n is the amino acid concentration, and C_p , n , and l are the path length of 1 mm and residues (582 for BSA), respectively. The value of the pure α -helix at 209 nm was 33,000, and the MRE for the β -form and random coiling conformations at 209 nm were 4000.

The calculated α -helix values are listed in Table 4.1. The reduction in the presence of Se-Met-Fa NPs and BSA helicity was approximately 3.9% to 4.4%.

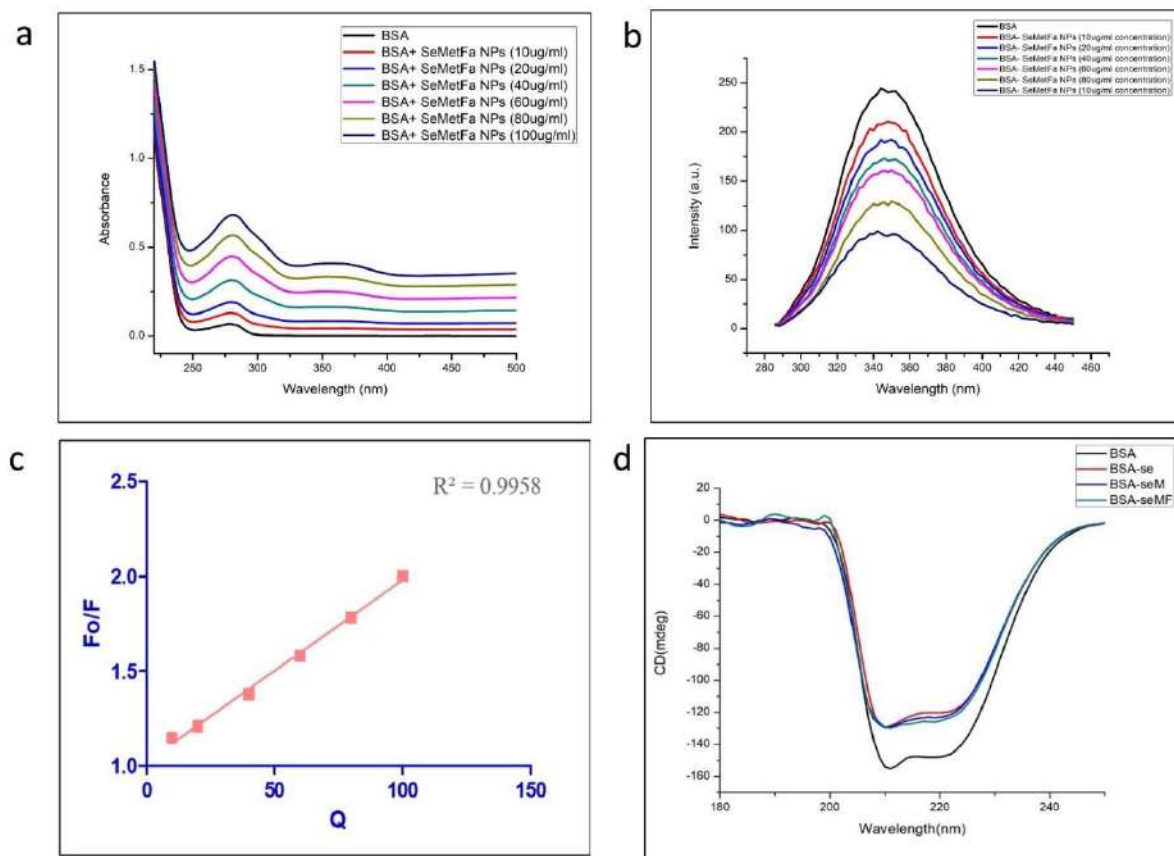


Figure 4.4 (A) UV-visible spectroscopy of BSA protein and BSA binding to Se-MetFa NPs at various doses (10-100 $\mu\text{g/ml}$). (B) Steady-state BSA fluorescence spectra with and without increasing amounts of Se-Met-Fa NPs. (C) Stern-Volmer plot of BSA protein fluorescence quenching by Se-Met-Fa NPs, plotted as F_0/F versus $[Q]$. (D) Circular dichroism spectra of BSA in the presence of Se, Se-Met, and Se-Met-Fa NPs.

Table 4.1: Helicity variations when nanoparticles are present

Samples	% α -Helix (209nm)
BSA	29.62
BSA-Se NPs	25.45
BSA-Se-Met NPs	25.47
BSA-Se-Met-Fa NPs	25.22

4.7.3 *In vitro* cytotoxicity of NPs

- AO/EB staining method

AO/EB staining in NIH-3T3 cells, with the following controls: untreated cells, methionine, sodium selenite, and folic acid. Control with sodium selenite, which shows complete red cells, resulted in 100% death, which justifies its high toxicity. As shown in Figure 4.5, approximately 80% viability was observed for 100 $\mu\text{g/ml}$ nanomaterial incubated for 24 and 48 h, while 70% viability was reported for 100 $\mu\text{g/ml}$ nanomaterial incubated for 72 h. The AO/EB data in this study were collected using a phase-contrast microscope and fluorescent lamp.

- MTT viability assay

The MTT experiment was performed, (Figure 4.6 A and B) with time points such as 24, 48, and 72 hours. Less than 50% of the Se NPs were viable at the lowest dose of 50 $\mu\text{g/ml}$, the effective concentration at 24 hours was 0.05 μg . While Se-Met-Fa NPs increased cell viability by up to 70%–80% at a concentration of 100 $\mu\text{g/ml}$, the active concentration was 0.1 μg for 24 hours and 55%–60% cells for 72 hours. Figure 4.6 B shows the percentage viability of Se-Met-Fa NPs in macrophages, which were 80% viable at 100 $\mu\text{g/ml}$ for 24 hours and 55% viable for 72 hours.

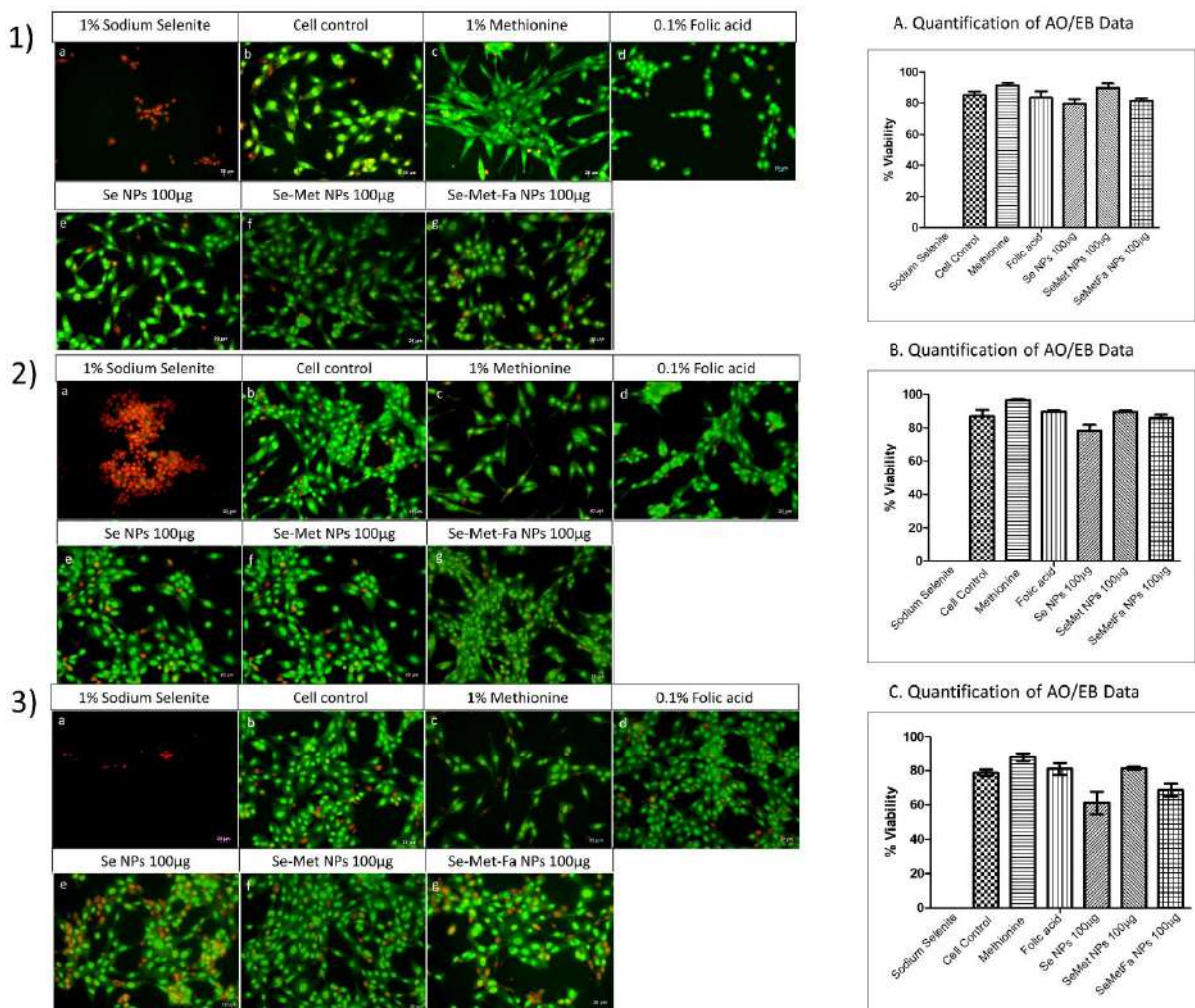


Figure 4.5 Images of AO/EB staining at 24, 48, and 72 h are shown in (1), (2), and (3), respectively. Each time point had the following seven images: (a) 1% sodium selenite, (b) cell control, (c) 1% methionine, (d) 0.1% folic acid, (e) 100 µg/ml of Se NPs, (f) 100 µg/ml of Se-Met NPs, and (g) 100 µg/ml of Se-Met-Fa NPs. Plots of (A)% cell viability at 100 µg/ml for 24 h One hundred µg/ml after 48 h (B). (C) Viability at 100 µg/mL after 72 h. The images were magnified by 20X.

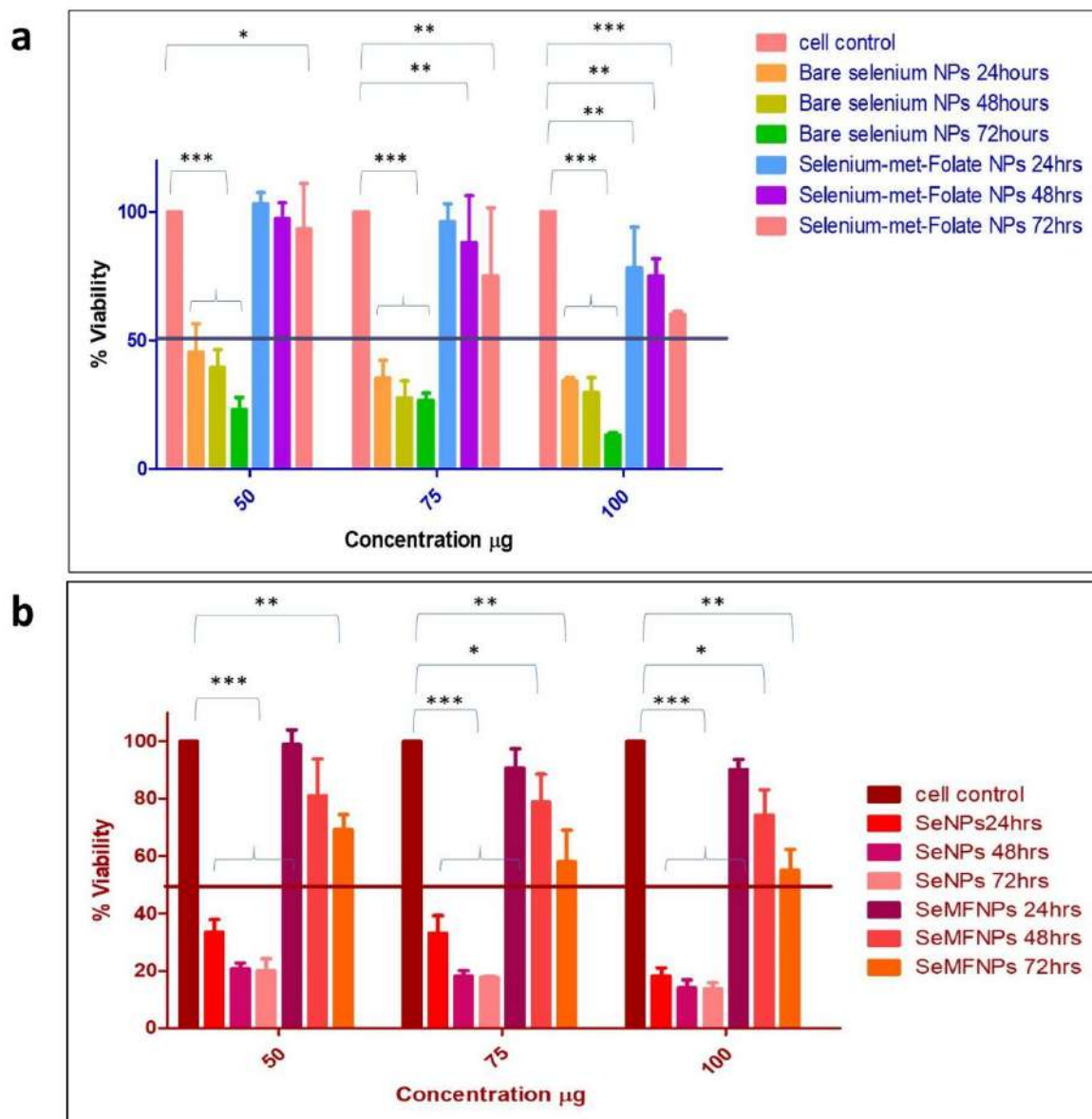


Figure 4.6 *In vitro* cytotoxicity of Se NPs and Se-Met-Fa NPs (50-100 µg) on NIH 3T3 and Raw 264.7 cells (A and B). Cell lines were investigated using two-way ANOVA with Bonferroni multiple comparisons. * $p < .05$, ** $p < .01$, *** $p < .001$

4.7.4 Antioxidant assay

Se-Met-Fa NPs were evaluated for antioxidant activity using the DPPH assay (Figure 4.7), and it was observed that 10 µg/ml of Se-Met-Fa NPs could scavenge roughly 41% of DPPH, despite the fact that the effective concentration of Se-Met-Fa NPs is 0.01 µg, demonstrating its significant antioxidant potential. At 60 µg/ml of Se-Met-Fa NPs, where the effective

concentration of Se-Met-Fa NPs is 0.06 μg , a maximum of 100% scavenging activity was recorded.

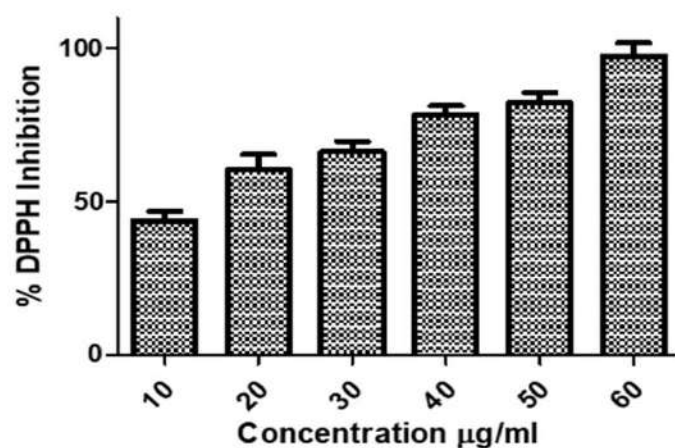


Figure 4.7 Radical scavenging assay showing the % suppression of DPPH by Se-Met-Fa NPs at various doses (10-60 $\mu\text{g/ml}$).

4.8 Discussion

Nanoparticle synthesis, coating materials, and microscopic and spectroscopic characterizations; each stage is critical for bio-nano interactions. The bio-nano interactions, stability, and therapeutic capabilities of nanomaterials combine to form important nanoparticles with the potential to become therapeutic agents. Selenium nanoparticles have been synthesized and coated with various coating materials, including dextrin, baicalin, folic acid, polyethylene glycol, and others (W. Chen et al., 2015; Fang et al., 2017; Hijaz et al., 2016; Kipper et al., 2015). Selenium in nano form offers various pro-activities such as antioxidant, anti-cancer, and anti-microbial potential, with a few negative effects such as cytotoxicity and bioavailability (Bjørklund et al., 2022; Menon, Shrudhi, et al., 2019).

The antioxidant activity and cytotoxicity of dual-coated selenium nanoparticles with methionine and folic acid were investigated in this study. In addition to cell cytotoxicity testing, nanoparticles were found to interact with macromolecules such as proteins and DNA. An investigation of DNA interactions with varied doses of SeNP not only aided in analyzing its toxic effect on DNA but also its antioxidant behavior against H₂O₂. A qualitative test was performed using basic agarose gel electrophoresis in which the DNA was subjected to Fenton-type damage using copper and H₂O₂, and the prevention of this damage was tested by treating different amounts of SeNP. The metal coordination mechanism is known to reduce oxidative damage caused by selenium compounds.

The primary benefits of *in vitro* cell toxicity experiments are as follows: 1) reduction in the number of animal models by screening the majority of substances in animal cells, 2) controlled exposure of materials, 3) less variance in results, and 4) quick investigation (V. Kumar et al., 2017). In a recent study by Ramamurthy, the *in vitro* cell viability of 25 g/ml Selenium NPs was 95%, which dropped to 45% when coupled with doxorubicin, indicating enhanced cytotoxicity (Ramamurthy et al., 2013).

Selenium NPs also shield cells from the harmful effects of arsenic by maintaining cell viability after treating arsenic-treated cells with selenium NPs. The major goal of this study was to make Se-Met-Fa NPs suitable for therapies by reducing their cytotoxicity compared to dextrin-coated Se NPs. The dyes used in this method were acridine orange, which stains dead cells and gives them red fluorescence, and ethidium bromide, which stains the DNA/RNA of the cells as green fluorescence, indicating their intact nature and viability (K. Liu et al., 2015), it was possible to

determine approximately how viable the NIH-3T3 cell lines were. According to preliminary findings, the survivability (Figure 4.5) was approximately 80%. By preserving cell viability in NIH-3T3 and raw 264.7 cell lines in the range of 70%-75% and 80%, respectively, at 0.1 μg concentration after 24 h of incubation, dual-coated Se-Met-Fa NPs have clearly solved the difficulty of toxicity, as seen in Figures 4.6 A and B. Compared to dextrin-coated Se NPs, the viability of cells increased by 10–15% with dual-coated Se–Met–Fa NPs (Malhotra et al., 2016).

Supercoiled DNA is introduced with DNA breaks into single and double strands by oxidative stress, which creates nicked DNA. Therefore, the key to seeing plasmid DNA by gel electrophoresis is to distinguish between intact DNA by observing the supercoiled bands and damaged DNA by observing the nicked circular bands (C. H. Gao et al., 2019; Guo et al., 2015). As a control, 1% sodium selenite was unable to shield the DNA from oxidative stress. This demonstrates that the ability of selenium to scavenge reactive oxygen species is enhanced at optimal concentrations and nanoscale sizes. In a previous study, the protective ability of selenium coated with dextrin against plasmid DNA damage (Malhotra et al., 2016). Selenium coated with dextrin could prevent DNA damage at a concentration of 250 μg . Similarly, as shown in Figure 4.3, Se-Met-fa NPs can preserve plasmid DNA at a concentration of 250 μg . Selenium, in various organic forms, has also been studied (Flemer, 2011; Kumar et al., 2011) because of its ability to protect against metal-induced oxidative damage. It was previously recognized that selenomethionine can protect approximately 96% of DNA from harm.

The process by which the fluorescence intensity of any biological component gradually lowers in the presence of other interacting molecules (Praktikum & Quenching, 2016) is known as quenching. Previously, protein interactions with dextrin-coated Se NPs were investigated. It was discovered that increasing the concentration of Se NPs gradually reduced BSA emission without causing a shift in the excitation wavelength. This indicates that selenium nanoparticles do not react violently with albumin. Figures 4.4 A and B show comparable results. There was no shift in the excitation wavelength peak in the UV-Vis and fluorescence spectra, and the BSA emission spectra decreased gradually as the Se NPs concentration increased. Trp-134 and Trp-212 residues of BSA exhibit this distinctive quenching behavior when they interact with tiny molecules (Papadopoulou et al., 2005; Vaughns, 2007). To further understand the protein

interactions with Se NPs, the current study used CD spectroscopy to learn more about alterations in the secondary structure of BSA.

Circular dichroism spectroscopy is a potent tool for analysing structural changes in protein molecules caused by reactive or non-reactive chemicals. The α -helix makes up approximately 67% of the BSA structure. As a result, changes in the α -helical structure can result in increased intensity in the far-UV region (Saptarshi et al., 2013). The interaction of 3-carboxyphenoxathiin with BSA reduces the intensity of the α -helical content of BSA by up to 2.7% (Varlan & Hillebrand, 2010). When Atomoxetine interacts with BSA (Buddanavar & Nandibewoor, 2017), the intensity decreases by 5.65%. When Se-Met-Fa NPs interacted with BSA, a 4.4% decrease in intensity was observed. This illustrates the safe interaction of Se-Met-Fa NPs with BSA, as the majority of the BSA structure was preserved even after conjugation.

As shown in Figure 4.7, Se-Met-Fa NPs had 50 % antioxidant activity at a concentration of 27 $\mu\text{g/ml}$, which is low compared with previous research. Boroumand et al. (2019) synthesized green selenium nanoparticles and selenium nanoparticles using polyvinyl alcohol and chitosan, respectively. Polyvinyl alcohol-Se NPs could scavenge up to 100% DPPH at 850 $\mu\text{g/ml}$, whereas chitosan-stabilized selenium nanoparticles could block approximately 82% DPPH (Zhai et al., 2017). Selenium nanoparticles synthesized from ginger extract demonstrated 50% DPPH scavenging activity at a concentration of 62.5 μg (Menon, Shrudhi, et al., 2019).

4.9 Conclusion

Se-Met-Fa NPs were tested for cytotoxicity and were found to be safe for both cell lines (NIH-3T3 and raw 267.4) at a concentration of 100 $\mu\text{g/ml}$ after 48 h of incubation. The interaction of Se-Met-Fa NPs with BSA protein was confirmed at three levels: UV spectroscopic absorbance, ground-state complex formation of BSA and nanoparticles, fluorescence emission study, which proved that the binding of BSA with nanoparticles was due to static quenching, and CD spectroscopy, which confirmed weak unfolding in the BSA peptide strands. Interaction with DNA revealed that Se-Met-Fa NPs protect against the extremely reactive OH radicals generated by metal-mediated processes. The DPPH assay yielded positive results, indicating that nanoparticles were antioxidants. Overall, it can be claimed that Se-Met-Fa NPs are simple to make, effective models, unique techniques, extremely safe for cell lines, protect against oxidative stress, naturally occurring antioxidants, and interact with albumin protein at a basic level. Therefore, it can be utilized as a therapeutic agent in biomedical applications.

Chapter 5:
Bioavailability and in
Vivo efficacy against
chronic RA

5.1 Introduction

Selenoproteins, whose functions, such as reactive oxygen species (ROS) defense, are frequently dependent on the presence of Se in their active site. As a result, both Se deficiency and excess can cause toxicity in humans, with cardiovascular and inflammatory ailments, immunosuppression and neurological conditions, type 2 diabetes, fertility/reproduction challenges, thyroid autoimmunity, and malignancy linked to Se deficiency and excess (Hariharan & Dharmaraj, 2020). Se nanoparticles (SeNPs) have a lower toxicological profile and greater biological compatibility than organic or inorganic Se molecules, drawing scientific interest for their use as therapeutic and theranostic agents (Fernandes & Gandin, 2015). SeNPs are defined as nanomaterials with an organic therapeutic core that can be stabilized/functionalized with specific chemicals or loaded with active medicines. SeNPs caused larger levels of ROS to be produced than when cancer cells were treated with selenite, implying that they had better anticancer capabilities than Se salts (Y. Huang et al., 2013). Furthermore, SeNPs have adaptable physical features such as the ability to create varied shapes based on the chemicals or solvents employed in their synthesis.

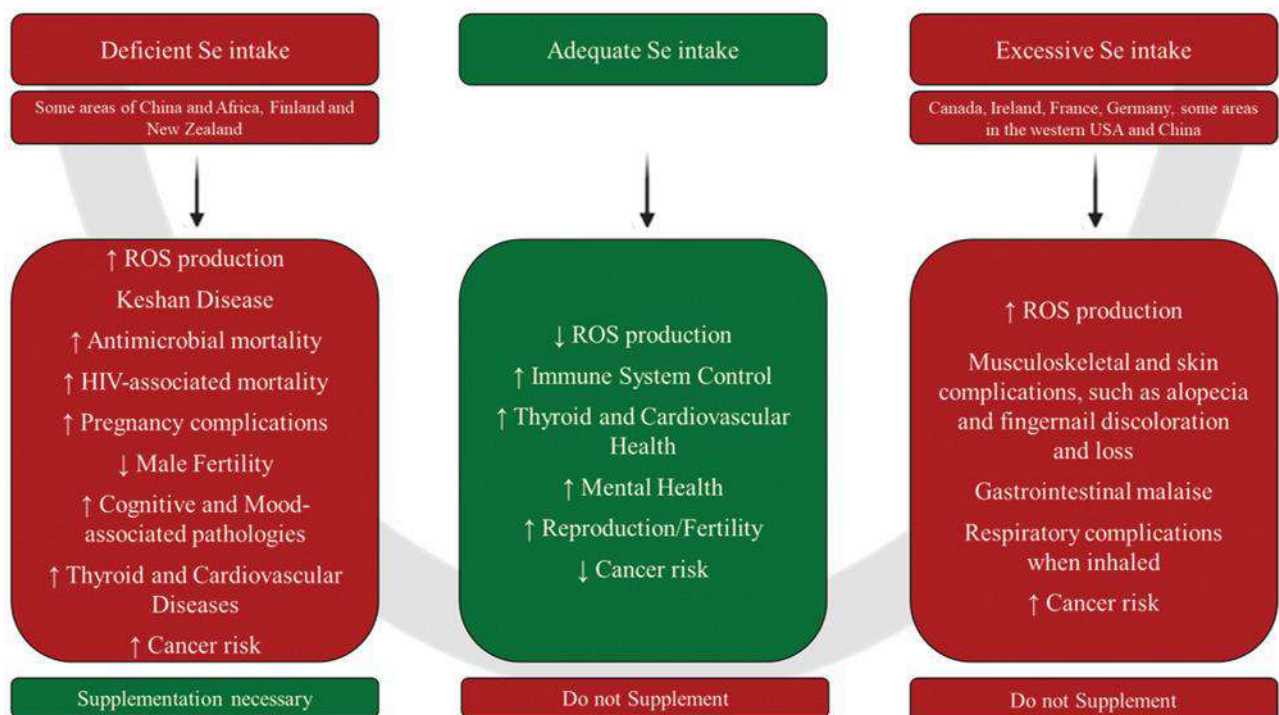


Figure 5.1 Relationship between Selenium and human health (Ferro et al., 2021).

Particle size, shape, and surface charge are all characteristics that can influence particle absorption inside the body. The size of a nanoparticle is a significant factor in its uptake by the cell and its subsequent interaction with organelles. The smaller the particle, the more efficient the uptake. Particle size also contributes to improved surface characteristics, leading to higher biological activity. This could potentially be a source of toxicity and other negative effects on the overall system. Diverse coatings on the surfaces of nanostructures also aid in particle dispersal. The surface of a NP is designed to be either hydrophobic or hydrophilic, which influences cell surface adherence, protein denaturation, and selective adsorption (Jana, 2019; Lin & Wang, 2005).

All the aforementioned variables influence particle dispersion in the system; thus, it is critical to investigate their negative impacts and enhance the design of nanoparticles to make them more biocompatible. The accumulation or delayed excretion of these particles also has negative consequences in the system; thus, long-term biocompatibility studies must be performed before employing these particles in biomedical applications.

5.1.1 Bioavailability

The ability of a dosage form to carry the medication to its site of action at a rate and amount adequate to elicit the intended pharmacological response determines the therapeutic effectiveness of any drug, whether taken from plants, animals, seafood, or synthetic sources. This feature of the dose form is known as bioavailability, biological availability, or physiological availability (Pouri et al., 2017b).

For most medications, a direct correlation exists between plasma levels and pharmacological responses. Thus, the rate and extent (quantity) of absorption of an unmodified drug from its dose form are characterized as bioavailability. When treating acute illnesses such as an asthma attack or pain, a quick commencement of the effect is sometimes sought. When the goal is to extend the duration of action or mitigate the detrimental effect and extent of absorption, which is important in the treatment of chronic illnesses such as hypertension and epilepsy, a slow rate of absorption is required. This can be accomplished by changing the dosage form's features and physicochemical qualities of the drug (Acosta, 2009; “Guidelines for Bioavailability &,” 2005).

Se bioavailability is affected by the diet consumed, with animal items having higher bioavailability than vegetables. The presence of heavy metal pollutants, such as mercury, which binds to Se to create insoluble inorganic compounds, can also influence Se levels in fish. SeMet can be found in both plants and animals, whereas selenocysteine is mostly found in animal products. SeMet improves the Se status more efficiently because it is immediately integrated into proteins, despite the fact that its breakdown into an inorganic precursor is required for it to enter the Se pool (Iwaoka et al., 2008; Schrauzer, 2000).

With the exception of selenite, which has an absorption rate of less than 60%, several Se forms exhibit an absorption rate of 70–90% under normal physiological conditions. In addition to heavy metals other than mercury, such as zinc and cadmium (Halliwell & Gutteridge, 1984), ethanol and sulfur compounds also have an impact on their bioavailability. Additionally, as higher temperatures increase protein digestion and Se release and bioavailability, food processing can also affect Se bioavailability. Owing to additive, antagonistic, or synergic interactions with Se, the overall amount of fat, protein, carbohydrates, and fiber in the meal consumed can also affect the bioavailability of Se. The overall Se level in the human body ranges from 10 to 20 mg, primarily as selenocysteine, with skeletal muscles providing half of that amount. The organs with the highest concentrations of Se are the kidneys, testes, and liver, which are primarily utilized by the immune system, erythrocytes, and platelets. Depending on the form, several Se metabolic processes may occur. The inorganic forms are reduced to selenite, whereas the organic forms are cleaved by β -lyase, and both are then employed to synthesize selenoproteins (Böck et al., 1991; Cohen et al., 2015; Johansson et al., 2005; Stadtman, 1996).

Despite their unexpected *in vitro* potential, many phytomedicines and nanomedicines have little or no substantial *in vivo* activity due to low solubility, poor lipid solubility, and incorrect size, resulting in poor absorption and bioavailability (Pouri et al., 2017c). Another issue is their structural fragility in biological environments, which leads to premature drug loss due to fast clearance and biotransformation, and some drugs are destroyed in gastric juice during gastric emptying when taken orally (Gunasekaran et al., 2014). Hence, to better understand the acceptance, solubility, and various factors that lead to drug formation, it is necessary to incorporate bioavailability and biocompatibility assays.

5.1.2 Intestinal permeability

Medications are typically administered orally because they are considered to be the safest and easiest to administer. However, it has limitations in that the medication must be absorbed from the site of absorption to the systemic circulation and then transported to the target organs to generate a pharmacological effect. Drugs are classified according to the US Food and Drug Administration's Biopharmaceutics Classification System (BCS) (Samineni et al., 2022) based on two inherent qualities that govern their oral absorption: aqueous solubility and intestinal permeability. Knowledge of these drug qualities not only aids in drug classification in the BSC but also helps candidate drug selection during the drug development process. According to the Noyes Whitney test, solubility is one of the qualities that most determines bioavailability because of its function in the dissolution process. Solubility is one of the most important and commonly studied physicochemical properties of candidate medications, because it is a thermodynamic parameter that describes the quantity of material that may dissolve in a particular solvent at equilibrium.

Permeability controls how quickly a dissolved medicine passes past the gut wall and enters the systemic circulation. Permeability is regarded as one of the most critical aspects of drug absorption. This is a complex kinetic process that is dependent on various physiological and physiochemical aspects of the drug, as well as the biophysiochemical properties of the gastrointestinal barrier membrane. The most important processes for permeation through biological barriers include passive diffusion (transcellular and paracellular), active uptake, and efflux transport (Bischoff et al., 2014).

Various techniques have been used to study intestinal absorption in detail; some include the Caco-2 cell line (human colon epithelial cell line) through the chamber, rat gut sac method (rat small intestine *ex vivo*), and working plates with paracellular movement, which consists of membranes that mimic the intestinal layer.

5.1.2.1 Caco-2 cell chamber

Caco-2 cells are a type of colon epithelial cancer cell line that are absorbed in the human digestive tract. Caco-2 cells develop tight connections between cells when cultivated as a monolayer, serving as a model of paracellular compound movement across the monolayer. Caco-2 cells also express transporter proteins, efflux proteins, and Phase II conjugation

enzymes to replicate a range of transcellular pathways as well as the metabolic transformation of test compounds. The Caco-2 cell monolayer closely resembles the human intestinal epithelium in several ways. The lack of expression of cytochrome P450 isozymes, particularly CYP3A4, which is normally expressed at high levels in the gut, is one of the functional differences between normal and Caco-2 cells. However, treatment with vitamin D3 may induce Caco-2 cells to exhibit greater amounts of CYP3A4 (Yee, 1997).

In multiwell culture plates, semipermeable plastic supports that can be placed into wells are typically used to culture Caco-2 cell monolayers. The test substances were subsequently introduced into the apical or basolateral sides of the monolayer. After incubation for varying times, aliquots of the buffer in opposing chambers were extracted to determine the concentration of test compounds and the rates of permeability for each compound (known as the apparent permeability coefficients). Although radiolabelled chemicals were employed in the original Caco-2 cell monolayer experiments, radiolabelled compounds were superseded using liquid chromatography-mass spectrometry (LC-MS) and LC-tandem mass spectrometry (LC-MS-MS). Radiolabelled substances are no longer necessary because of mass spectrometry, which also makes it possible to simultaneously measure several compounds. The detection of numerous substances per assay minimizes the number of incubations required, thus boosting the throughput of investigations. Furthermore, LC-MS and LC-MS-MS bring a new dimension to Caco-2 experiments by allowing researchers to investigate drug metabolism in Caco-2 cells (Ingels et al., 2002; Masungi et al., 2004; Van Breemen & Li, 2005).

5.1.2.2 Rat Gut sac method

Drug interactions, metabolism, and absorption are complex processes, and understanding their underlying mechanisms necessitates in-depth research. In addition to passive absorption, intestinal absorption is aided by the presence of different carriers and pumps in the intestinal epithelium. One form of pump transfers drug substrates from the intestinal mucosa to the serosal side (influx transporter), whereas another type, known as efflux pump, transports drug substrates from the serosal side to the mucosa (efflux transporter). Several inflow and efflux transporters have been identified in the intestine. P-glycoprotein (P-gp), a breast cancer resistance protein, and multidrug resistance-associated proteins are the most well-known efflux transporters that decrease intestinal absorption (M. Li et al., 2011).

Drug bioavailability decreases when efflux transporters interfere with drug absorption, which is generally undesirable. The P-gp pump is involved in various interactions with various P-gp substrates. In addition to drug-drug interactions, P-gp interacts with dietary components such as apricot extract and herbal medications. P-gp has been implicated in the development of multidrug resistance in cancer chemotherapy and numerous modulators have been identified. The influx transporters belong to the solute carrier transporter (SLC) family, several of which have been identified.

This saturable carrier-mediated transport can be influenced by both external and internal factors. Food, pharmacological compounds, ions, and other transport modulators are examples of the external stimuli that influence carrier-mediated transport. The everted sac model can be used to determine the function of carrier-mediated transport in medication absorption and interactions. The everted sac and *in vivo* models do not have an *in vitro* or *in vivo* link. Under several circumstances, two independent *in vitro* models demonstrated the same or differing absorption of the same drug. However, results from the everted intestinal sac model usually agree with *in vivo* data. Live systems are more complex than *in vitro* models; *in vitro* conditions have lower or no enzymatic activity (Alam et al., 2012; Tambe et al., 2019).

Wilson and Wiseman first presented the *in vitro* everted gut sac model in 1954, after which adjustments and enhancements were made to the model to boost tissue viability and retain intact mucosal epithelium that mimics *in vivo* circumstances. An enhanced everted gut sac model can be used to explore the processes and kinetics of drug absorption *in vitro*. The everted sac model has been extensively investigated for pharmacokinetic studies, such as drug absorption, drug metabolism or pro-drug conversion in gastrointestinal segments, efflux transport, multidrug resistance, drug interactions, and the effect of efflux transport modulators on drug absorption. The presence of a mucus layer and relatively large surface area available for absorption are the advantages of this model. However, one of the limiting criteria is the tissue viability. Under physiological conditions, the suggested tissue viability and metabolic activity of the gut were two hours. Another potential disadvantage of this method is the presence of muscularis mucosa, which is typically left in everted sac preparations (Barthe et al., 1998).

5.1.2.3 Permeapad plate technique

The most commonly described and reliable non-cellular *in vitro* permeability assays are the Parallel Artificial Membrane Permeation Assay (PAMPA) and Phospholipid Vesicle-based Permeation Assay (PVPA). As these *in vitro* approaches are only capable of assessing passive drug diffusion over different barriers, neither active nor paracellular transport can be evaluated. Since its debut, PAMPA has been shown to be a reliable and efficient approach for high-throughput screening of medicines and drug candidates in terms of permeability. The barrier that drug molecules must pass through in PAMPA is composed of filter supports that have been soaked (by immersion or spraying) in organic solvents (hexadecane/dodecane) and a small fraction of lipids. Although the PAMPA test is expensive to use, it is more time-effective than cell-based techniques. Furthermore, even in recently optimized versions, the PAMPA barrier does not reflect the biological membrane lipid composition and structure (e.g., drug permeability via a paracellular mechanism is not reflected). Because the barriers are made of phosphatidylcholine liposomes immobilized on a nitrocellulose filter substrate (similar to the cell membrane structure and tissue shape), the PVPA model produced a more biomimetic assay. Despite the fact that the PVPA barrier has a considerably higher similarity to biological tissues, its use in drug discovery research has been limited owing to the arduous and time-consuming fabrication techniques, as well as a general low resistance to additives and a short shelf life (Berben et al., 2018; Palumbo et al., 2008).

We included the most recent Permeapad™ barrier plate approach for unusual research on the intestinal permeability of selenium nanoparticles after learning about all new permeability techniques. For the drug permeability experiments, the newly released biomimetic artificial barrier Permeapad™ plate was investigated. This revolutionary barrier is projected to be more cost-effective, easy to use, and resistant to pH fluctuations than any other available type because of its unique design. The permeability barriers were fitted to Franz cell diffusion chambers and compared to log *P*_{cal} values, as well as PAMPA and Caco-2 permeability reference values (Di Cagno et al., 2015; Jacobsen et al., 2020).

5.1.3 Blood compatibility

Because nanomedicines have the potential to solve many currently unmet medical needs, it is critical to identify regulatory limitations that may impede the smooth translation of nanomedicines from laboratory to clinical applications. The blood system is especially important because many nanomedicinal products currently in development are intended for intravenous delivery, and blood system cells are among the first biological systems to be exposed to injected nanomedicine.

According to the ISO 10993-4's specified categories and assays, three blood incompatibilities were examined for *in vivo* studies: hematology (including hemolysis and leukocyte count), thrombosis, and complement activation. Endpoints for *in vitro* investigations included hematology, coagulation, platelet (aggregation and/or activation), and complement activation. (H. Huang et al., 2016a; Nimi et al., 2011).

5.1.4 Types of Arthritis

Arthritis is divided into two types: inflammatory and noninflammatory arthritis. Inflammatory arthritis is characterized by joint inflammation, pain, and swelling, caused by an overactive immune system. Examples of inflammatory arthritis include rheumatoid and psoriatic arthritis. On the other hand, non-inflammatory arthritis, also known as osteoarthritis, is caused by wear and tear on the joints over time. This type of arthritis typically occurs with age and is characterized by joint stiffness and pain.

5.1.4.1 Gout

Gout is an inflammatory arthritis that causes joint pain and swelling, usually in flares that last a week or two, and then resolves. Gout flares frequently start in the large or lower limbs. Gout occurs when high levels of serum urate accumulate in the body, which can then form needle-shaped crystals in and around the joint. This leads to joint inflammation and arthritis. Urate levels rise when the body produces too much urate or removes too little. (*Overview of Gout*, n.d.).

5.1.4.2 Reactive arthritis

Reactive arthritis is a type of seronegative spondyloarthritis characterized by inflammatory back pain, additive or migratory oligoarthritis, and extra-articular symptoms that typically occur 1–3–6 weeks after a gastrointestinal or urogenital infection. However, once arthritis is diagnosed, microbial tests and blood or synovial fluid cultures are negative, and only serum antibodies are detected. Reactive arthritis is most common in young adults who are white and harbor the HLA-B27 allele. Only 1-15% of cases of infection cases develop reactive arthritis, implying that genetic susceptibility is required. The clinical symptoms differ from those of septic arthritis, which include fever, systemic signs of infection, and monoarthritis. Reiter's syndrome is defined as a clinical subtype by the presence of large joint oligoarthritis, urogenital tract infection, and uveitis. Ocular, skin, and heart involvement is not uncommon, and their severity can vary greatly. Additionally, Reiter's syndrome is often associated with gastrointestinal symptoms such as diarrhea and abdominal pain. It is important to note that the

severity and combination of symptoms can vary greatly among individuals with Reiter's (Selmi & Gershwin, 2014).

5.1.4.3 Juvenile Idiopathic Arthritis

Juvenile idiopathic arthritis (JIA) is a diverse group of conditions that includes all forms of arthritis with unknown etiology that last for at least 6 weeks and begin before the age of 16. Due to the lack of pathognomonic features, the diagnosis of JIA is one of the exclusion criteria among all possible causes of childhood chronic arthritis. The number of joints involved, presence or absence of systemic symptoms, and presence or absence of specific antibodies were used to classify JIA. Furthermore, JIA can have long-term effects on children's physical and emotional well-being; therefore, early detection and treatment are critical for optimal outcomes.

In European and North American populations, the reported incidence and prevalence range from 2 to 20 and 16 to 150 per 100,000, respectively. However, there is a significant disparity in the frequency of the JIA subtypes across geographical areas and ethnic groups. Oligoarthritis is the most common subtype in Western countries, whereas polyarthritis predominates in Costa Rica, India, New Zealand, and South Africa. Systemic arthritis accounts for a higher proportion of childhood arthritis cases in Asia. Enthesitis-related arthritis (ERA) is more common in India, Mexico, and Canada, possibly because of the high prevalence of human leukocyte antigen (HLA)-B27. The differences in the prevalence of different subtypes of childhood arthritis across geographical areas or ethnic groups can be attributed to various factors such as genetic predisposition and environmental influences. Additionally, variations in subtype distribution highlight the importance of considering regional factors when studying and managing childhood arthritis (Giancane et al., 2016; Petty, 2016).

5.1.4.4 Fibromyalgia

Fibromyalgia is a diagnosis given to people who have chronic widespread musculoskeletal pain and no other cause, such as tissue inflammation or damage. Fibromyalgia is now thought to be, at least in part, a disorder of central pain processing that results in hyperalgesia and painful responses to nonpainful stimuli (allodynia). Changes in central pain processing may also play a role in the symptoms of several chronic pain disorders that coexist with fibromyalgia caused by genetic and environmental factors. Thus, abnormal central pain processing is linked to irritable bowel syndrome, temporomandibular disorder, chronic lower back pain, and other chronic pain conditions (Clauw, 2009).

5.1.4.5 Septic arthritis

Septic arthritis is a major concern among adults with acute monoarticular arthritis. If appropriate antibiotic therapy is not initiated within the first 24 to 48 h of onset, subchondral bone loss and permanent joint dysfunction can occur. Septic arthritis has a wide range of incidence, ranging from four to 29 cases per 100,000 person-years, and is affected by population factors, as well as pre-existing structural joint abnormalities. Because synovial tissues lack a limiting basement plate, hematogenous spread during bacteremia is the most common route of entry into the joint. Pathogens can also enter via direct inoculation (e.g., arthrocentesis, arthroscopy, trauma) or through contiguous spread from local infections (e.g., osteomyelitis, septic bursitis, abscesses). Microorganisms are deposited in the synovial membranes of joints, causing an acute inflammatory response. Inflammatory mediators and pressure from large effusions can cause joint cartilage destruction and bone loss. To ensure timely joint-preserving interventions, history, physical examination, and joint fluid analysis are required. Anti-inflammatory medications such as nonsteroidal anti-inflammatory drugs (NSAIDs) may be used in these interventions to reduce inflammation and pain. In severe cases, surgical interventions, such as joint aspiration or joint replacement, may be required to relieve symptoms and restore joint function (Lewis Horowitz & Katzap, 2011).

5.1.4.6 Osteoarthritis

Osteoarthritis is a debilitating and painful disease that affects millions of people worldwide. Its cause is unknown, but is most likely multifactorial. Osteoarthritis presents a conundrum: it frequently begins attacking various joint tissues well before middle age but cannot be diagnosed until it becomes symptomatic decades later, by which time structural alterations are well advanced. Osteoarthritis (OA) is one of the most common musculoskeletal diseases worldwide. Every 1.5 minutes, a joint in Europe is replaced due to OA. The situation is even worse in the United States, where 500,000 joint replacements are performed each year. According to conservative estimates, symptomatic OA cases represent a sizable population. Pain and functional impairment, including joint stiffness and dysfunction, are the clinical symptoms of OA. Movement is restricted to some extent in 80% of the patients with OA. This impairs workplace performance, and 25% of patients are unable to perform daily activities, which often leads to social isolation and depression. Furthermore, the economic toll of OA is substantial, with healthcare costs and lost productivity totalling billions of dollars annually. Moreover, the impact of OA extends beyond the individual, as family members and caregivers may experience increased stress and decreased quality of life because of the demands of caring for someone with OA (Bingham, 2002; Ursini & Pipicelli, 2009; Wieland et al., 2005).

5.1.4.7 Rheumatoid arthritis (RA)

Rheumatoid arthritis (RA) is a symmetric polyarticular arthritis that primarily affects the small diarthrodial joints of the forearms and feet. In addition to inflammation of the synovium, the joint lining, an aggressive front of tissue known as the pannus, invades and destroys local articular structures. Normally, the synovium is a relatively acellular structure with delicate intimal lining. In RA, CD4⁺ T cells, B cells, and macrophages infiltrate the synovium and occasionally form distinct lymphoid aggregates with germinal centers. Intimal lining hyperplasia is caused by an increase in the number of macrophage-like and fibroblast-like synoviocytes. Degradative enzymes, such as metalloproteinases, serine proteases, and aggrecanases, digest the extracellular matrix and destroy articular structures. RA affects 0.5-1.0% of the adult population worldwide, although its prevalence varies (Handa et al., 2016).

5.1.5 Evolving concepts of RA

Since the mid-twentieth century, when the first concepts of immune hyper-reactivity were considered, ideas about the pathogenesis of RA have evolved. The discovery of 'rheumatoid factor' in the blood of patients with RA provided the first indication that self-reactivity is important in the disease. The rheumatoid factor was discovered by Waaler in 1939 and rediscovered by Rose in 1948 because of its ability to agglutinate sheep red blood cells coated with rabbit serum. Kunkel's seminal research eventually identified an unknown factor as an antibody that binds to the Fc portion of immunoglobulins. This finding led to the logical conclusion that RA is an autoimmune disease that is caused by self-reactive antibodies. The rheumatoid factor is 'seropositive' in approximately 80% of patients, and its presence predicts a more aggressive and destructive course (Firestein, 2003).

5.1.6 Etiopathogenesis of RA

Synovial joint is the most common joint involved in RA. It is surrounded by articulating surfaces and synovial fluid, which aid in lubrication. The synovial joint is composed of various tissues, including the bone, cartilage, synovium, synovial fluid, ligaments, and tendons. The structural design of cartilage, which consists of chondrocytes and extracellular matrix, determines its function. RA pathogenesis is caused by a combination of genetic and environmental factors, including the HLADR4 gene, sex, and age. Viruses such as Epstein-Barr virus, herpes virus, and mycoplasma have also been implicated as etiological agents of RA. IgG antibodies against collagen type II proteins have been observed during inflammation progression. These antibodies have the potential to destroy cartilage in the early stages of RA, and rheumatoid factors exacerbate inflammation (COHEN and GOLDMAN, 1964). The presence of IgG antibodies against collagen type II proteins contributes to the destruction of cartilage in affected joints as the disease progresses. Furthermore, rheumatoid factor promotes the production of other pro-inflammatory molecules, leading to more severe symptoms and joint damage in patients with RA. Because IgG autoantibodies, macrophages, phagocytes, and cytokines, among other substances, are produced by the immune system and accumulate in the synovium to cause inflammation, they play a significant role in the pathogenesis of RA. Thickened synovial tissue can attack the cartilage and destroy the subchondral bone. Pannus

enzymes degrade nearby cartilage, infiltrating white cells, such as macrophages, and cause inflammation. Inflammation causes synovitis. The pathophysiology of RA is complex, with a network of cytokines, proteolytic enzymes, and prostanoids playing a major role. Interleukin (IL) 1 mediates pannus formation in RA and impairs the tissue repair system, causing bone and cartilage damage. Inflammation causes neutrophils, macrophages, T cells, and B cells to proliferate and differentiate. Synoviocytes produce IL-6 and MMPs in response to IL-1, resulting in proteoglycan degradation and cartilage destruction (Dell et al., 1991; Firestein, 2013; Huber et al., 2006).

Autoantibodies, known as rheumatoid factors, are produced by B cells that carry surface immunoglobulins and form immune complexes, complement fixation, neutrophil activation, and inflammation. T cells also generate autoantibodies that cause inflammation. Heat shock proteins, which are produced by all cells in response to stress, promote cross-reactivity between lymphocytes and host cells, triggering an immune response in RA. Several recent studies have found reactive oxygen species and other free radicals to be involved as mediators of tissue damage and joint inflammation via a variety of pathways. Inflammation, which is an early sign of arthritis, also causes the production of other markers such as tumor necrosis factor alpha (TNF-), interleukins, and transforming growth factor beta (TGF-). Fibroblast growth factor (FGF) and platelet-derived growth factor (PDGF) have been implicated in RA. These markers are important for the recruitment and activation of immune cells, which leads to the perpetuation of inflammation and joint destruction. Furthermore, dysregulation of these markers has been linked to systemic manifestations and extra-articular complications in RA patients (Bax et al., 2011; Gouveia et al., 2015; Hart, 1970).

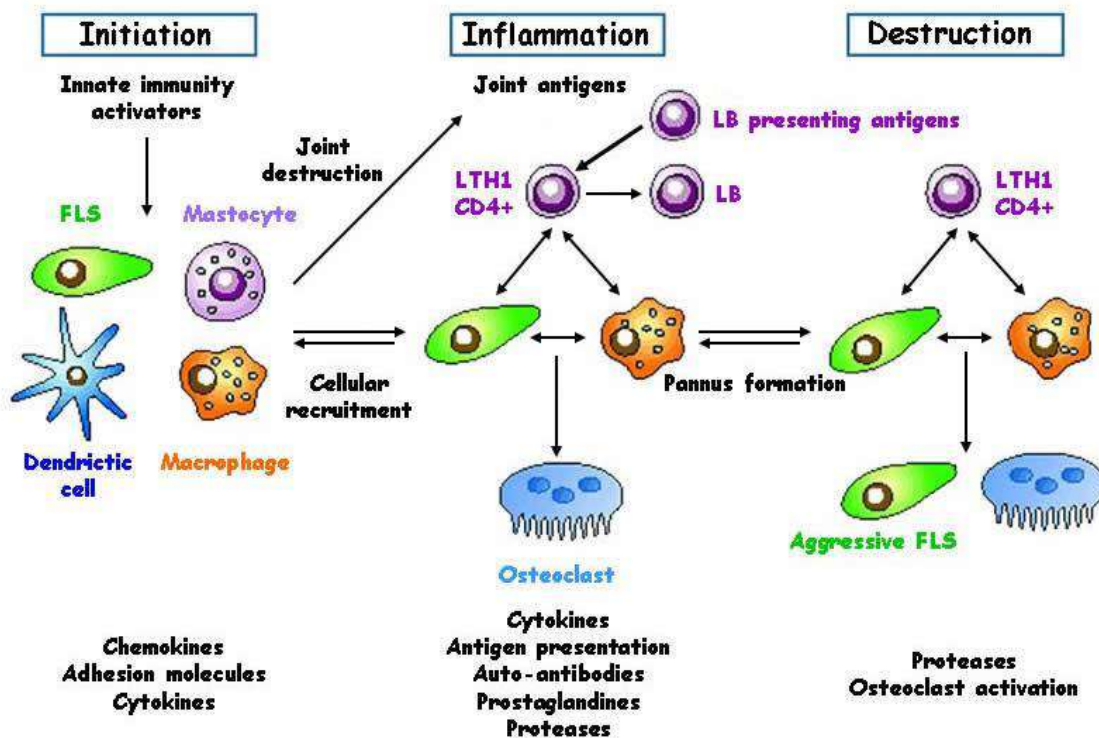


Figure 5.2 Multiple pathogenic mechanisms underlying RA (*Evolving Concepts of RA*, n.d.).

5.1.7 Potential role of reactive oxygen species (ROS) in RA

Oxidative stress is characterized by an imbalance between oxidant production and the antioxidant capacity of the cell to prevent oxidative injury. According to current thinking, oxidative stress plays a role in the pathogenesis of many human diseases, such as RA, pulmonary fibrosis, cancer, and age-related diseases. Oxidative stress occurs when the accumulation of ROS increases above physiologically normal levels. The main causes of disturbance of the oxidant-antioxidant balance and acceleration of free radical generation are stress, trauma, nutrition, exercise, immune disturbance, degenerative diseases, and hormonal imbalance (Phull et al., 2018). Different redox reactions generate partially reduced or extremely reactive oxygen metabolites; the latter are known as reactive oxygen species (ROS) and are more reactive in nature. Reactive oxidative species exist in a variety of forms and can be either radical (superoxide, hydroxyl, etc.) or non-radical (hydrogen peroxide, singlet oxygen, etc.).

Nowadays, ROS are mainly regarded as novel signal mediators that are involved in cell growth, progression, differentiation, and death. ROS are produced through a variety of extracellular and intracellular processes. Due to oxidative stress and the peroxidation of double-chain fatty

acids, DNA, and proteins, free radicals have a cytotoxic effect and are linked to a number of diseases. Cellular ROS are toxic byproducts produced during cellular metabolism that originate from a variety of sources, including mitochondria. ROS were once thought to be a host defense molecule released by neutrophils to destroy foreign pathogens, such as bacteria, but mounting evidence now indicates that ROS play a critical role as a second messenger to determine cell fate and modify a variety of signalling molecules (Paola Rosanna & Salvatore, 2012).

Oxidative stress plays a crucial role in RA pathophysiology. In RA, an altered antioxidant system and higher levels of lipid peroxidation in the serum and synovial fluid have been reported. The presence of oxidized IgG, modified low-density lipoprotein (LDL), a nitrous type II collagen peptide, and peroxidation products derived from cartilage in the serum and urine of patients with arthritis provides indirect evidence that ROS play a role in ligament deterioration. An immediate complication of ROS in chronic arthritis has been proposed because nitrated proteins, nitrotyrosine, and oxidized LDL have been seen to aggregate in the cartilage of patients with arthritis. A case-control study conducted on a cohort of 1419 grown men and women in Finland also revealed that a low antioxidant status appeared to be a risk factor for the onset and development of RA. A prospective case-control study conducted on various blood donors who developed RA found that their levels of β -carotene were significantly lower (Gracie et al., 1999; Phull et al., 2018; Sanam Dolatia, Sanam Sadreddinic, Davoud Rostamzadeha & Farhad Jadidi-Niaraghe, 2016).

5.1.8 Antioxidant System

Antioxidants, both enzymatic and non-enzymatically active, are widely used to combat ROS. By directly scavenging ROS or repairing the damage they cause, these antioxidants are essential for reducing their negative effects. Additionally, maintaining cellular homeostasis and avoiding diseases linked to oxidative stress require a balance between ROS production and antioxidant defense.

5.1.8.1 Enzymatically active antioxidants

- Superoxide dismutase (SOD)

SOD converts the harmful superoxide radical (O_2^-) into H_2O_2 , which is created when polymorphonuclear leukocytes phagocytose and partially reduce oxygen in the tissues. Arachidonic acid is converted into prostaglandin G_2 (PGG_2) and prostaglandin H_2 (PGH_2), which results in the production of ROS that are neutralized by SOD. There are

three known isoforms in the system: manganese-SOD, which is found in the mitochondrial membrane and manages oxidative stress resistance by forming non-proteinaceous manganese-based antioxidants; copper-zinc SOD, a constitutive homodimer that dismutates harmful superoxide radicals in the cytosol; and extracellular SOD, which protects type I collagen from oxidative fragmentation and maintains its integrity (MARKLUND & MARKLUND, 1974; Nandi & Chatterjee, 1988). SOD's role of SOD in the scavenging of ROS is essential for preserving cellular homeostasis and avoiding oxidative damage. The existence of these various isoforms also emphasizes the significance of compartmentalized antioxidant defense mechanisms in different cellular compartments.

- The breakdown of H₂O₂, which is produced by SOD, is carried out by the enzymes glutathione peroxidase (GPx) and catalase (CAT). GPx, a selenium-dependent enzyme, serves as a second line of defense by degrading the H₂O₂ produced in the nucleus, which is transported to the cytoplasm with the help of the tubules in the nuclear membrane. CAT degrades the H₂O₂ that is produced in the matrix and not in the peroxisome core to form water using two hydrogen atoms of H₂O₂ and liberated oxygen from the reaction (Mekail & Sharafaddin, 2009; Serfass & Ganther, 1976). By converting H₂O₂ into water and oxygen, GPx is an essential component of the nuclear defense against oxidative damage. Additionally, the nuclear membrane tubules ensure that H₂O₂ does not build up and harms the nucleus by transporting it to the cytoplasm.

Several studies have been conducted to better understand the antioxidant defence system and its role in RA. The antioxidant status was observed in male and female Wistar and Lewis rats with collagen-induced arthritis (Leonavičienė et al., 2008). Changes in the levels of serum oxidative products, such as malondialdehyde, as well as antioxidative enzymes, such as catalase, were observed in both rat strains, as well as differences in the sex of the rats. They discovered that the clinical course of the disease, as well as histological analysis, revealed that the disease is less severe in Wistar rats than in Lewis rats and that female rats are more affected than male rats. Both rat strains produced less malondialdehyde and catalase, indicating that arthritis rats were also subjected to oxidative stress. These findings indicate that oxidative stress is important for the development and progression of arthritis in both the rat strains. Furthermore, the observed sex differences highlight the potential influence of hormonal factors

on disease severity. Ramos investigated antioxidant enzymes, such as catalase and superoxide dismutase, in the spleens of female Wistar rats with Freund's adjuvant-induced arthritis. The rats were then fed with 5% cocoa laced with quercetin (Pérez-Cano et al., 2013). The effects of cocoa consumption on oxidative stress have been studied in rats with chronic inflammatory arthritis. A 5% cocoa diet supplemented with quercetin reduced ROS production and normalized SOD and CAT enzyme activities in the spleen. This suggests that drinking cocoa containing quercetin may protect against oxidative stress in chronic inflammatory arthritis. These findings highlight the potential therapeutic benefits of cocoa and quercetin in the diet of people with arthritis.

5.1.8.2 Non-enzymatically active antioxidants

Non-enzymatic antioxidant defence systems that participate in redox reactions include vitamin E, C, -carotene, and glutathione. Glutathione, a GPx substrate, is involved in several activities of the system, including ascorbic acid metabolism, cell communication, prevention of oxidation of protein thiol groups, and detoxification of reactive oxygen species. It functions as an important free-radical scavenger and aids in the maintenance of the body's oxidative stress balance. Furthermore, glutathione is important for supporting the immune system and promoting overall cellular health (Oktyabrsky & Smirnova, 2007). The plasma levels of SOD, GSH, and PGE2 were measured, and it was discovered that in the arthritis control group, the levels of SOD and GSH were reduced, while PGE2 was increased, whereas treatment with antioxidants, such as allopurinol (50 mg) and Vitamin E (100 mg), significantly increased the levels of SOD and GSH and decreased the levels of PGE2. These findings imply that allopurinol and Vitamin E may have therapeutic effects in reducing oxidative stress and inflammation in collagen-induced mice. However, further research is needed to determine the optimal dosage and combination of these antioxidants for maximum efficacy.

Previous studies have investigated the impact of oxidative stress on materials adjacent to joints, such as synovial fluid and tissues surrounding the joints, oxidative damage of hyaluronic acid (Tamer, 2013), DNA damage, oxidative damage of extracellular collagen, and oxidation of low-density lipoproteins. Researchers have determined that low levels of antioxidants, such as vitamins E and C, selenium, zinc, α -tocopherol, and β -carotene, can also be a cause of

autoimmune diseases (Galan et al., 2005). Therefore, proper disease diagnosis is required before determining the cause of the disease.

The presence or absence of clinical, laboratory, and radiological abnormalities, such as morning stiffness, arthritis in three or more joint areas, symmetric arthritis, rheumatoid nodules, and serum rheumatoid factor, were used to diagnose RA. RF is no longer regarded as a reliable method; instead, anti-cyclic citrulline proteins (ACCP) are monitored (Professor of Microbiology, 2015).

5.1.9 Biomarkers for Rheumatoid arthritis

ESR serves as an indirect indicator of the concentrations of acute-phase reactants (mainly fibrinogen). (Orr et al., 2018). C-Reactive protein (CRP) belongs to the pentraxin protein family, which includes pattern-recognition molecules involved in the innate immune response. CRP can be found in both acute and chronic inflammatory states as well as in infectious and non-infectious conditions. Low-grade CRP elevation is linked to a variety of metabolic stressors, including but not limited to atherosclerosis, obesity, type 2 diabetes, sedentary lifestyles, poor diet, and being single. CRP levels vary with age, sex, and race, but not as much as ESR levels. In addition, there is no standardized reference range or unit of measurement for CRP values, which varies between laboratories. The abundance of proinflammatory cytokines in the RA synovium stimulates the production of CRP in the liver, making it a promising candidate as a biomarker of disease activity. However, measuring CRP levels in RA is not without risks. For example, elevated CRP levels have been linked to truncal adiposity in women with RA, regardless of articular involvement or the use of biological agents (Atzeni et al., 2017; Selmi & Gershwin, 2014).

5.1.10 Rheumatoid Factor

In clinical practice, RF is an IgM antibody directed against IgG. Agglutination with sheep red blood cells (RF cross-reacts with IgG from other species) or latex particles attached to human IgG have traditionally been used to detect IgG. The dilution required to eliminate reactivity was expressed as the antibody titer. However, RF's biological functions is unknown. It is most commonly found in RA, the elderly (usually with low titers), a variety of rheumatic diseases other than RA, and a variety of neoplastic and infectious diseases. Chronic antigenic stimulation appears to be a common theme among these disorders, as might be expected in infective endocarditis or chronic active hepatitis (Shmerling & Delbanco, n.d.).

5.1.10.1 Anti-cyclic Citrullinated Peptide (ACCP)

ACCP is an autoantibody group that includes anti-perinuclear factor, anti-keratin, and anti-filaggrin antibodies. The measurement of antibodies that recognize citrullinated antigens has been developed as a diagnostic test for RA. Citrulline is a non-standard amino acid produced by the post-translational modification of arginine during inflammation. Citrulline is incorporated into proteins via a process known as citrullination. Several studies have demonstrated that ACCP is a superior diagnostic test for RF owing to its high sensitivity and specificity. According to these studies, ACCP antibodies have been detected in the early stages of RA, even before symptoms appear. Furthermore, ACCP antibodies have been discovered to be more specific to RA than to RF, implying that they are less likely to be present in other autoimmune diseases. Consequently, the use of ACCP as a diagnostic test for RA has grown in popularity in clinical practice (Niewold et al., 2007; Puszczewicz & Iwaszkiewicz, 2011).

5.1.10.2 Prostaglandin E2 (PGE₂)

PGE₂ is the most common PG produced under both physiological and pathophysiological conditions and has long been used as an immunosuppressant. This is partly because it inhibits macrophage production of inflammatory cytokines, such as IL-1 and TNF, as well as its well-documented inhibitory action on Th1 differentiation. PGE₂ was discovered in the 1980s to be produced by APCs, to inhibit the production of IL-2 and IFN-, and to suppress the proliferation of murine and human T cells *in vitro*. The effect of PGE₂ on cytokine production from Th1,

Th2, and Th0 clones was then investigated, and it was discovered that PGE₂ inhibited the production of two Th1 cytokines, IL-2 and IFN- γ , while sparing the production of the Th2 cytokine IL-4 (Deraedt et al., 1980; Kalinski, 2012).

Numerous studies have confirmed that PGE₂ affects Th1 and Th2 cells differently. Because the best-known action of PGE₂ at the time was intracellular cAMP elevation, and cAMP exerted similar Th1-selective suppression, most, if not all, studies have assigned PGE₂ as a modulator of T cells, increasing intracellular cAMP levels. EP2 and EP4 are the two PGE receptor subtypes that are linked to an increase in cAMP. T cells obtained from mice deficient in each EP subtype individually, and discovered that the immunosuppressive action of PGE₂ was significantly reduced in T cells obtained from either EP2^{-/-} or EP4^{-/-} mice, implying that both EP2 and EP4 mediate PGE₂ suppression in T cells. There is considerable evidence that PGE₂ has a Th1-suppressive effect. Surprisingly, these T cell-suppressive effects of PGE₂ have been demonstrated mostly *in vitro* and are rarely seen *in vivo*, leaving the action of PGE₂ in the immune system *in vivo*. Further research is needed to understand the disparity between *in vitro* and *in vivo* studies of the suppressive effects of PGE₂ on T cells. Other factors in the *in vivo* environment may modulate PGE₂ action on T cells, highlighting the complexity (Prempeh & Mensah-Attipoe, 2008; Ricciotti et al., 2011; Sakata et al., 2010) al., 2011; Sakata et al., 2010).

5.1.10.3 Tumor necrosis factor- α (TNF- α)

Many efforts have been made to develop medications to specifically target the important molecules involved in the pathogenesis of RA. Maini et al. made one of the first attempts to target TNF- α as one of the main cytokines in inflamed synovium, leading to one of the major advances in the treatment of inflammatory arthritis (Maini et al., 1995). Since then, more than one million patients have been treated with TNF-blocking agents and various mechanisms of action have been identified. However, TNF does not appear to be the only cytokine involved in the pathogenesis of RA. Interleukin-1 (IL-1) and IL-6 also play important roles, as inhibition of either can allow effective disease control. Other effective approaches include depleting circulating CD20⁺ B lymphocytes with a monoclonal anti-CD20 antibody and blocking the costimulatory signal (CD28-CD80/86) for T cell/APC interactions (Brennan et al., 1984).

Soluble receptors or monoclonal antibodies that bind to cytokines and compete for binding with cell surface receptors can inhibit the action of inflammatory cytokines. On the other hand,

receptor antagonists or monoclonal antibodies bind to cell surface receptors and prevent the binding of cytokines. To date, all studies have shown that targeted therapies are more effective than traditional DMARDs in reducing symptoms, reducing or stopping joint damage, and preventing functional disabilities. They have also been shown to be effective in patients with long-standing disease refractory to conventional DMARDs as well as in those with early disease. Furthermore, the majority of trials have shown that combining a TNF inhibitor with MTX is especially effective and superior to either drug alone (Caporali et al., 2009; Feldmann et al., n.d.).

5.1.11 Arthritis-Related Therapeutic Agents

Various therapeutic agents have been used to treat rheumatoid arthritis by preventing and curing its symptoms. Nonsteroidal anti-inflammatory drugs (NSAIDs), disease-modifying antirheumatic drugs (DMARDs), and biological response modifiers are examples of such therapeutic agents. NSAIDs help reduce pain and inflammation, whereas DMARDs slow disease progression. To control inflammation and joint damage, biological response modifiers target specific components of the immune system.

Analgesics, anti-inflammatory and anti-rheumatic drugs, corticosteroids, and anti-tumor necrosis factor (anti-TNF) are common therapeutic agents. Nonsteroidal anti-inflammatory drugs (NSAIDs) such as salicylates are used to reduce joint pain, swelling, and symptoms. NSAIDs have a number of side effects, including gastrointestinal (GI) tract and renal toxicity, gastric erosions, and peptic ulcers. Even if the symptoms of joint pain are relieved, the destruction continues; disease-modifying anti-rheumatic drug (DMARD) therapy such as hydroxychloroquine, sulfasalazine, methotrexate, and others are initiated to reduce or prevent joint damage and preserve joint integrity. DMARDs can cause macular damage, myelosuppression, alopecia, and hepatotoxicity. To reduce the risk of these toxicities, healthcare providers should carefully monitor patients for DMARD therapy. Regular eye examinations and liver function tests are also advised to detect any potential complications early. Low doses of glucocorticoids such as prednisolone may also be used to restore lost joint motion and alleviate symptoms that cause adverse effects, such as renal sepsis, hypertension, and hyperglycemia. Phytochemicals have been extensively studied for the treatment of arthritis. In the treatment of arthritis, various plants such as Aloe vera, Ashwagandha, Shallaki, black

pepper, black cohosh, cat claw, ginger, turmeric, and green tea are used. Recently, new biological therapies such as anti-TNF (etanercept, infliximab) have been introduced into rheumatology practice, but these may increase the risk of other infections, such as tuberculosis (Yazici & Regens, 2011). As a result, emphasis has shifted to complementary medicine. Complementary medicines, such as herbal remedies and dietary supplements, are gaining popularity as arthritis treatment. These natural remedies may be beneficial for reducing inflammation and managing pain without the risks associated with conventional medications. To ensure safety and effectiveness, consult a healthcare professional before incorporating any complementary medicine into the arthritis treatment plan. With growing evidence of the role of free radicals, antioxidant therapy may represent an alternative approach. Antioxidant therapy aims to reduce oxidative stress and neutralize free radicals, which are thought to contribute to the development and progression of arthritis (Wright 1986).

Vitamin E, folate, zinc, iron, selenium, and other antioxidant supplements have long been advocated for the treatment of rheumatoid arthritis (RA), osteoarthritis (OA), and other inflammatory arthritis. Patients with RA have lower selenium concentrations than healthy individuals do. An epidemiological study suggested that low selenium and -tocopherol levels may increase the risk of developing diseases, such as rheumatoid arthritis. Selenium is an essential micronutrient found in foods, such as fish and wheat (Fairweather-Tait et al., n.d.). This metalloid is the primary constituent of selenoenzymes, which have been shown to protect animal cells from oxidative damage. By increasing glutathione (GSH) synthesis and release in the liver along with a corresponding rise in plasma GSH, Se deficiency affects glutathione (GSH) metabolism, which further causes cysteine depletion and impairs protein synthesis (Mekail & Sharafaddin, 2009; Y. Wang, 2009). Although selenium is a potential micronutrient supplement for the treatment of rheumatoid arthritis, its dose and chemical form play an important role in its bioavailability, toxicity, and biological properties. Selenium nanoparticles, as an alternative to seleno-compounds, may be potential antioxidant therapeutic agents for the treatment of RA.

Nanotechnology is a relatively new line of treatment, and various forms of nanoparticles are used to treat rheumatology. Effect of AuNPs in the treatment of collagen-induced arthritis in Wistar rats (Khan et al., 2012). AuNPs of 13 nm (50 µg/ml initial concentration of gold) and 50 nm (188 µg/ml initial concentration of gold) were injected intra-articularly at the ankle joints of rats in this study. The treatment consisted of 12 injections. Body and organ weights, arthritic

profiles based on paw swelling, histological changes in joints and internal organs, blood indices, and serum catalase activity were investigated. Serum enzyme levels were elevated, and arthritis symptoms were lessened by using nanoparticles of both sizes. Thomas et al. (2012) investigated the use of folic acid-G5 dendrimer nanoparticles to target macrophages and deliver methotrexate in rats with collagen-induced arthritis. Three times per week for 17 days, a treatment regimen of 70 mg/kg conjugated nanoparticles containing 5 mg/kg methotrexate was used. The conjugate reduced arthritis symptoms, such as paw volume, joint swelling, cartilage damage, and bone resorption, by acting as an anti-inflammatory agent. Therefore, several animal models must be experimentally induced with particular agents to cause arthritis in order to test for arthritis and demonstrate the safety, dosage, and efficacy of these therapeutic agents.

5.1.12 Animal Models for Chronic inflammatory arthritis

Several animal models have been used in this study. These models have unique benefits and constraints at the beginning of a clinical process. However, crucial standards for selecting an appropriate RA animal model include the following: 1) the ability to assess the effectiveness of therapeutic interventions in humans, 2) the model's striking resemblance to human RA, 3) simple handling, 4) repeatable data, 5) a test period with a reasonable length, 6) an easy start, and 7) the target must be verified. To better understand disease mechanisms and potential treatments, it is essential for animal models to display similar pathological traits and immune responses to human RA. To extrapolate the results to patients with RA more accurately, the chosen animal model should also have a genetic predisposition or be prone to developing RA-like symptoms (Dustin, 2003).

Adjuvant-induced arthritis, collagen-induced arthritis, cartilage oligometric matrix protein-induced arthritis, pristane-induced arthritis, and *streptococcal* cell wall-induced arthritis are some of the animal models used for the experimental induction of rheumatoid arthritis in rats.

5.1.12.1 Adjuvant induced arthritis (AIA)

This popular rat model has been used to evaluate the effectiveness of various anti-arthritic medications. Complete Freund's adjuvant is intradermally injected into rats to cause it in the

area around the paws or the base of the tail (CFA) (Bauerova et al., 2012). Their susceptibility to AIA is influenced by the MHC and non-MHC genes. In contrast to human RA, CFA is characterized by a rapid onset of the disease, with symptoms such as joint swelling, lymphocyte infiltration, cartilage degradation, and polyarticular inflammation appearing within seven days. The primary cause of every immune response produced in rats with AIA is the T cells. The antigens in CFA activate these T cells, causing the release of cytokines and chemokines that promote inflammation. The pathogenesis of AIA in rats is also aided by the activation of B cells and creation of autoantibodies (Freund et al., 2011).

5.1.12.2 Collagen induced arthritis (CIA)

The most popular Th1-mediated model is controlled by both innate and adaptive immunities. Type II collagen, which is prevalent in articular cartilage, is a target of autoimmune diseases that result in chronic inflammatory joint disease. The disease begins after 12–18 days and progresses over 35–42 days. The fore and hind paws are the only joints in which CIA can occur. CIA lesions are comparable to RA lesions in humans. Inflammatory cells and proteolytic enzymes are released by neutrophils and monocytes in the joints, which control CIA pathogenesis. In the CIA model, MHC class II molecules were responsible for RA development. Collagen-specific B cells are essential for maintaining disease severity in CIA rats. Additionally, the development of CIA is aided by the activation of T cells and the production of pro-inflammatory cytokines, such as TNF- α and IL-1. Likewise, research has demonstrated that inhibiting these cytokines can lessen symptoms and joint damage in CIA rats (Chunxia et al., 2011; Leonavičienė et al., 2008; Zahidah et al., 2012; Zhou et al., 2007).

5.1.12.3 Cartilage oligometric matrix protein induced arthritis

RA affects peripheral cartilaginous joints, and one of the underlying causes may be an immune reaction to proteins in the cartilage, such as cartilage oligometric matrix proteins. This is comparable to the response to RA in humans. It is a self-limiting illness that can last for a maximum of 43 days without the development of chronic lesions. The immune reaction to COMP is genetically controlled by the MHC. Compared with AIA or CIA, many more genes are involved in the pathophysiology of arthritis in rats. Additionally, rats were administered intradermal injections of COMP at the base of their tail. This injection site was selected because

it is simple to track and gauge immune response. Furthermore, intradermal injections of COMP have been shown to induce a localized inflammatory response in joints, mimicking the pathogenesis of arthritis (Webb, 2018).

5.1.12.4 Pristane induced arthritis

It is a preclinical model of arthritis that exhibits traits similar to those of human RA, such as the chronic relapsing nature of the disease, erosive destruction of joints, inflammation, and T cell infiltration. The rats receive a 150 µl intradermal injection of pristane. The rat immune system reacts to the injection of pristane by developing symptoms of arthritis. With the aid of this preclinical model, researchers can examine the effectiveness of potential rheumatoid arthritis treatments and gain a deeper understanding of the underlying mechanisms of RA. Within two to three weeks, the disease manifests. The study lasted for 28 days in these rats. This preclinical model offers important insights into the onset and progression of systemic lupus, in addition to investigating the effectiveness of potential treatments for rheumatoid arthritis (SLE). Researchers can learn more about the underlying mechanisms of SLE and consider novel therapeutic modalities by observing the production of autoantibodies in rats (Bauerova et al., 2012; Dustin, 2003).

5.1.12.5 *Streptococcal* cell wall induced arthritis

Streptococcus pyogenes was used for cell wall-induced arthritis in rats. It is capable of using a purified peptidoglycan-polysaccharide (PG-PS) polymer, which causes severe inflammation and arthritis in rats. In rats, this polymer stimulates the immune system and initiates an inflammatory process that results in the onset of arthritis. *Streptococcus pyogenes* was used in this experimental model to shed light on the pathogenesis of arthritis in humans and possible treatments. Initiating two distinct models, Polyarticular and Monoarticular, two different types of PGPS fragments are used via two different routes of administration. These models are not used as often because of their expensive maintenance requirements. This model has an advantage over other models because it can be used to study acute arthritis (Bauerova et al., 2012; Bevaart et al., 2010).

5.2 Materials

Molychem supplied analytical-grade sodium selenite (product code 18770), HPLC (deionized water), L-methionine (product code 15900), and ascorbic acid (product code 12480). For both assays, prepared in ultra-pure HPLC water, 1X Phosphate Buffer Saline (PBS) buffer was used (Molychem). Human blood was drawn using EDTA-coated vacutainers (BECTON DICKINSON). Human blood was acquired from 6 volunteers. This study was approved by university ethics committee (NMIMS/IEC/016/2020). Permeability assays were performed using an ElectroLab Permeapad 96-well plate. Folic acid (product code F8758) and complete Freund's adjuvant (CFA) were procured from Sigma-Aldrich. (St. Louis Mo. USA)

5.3 Methodology

SeMetFa NPs were prepared by reducing sodium selenite with ascorbic acid as the precursor. To improve bioavailability and stability, NPs were coated with methionine and folic acid. They were examined using several characterization procedures, such as UV-Vis spectrophotometry, FTIR, ZETA potential, XRD, Raman spectroscopy, ICP-AES, DSC, and TEM. The average size of SeMetFa NPs was approximately 50 nm.

5.3.1 Blood compatibility of SeMetFa NPs

Freshly drawn EDTA-stabilized human blood was collected in a vacutainer. A total of 5.0 ml of blood was drawn from six healthy volunteers. The institutional ethics committee of NMIMS/IEC/016/2020 approved this study.

A preliminary assay used as a safety precaution for dual-coated Se NPs is the blood hemolysis assay. Basic biocompatibility and bioavailability procedures should be applied in any study that has the potential to result in animal efficacy or clinical trials. Before conducting animal efficacy studies, one of the preliminary procedures was the hemolysis assay, which can reveal any harm caused by Se NPs.

5.3.1.1 Hemolysis assay

A 5.0 ml sample of human blood was stabilized with EDTA and centrifuged at 127.18 g for 5 min. The red blood cell pellets obtained were washed twice with PBS after centrifugation. Subsequently, the RBC were suspended in 5 ml of PBS and this was further diluted in 1:4 ratio. Se NPs were suspended in 0.8 ml of PBS at three different concentrations (50, 100, and 200 g/ml). A 0.2 ml RBC suspension was added to a 0.8 ml Se NPs + PBS solution. Positive and negative controls were prepared by combining 0.2 mL of RBC suspension (0.8 mL with distilled water and PBS, respectively). The samples were then incubated for 2 h at 37 °C with 15-minute intervals of shaking. The samples were centrifuged again (PerkinElmer) for 5 min at 1200 rpm for 2 h to check for any signs of hemolysis. Later, 100 µL samples were transferred to 96 well plates and absorbance was measured at 570 nm and 655 nm on using a microplate reader (Biotek, Epoc). The following formula was used to calculate the percentage of hemolysis:

$$\% \text{Hemolysis} = \frac{(\text{Absorbance of sample} - \text{Absorbance of negative control})}{(\text{Absorbance of positive control} - \text{Absorbance of negative control})} \times 100$$

5.3.2 Intestinal permeability assay

A 96-well microtiter plate system that is ready to use is the Permeapad® plate (Electro Lab). Permeapad® plate barrier layer mimics the intestinal barrier, allowing for quick and repeatable *in vitro* permeability studies. The electro lab provided prototypes of the Permeapad® plate. The Permeapad® 96 well plate was divided into two compartments: the upper (donor) and lower (recipient) compartments (receiver). A phospholipid-based barrier separates the compartments. In addition, there is another inlet in the donor-receiver well that allows direct sampling from the receiver end without disturbing the membrane or donor compartment. Permeation was possible over a total area of 0.15 cm².

5.3.2.1 Sample preparation

A Permeapad® plate was used to test the intestinal permeability of selenium nanoparticles with dual coatings (SeMetFa NPs) and without coating (SeMetFa NPs). Colloidal solutions of 100 µg/ml concentration were prepared in phosphate-buffered saline (PBS). Before the experiment, six different pH solutions (2, 4, 6, 7, 8, and 10) were prepared for each sample. For each time point, three sets of SeMetFa and Se NPs were prepared. The Permeapad® plate was incubated at 37 °C for 2 hours-4 hours-24 hours after carefully adding 200 µl of each sample to the donor compartment. Following each time point, specimens were taken using an extra inlet via syringe and collected on a glass 6-well plate, and the spectrum was checked from 200-500 nm on a Bio-Rad ELISA reader. The results were read at 265 nm.

5.3.2.2 Data analysis

The estimated number of nanoparticles that successfully crossed the Permeapad® barrier, as measured by the apparent permeability (Papp), for SeMetFa NPs was calculated. The total number of nanoparticles that successfully crossed the Permeapad® barrier, as measured in grams per ml of concentration, is known as the apparent permeability (Papp) of SeMetFa NPs. The surface area of the well (A:0.15 cm²) and amount of time (dt) were used to normalize the permeated nanoparticles (dQ). The steady-state permeation time points were 2, 4, and 24 h. J

represents the flux, which represents the linearity of the graph. For this permeability experiment, the flux J is given by the following equation:

$$J = \frac{dQ}{A \cdot dt}$$

In this permeation experiment, the flux J was divided by the amount of drug present in the donor compartment C_0 to determine the apparent permeability coefficient (P_{app}) (Gunasekaran et al., 2014).

$$P_{app} = \frac{J}{C_0}$$

The percentage permeation was calculated as follows:

$$P\% = \frac{P_{app}}{\text{Control}P_{app}} \times 100$$

The control sample is a blank sample containing only Phosphate buffered saline (PBS). The permeation experiment was repeated thrice. The standard deviations of each sample were determined independently and cumulatively and are shown with error bars.

5.3.3 Housing of animal models

All animal investigations were conducted after the IAEC granted animal ethical clearance (CPCSEA/IAEC/P-11/2019). Bharat Serum and Vaccines Pvt. Ltd., Mumbai, India, were the suppliers of Wistar rats. The animals were acclimatized to laboratory conditions prior to the start of the investigation. These animals were housed for 14 days prior to the commencement of the experiment under regular conditions of temperature (23 \pm 1 °C) and 12 h of light and dark cycles and were provided food and water ad libitum until the end of the study.

5.3.4 Grouping of animals

Six animals per group were randomly assigned to the 42 male Wistar rats (180-200 g; 8-10 weeks) in the following groups:

Group I: Unaffected by disease.

Group II: Arthritic control, induced by 0.1 mL of CFA.

Carboxymethylcellulose (CMC-Vehicle control) Group III

Group IV: Prednisolone (10 µg/kg body weight).

SeMetFa nanoparticles (250 µg/kg.b.w.) were observed in Group V.

SeMetFa nanoparticles (500 µg/kg body weight) were observed in Group VI.

SeMetFa nanoparticles (750 µg/kg body weight) were observed in Group VII.

5.3.5 Anti-arthritic study

Different concentrations of SeMetFa NP (250, 500, and 750 g/kg b.w.) were compared with the positive control group, which consisted of prednisolone (10 mg/kg b.w.), a commonly prescribed medication. Groups II, III, IV, V, VI, and VII received 0.1 ml CFA intradermally in the paw region. During the first 21 days of inflammation, the animals were administered the standard drug as well as different concentrations of SeMetFa NP. For 21 days, the percent increase in inflammation of the paw volume was measured using a digital Vernier caliper. After 21 days, the animals were humanely sacrificed, and various organs, such as the spleen, kidney, and liver, were dissected. Blood was collected from each animal through a heart puncture. For histopathological and radiological analysis, the paw region was dissected and preserved in 10% formalin at RT.

5.3.5.1 Inflammatory marker study

Following sacrifice, the blood samples were collected in vials. Serum was separated from blood immediately by centrifuging at 1000 g for 10 minutes at 4°C. Serum was then tested for C-reactive protein (OVI diagnostics), prostaglandin E2 (PGE2), and TNF-α using the Biotech desk kit from India and the Everon life sciences kit from India.

- CRP protein

A quantitative turbidimetric assay was used to measure serum CRP levels. Before use, the CRP calibrator was reconstituted with 1 ml distilled water and incubated for 10 min at room temperature. The diluent (450 μ L) and latex reagent (50 μ L) were combined to prepare the working reagent. The reaction mixture contained 500 μ L of the working reagent and 5 μ L of the sample or calibrator. At 540 nm, readings were taken 10 s (A1) and 120 s (A2) after the addition of the sample.

Formula for calculations,

$$\text{CRP (mg/L)} = \frac{\text{O.D.of test (A2-A1)}}{\text{O.D.of calibrator (A2-A1)}} \times \text{Conc. of calibrator}$$

- Prostaglandin PGE₂ assay

This was a quantitative test. Before use, the wash buffer was brought to room temperature and the crystals were dissolved. Distilled water was used to dilute the wash buffer (20 ml wash buffer to 500 ml). Substrate solutions were prepared and light-protected by mixing equal volumes of color reagents A and B within 15 minutes of use. Distilled water was used to rehydrate PGE₂ standards. Standard stock solutions of 25,000 pg/ml were prepared and allowed to stand for 15 minutes before use. Dilutions are made. As shown in Fig 5.3, 900 μ L of calibrator diluent was added to the first dilution tube, and 500 μ L was added to the remaining six tubes. Subsequently, light mixing was performed. The highest dilution among the seven dilution tubes was 2500 pg/ml, whereas the blank tube contained only the calibrator diluent. After preparing dilutions of the sample and standard, all additions were performed in a 96 well plate. Nonspecific Binding (NSB) wells, Zero Standard (B0) wells, Standard wells, and Sample wells were labelled on the plate. Calibrator diluent RD5-56 was added to the wells as follows: 200 μ L in the NSB well and 150 μ L in all other wells. Next, 50 μ L of Primary Antibody Solution was added to each well, except the NSB well, turning the solution blue. The plate was sealed and incubated for an hour at room temperature on a horizontal shaker set to 500 rpm. Following incubation, 50 μ L of PGE₂

Conjugate was added to each well, except the NSB well, changing the color to violet. The plate was then incubated for 2 h under the same conditions as described above.

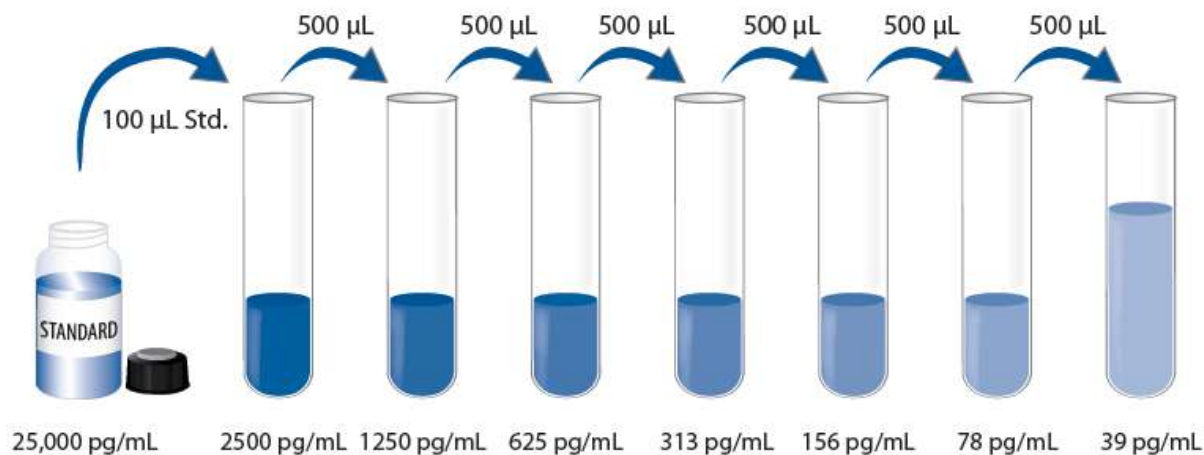


Figure 5.3 Preparations of PGE₂ standards

Each well was aspirated and washed four washes after two hours of incubation by adding 400 µL Wash Buffer using a squirt bottle. To achieve a good performance, the liquid was completely removed at each step. After the last wash, the plate was inverted on clean paper towels to blot the remaining liquid. Each well received 200 µL of the Substrate Solution, and the plate was incubated for 30 min at room temperature under static conditions in the dark. Following incubation, 100 µL Stop Solution was added to each well and thoroughly mixed, changing the color from violet to yellow.

Calculations:

The average of duplicate readings for each sample was subtracted from the average NSB O.D.. The corresponding mean absorbance for each standard was plotted against concentration to create a standard curve. The concentration of PGE₂ was calculated from the mean absorbance of the standard curve. Finally, the curve values were multiplied by a dilution factor to obtain the actual concentration.

- Tumor Necrosis Factor- α (TNF- α)

Rat TNF- α can be quantitatively measured in serum, plasma, and cell culture supernatants using the rat TNF- α ELISA kit, an *in vitro* enzyme-linked immunosorbent assay. This assay

uses a 96-well plate coated with an antibody specific for rat TNF- α . TNF- α present in a sample was bound to the wells by the immobilized antibody after the standards and samples were pipetted into the wells. After washing the wells, biotinylated anti-Rat TNF- α antibody was added. Following removal of the unbound biotinylated antibody, HRP-conjugated streptavidin was pipetted into the wells. A TMB substrate solution was added to the wells after the wells had been washed once more, and color developed in direct proportion to the amount of TNF- α bound. The Stop Solution changed color from blue to yellow, and the color intensity was measured at 450 nm.

Assay Procedure:

Before use, all the reagents and samples were stored at room temperature (18 – 25 °C). It is recommended to run all standards and samples at least twice. Appropriate wells were filled with 100 μ L of each standard (provided in the kit) and sample. The wells were covered and shaken gently for 2.5 hours at room temperature. The solution was discarded after four washes with a 1X Wash Solution. Each well was then filled with wash buffer using a multichannel pipette or auto-washer. To achieve optimal performance, the liquids were completely removed. After the last wash, any remaining Wash Buffer was aspirated or decanted. The plate was inverted and blotted using clean paper towels. To each well, 100 μ l of 1X prepared biotinylated antibody was added. The mixture was then incubated at room temperature for 1 h with gentle shaking. The solution was discarded. The washing procedure was repeated in step 4. Each well received 100 μ L of streptavidin solution. The mixture was then incubated at room temperature for 45 min with gentle shaking. The solution was discarded. The washing procedure was repeated in step 4. Each well received 100 μ L of TMB One-Step Substrate Reagent (Item H). The mixture was then incubated at room temperature in the dark for 30 min with gentle shaking. Finally, 50 μ L of the Stop Solution (Item I) was added to each well. Immediately read at 450 nm

Calculation of the results

The average optical density of the zero standard was subtracted after calculating the mean absorbance of each set of duplicate standards, controls, and samples. The standard curve was plotted on a log-log graph paper or with Sigma plot software, with the standard

concentration on the x-axis and absorbance on the y-axis. The best-fit straight line was drawn using the standard points.

5.3.5.2 Antioxidant enzyme assay

The dissected organs were weighed (1 g each) and homogenized in 5 ml of 10 mM cold phosphate buffer (pH 7.0 before being centrifuged at $8000 \times g$ for 10 min at 4 °C. The supernatant was aliquoted and the protein content in each organ tissue was estimated using Lowry's method (LOWRY et al., 1951). Protein concentrations were estimated using a standard curve, with BSA serving as the standard protein. Several solutions were prepared using this method, including Solution A, which contained 2% (w/v) Na₂CO₃ in 0.1 N NaOH, Solution B, which contained 1% (w/v) CuSO₄·5H₂O in DW, and Solution C, which contained 2% (w/v) sodium potassium tartrate in DW. Table 5.1 shows how the dilutions were prepared. Levels of enzymes such as Superoxide Dismutase (SOD), catalase (CAT), and Glutathione Peroxidase (GPx) were measured in these organs (GPx).

- Assay for Superoxide dismutase (SOD)

SOD activity was measured using assay of Marklund and Marklund and Malhotra et al's with modifications (Malhotra et al., 2016; MARKLUND & MARKLUND, 1974). The autoxidation of pyrogallol was determined 3 mins and this was used as a blank. The reaction mixture contained 50 mM Tris-EDTA buffer (pH 8.2), 4 mM pyrogallol, and 100 mg liver protein or 200 mg kidney and spleen proteins, as appropriate. Absorbance was measured at 420 nm for 3 min. Enzyme activity was expressed in units/mg protein, where one unit is the amount of enzyme required to inhibit pyrogallol autooxidation by approximately 50%.

- Assay for Catalase (CAT)

Liu and Wang's method was used with modifications to estimate the level of catalase enzyme. Protein (200 mg) was extracted from various tissues, along with 10 mM potassium phosphate buffer (pH 7.4), to make up the reaction mixture. 19.6 mM H₂O₂ was added to start the reaction, and a 2-minute decrease in absorbance at 240 nm was noted. One unit of enzyme is equal to the quantity needed to break down 1.0 mmol of H₂O₂ in one minute, and enzyme activity was expressed as units/mg of protein.(L. Wang et al., 2011)

- Assay for Glutathione peroxidase (GPx)

Rotruck et al. evaluated the glutathione peroxidase enzyme activity and described their findings (D. Peng et al., 2007; Saalu et al., 2010). The reaction mixture included 2 ml of deionized water, 100 mg of tissue-derived protein, 0.2 ml of 1 mM reduced GSH, 0.1 ml of 2 mM H₂O₂, 0.1 ml of 10 mM sodium azide, and 0.2 ml of 0.2 M phosphate buffer with a pH of 7.6. The mixture was then incubated for 10 min at 37 °C. This mixture was post-incubated with 0.4 ml of 5% TCA and centrifuged at 3200 g for 20 min. Ellman's reagent (1 ml of Ellman reagent was added to 0.2 ml of supernatant, and the mixture was incubated at 20 °C for 5 min. Absorbance was measured at 412 nm. One unit of GPx enzyme was used to express enzyme activity in units/mg protein. 1 unit of GPx is the amount of enzyme necessary to catalyze the oxidation (by H₂O₂) of 1 μmole GSH to GSSG, per minute at 25 °C, pH 7.0.

5.3.6 Histopathological findings

Selective organ histopathology, including that of the liver, kidneys, spleen, and hind paw, was performed. The animal paws were removed, dissected, and preserved in 10% formalin for three days. By treating the tissue with 5% nitric acid for 72 h with four changes in the acid solution, decalcification of the bones was achieved. The softened bony tissues were processed for a histological procedure using alcohol-xylene for 24 h while being kept in 10% formalin solution (for dehydration and cleansing of tissue). To remove fixative from the tissues, 4–6 h of exposure to 50% absolute alcohol was used. Following this, the tissues were kept in increasing concentrations of alcohol (70–90%) for two hours each and then in pure alcohol for two hours. Xylene was used to clean tissues for three to four cycles lasting two hours each. The tissues were then transferred and left in liquid paraffin for three–five hours. Subsequently, the tissues were sectioned (4-5 m) using an automated microtome after being embedded in paraffin blocks (OVI diagnostics). According to the modified Drury method, the tissue sections were stained with hematoxylin and eosin (Malhotra et al., 2016). All tissues were examined microscopically, and microphotographs were taken. A skilled veterinary histopathologist at OVI Diagnostics in Mumbai performed histopathological evaluation. Scores were assigned to H&E slides based on the level of

inflammation seen: minimal lesions 10% (+), mild lesions 11-25% (++) , moderate lesions 26-75% (+++), and severe lesions 76-100% (++++).

5.3.7 Radiographical findings

The hind paws of each group of rats were radiographically evaluated (Wipro GE Dx300 X-ray unit at OVI diagnostics, Mumbai). Lateral imaging was performed on Days 0 and 21. According to the following criteria, radiographic assessment was graded from 0 to 4 as follows: 0, no change; 1, minimal changes; 2, mild changes; 3, moderate changes; and 4, severe changes.

5.3.8 Statistical data analysis

Each piece of data is presented as the mean \pm standard deviation. Using the Prism 5.0 program, data interpolation, including data from standard curves, was carried out (GraphPad Software Inc., CA, USA). Dunnett's multiple comparison tests were used after the one-way ANOVA to determine the statistical significance. Differences between groups were deemed significant at $p < 0.05$.

5.4 Results

5.4.1 Blood Compatibility assay

RBC hemolysis, which denotes blood incompatibility, and no hemolysis, which denotes blood compatibility, were used to interpret the results. When comparing the tube containing Se nanoparticles to the positive control (distilled water) used for the assay shown in figures 5.4, RBC hemolysis was not observed (a, c, and d). At 570 nm, the positive control had the highest optical density (OD), which was 1.3 and indicated blood hemolysis. However, neither the coated nor uncoated Se nanoparticles displayed an OD greater than 0.03, indicating the absence of blood hemolysis. Phosphate-buffered saline (PBS) was used as a negative control, with an optical density (OD less than 0.03 indicating no hemolysis. The percentage of hemolysis for each sample is shown in Figure 5.4(b). Hemolysis was observed in 100% of positive controls. Concentrations of 50, 100, and 200 $\mu\text{g/ml}$ were used for each set of coated and uncoated Se NPs. Compared to other concentrations, RBC hemolysis was the lowest with SeMetFa NPs at a concentration of 50 $\mu\text{g/ml}$.

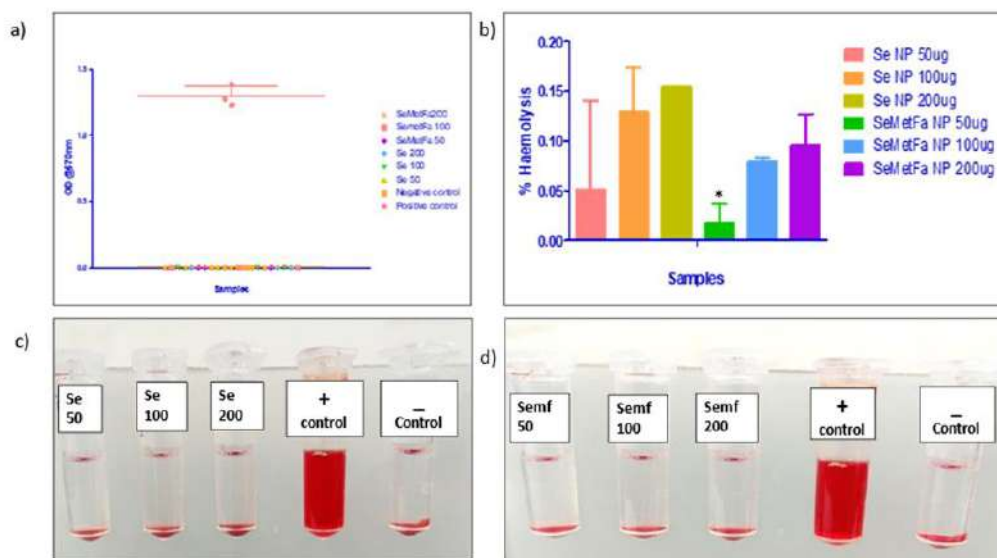


Figure 5.4 (a) shows a graph of coated and uncoated objects. Compare the nanoparticles in nm was compared to their size. (b) Graph showing Se and SeMetFa NPs against percentage of hemolysis. (C and d) Illustrations of Se NPs and SeMetFa NPs at concentrations of 50, 100, and 200 $\mu\text{g/ml}$, respectively. Distilled water and blood samples were used as positive

and negative controls, respectively. Taking into account the mean and standard deviation, each plot contained readings in triplicate. One-way ANOVA with Tukey's test and multiple comparisons taking into account * $p < .05$, ** $p < .01$, and *** $p < .001$ were used to analyze the percentage of hemolysis. The SeMetFa NPs were denoted as SeMF.

5.4.2 Intestinal permeability

A wide pH range (2, 4, 6, 7, 8, and 10) and various time points (2, 4, and 24 h) were added to the permeability assay. The apparent permeabilities of the Se and SeMetFa NPs are plotted in figures 5.5(a) and (b), respectively. For samples incubated for 2 and 4 h, the proton transfer of NPs in both samples did not vary significantly in the pH range of 2 to 8. At pH 10, the plot exhibited variability with an increase in apparent permeability. Papp for SeMetFa NPs increased by 1.5×10^{-6} cm/s in comparison to Se NPs at the same pH 10 when figures 5.5 (a) and (b) are compared in a single graph plotted in Figure 5.5 (c) (incubated for 24 h). Similarly, after 4 h of incubation, the Papp of SeMetFa NPs increased by 1.2×10^{-6} cm/s in comparison to Se NPs. There was no discernible difference in Papp between the samples incubated for 2 h.

Various time points were considered in the study of the barrier integrity. Figure 5.5 c shows that Papp for both samples increased as the incubation time increased. For Se NPs, the difference between samples incubated for 2- and 4-hours was 3.5×10^{-6} cm/s, at 4- and 24-hours, 4.5×10^{-6} cm/s, and between 2- and 24-hours, about 16×10^{-6} cm/s. For SeMetFa NPs, the difference between 2- and 4-hour samples was approximately 4.5×10^{-6} cm/s, between 4- and 24-hour samples was approximately 5×10^{-6} cm/s, and between 2- and 24-hour samples was approximately 22.5×10^{-6} cm/s. % Permeability has been calculated for each sample at each pH level for a 24-hour period in figure 5.5 d. Overall, for both sets of NPs, the 24-hour Papp was the highest. The percentage of the control group was assumed to be 100%. When comparing coated and uncoated NPs, it was found that SeMetFa NPs had a permeability of approximately 70% at pH 10. Between 50 and 70 percent permeability was observed for SeMetFa NPs in the pH range of 2 to 10. Similarly, it can be seen that the % Permeability for Se NPs in the pH range of 2 to 10 is between 35 and 45%.

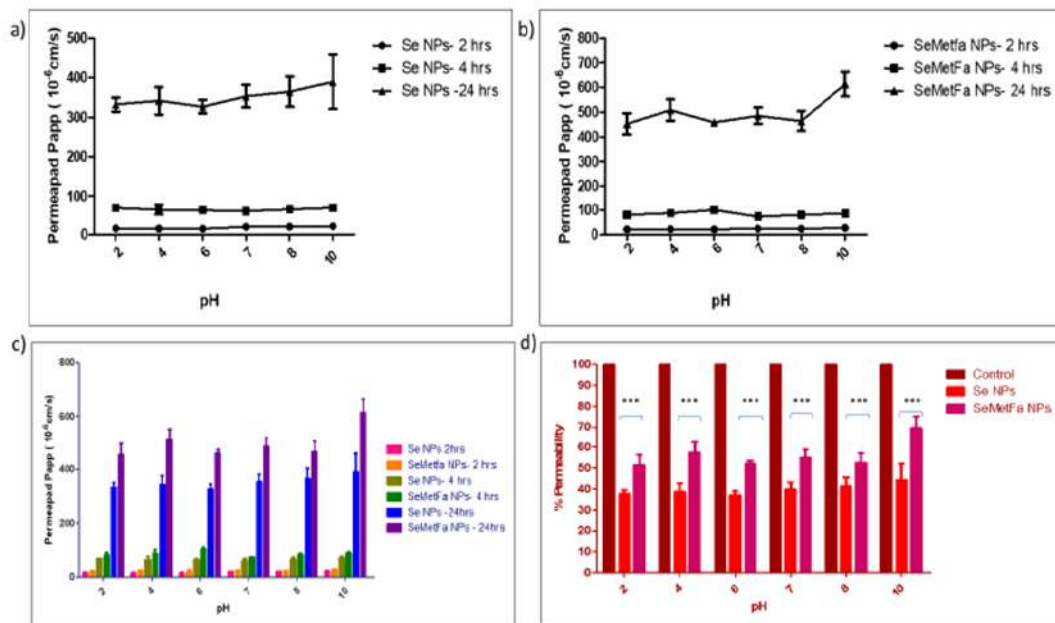


Figure 5.5 Shows the permeability data. a) A graph was created for Se NPs against apparent permeability in the required pH range at three different time points (2,4 and 24 h). b) Graph with three different time points that compares the apparent permeability of SeMetFa NPs at each required pH (2,4 and 24 h). c) A bar graph is used to compare steps a) and b) d) Bar graph demonstrating the percentage of permeability of control samples, SeMetFa NPs, and Se NPs over a wide pH range (2,4,6,7,8 and 10). Considering the mean and standard deviation, each plot contained readings in triplicate. With Bonferroni test multiple comparisons considering * $p < .05$, ** $p < .01$, and *** $p < .001$, the percentage of permeability was analyzed using two-way ANOVA.

5.4.3 Arthritic rat model study

5.4.3.1 Assessment of rat paw edema and weight

The hind paws of Wistar rats were used to induce chronic inflammatory arthritis. 0.1 ml of CFA was used for the induction process. Following paw injection, paw sizes of all animals were measured on days 1, 7, 14, and 21. On day 1, all animals administered CFA injections displayed inflammation near their paws, which was regarded as a 100% increase. The

results of the Bonferroni post hoc test demonstrated that the variances of the arthritic and treated groups were not significantly different in terms of homogeneity. From days 1 to 21, paw edema was significantly reduced in all groups (Table 5.1). On day 21, inflammation in the injected paw was significantly reduced by treatment with SeMetFa NPs 250, 500, and 750 g/kg b.w. and prednisolone, with percentages of 43.43%, 45.83%, 61.60%, and 46.43%, respectively.

The body weights of all control and treatment groups were recorded. Figure 5.6 shows the gradual increase in weight of the normal and vehicle control groups of approximately 100 g. The weight of the treatment groups steadily increased (80–90 g), whereas that of the arthritic control group increased only slightly (40 g).

Table 5.1 The effect of different concentrations of SeMetFa NPs on paw edema in adjuvant-induced arthritis.

Groups	Day 21 (% reduction)
Arthritic control	18.40 ± 1.76
Prednisolone (10 mg/kg b.w.)	46.43 ± 2.259
SeMetFa nanoparticles (250 mg/kg b.w.)	43.45 ± 1.63
SeMetFa nanoparticles (500 mg/kg b.w.)	45.83 ± 4.156
SeMetFa nanoparticles (750 mg/kg b.w.)	61.60 ± 1.67

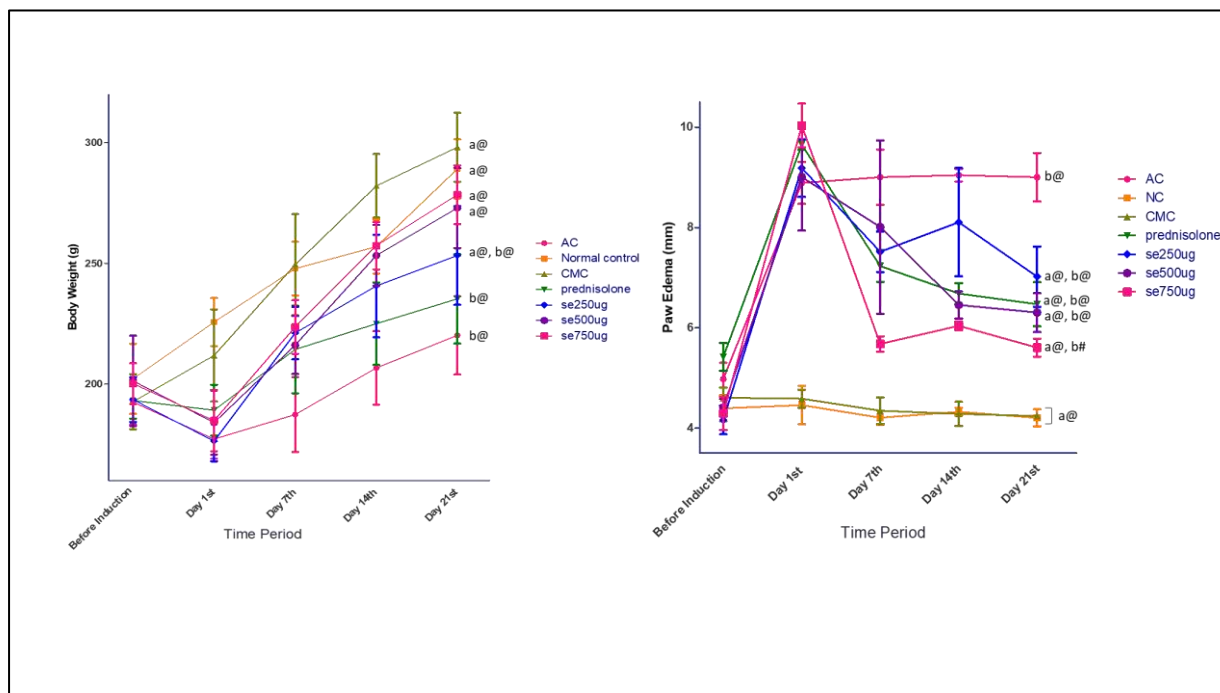


Figure 5.6 A shows the average body weight of the rats used as an animal model and how it changed in each group from before CFA induction to day 21 of the experiment. B) Prednisolone and SeMetFaNPs (250, 500, and 750 g/kg b.w.) Effect on Paw Edema in CFA-induced Rats. Two-way ANOVA with the "Bonferroni Posthoc test "a" was used for the statistical analysis, and the results show a significant difference from the arthritic control group at (*) $P < 0.05$, (#) $P < 0.01$, and (@) $P < 0.001$. "b" denotes a significant difference when (*) $P < 0.05$, (#) $P < 0.01$, and (@) $P < 0.001$ are taken into account in comparison to the normal control group. Data are presented as mean SD ($n=6$).

5.4.3.2 Effect of SeMetFa NPs on antioxidant enzymes

SOD, GPX, and Catalase levels were assessed in both the control and treatment groups at the end of the 21-day study. The variances of the liver, spleen, and kidney treatment groups were not significantly different from those of the normal control, arthritic, and normal control groups according to the results of Dunnett's test. The equality of means for these enzymes in each organ sample led researchers to consider a one-way ANOVA. Dunnett's multiple comparison test revealed a statistically significant difference between the control and treatment groups of ($p < 0.05$). Figure 5.7 shows a statistical breakdown of the decrease in antioxidant levels between the arthritic and healthy control groups. Dunnett's tests revealed that the liver, spleen, and kidney SOD levels of Se 750 were returning to normal,

which is a two-fold improvement when compared to the arthritic group. Prednisolone, Se 250, and Se 500, on the other hand, all demonstrated a one-fold improvement over the arthritic group. When compared to the diseased control, catalase levels in the spleen were significantly increased, roughly threefold in the Se 750 group and twice as much in the Se 250, Se 500, and prednisolone groups. All treatment groups demonstrated a two-fold increase in catalase levels in the liver and kidney compared with the arthritic group. GPx levels of GPx significantly increased in the liver, spleen, and kidney; treatment were restored to levels comparable to those in the normal group.

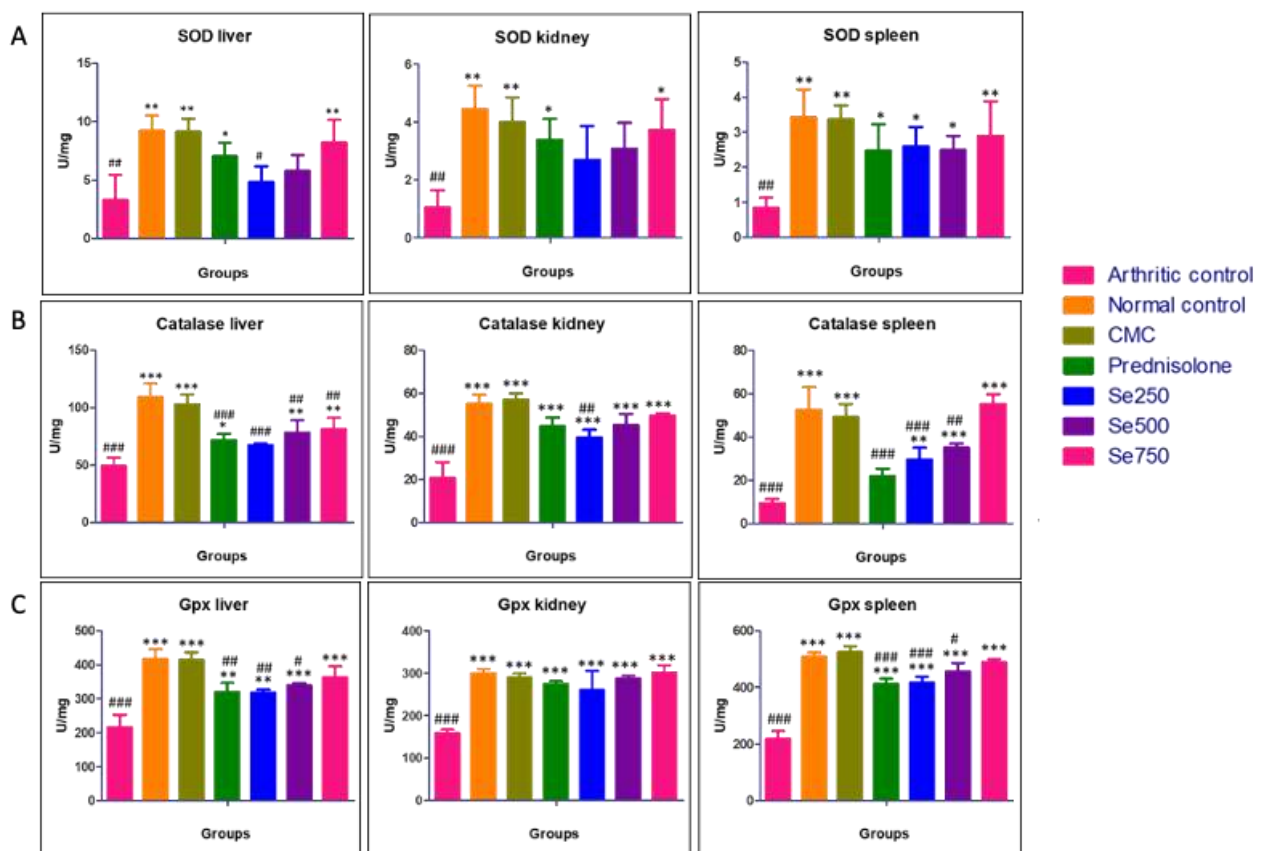


Figure 5.7 shows the impact of SeMetFaNPs (250, 500, and 750 $\mu\text{g}/\text{kg}$ b.w.) and prednisolone on the levels of A) SOD, B) catalase, and C) Gpx in rats administered CFA. Dunnett's Multiple Comparison Test was used in the one-way ANOVA statistical analysis. The asterisk (*) denotes a significant difference compared with the control group. $P < 0.05$, (**) $P < 0.01$, (***) $P < 0.001$. # denotes significant deviation from the normal control group when considering (#). $P < 0.05$, (##) $P < 0.01$, (###) $P < 0.001$. Data are presented as mean SD (n=3).

5.4.3.3 Effect of SeMetFa NPs on inflammatory biomarkers

(Figure 5.8) shows the measurements of inflammatory biomarkers such as TNF- α , CRP, and PGE2 in rat serum. Serum levels of TNF- α , CRP, and PGE2 were higher in the arthritic control group. However, TNF- α and CRP levels significantly declined in animals in the treatment groups. In the PGE2 treatment groups, a one-fold reduction was observed.

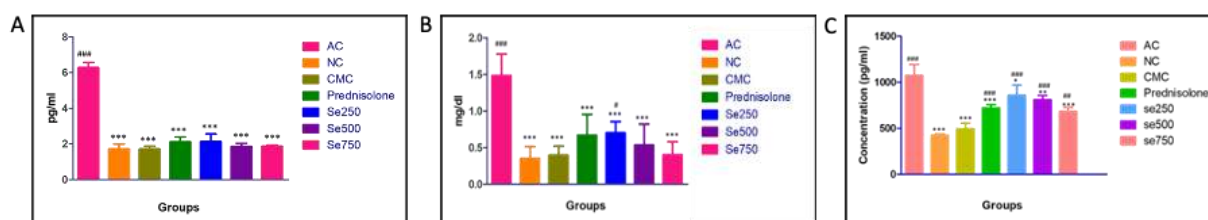


Figure 5.8 Shows of prednisolone and SeMetFaNPs (250, 500, and 750 $\mu\text{g/kg}$ b.w.) on the levels of TNF alpha, CRP, and prostaglandins in rats administered CFA. Dunnett's Multiple Comparison Test was used in the one-way ANOVA statistical analysis. * denotes a significant difference from the arthritic control group when (*) $P < 0.05$, (**) $P < 0.01$, and (***) $P < 0.001$ are taken into account. # denotes a significant deviation from the normal control group when (#) $P < 0.05$, (##) $P < 0.01$, and (###) $P < 0.001$ were considered. Data are presented as mean SD ($n = 6$).

5.4.3.4 Histopathological and Radiological findings of rat paw

Figure 5.9 shows the histopathology and radiographic images. In the paw region photographs, both the arthritic group and other treatment groups showed paw edema. The reduction in paw edema in all treatment groups compared to the diseased arthritic group was visually observed when these results were compared with normal and vehicle controls. Microphotographs of the paw region in the arthritic control group show a disturbed architectural pattern. Both the standard drug group and groups administered different doses of SeMetFa NPs displayed recovered tissue patterns. Table 5.2 includes information on the severity of lesions in the paw region.

The arthritic control group had severe lesions and changes in radiographic parameters, which raised the radiographic score to 4 according to the radiographic images (Figure 5.9) and radiographic score (Table 5.2). Se 750 displayed a radiographic score of 1, while the standard drug, Se 250, and Se 500 treatment groups displayed a score of 2. When compared with the scores given to the various groups, the radiographic paw images also showed comparable outcomes.

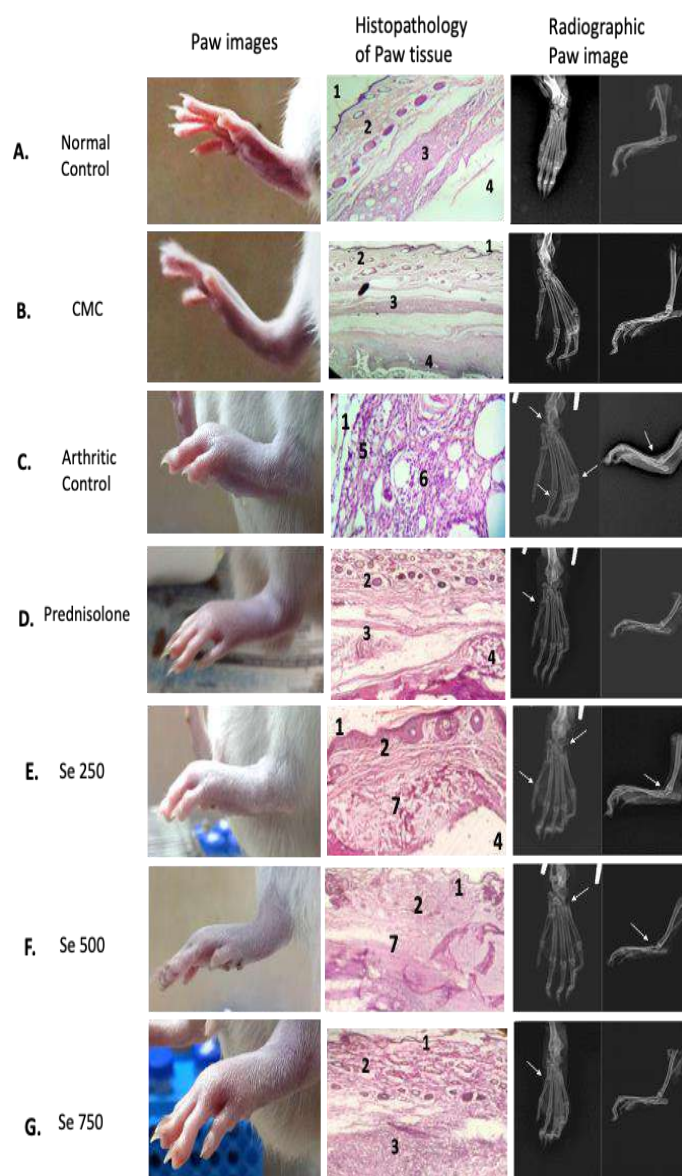


Figure 5.9 Images of the individual group's paws, histopathology of the tissue, and a microphotograph of the paw area (1) The outermost layer of skin. (2) Subcutaneous tissue containing fluid-filled vacuoles and mononuclear cell infiltrates. (3) Bone surrounding the muscle layer, (4) normal bone marrow tissue, (5) inflammation in the muscle layer, and (6)

bone tissue death. (7) Subcutaneous tissue exhibits only slight inflammatory alterations. (100x); Radiographic Paw images of the left hind paw in rats with arthritis brought on by CFA. The arrows show articular changes, swelling around the soft tissues, and degenerative changes in the ankle joint.

Table 5.2 liver, spleen, kidney, and paw tissues were graded histopathologically, as well as the radiographic condition of the paws.

Groups	Description	Histopathology				Radiographic score
		Liver	Spleen	kidney	Paw	
1	Healthy control	NAD	NAD	NAD	NAD	0
2	Arthritic control	++	++	++	++++	4
3	Vehicle control-CMC	NAD	NAD	NAD	NAD	0
4	Prednisolone	+	+	+	++	2
5	Se250	+	NAD	+	++	2
6	Se500	+	NAD	+	++	2
7	Se750	+	NAD	+	+	1

Grades of Severity of Lesions: + Minimal (< 10%), ++ Mild (11- 25%), +++ Moderate (26- 75%), ++++ Severe (> 75%), NAD (No abnormality detected).

Table 5.3 (a) Histopathology report of liver.

Sr. No	Study Group	Treatment Details	Microscopic Observations
1	A	Healthy control	NAD
2	B	Diseased control	Multifocal congestion (++); Focal hemorrhages (++); Multifocal hepatic degeneration (++); Multifocal cellular swelling (++), Focal MNC infiltration (++)
3	C	Vehicle control-placebo	Focal congestion (+); Focal hemorrhages (+).
4	D	Se 250	Focal congestion (+); Focal hemorrhages (+).
5	E	Se 500	Focal congestion (+); Focal hemorrhages (+).
6	F	Se 750	Focal congestion (+); Focal hemorrhages (+).
7	G	Prednisolone	Focal congestion (+); Focal hemorrhages (+).

Key:

NAD : No Abnormality Detected.	MNC : Mononuclear Cell Infiltration.
Grades of Severity of Lesions:	
+ : Minimal: Very small amount of change < 10%	++ : Mild : Lesion is easily identified but of limited severity 11-25%
+++ : Moderate: Lesion is prominent 26 to 75%.	++++ : Severe: the degree of changes is either as complete 76 – 100% as possible or great enough in intensity or extent to expect significant tissue or organ dysfunction.
Grades of extent of lesions: Focal, Multifocal, Diffuse// Whole of the section.	

Table 5.3 (b) Summary of the Histopathological Findings in Liver tissue

Organ	Lesions	Study Groups						
		A	B	C	D	E	F	G
Liver	Congestion	-	MF++	F++	F+	F+	F+	F+
	Hemorrhages	-	F++	F++	F++	F+	F+	F+
	Hepatic Degeneration	-	MF++	-	-	-	MF+	MF+
	Cellular swelling	-	MF++	-	-	-	-	-
	MNC infiltration	-	F++	-	-	-	-	-

Criteria's:

- I. **Grades of severity of lesions:** + Mild, ++ Moderate, +++ Severe.
- II. **Grades of extent of lesions:** F- Focal, MF-Multifocal, D-Diffuse/ Whole of the section.

Table 5.4 (a) Histopathology report of Kidney.

Sr. No	Study Group	Treatment Details	Microscopic Observations
1	A	Healthy control	NAD
2	B	Diseased control	Multifocal congestion (++); Multifocal hemorrhages (++); Focal glomerular atrophy (++) , Focal tubular degeneration (++) ; Multifocal necrotic changes (++) ; Multifocal deposition of pink eosinophilic material [Protein casts] (++) within renal tubules ; Focal MNC infiltration (++) .
3	C	Vehicle control-placebo	Focal congestion (+); Focal hemorrhages (+).
4	D	Se 250	Focal congestion (+); Focal hemorrhages (++) ; Focal tubular degeneration (+).
5	E	Se 500	Multifocal congestion (++) ; Multifocal hemorrhages (+); Focal necrotic changes (+); Focal tubular degeneration (+)
6	F	Se 750	Multifocal congestion (+); Multifocal hemorrhages (+); Focal tubular degeneration (+).
7	G	Prednisolone	Focal congestion (+); Focal hemorrhages (+); Focal tubular degeneration (+)

Key:

NAD : No Abnormality Detected.	MNC : Mononuclear Cell Infiltration.
Grades of Severity of Lesions:	
+	Minimal: Very small amount of change < 10%
++	Mild : Lesion is easily identified but of limited severity 11-25%
+++	Moderate: Lesion is prominent 26 to 75%.
++++	Severe: the degree of changes is either as complete 76 – 100% as possible or great enough in intensity or extent to expect significant tissue or organ dysfunction.
Grades of extent of lesions: Focal, Multifocal, Diffuse// Whole of the section.	

Table 5.4 (b) Summary of the Histopathological Findings in Kidney tissue

Organ	Lesions	Study Groups						
		A	B	C	D	E	F	G
Kidneys	Congestion	-	MF++	F+	MF+	MF+	F+	MF+
	Hemorrhages	-	MF++	F+	MF+	F+	F+	F+
	Glomerular atrophy	-	F++	-	-	-	-	F+
	Tubular Degeneration	-	F++	-	F+	F+	MF+	F+
	Necrotic changes	-	MF++	-	-	-	-	-
	Proteinous cast deposition	-	MF++	-	-	-	-	-
	MNC infiltration	-	F++	-	-	-	-	-

Criteria's:

- I. **Grades of severity of lesions:** + Mild, ++ Moderate, +++ Severe.
- II. **Grades of extent of lesions:** F- Focal, MF-Multifocal, D-Diffuse/ Whole of the section.

Table 5.5 (a) Histopathology report of Spleen.

Sr. No	Study Group	Treatment Details	Microscopic Observations
1	A	Healthy control	NAD
2	B	Diseased control	Multifocal congestion (++); Multifocal hemorrhages (++); Multifocal lymphoid hyperplasia (++)
3	C	Vehicle control-placebo	NAD
4	D	Se 250	NAD
5	E	Se 500	NAD
6	F	Se 750	Focal congestion (+); Focal hemorrhages (+).
7	G	Prednisolone	Focal congestion (+); Focal hemorrhages (+)

Key:

NAD : No Abnormality Detected.	MNC : Mononuclear Cell Infiltration.
Grades of Severity of Lesions:	
+ : Minimal: Very small amount of change < 10%	++ : Mild : Lesion is easily identified but of limited severity 11-25%
+++ : Moderate: Lesion is prominent 26 to 75%.	++++ : Severe: the degree of changes is either as complete 76 – 100% as possible or great enough in intensity or extent to expect significant tissue or organ dysfunction.
Grades of extent of lesions: Focal, Multifocal, Diffuse// Whole of the section.	

Table 5.5 (b) Summary of the Histopathological Findings in Spleen tissue

Organ	Lesions	Study Groups						
		A	B	C	N	O	P	Q
Spleen	Congestion	-	MF++	-	-	-	-	F+
	Hemorrhages	-	MF++	-	-	-	-	F+
	Lymphoid hyperplasia	-	MF++	-	-	-	-	-

Criteria's:

- I. **Grades of severity of lesions:** + Mild, ++ Moderate, +++ Severe.
- II. **Grades of extent of lesions:** F- Focal, MF-Multifocal, D-Diffuse/ Whole of the section.
- III.

Table 5.6 Microscopic Observations and Grades of Pathological Changes observed for paw Joints

Study Groups	Treatment Details	Microscopic Observations						Overall grade of pathological change
		Disturbed architectural pattern	Degenerative changes in inner region of tissue	Necrotic Changes in inner region of tissue	MNC & poly morpho nuclear cells infiltrations	Congestion	Deposits of adipose tissue	
1 A	Healthy control	NAD	F (+)	NAD	NAD	F (+)	F (+)	No Pathology grade changes seen.
2 B	Diseased control	MF (++++)	MF (+++)	MF (++)	MF (+++)	F (++)	MF (++)	Pathology grade +++ changes seen
3 C	Vehicle control-placebo	F (+)	F (+)	NAD	NAD	F (+)	F (+)	No significant pathology grade changes seen
4 D	Se 250	MF (++++)	MF (+++)	MF (++)	MF (+++)	F (++)	MF (++)	Pathology grade +++ changes seen
5 E	Se 500	MF (++)	MF (++)	MF (+)	MF (++)	F (+)	MF (++)	Pathology grade ++ changes seen
6 F	Se 750	MF (++)	MF (++)	F (++)	MF (++)	F (++)	MF (++)	Pathology grade ++ changes seen
8 H	Prednisolone	MF (++)	MF (++)	F (++)	MF (++)	F (++)	MF (++)	Pathology grade ++ changes seen

Key:

Grades of Severity of Lesions:

+ Minimal (< 10%)

++ Mild (11- 25%)

+++ Moderate (26- 75%)

++++ Severe (> 75%)

Grades of extent of lesions: Focal, Multifocal, Diffuse// Whole of the section.

5.4.3.5 Histopathological findings of rat liver, spleen and kidney

The histopathology of the liver, spleen, and kidneys in rats from various treatment groups is shown in Figure 5.10. Liver and kidney tissues in all treatment groups exhibited only slight lesions. The only abnormalities found in spleen samples were minor lesions in the prednisolone group and mild lesions in the arthritic group. The severity of the lesions for each sample is provided in detail in Table 5.2.

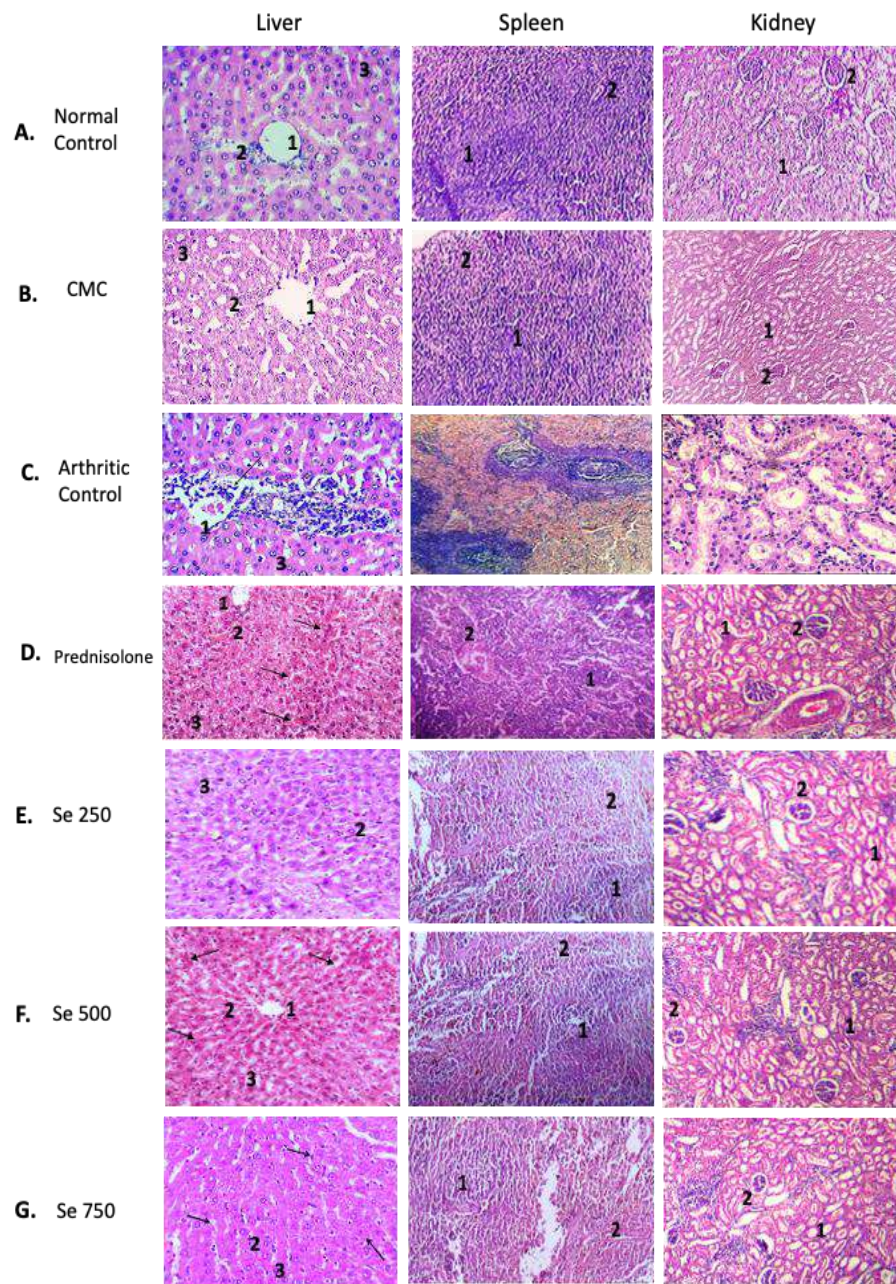


Figure 5.10 Microphotographs of 1) Liver, 2) Spleen and 3) Kidney

1. (1) Normal central vein, (2) hepatocytes arranged cord-like around the central vein, and (3) normal intact hepatocytes with nucleus (400x).
2. (1) Normal red pulp and (2) normal white pulp (100x).
3. (1) Normal renal parenchyma showing intact renal tubules and (2) normal intact glomeruli (200x).

Grades of Severity of Lesions: + Minimal (< 10%), ++ mild (11–25%), +++ moderate (26–75%), ++++ severe (> 75%), NAD (no abnormality detected).

5.5 Discussion

Se NPs have a limited therapeutic window because of their toxicity, biocompatibility, and off-target effects. According to previous reports, macrophages in the bloodstream eliminate all nanoparticles with unmodified surfaces and stop opsonin from adhering to them. A hemolysis assay should be part of the initial biocompatibility examination, primarily because of this. Studies have been conducted on the cytotoxicity and intraocular biocompatibility of graphene oxide (GO), a drug delivery system for human eyes (Naahidi et al., 2013). Preliminary findings showed good *in vivo* and *in vitro* biocompatibility, decreased toxicity, and minimal side effects. Apoptosis, membrane integrity, and cell survival are affected by GO accumulation and aggregation (Yan et al., 2012). The mechanisms underlying GO accumulation and aggregation, as well as their potential effects on long-term biocompatibility, require further investigation. The overall safety and effectiveness of GO as a drug delivery agent for ocular applications may also be improved by developing methods to reduce these side effects. SeMetFa NPs demonstrated no cytotoxicity in *in vitro* tests up to a concentration of 250 µg/ml and demonstrated an antioxidant effect using the DPPH assay at a concentration of 10 µg/ml (Shinde, 2022). By combining our experimental data with blood hemolysis and Permeapad® plates, we were able to analyze the biocompatibility and permeability of coated and non-coated Se NPs. The safe transfer of NPs in the bloodstream was determined using a preliminary test called a hemolysis assay. Blood biocompatibility is a crucial factor because erythrocytes serve as the best indicator of the impact of nanoparticles on the human body. NPs may cause the blood to clump or lyse as they enter the bloodstream. Figure 5.4(b) shows that less than 5% hemolysis was observed, further proving the biocompatibility of Se NPs (Hoonjan et al., 2018).

The permeability of the Se NPs was examined for the first time using a Permeapad® plate. It has previously been used to study the permeability of oral and nasal medications (Z. Huang et al., 2012). Southern Danish University created the Permeapad® plate in 2015. It is entirely artificially produced and composed of phospholipids (soybean phosphatidylcholine S-100) deposited between two adjacent sheets to mimic the intestinal membrane. The system functions as follows: the stack of intercalating steroids mimics the cell membrane, and the lipid crystals swell up when they come into contact with water. Phospholipids mimic the morphology of the tissue by filling the spaces between the support sheets. Determination of a drug's hydrophilicity or lipophilicity and apparent permeability, commonly abbreviated as Papp, is a crucial parameter for the prediction of passive drug diffusion (Di Padova, 1987). Phosphate buffer (pH

2–10) also replicates the conditions inside the stomach, intestine, and blood. Passive diffusion, which aids in the oral consumption of drugs, is a transmembrane process in which small drugs diffuse from a higher-concentration region (the gastrointestinal tract) to a lower-concentration region (the blood) (Shen et al., 2011). An ideal drug must also have sufficient solubility and permeability to achieve effective concentrations in the necessary tissues (Sylvain Chemtob, 2004). Therefore, the better the diffusion, the higher the permeability. The coated SeMetFa NPs had the highest P_{app} at pH 10 when incubated for 24 h, as shown in Figure 3c, in comparison to the non-coated Se NPs (Cárdenas et al., 2006).

This demonstrated the higher proton transfer of the coated NPs. Less variation in proton transfer also indicates high barrier resistance. The percentage of permeability was calculated using apparent permeability. The effective concentration of NPs with a high permeability at a specific pH and temperature can be easily determined using this permeability. SeMetFa NPs exhibit the highest permeability of 70% when compared to Se NPs, as shown in Figure 3d. Additionally, at any pH between 2 and 10, the permeability was approximately 50–70%. P_{app} is a highly permeable drug in both directions, according to a valid drug study of 6-methyl coumarin, which shows P_{app} to be 9.1×10^{-5} cm/s. Passive diffusion and the absence of efflux were indicated by the efflux ratio, which was less than 2. The P_{app} for SeMetFa NPs in the current study was found to be greater than 1.5×10^{-6} cm/s, indicating that the nanoparticles have a high penetration rate (L. K. Prasad et al., 2015).

Unknown in its aetiology, rheumatoid arthritis is a debilitating inflammatory condition that disturbs the oxidative balance of tissue. Dietary interventions can help manage RA-related symptoms, such as pain, tender joints, swelling, and disease progression (Silva et al., 2016). Zinc, selenium, calcium, and vitamin D play cofactor roles in immune responses in articular tissues, which are related to the significance of these micronutrients. Additionally, selenium levels are low in patients with RA. The difference between the advantageous and harmful effects of selenium is relatively small. This was an essential factor. According to a comparative study by Zhang et al. using elemental selenium (Se) and e-methyl selenocysteine (SeMSC), elemental selenium in the nano form is equally effective, with little toxicity and higher levels of Se. (D. Peng et al., 2007) carried out a similar study in mice and concluded that Che-SeNP was seven times less toxic than sodium selenite, while also increasing tissue selenium levels and glutathione peroxidase activity. These findings unequivocally establish the toxicity of Se in its organic form, but nanoscale Se may be less toxic and may increase GPx activity at lower

concentrations. Therefore, Se nanoparticles may be a superior choice for Se as a micronutrient. With the aid of animal models, the pathogenesis of inflammatory arthritis has been thoroughly investigated. In the current study, we focused on the rat adjuvant arthritis model from all possible models. An experimental model of polyarthritis, called rat adjuvant arthritis, has been used extensively for a decade in preclinical and clinical studies on various anti-arthritic agents as well as therapeutics (Webb, 2018). The created and thoroughly characterized SeMetFa NPs were tested on Wistar rats with arthritis induced by CFA. All treatment groups showed a significant decline in paw inflammation. The inherent immunity of rats may be responsible for the reduction in paw inflammation in the arthritis group. In treated groups consisting of SeMetFa NPs 250, 500, and 750 $\mu\text{g}/\text{kg}$ b.w. with an effective selenium concentration of 137.5, 275, and 412.5 mg/kg b.w respectively, paw edema decreased from day 1 to day 21 without any indications of severe toxicity (figure 5.6). Researchers Malhotra and Desai found that selenium nanoparticles coated with dextrin were effective in CFA-induced rats at 500 mg/kg body weight (Malhotra et al., 2016). In dextrin-coated Se NPs at 250, 500, and 750 $\mu\text{g}/\text{kg}$ b.w., the effective selenium concentrations were 229.25, 458.5, and 687.75 mg/kg b.w. Regarding the outcomes of Se NPs coated in dextrin, it can be said that SeMetFa NPs, which had a 2-fold lower concentration, reduced paw edoema more effectively at 500 $\mu\text{g}/\text{kg}$ b.w. without exhibiting any toxic effects. Additionally, SeMetFa NPs may be more potent at lower concentrations, suggesting an improved oral bioavailability and targeted delivery. The effects of the newly developed nanoparticles on the levels of inflammatory cytokines were investigated. After 21 days, several enzymatic and non-enzymatic parameters, including SOD, CAT, GPx, CRP, PGE2, and TNF- α , were analyzed. For the control and treatment groups, tests for CRP, PGE2, and TNF- α were performed to evaluate disease conditions.

Activated macrophages secrete a variety of cytokines that have a significant impact on the development, progression, and pathogenesis of this illness. These activated macrophages have higher levels of folate receptor overexpression than normal macrophages, which barely express folate receptor. FA-conjugated therapies are, therefore, focused on inflammatory diseases. A previous study (Zeng et al., 2013). examined the impact of dexamethasone phosphate nanoparticles conjugated with FA on inflammatory disease and found that FA-conjugated NPs demonstrated a better reduction in inflammation than non-FA-conjugated NPs. The SeMetFa NPs results were consistent with those of Cao et al., and it was found that the TNF- α and CRP protein levels decreased by up to 3- and 2-fold, respectively. When compared to the results of

the CRP and TNF- α tests, the PGE2 test did not reveal a significantly lower level in the treated groups. The lack of a change in the levels of COX 1/ COX 2 could be explained by the fact that the standard medication is a glucocorticoid and selenium has an activity that is selective for the COX 2 enzyme, given that COX 1 and COX 2 are both enzymes that increase the levels of prostaglandin in the body. This might also be a result of the drug dosage being used, which might not be sufficient to change COX 1 and COX 2 enzyme levels or PGE2 levels. These findings are consistent with those of an earlier study by Malhotra et al., in which Se nanoparticles and an analogous standard glucocorticoid drug failed to significantly reduce the activity of COX 2 due to specificity. (Prempeh & Mensah-Attipoe, 2008) Prempeh et al. also came to the conclusion that glucocorticoids have a selective activity towards the COX 2 enzyme, and that the drug's crude aqueous extract of the root bark of *Zanthoxylum xanthoxyloides* did not affect PGE2 levels in any way. Since the infiltration of these cytokines, along with T- and B-cells and matrix metalloproteins, has been known to contribute to the development of RA, the significant decrease in their levels suggests that SeMetFa NPs have the ability to delay the progression of chronic inflammation (Cao et al., 2015; Malhotra et al., 2016).

After 21 days of NPs treatment, antioxidant enzyme status was observed in several organs, including the liver, spleen, and kidneys. Owing to oxidative stress in the body, lower levels of SOD, CAT, and GPx were observed in the arthritis control group. This explains how CFA triggers chronic inflammatory arthritis. An intriguing finding of the study was that SeMetFa NPs significantly restored antioxidant enzyme levels in animals when combined with the commonly used prednisolone medication. With a 2-fold higher concentration of selenium, the dextrin-coated Se NPs demonstrated a similar pattern of increase in antioxidant enzymes. To treat chronic inflammatory arthritis, dual coating with SeMetfa NPs is advantageous. The toxicity factor was adequately supported by histopathological data; little to no toxicity was observed in any of the groups that received the NP treatment. highlight the safety of SeMetFa NPs in this process. The observation of a decrease in paw edema was also supported by the X-ray data, the Radiography score demonstrating the improved and targeted therapeutic effectiveness of SeMetFa NPs.

5.6 Conclusion

The in-situ technique was used to successfully prepare SeMetFa NPs through chemical precipitation and dual coating. The safety and therapeutic potential of the developed NPs were determined using *in vivo* data. Compared to a previous study, SeMetFa NPs produced significantly greater reductions in paw edema, proinflammatory cytokines, and toxicity. SeMetFa NPs were effective even at lower doses, indicating improved oral bioavailability and potential for targeted delivery because of the Fa coating. Histopathological and radiological studies verified these findings. Thus, this study showed that the 2-fold lower selenium concentration used for the targeted delivery of SeMetfa NPs resulted in enhanced efficacy and decreased toxicity. The NPs created may be modified to aid RA maintenance.

Chapter 6:
Conclusion and Future
prospects

Over the last three decades, nanoparticle manufacturing has expanded tremendously owing to the rapid growth of nanotechnology. As a result, nanoparticles have a wide range of uses, including in gadgets, engineering medicinal/medical devices for diagnosis, personal hygiene products, food/beverages, and pollution remediation. Because of their size and condition, nanoparticles offer a higher surface area than macro sized materials. Nanoparticles expose actual sections of a material's atomic structure to the outside world. This leads to a different contact surface than that of a larger-sized substance, as well as a different chemical and physical reactivity to the environment. This distinguishing feature of nanoparticles allows them to behave differently in terms of responsiveness and lethality compared to their bulk counterparts. The purpose of this thesis was to create non-toxic, bioavailable, and, most importantly, biocompatible selenium nanoparticles. This demonstrated their efficacy in the treatment and management of chronic inflammatory arthritis in a Wistar rat model.

SeNP have been synthesized utilising a variety of ways in recent years, including biological, chemical, and physical processes. In this study, SeNPs were chemically synthesized using biocompatible materials that are extremely effective in maintaining particle homogeneity. Various biocompatible reducing agents, such as amino acids and reducing sugars, have been tested for their synthesis, including ascorbic acid as a green source of powerful chemical reducing agents, which was subsequently used for one-step simple synthesis of SeNPs.

The generated SeNPs were then characterized using a variety of advanced analytical techniques, including UV-visible spectrophotometry, FTIR, Zeta potential, XRD, Raman spectroscopy, and TEM, to determine the particle size and morphology. These SeNPs were subsequently stabilized and rendered accessible by covering the surface of the nanoparticles with Methionine and Folic acid, biocompatible amino acids, and vitamin B9. The overall size of the nanoparticles with their covering was confirmed by TEM measurements to be 50 ± 2.0 nm. SeNP (SeMetFa NPs) stabilized with methionine and folic acid were used throughout the investigation.

SeNPs stabilized with methionine and folic acid were tested for toxicity *in vitro*. In the cytotoxicity study, the following kinds of selenium were examined for their *in vitro* toxicity on NIH/3T3 and Raw 264.7 cell lines: uncoated SeNP, Methionine coated SeNP, Methionine + folic acid coated SeNP, and 1% sodium selenite (precursor). According to the findings of this

investigation, the coated and uncoated forms of selenium exhibited 15% and 40% toxicity, respectively, whereas the bulk form of sodium selenium exhibited 99% toxicity to cells.

The bioavailability of SeMetFa NPs was also investigated via intestinal permeability and blood compatibility to determine their biocompatibility. It has been demonstrated to be bioavailable because it has 70% permeability, and is biocompatible because it has less than 5% hemolysis.

The SeNPs were focused on the eventual goal of their role in the treatment/maintenance) of chronic inflammatory arthritis after preliminary examination. Wistar rats were used as an experimental model to treat CFA-induced arthritis using these nanoparticles. Various parameters, including paw volume; anti-inflammatory markers in the blood (CRP, PGE₂, and TNF- α); antioxidant enzyme (SOD, CAT, GPx) status of the liver, kidney, and spleen; histopathology; and radiology of the paw region, were examined for disease prognosis and the effect of the SeMetFa NPs and standard drug (prednisolone 10 mg).

Taking into account all of the variables investigated, it was discovered that oral administration of SeMetFa NPs at a concentration of 500 g/kg b.w. for up to 21 days had a significant effect on experimentally induced chronic inflammatory arthritis in rats and can be considered as an additional therapy for the treatment of RA as a therapeutic drug supplement.

In addition to the industrial revolution, nanotechnology has the potential to revolutionize society. Everyone is affected or influenced by this. Nanotechnology is evolving rapidly and has a promising future. The applications of nanotechnology are impressive when compared to competing applications. Thus, speculation on the future of nanotechnology may be of interest. Because the current study fulfilled all the objectives, we must now decide on the future scope of the work. This study aids in determining the two ways in which the study can be extrapolated.

- Kinetic studies of SeMetFa NP bioavailability can be performed to gain a better understanding of particle excretion and half-life. Furthermore, these studies provide important information regarding the potential bioaccumulation and toxicity of SeMetFa NP in various biological systems. Understanding the kinetic behavior of SeMetFa NP can also aid in the development of effective strategies for their safe and efficient use in a variety of applications.

- These nanoparticles can either be administered alongside drugs that are currently on the market, coated on the nanoparticles, or made into mesopores that can hold and release the drugs as needed. Lowering the effective concentration and raising the reactivity in synergy may reduce the toxicity of drugs.

Bibliography

- About the National Science and Technology Council About this Document.* (n.d.).
<http://www.ostp.gov>.
- Acharya, J. D., & Ghaskadbi, S. S. (2013). Protective effect of Pterostilbene against free radical mediated oxidative damage. *BMC Complementary and Alternative Medicine*, *13*(1), 1. <https://doi.org/10.1186/1472-6882-13-238>
- Acosta, E. (2009). Bioavailability of nanoparticles in nutrient and nutraceutical delivery. *Current Opinion in Colloid and Interface Science*, *14*(1), 3–15.
<https://doi.org/10.1016/j.cocis.2008.01.002>
- Ahmed, H. H., Abd El-Maksoud, M. D., Abdel Moneim, A. E., & Aglan, H. A. (2017). Pre-Clinical Study for the Antidiabetic Potential of Selenium Nanoparticles. *Biological Trace Element Research*, *177*(2), 267–280.
<https://doi.org/10.1007/s12011-016-0876-z>
- Alagesan, V., & Venugopal, S. (2019). Green Synthesis of Selenium Nanoparticle Using Leaves Extract of *Withania somnifera* and Its Biological Applications and Photocatalytic Activities. *BioNanoScience*, *9*(1), 105–116.
<https://doi.org/10.1007/s12668-018-0566-8>
- Alam, M. A., Al-Jenoobi, F. I., & Al-Mohizea, A. M. (2012). Everted gut sac model as a tool in pharmaceutical research: Limitations and applications. *Journal of Pharmacy and Pharmacology*, *64*(3), 326–336. <https://doi.org/10.1111/j.2042-7158.2011.01391.x>
- Ali, O. (2023, July 13). *Nanotechnology Market Report: India*. AZoNano.
- Attia, M. F., Anton, N., Wallyn, J., Omran, Z., & Vandamme, T. F. (2019). An overview of active and passive targeting strategies to improve the nanocarriers efficiency to tumour sites. In *Journal of Pharmacy and Pharmacology* (Vol. 71, Issue 8, pp. 1185–1198). Blackwell Publishing Ltd. <https://doi.org/10.1111/jphp.13098>
- Atzeni, F., Talotta, R., Masala, I. F., Bongiovanni, S., Boccassini, L., & Sarzi-Puttini, P. (2017). Biomarkers in rheumatoid arthritis. In *Israel Medical Association Journal* (Vol. 19, Issue 8, pp. 512–516). Israel Medical Association.
<https://doi.org/10.7759/cureus.15063>
- Ayyub, P., Chandra, R., Taneja, P., Sharma, A. K., & Pinto, R. (2001). Synthesis of nanocrystalline material by sputtering and laser ablation at low temperatures. *Applied Physics A: Materials Science and Processing*, *73*(1), 67–73.
<https://doi.org/10.1007/s003390100833>
- Baba, K., Kasai, H., Nishida, K., & Nakanishi, H. (2011). Functional Organic Nanocrystals. In *Nanocrystal*. InTech. <https://doi.org/10.5772/16948>
- Bafghi, M. H., Darroudi, M., Zargar, M., Zarrinfar, H., & Nazari, R. (2021). Biosynthesis of selenium nanoparticles by *Aspergillus flavus* and *Candida albicans*

- for antifungal applications. *Micro and Nano Letters*, 16(14), 656–669. <https://doi.org/10.1049/mna2.12096>
- Baines, A., Taylor-Parker, M., Goulet, A. C., Renaud, C., Gerner, E. W., & Nelson, M. A. (2002). Selenomethionine inhibits growth and suppresses cyclooxygenase-2 (COX-2) protein expression in human colon cancer cell lines. *Cancer Biology and Therapy*, 1(4), 370–374. <https://doi.org/10.4161/cbt.1.4.9>
- Barthe, L., Woodley, J. F., Kenworthy, S., & Houin, G. (1998). An improved everted gut sac as a simple and accurate technique to measure paracellular transport across the small intestine. *European Journal of Drug Metabolism and Pharmacokinetics*, 23(2), 313–323. <https://doi.org/10.1007/BF03189357>
- Battin, E. E., Perron, N. R., & Brumaghim, J. L. (2006). The central role of metal coordination in selenium antioxidant activity. *Inorganic Chemistry*, 45(2), 499–501. <https://doi.org/10.1021/ic051594f>
- Bauerova, K., Ponist, S., Nosal, R., Stancikova, M., & Rovensky, J. (2012). Modern Pharmacological Approaches to Therapies: Substances Tested in Animal Models of Rheumatoid Arthritis. *Rheumatoid Arthritis - Treatment*. <https://doi.org/10.5772/27097>
- Bax, M., Van Heemst, J., Huizinga, T. W. J., & Toes, R. E. M. (2011). Genetics of rheumatoid arthritis: What have we learned? *Immunogenetics*, 63(8), 459–466. <https://doi.org/10.1007/s00251-011-0528-6>
- Beheshti, N., Soflaei, S., Shakibaie, M., Yazdi, M. H., Ghaffarifar, F., Dalimi, A., & Shahverdi, A. R. (2013). Efficacy of biogenic selenium nanoparticles against *Leishmania major*: In vitro and in vivo studies. *Journal of Trace Elements in Medicine and Biology*, 27(3), 203–207. <https://doi.org/10.1016/j.jtemb.2012.11.002>
- Behzadi, S., Ghasemi, F., Ghalkhani, M., Ashkarran, A. A., Akbari, S. M., Pakpour, S., Hormozi-Nezhad, M. R., Jamshidi, Z., Mirsadeghi, S., Dinarvand, R., Atyabi, F., & Mahmoudi, M. (2015). Determination of nanoparticles using UV-Vis spectra. *Nanoscale*, 7(12), 5134–5139. <https://doi.org/10.1039/c4nr00580e>
- Behzadi, S., Serpooshan, V., Tao, W., Hamaly, M. A., Alkawareek, M. Y., Dreaden, E. C., Brown, D., Alkilany, A. M., Farokhzad, O. C., & Mahmoudi, M. (2017). Cellular uptake of nanoparticles: Journey inside the cell. In *Chemical Society Reviews* (Vol. 46, Issue 14, pp. 4218–4244). Royal Society of Chemistry. <https://doi.org/10.1039/c6cs00636a>
- Benjamin, M. (1881). Some Chemical Reagents. *Scientific American*, 12(296supp), 4725–4725. <https://doi.org/10.1038/scientificamerican09031881-4725asupp>
- Berben, P., Bauer-Brandl, A., Brandl, M., Faller, B., Flaten, G. E., Jacobsen, A. C., Brouwers, J., & Augustijns, P. (2018). Drug permeability profiling using cell-free permeation tools: Overview and applications. *European Journal of Pharmaceutical Sciences*, 119(March), 219–233. <https://doi.org/10.1016/j.ejps.2018.04.016>

- Bevaart, L., Vervoordeldonk, M. J., & Tak, P. P. (2010). Evaluation of therapeutic targets in animal models of arthritis: How does it relate to rheumatoid arthritis? *Arthritis and Rheumatism*, 62(8), 2192–2205. <https://doi.org/10.1002/art.27503>
- Bingham, C. O. (2002). Development and clinical application of COX-2-selective inhibitors for the treatment of osteoarthritis and rheumatoid arthritis. *Cleveland Clinic Journal of Medicine*, 69(SUPPL. 1), 5–12. https://doi.org/10.3949/ccjm.69.suppl_1.si5
- Biriukov, D., Fibich, P., & Předota, M. (2020). Zeta Potential Determination from Molecular Simulations. *Journal of Physical Chemistry C*, 124(5), 3159–3170. <https://doi.org/10.1021/acs.jpcc.9b11371>
- Bischoff, S. C., Barbara, G., Buurman, W., Ockhuizen, T., Schulzke, J. D., Serino, M., Tilg, H., Watson, A., & Wells, J. M. (2014). Intestinal permeability - a new target for disease prevention and therapy. In *BMC Gastroenterology* (Vol. 14, Issue 1). BioMed Central Ltd. <https://doi.org/10.1186/s12876-014-0189-7>
- Bjørklund, G., Shanaida, M., Lysiuk, R., Antonyak, H., Klishch, I., Shanaida, V., & Peana, M. (2022). Selenium: An Antioxidant with a Critical Role in Anti-Aging. In *Molecules* (Vol. 27, Issue 19). MDPI. <https://doi.org/10.3390/molecules27196613>
- Böck, A., Forchhammer, K., Heider, J., Leinfelder, W., Sawers, G., Veprek, B., & Zinoni, F. (1991). Selenocysteine: the 21st amino acid. *Molecular Microbiology*, 5(3), 515–520. <https://doi.org/10.1111/j.1365-2958.1991.tb00722.x>
- Book, . (2017). *Green Synthesis of Copper oxide Nanoparticles & Biomedical Application*. <https://www.researchgate.net/publication/321183963>
- Boroumand, S., Safari, M., Shaabani, E., Shirzad, M., & Faridi-Majidi, R. (2019). Selenium nanoparticles: Synthesis, characterization and study of their cytotoxicity, antioxidant and antibacterial activity. *Materials Research Express*, 6(8). <https://doi.org/10.1088/2053-1591/ab2558>
- Brady, N. C. (1984). *Advances in agronomy. Volume 37*. Academic Press.
- Braun, C. E., Cook, C. D., Charles, Merritt, Jr., & Rousseau, J. E. (1951). Reliable Methods for the Preparation of Organic Compounds Working with Hazardous Chemicals 9-Nitroanthracene. *Organic Syntheses*, 31(September), 77. <https://doi.org/10.15227/orgsyn.031.0077>
- Brennan, F. M., Jackson, A., Chantry, D., Maini, R., & Feldmann, M. (1984). Preliminary Communication INHIBITORY EFFECT OF TNF&agr; ANTIBODIES ON SYNOVIAL CELL INTERLEUKIN-1 PRODUCTION IN RHEUMATOID ARTHRITIS. In *J Clin Invest* (Vol. 74).
- Buddanavar, A. T., & Nandibewoor, S. T. (2017). Multi-spectroscopic characterization of bovine serum albumin upon interaction with atomoxetine. *Journal of Pharmaceutical Analysis*, 7(3), 148–155. <https://doi.org/10.1016/j.jpha.2016.10.001>

- Bunaciu, A. A., Udriștioiu, E. gabriela, & Aboul-Enein, H. Y. (2015). X-Ray Diffraction: Instrumentation and Applications. In *Critical Reviews in Analytical Chemistry* (Vol. 45, Issue 4, pp. 289–299). Taylor and Francis Ltd. <https://doi.org/10.1080/10408347.2014.949616>
- Butterworth, C. E., & Tamura, T. (1989). Folic acid safety and toxicity: a brief review. *The American Journal of Clinical Nutrition*, 50(2), 353–358.
- Byrappa, K., Ohara, S., & Adschiri, T. (2008). Nanoparticles synthesis using supercritical fluid technology - towards biomedical applications. In *Advanced Drug Delivery Reviews* (Vol. 60, Issue 3, pp. 299–327). Elsevier. <https://doi.org/10.1016/j.addr.2007.09.001>
- Cadet, F., Garrigues, S., & de la Guardia, M. (2012). Quantitative Analysis, Infrared Update based on the original article by Frederic Cadet, *Encyclopedia of Analytical Chemistry*, © 2000, John Wiley & Sons, Ltd. . In *Encyclopedia of Analytical Chemistry*. John Wiley & Sons, Ltd. <https://doi.org/10.1002/9780470027318.a5610.pub2>
- Callejas, D., Mann, C. J., Ayuso, E., Lage, R., Grifoll, I., Roca, C., Andaluz, A., Ruiz-de Gopegui, R., Montané, J., Muñoz, S., Ferre, T., Haurigot, V., Zhou, S., Ruberte, J., Mingozzi, F., High, K. A., Garcia, F., & Bosch, F. (2013). Treatment of diabetes and long-term survival after insulin and glucokinase gene therapy. *Diabetes*, 62(5), 1718–1729. <https://doi.org/10.2337/db12-1113>
- Camargo, P. H. C., Satyanarayana, K. G., & Wypych, F. (2009). Nanocomposites: Synthesis, structure, properties and new application opportunities. *Materials Research*, 12(1), 1–39. <https://doi.org/10.1590/S1516-14392009000100002>
- Cao, J., Naeem, M., Noh, J. K., Lee, E. H., & Yoo, J. W. (2015). Dexamethasone phosphate-loaded folate-conjugated polymeric nanoparticles for selective delivery to activated macrophages and suppression of inflammatory responses. *Macromolecular Research*, 23(5), 485–492. <https://doi.org/10.1007/s13233-015-3065-6>
- Caporali, R., Pallavicini, F. B., Filippini, M., Gorla, R., Marchesoni, A., Favalli, E. G., Sarzi-Puttini, P., Atzeni, F., & Montecucco, C. (2009). Treatment of rheumatoid arthritis with anti-TNF-alpha agents: A reappraisal. In *Autoimmunity Reviews* (Vol. 8, Issue 3, pp. 274–280). <https://doi.org/10.1016/j.autrev.2008.11.003>
- Cárdenas, M., Barauskas, J., Schullén, K., Brennan, J. L., Brust, M., & Nylander, T. (2006). Thiol-specific and nonspecific interactions between DNA and gold nanoparticles. *Langmuir*, 22(7), 3294–3299. <https://doi.org/10.1021/la0530438>
- Chakraborty, D., Chauhan, P., Alex, S. A., Chaudhary, S., Ethiraj, K. R., Chandrasekaran, N., & Mukherjee, A. (2018). Comprehensive study on biocorona formation on functionalized selenium nanoparticle and its biological implications. *Journal of Molecular Liquids*, 268, 335–342. <https://doi.org/10.1016/j.molliq.2018.07.070>

- Chaudhary, N., Gomez, G. A., Howes, M. T., Lo, H. P., McMahon, K. A., Rae, J. A., Schieber, N. L., Hill, M. M., Gaus, K., Yap, A. S., & Parton, R. G. (2014). Endocytic Crosstalk: Cavins, Caveolins, and Caveolae Regulate Clathrin-Independent Endocytosis. *PLoS Biology*, *12*(4). <https://doi.org/10.1371/journal.pbio.1001832>
- Chaudhary, S., Chauhan, P., Kumar, R., & Bhasin, K. K. (2018). Toxicological responses of surfactant functionalized selenium nanoparticles: A quantitative multi-assay approach. *Science of the Total Environment*, *643*, 1265–1277. <https://doi.org/10.1016/j.scitotenv.2018.06.296>
- Chaudhary, S., Umar, A., & Mehta, S. K. (2014). Surface functionalized selenium nanoparticles for biomedical applications. *Journal of Biomedical Nanotechnology*, *10*(10), 3004–3042. <https://doi.org/10.1166/jbn.2014.1985>
- ChemBAM. (n.d.). *Nanotechnology*. Wordpress.Com.
- “Chemistry-It’s Elemental!” *eResources for K-12 National Chemistry Week-A Periodic Table of the Elements : A Resource for Elementary, Middle School, and High School Students (E,I,HS)*. (n.d.). <http://www.americanelements.com/infocenter.html><http://umbbd.msi.umn.edu/periodic/>
- Chen, W., Li, Y., Yang, S., Yue, L., Jiang, Q., & Xia, W. (2015). Synthesis and antioxidant properties of chitosan and carboxymethyl chitosan-stabilized selenium nanoparticles. *Carbohydrate Polymers*, *132*, 574–581. <https://doi.org/10.1016/j.carbpol.2015.06.064>
- Chen, Y., Liu, W., Leng, X., & Stoll, S. (2022a). Toxicity of selenium nanoparticles on *Poteroochromonas malhamensis* algae in Waris-H culture medium and Lake Geneva water: Effect of nanoparticle coating, dissolution, and aggregation. *Science of the Total Environment*, *808*. <https://doi.org/10.1016/j.scitotenv.2021.152010>
- Chen, Y., Liu, W., Leng, X., & Stoll, S. (2022b). Toxicity of selenium nanoparticles on *Poteroochromonas malhamensis* algae in Waris-H culture medium and Lake Geneva water: Effect of nanoparticle coating, dissolution, and aggregation. *Science of the Total Environment*, *808*. <https://doi.org/10.1016/j.scitotenv.2021.152010>
- Chunxia, C., Peng, Z., Huifang, P., Hanli, R., Zehua, H., & Jizhou, W. (2011). Extracts of *Arisaema rhizomatum* C.E.C. Fischer attenuate inflammatory response on collagen-induced arthritis in BALB/c mice. *Journal of Ethnopharmacology*, *133*(2), 573–582. <https://doi.org/10.1016/j.jep.2010.10.035>
- Clauw, D. J. (2009). Fibromyalgia: An Overview. *American Journal of Medicine*, *122*(12 SUPPL.). <https://doi.org/10.1016/j.amjmed.2009.09.006>
- COHEN, A., & GOLDMAN, J. (1964). Bromelains Therapy in Rheumatoid Arthritis. *Pennsylvania Medical Journal* (1928), *67*(6), 27–30.
- Cohen, D. T., Zhang, C., Pentelute, B. L., & Buchwald, S. L. (2015). An Umpolung Approach for the Chemoselective Arylation of Selenocysteine in Unprotected

- Peptides. *Journal of the American Chemical Society*, 137(31), 9784–9787.
<https://doi.org/10.1021/jacs.5b05447>
- Crosland, A. R., Zhao, F. J., Mcgrath, S. P., Lane, P. W., & Experimental, R. (2008). *Communications in Soil Science and Plant Analysis digestion with sodium carbonate fusion for the determination of total phosphorus in soils by inductively coupled plasma atomic emission spectroscopy (ICP). July 2011*, 1357–1368.
- de Matos, R. A., Iwasaki, M. T., Tomita, R. J., & Courrol, D. L. C. (2013). *Green Synthesis of Spherical Gold Nanoparticles Using Amino Acids. 01*, LM2A.26.
<https://doi.org/10.1364/laop.2012.lm2a.26>
- Dell, J. R. O., Lemley-Gillespie, S., Palmer, W. R., Weaver, A. L., Moore, G. F., & Klassen, L. W. (1991). Serum selenium concentrations in rheumatoid arthritis. *Annals of the Rheumatic Diseases*, 50(6), 376–378.
<https://doi.org/10.1136/ard.50.6.376>
- Deraedt, R., Jouquey, S., ~e, D.], & Flahaut, M. (1980). RELEASE OF PROSTAGLANDINS E AND F IN AN ALGOGENIC REACTION AND ITS INHIBITION. In *European Journal of Pharmacology*.
- Di Cagno, M. biomimetic barrier P. for efficient investigation of passive permeability of drugs, Bibi, H. A., & Bauer-Brandl, A. (2015). New biomimetic barrier Permeapad™ for efficient investigation of passive permeability of drugs. *European Journal of Pharmaceutical Sciences*, 73, 29–34.
<https://doi.org/10.1016/j.ejps.2015.03.019>
- Di Padova, C. (1987). S-Adenosylmethionine in the treatment of osteoarthritis. Review of the clinical studies. *The American Journal of Medicine*, 83(5 SUPPL. 1), 60–65.
[https://doi.org/10.1016/0002-9343\(87\)90853-9](https://doi.org/10.1016/0002-9343(87)90853-9)
- Dmitrenko, M., Liamin, V., Kuzminova, A., Lahderanta, E., Solovyev, N., & Penkova, A. (2021). Modification approaches to enhance dehydration properties of sodium alginate-based pervaporation membranes. *Membranes*, 11(4).
<https://doi.org/10.3390/membranes11040255>
- Dobias, J., Suvorova, E. I., & Bernier-Latmani, R. (2011). Role of proteins in controlling selenium nanoparticle size. *Nanotechnology*, 22(19). <https://doi.org/10.1088/0957-4484/22/19/195605>
- Dustin, M. L. (2003). In vivo imaging approaches in animal models of rheumatoid arthritis. *Arthritis Research and Therapy*, 5(4), 165–171.
<https://doi.org/10.1186/ar768>
- EFSA. (2009). L-selenomethionine as a source of selenium added for nutritional purposes Scientific Opinion of the Panel on Food Additives and Nutrient Sources added to Food Adopted on 14 May 2009. *The EFSA Journal*, 1082, 1–38.
- El-Ramady, H. R., Domokos-Szabolcsy, É., Shalaby, T. A., Prokisch, J., & Fári, M. (2015). *Selenium in Agriculture: Water, Air, Soil, Plants, Food, Animals and Nanoselenium* (pp. 153–232). https://doi.org/10.1007/978-3-319-11906-9_5

- Epple, M. (n.d.). *Synthesis and characterization of inorganic nanoparticles*.
- Evans, C. H., Ghivizzani, S. C., & Robbins, P. D. (2009). Gene therapy of the rheumatic diseases: 1998 to 2008. *Arthritis Research and Therapy*, *11*(1), 1–12. <https://doi.org/10.1186/ar2563>
- Evolving concepts of RA*. (n.d.).
- Ezhuthurakkal, P. B., Polaki, L. R., Suyavaran, A., Subastri, A., Sujatha, V., & Thirunavukkarasu, C. (2017). Selenium nanoparticles synthesized in aqueous extract of *Allium sativum* perturbs the structural integrity of Calf thymus DNA through intercalation and groove binding. *Materials Science and Engineering C*, *74*, 597–608. <https://doi.org/10.1016/j.msec.2017.02.003>
- Faghihzadeh, F., Anaya, N. M., Schifman, L. A., & Oyanedel-Craver, V. (2016). Fourier transform infrared spectroscopy to assess molecular-level changes in microorganisms exposed to nanoparticles. *Nanotechnology for Environmental Engineering*, *1*(1). <https://doi.org/10.1007/s41204-016-0001-8>
- Fairweather-Tait, S. J., Bao, Y., Broadley, M. R., Collings, R., Ford, D., Hesketh, J. E., & Hurst, R. (n.d.). *COMPREHENSIVE INVITED REVIEW Selenium in Human Health and Disease*.
- Fang, X., Wu, X., Li, C., Zhou, B., Chen, X., Chen, T., & Yang, F. (2017). Targeting selenium nanoparticles combined with baicalin to treat HBV-infected liver cancer. *RSC Advances*, *7*(14), 8178–8185. <https://doi.org/10.1039/C6RA28229F>
- Fardsadegh, B., & Jafarizadeh-Malmiri, H. (2019). Aloe vera leaf extract mediated green synthesis of selenium nanoparticles and assessment of their in vitro antimicrobial activity against spoilage fungi and pathogenic bacteria strains. *Green Processing and Synthesis*, *8*(1), 399–407. <https://doi.org/10.1515/gps-2019-0007>
- Faria, M., Björnmalm, M., Thurecht, K. J., Kent, S. J., Parton, R. G., Kavallaris, M., Johnston, A. P. R., Gooding, J. J., Corrie, S. R., Boyd, B. J., Thordarson, P., Whittaker, A. K., Stevens, M. M., Prestidge, C. A., Porter, C. J. H., Parak, W. J., Davis, T. P., Crampin, E. J., & Caruso, F. (2018). Minimum information reporting in bio-nano experimental literature. *Nature Nanotechnology*, *13*(9), 777–785. <https://doi.org/10.1038/s41565-018-0246-4>
- Feldmann, M., Brennan, F. M., Elliott, M. J., Williams, R. O., & Maini, R. N. (n.d.). *TNF α Is an Effective Therapeutic Target for Rheumatoid Arthritis*. www.pdflib.com
- Feng, Y., Su, J., Zhao, Z., Zheng, W., Wu, H., Zhang, Y., & Chen, T. (2014). Differential effects of amino acid surface decoration on the anticancer efficacy of selenium nanoparticles. *Dalton Transactions*, *43*(4), 1854–1861. <https://doi.org/10.1039/c3dt52468j>
- Fernandes, A. P., & Gandin, V. (2015). Selenium compounds as therapeutic agents in cancer. *Biochimica et Biophysica Acta - General Subjects*, *1850*(8), 1642–1660. <https://doi.org/10.1016/j.bbagen.2014.10.008>

- Ferro, C., Florindo, H. F., & Santos, H. A. (2021a). Selenium Nanoparticles for Biomedical Applications: From Development and Characterization to Therapeutics. *Advanced Healthcare Materials*, 10(16), 1–50. <https://doi.org/10.1002/adhm.202100598>
- Ferro, C., Florindo, H. F., & Santos, H. A. (2021b). Selenium Nanoparticles for Biomedical Applications: From Development and Characterization to Therapeutics. In *Advanced Healthcare Materials* (Vol. 10, Issue 16). John Wiley and Sons Inc. <https://doi.org/10.1002/adhm.202100598>
- Findik, F. (2021). *Nanomaterials and their applications*. 9(3), 62–75.
- Firestein, G. S. (2003). Evolving concepts of rheumatoid arthritis. *Nature*, 423(6937), 356–361. <https://doi.org/10.1038/nature01661>
- Firestein, G. S. (2013). Etiology and Pathogenesis of Rheumatoid Arthritis. *Kelley's Textbook of Rheumatology*, 1059-1108.e5. <https://doi.org/10.1016/b978-1-4377-1738-9.00069-4>
- Flemer, S. (2011). Selenol protecting groups in organic chemistry: Special emphasis on selenocysteine Se-protection in solid phase peptide synthesis. *Molecules*, 16(4), 3232–3251. <https://doi.org/10.3390/molecules16043232>
- Foroozandeh, P., & Aziz, A. A. (2018). Insight into Cellular Uptake and Intracellular Trafficking of Nanoparticles. In *Nanoscale Research Letters* (Vol. 13). Springer New York LLC. <https://doi.org/10.1186/s11671-018-2728-6>
- Freund, C., Arthritis, A., Various, A., The, O., Freund, I., & Freund, D. I. (2011). *Protocol for Induction of Adjuvant-Induced Arthritis (AIA) in Rats*. 1–4.
- Fultz, B., & Howe, J. (2013). *Transmission Electron Microscopy and Diffraction of Materials*. Springer Berlin Heidelberg. <https://doi.org/10.1007/978-3-642-29761-8>
- Galan, P., Viteri, F. E., Bertrais, S., Czernichow, S., Faure, H., Arnaud, J., Ruffieux, D., Chenal, S., Arnault, N., Favier, A., Roussel, A. M., & Herberg, S. (2005). Serum concentrations of β -carotene, vitamins C and E, zinc and selenium are influenced by sex, age, diet, smoking status, alcohol consumption and corpulence in a general French adult population. *European Journal of Clinical Nutrition*, 59(10), 1181–1190. <https://doi.org/10.1038/sj.ejcn.1602230>
- Gao, C. H., Mortimer, M., Zhang, M., Holden, P. A., Cai, P., Wu, S., Xin, Y., Wu, Y., & Huang, Q. (2019). Impact of metal oxide nanoparticles on in vitro DNA amplification. *PeerJ*, 2019(6). <https://doi.org/10.7717/peerj.7228>
- Gao, F., Yuan, Q., Gao, L., Cai, P., Zhu, H., Liu, R., Wang, Y., Wei, Y., Huang, G., Liang, J., & Gao, X. (2014). Cytotoxicity and therapeutic effect of irinotecan combined with selenium nanoparticles. *Biomaterials*, 35(31), 8854–8866. <https://doi.org/10.1016/j.biomaterials.2014.07.004>
- Gao, T., Duan, P., Zhang, Q., & Yuan, S. (2021). Application of One-Dimensional Nanomaterials in Catalysis at the Single-Molecule and Single-Particle Scale. In

- Frontiers in Chemistry* (Vol. 9). Frontiers Media S.A.
<https://doi.org/10.3389/fchem.2021.812287>
- Gao, Z., Lee, S., & Huang, J. (2022). The Application of Nanoparticle Ceramic Materials in the Design of Modern Handicrafts. *Journal of Nanomaterials*, 2022. <https://doi.org/10.1155/2022/1998985>
- Geck, P., & Heinz, E. (1989). Secondary active transport: Introductory remarks. *Kidney International*, 36(3), 334–341. <https://doi.org/10.1038/ki.1989.201>
- Genwa, G. E. M., Kumari, K., & Singh, P. (2019). Editorial Nanotechnology: Beneficial or Harmful. In *Nanoscience & Nanotechnology-Asia* (Vol. 9, Issue 1).
- Ghaderi, R. S., Adibian, F., Sabouri, Z., Davoodi, J., Kazemi, M., Amel Jamehdar, S., Meshkat, Z., Soleimanpour, S., & Daroudi, M. (2022). Green synthesis of selenium nanoparticle by *Abelmoschus esculentus* extract and assessment of its antibacterial activity. *Materials Technology*, 37(10), 1289–1297. <https://doi.org/10.1080/10667857.2021.1935602>
- Giancane, G., Consolaro, A., Lanni, S., Davì, S., Schiappapietra, B., & Ravelli, A. (2016). Juvenile Idiopathic Arthritis: Diagnosis and Treatment. In *Rheumatology and Therapy* (Vol. 3, Issue 2, pp. 187–207). Adis. <https://doi.org/10.1007/s40744-016-0040-4>
- Giannousi, K., Lafazanis, K., Arvanitidis, J., Pantazaki, A., & Dendrinou-Samara, C. (2014). Hydrothermal synthesis of copper based nanoparticles: Antimicrobial screening and interaction with DNA. *Journal of Inorganic Biochemistry*, 133, 24–32. <https://doi.org/10.1016/j.jinorgbio.2013.12.009>
- Gill, P., Moghadam, T. T., & Ranjbar, B. (2010). *Differential Scanning Calorimetry Techniques: Applications in Biology and Nanoscience*.
- Goodpaster, J. V., & McGuffin, V. L. (1999). Rapid and accurate determination of Stern-Volmer quenching constants. *Applied Spectroscopy*, 53(8), 1000–1008. <https://doi.org/10.1366/0003702991947676>
- Gouveia, V. M., Lima, S. A. C., Nunes, C., & Reis, S. (2015). Non-biologic nanodelivery therapies for rheumatoid arthritis. *Journal of Biomedical Nanotechnology*, 11(10), 1701–1721. <https://doi.org/10.1166/jbn.2015.2159>
- Gozhong Cao (university of washington, U. (2008). Nanostructures and Nanomaterials. In *Nanostructures and Nanomaterials - synthesis, Properties and applications* (pp. 267–269). Imperial College Press.
- Gracie, J. A., Forsey, R. J., Chan, W. L., Gilmour, A., Leung, B. P., Greer, M. R., Kennedy, K., Carter, R., Wei, X. Q., Xu, D., Field, M., Foulis, A., Liew, F. Y., & McInnes, I. B. (1999). A proinflammatory role for IL-18 in rheumatoid arthritis. *Journal of Clinical Investigation*, 104(10), 1393–1401. <https://doi.org/10.1172/JCI7317>

- Grammatikopoulos, P., Steinhauer, S., Vernieres, J., Singh, V., & Sowwan, M. (2016). Nanoparticle design by gas-phase synthesis. In *Advances in Physics: X* (Vol. 1, Issue 1, pp. 81–100). Taylor and Francis Ltd. <https://doi.org/10.1080/23746149.2016.1142829>
- Guidelines for Bioavailability &. (2005). *Exposure, March*.
- Gunasekaran, T., Haile, T., Nigusse, T., & Dhanaraju, M. D. (2014). Nanotechnology: An effective tool for enhancing bioavailability and bioactivity of phytomedicine. In *Asian Pacific Journal of Tropical Biomedicine* (Vol. 4, pp. S1–S7). Asian Pacific Tropical Biomedicine Press. <https://doi.org/10.12980/APJTB.4.2014C980>
- Guo, X., Cui, H., Zhang, H., Guan, X., Zhang, Z., Jia, C., Wu, J., Yang, H., Qiu, W., Zhang, C., Yang, Z., Chen, Z., & Mao, G. (2015). Protective Effect of Folic Acid on Oxidative DNA Damage. *Medicine (United States)*, *94*(45), e1872. <https://doi.org/10.1097/MD.0000000000001872>
- Halliwell, B., & Gutteridge, J. M. C. (1984). Oxygen toxicity, oxygen radicals, transition metals and disease. *Biochemical Journal*, *219*(1), 1–14. <https://doi.org/10.1042/bj2190001>
- Handa, R., Rao, U. R. K., Lewis, J. F. M., Rambhad, G., Shiff, S., & Ghia, C. J. (2016). Literature review of rheumatoid arthritis in India. *International Journal of Rheumatic Diseases*, *19*(5), 440–451. <https://doi.org/10.1111/1756-185X.12621>
- Hariharan, S., & Dharmaraj, S. (2020). Selenium and selenoproteins: it's role in regulation of inflammation. In *Inflammopharmacology* (Vol. 28, Issue 3, pp. 667–695). Springer. <https://doi.org/10.1007/s10787-020-00690-x>
- Hart, F. D. (1970). Rheumatoid Arthritis: Extra-articular Manifestations. Part II. *British Medical Journal*, *2*(5712), 747–752. <https://doi.org/10.1136/bmj.2.5712.747>
- Hasan, S. (2014). A Review on Nanoparticles : Their Synthesis and Types. *Research Journal of Recent Sciences Res . J. Recent . Sci . Uttar Pradesh (Lucknow Campus)*, *4*(February), 1–3.
- Hijaz, M., Das, S., Mert, I., Gupta, A., Al-Wahab, Z., Tebbe, C., Dar, S., Chhina, J., Giri, S., Munkarah, A., Seal, S., & Rattan, R. (2016). Folic acid tagged nanoceria as a novel therapeutic agent in ovarian cancer. *BMC Cancer*, *16*(1), 1–14. <https://doi.org/10.1186/s12885-016-2206-4>
- Hoang, N. H., Thanh, T. Le, Sangpueak, R., Treekoon, J., Saengchan, C., Thepbandit, W., Papatthoti, N. K., Kamkaew, A., & Buensanteai, N. (2022). Chitosan Nanoparticles-Based Ionic Gelation Method: A Promising Candidate for Plant Disease Management. In *Polymers* (Vol. 14, Issue 4). MDPI. <https://doi.org/10.3390/polym14040662>
- Hoonjan, M., Sachdeva, G., Chandra, S., Kharkar, P. S., Sahu, N., & Bhatt, P. (2018). Investigation of HSA as a biocompatible coating material for arsenic trioxide nanoparticles. *Nanoscale*, *10*(17), 8031–8041. <https://doi.org/10.1039/c7nr09503a>

- Hosnedlova, B., Kepinska, M., Skalickova, S., Fernandez, C., Ruttkay-Nedecky, B., Peng, Q., Baron, M., Melcova, M., Opatrilova, R., Zidkova, J., Bjørklund, G., Sochor, J., & Kizek, R. (2018). Nano-selenium and its nanomedicine applications: A critical review. *International Journal of Nanomedicine*, *13*, 2107–2128. <https://doi.org/10.2147/IJN.S157541>
- Htun, T. (2004). A Negative Deviation from Stern-Volmer Equation in Fluorescence Quenching. In *Journal of Fluorescence* (Vol. 14, Issue 2).
- Hü Bner, C. A., & Jentsch, T. J. (n.d.). *Ion channel diseases*. <https://academic.oup.com/hmg/article/11/20/2435/615688>
- Hu, T., Mei, X., Wang, Y., Weng, X., Liang, R., & Wei, M. (2019). Two-dimensional nanomaterials: fascinating materials in biomedical field. In *Science Bulletin* (Vol. 64, Issue 22, pp. 1707–1727). Elsevier B.V. <https://doi.org/10.1016/j.scib.2019.09.021>
- Huang, H., Lai, W., Cui, M., Liang, L., Lin, Y., Fang, Q., Liu, Y., & Xie, L. (2016a). An Evaluation of Blood Compatibility of Silver Nanoparticles. *Scientific Reports*, *6*(January), 1–15. <https://doi.org/10.1038/srep25518>
- Huang, H., Lai, W., Cui, M., Liang, L., Lin, Y., Fang, Q., Liu, Y., & Xie, L. (2016b). An Evaluation of Blood Compatibility of Silver Nanoparticles. *Scientific Reports*, *6*. <https://doi.org/10.1038/srep25518>
- Huang, Y., He, L., Liu, W., Fan, C., Zheng, W., Wong, Y. S., & Chen, T. (2013). Selective cellular uptake and induction of apoptosis of cancer-targeted selenium nanoparticles. *Biomaterials*, *34*(29), 7106–7116. <https://doi.org/10.1016/j.biomaterials.2013.04.067>
- Huang, Z., Rose, A. H., & Hoffmann, P. R. (2012). The role of selenium in inflammation and immunity: From molecular mechanisms to therapeutic opportunities. *Antioxidants and Redox Signaling*, *16*(7), 705–743. <https://doi.org/10.1089/ars.2011.4145>
- Huber, L. C., Distler, O., Tarner, I., Gay, R. E., Gay, S., & Pap, T. (2006). Synovial fibroblasts: Key players in rheumatoid arthritis. *Rheumatology*, *45*(6), 669–675. <https://doi.org/10.1093/rheumatology/ke1065>
- Hulla, J. E., Sahu, S. C., & Hayes, A. W. (2015). Nanotechnology: History and future. In *Human and Experimental Toxicology* (Vol. 34, Issue 12, pp. 1318–1321). SAGE Publications Ltd. <https://doi.org/10.1177/0960327115603588>
- Husen, A., & Siddiqi, K. S. (2014). Plants and microbes assisted selenium nanoparticles: Characterization and application. *Journal of Nanobiotechnology*, *12*(1), 1–10. <https://doi.org/10.1186/s12951-014-0028-6>
- Ibrahim, R. K., Hayyan, M., AlSaadi, M. A., Hayyan, A., & Ibrahim, S. (2016). Environmental application of nanotechnology: air, soil, and water. In *Environmental Science and Pollution Research* (Vol. 23, Issue 14, pp. 13754–13788). Springer Verlag. <https://doi.org/10.1007/s11356-016-6457-z>

- Ijaz, I., Gilani, E., Nazir, A., & Bukhari, A. (2020). Detail review on chemical, physical and green synthesis, classification, characterizations and applications of nanoparticles. In *Green Chemistry Letters and Reviews* (Vol. 13, Issue 3, pp. 59–81). Taylor and Francis Ltd. <https://doi.org/10.1080/17518253.2020.1802517>
- Indumathy, M., Raj, S. S., Arumugham, I. M., & Kumar, R. P. (2020). Assessment of Toxicity of Selenium Nanoparticle Varnish Using HepG2 Cell Lines: In vitro Study. *Journal of Pharmaceutical Research International*, 33–39. <https://doi.org/10.9734/jpri/2020/v32i2730853>
- Ingels, F., Deferme, S., Destexhe, E., Oth, M., Van Den Mooter, G., & Augustijns, P. (2002). Simulated intestinal fluid as transport medium in the Caco-2 cell culture model. *International Journal of Pharmaceutics*, 232(1–2), 183–192. [https://doi.org/10.1016/S0378-5173\(01\)00897-3](https://doi.org/10.1016/S0378-5173(01)00897-3)
- Iwaoka, M., Ooka, R., Nakazato, T., Yoshida, S., & Oishi, S. (2008). Synthesis of selenocysteine and selenomethionine derivatives from sulfur-containing amino acids. *Chemistry and Biodiversity*, 5(3), 359–374. <https://doi.org/10.1002/cbdv.200890037>
- Jacobsen, A. C., Nielsen, S., Brandl, M., & Bauer-Brandl, A. (2020). Drug Permeability Profiling Using the Novel Permeapad® 96-Well Plate. *Pharmaceutical Research*, 37(6), 93. <https://doi.org/10.1007/s11095-020-02807-x>
- Jana, S. (2019). Particle Size, Surface Area, Crystallite Size, and Thermal Analysis of Consciousness Energy Healing Treated Selenium. *Research & Development in Material Science*, 9(3). <https://doi.org/10.31031/rdms.2019.09.000713>
- Jarvis, I., & Jarvis, K. E. (1992). Plasma spectrometry in the earth sciences: techniques, applications and future trends. In *Chemical Geology* (Vol. 95).
- Jeyaraj, M., Gurunathan, S., Qasim, M., Kang, M. H., & Kim, J. H. (2019). A comprehensive review on the synthesis, characterization, and biomedical application of platinum nanoparticles. In *Nanomaterials* (Vol. 9, Issue 12). MDPI AG. <https://doi.org/10.3390/nano9121719>
- Jo, J. H., Singh, P., Kim, Y. J., Wang, C., Mathiyalagan, R., Jin, C. G., & Yang, D. C. (2016). Pseudomonas deceptionensis DC5-mediated synthesis of extracellular silver nanoparticles. *Artificial Cells, Nanomedicine and Biotechnology*, 44(6), 1576–1581. <https://doi.org/10.3109/21691401.2015.1068792>
- Johansson, L., Gafvelin, G., & Arnér, E. S. J. (2005). Selenocysteine in proteins - Properties and biotechnological use. *Biochimica et Biophysica Acta - General Subjects*, 1726(1), 1–13. <https://doi.org/10.1016/j.bbagen.2005.05.010>
- John, A. T., & Tricoli, A. (2022). Flame assisted synthesis of nanostructures for device applications. In *Advances in Physics: X* (Vol. 7, Issue 1). Taylor and Francis Ltd. <https://doi.org/10.1080/23746149.2021.1997153>
- Kalinski, P. (2012). Regulation of Immune Responses by Prostaglandin E 2 . *The Journal of Immunology*, 188(1), 21–28. <https://doi.org/10.4049/jimmunol.1101029>

- Kaur, K., & Rath, G. (2019). Formulation and evaluation of UV protective synbiotic skin care topical formulation. *Journal of Cosmetic and Laser Therapy*, 21(6), 332–342. <https://doi.org/10.1080/14764172.2019.1658878>
- Kaye, P. M., & Aebischer, T. (2011). Visceral leishmaniasis: Immunology and prospects for a vaccine. In *Clinical Microbiology and Infection* (Vol. 17, Issue 10, pp. 1462–1470). Blackwell Publishing Ltd. <https://doi.org/10.1111/j.1469-0691.2011.03610.x>
- Ketterer, M. E. (n.d.). *Geology and Mineralogy Applications of Atomic Spectroscopy*.
- Khan, H. A., Abdelhalim, M. A. K., Al-Ayed, M. S., & Alhomida, A. S. (2012). Effect of gold nanoparticles on glutathione and malondialdehyde levels in liver, lung and heart of rats. *Saudi Journal of Biological Sciences*, 19(4), 461–464. <https://doi.org/10.1016/j.sjbs.2012.06.005>
- Khurana, A., Tekula, S., Saifi, M. A., Venkatesh, P., & Godugu, C. (2019). Therapeutic applications of selenium nanoparticles. In *Biomedicine and Pharmacotherapy* (Vol. 111, pp. 802–812). Elsevier Masson SAS. <https://doi.org/10.1016/j.biopha.2018.12.146>
- Kipper, A. I., Titova, A. V., Borovikova, L. N., & Pisarev, O. A. (2015). Morphological characteristics of selenium-polyethylene glycol nanocomposites. *Russian Journal of Physical Chemistry A*, 89(9), 1625–1627. <https://doi.org/10.1134/S0036024415090174>
- Kolb, M. J., Bourne, W. M., & Clinic, M. (1986). Supravital fluorescent staining of the corneal endothelium with acridine orange and ethidium bromide. *Current Eye Research*, 5(7).
- Kumar, M., Dwivedi, C., Shah, C. P., Singh, K., & Bajaj, P. N. (2011). An organic acid-induced synthesis and characterization of selenium nanoparticles. *Journal of Nanotechnology*. <https://doi.org/10.1155/2011/651971>
- Kumar, S. (2009). Synthesis and characterisation of selenium nanowires using template synthesis. *Journal of Experimental Nanoscience*, 4(4), 341–346. <https://doi.org/10.1080/17458080903055666>
- Kumar, V., Sharma, N., & Maitra, S. S. (2017). In vitro and in vivo toxicity assessment of nanoparticles. *International Nano Letters*, 7(4), 243–256. <https://doi.org/10.1007/s40089-017-0221-3>
- Kumari, S., Mg, S., & Mayor, S. (2010). Endocytosis unplugged: Multiple ways to enter the cell. In *Cell Research* (Vol. 20, Issue 3, pp. 256–275). <https://doi.org/10.1038/cr.2010.19>
- Langsdorf, A., And, J. R., & Segre, E. (n.d.). *Nuclear Isomerism in Selenium and Krypton*.
- Laslo, V., Pinzaru, S. C., Zagula, G., Kluz, M., Vicas, S. I., & Cavalu, S. (2022). Synergic effect of selenium nanoparticles and lactic acid bacteria in reduction

- cadmium toxicity. *Journal of Molecular Structure*, 1247.
<https://doi.org/10.1016/j.molstruc.2021.131325>
- Laurent, S., Forge, D., Port, M., Roch, A., Robic, C., Vander Elst, L., & Muller, R. N. (2008). Magnetic iron oxide nanoparticles: Synthesis, stabilization, vectorization, physicochemical characterizations and biological applications. *Chemical Reviews*, 108(6), 2064–2110. <https://doi.org/10.1021/cr068445e>
- Leonavičienė, L., Bradūnaitė, R., Vaitkienė, D., Vasiliauskas, A., & Keturkienė, A. (2008). Collagen-induced arthritis and pro-/antioxidant status in Wistar and Lewis rats. *Biologija*, 54(4), 290–300. <https://doi.org/10.2478/v10054-008-0059-8>
- Lewinski, N., Colvin, V., & Drezek, R. (2008). Cytotoxicity of nanoparticles. In *Small* (Vol. 4, Issue 1, pp. 26–49). <https://doi.org/10.1002/sml.200700595>
- Lewis Horowitz, D., & Katzap, E. (2011). *Approach to Septic Arthritis* (Vol. 84, Issue 6). www.aafp.org/afpAmericanFamilyPhysician653
- Li, L., Mu, Q., Zhang, B., & Yan, B. (2010). Analytical strategies for detecting nanoparticle-protein interactions. In *Analyst* (Vol. 135, Issue 7, pp. 1519–1530). Royal Society of Chemistry. <https://doi.org/10.1039/c0an00075b>
- Li, M., Si, L., Pan, H., Rabba, A. K., Yan, F., Qiu, J., & Li, G. (2011). Excipients enhance intestinal absorption of ganciclovir by P-gp inhibition: Assessed in vitro by everted gut sac and in situ by improved intestinal perfusion. *International Journal of Pharmaceutics*, 403(1–2), 37–45. <https://doi.org/10.1016/j.ijpharm.2010.10.017>
- Lin, H., Gerbec, J. A., Sushchikh, M., & McFarland, E. W. (2008). Synthesis of amorphous silicon carbide nanoparticles in a low temperature low pressure plasma reactor. *Nanotechnology*, 19(32). <https://doi.org/10.1088/0957-4484/19/32/325601>
- Lin, Z. H., & Wang, C. R. C. (2005). Evidence on the size-dependent absorption spectral evolution of selenium nanoparticles. *Materials Chemistry and Physics*, 92(2–3), 591–594. <https://doi.org/10.1016/j.matchemphys.2005.02.023>
- Liu, C., Hu, T., Wu, Y., Gao, H., Yang, Y., & Ren, W. (2019). 2D selenium allotropes from first principles and swarm intelligence. *Journal of Physics Condensed Matter*, 31(23). <https://doi.org/10.1088/1361-648X/ab059d>
- Liu, F. K. (2009). Analysis and applications of nanoparticles in the separation sciences: A case of gold nanoparticles. In *Journal of Chromatography A* (Vol. 1216, Issue 52, pp. 9034–9047). <https://doi.org/10.1016/j.chroma.2009.07.026>
- Liu, K., Liu, P. cheng, Liu, R., & Wu, X. (2015). Dual AO/EB staining to detect apoptosis in osteosarcoma cells compared with flow cytometry. *Medical Science Monitor Basic Research*, 21, 15–20. <https://doi.org/10.12659/MSMBR.893327>
- Lombardo, D., Calandra, P., Pasqua, L., & Magazù, S. (2020). Self-assembly of organic nanomaterials and biomaterials: The bottom-up approach for functional nanostructures formation and advanced applications. *Materials*, 13(5). <https://doi.org/10.3390/ma13051048>

- LOWRY, O. H., ROSEBROUGH, N. J., FARR, A. L., & RANDALL, R. J. (1951). Protein measurement with the Folin phenol reagent. *The Journal of Biological Chemistry*, 193(1), 265–275. [https://doi.org/10.1016/s0021-9258\(19\)52451-6](https://doi.org/10.1016/s0021-9258(19)52451-6)
- Lyons, G. H., Genc, Y., Soole, K., Stangoulis, J. C. R., Liu, F., & Graham, R. D. (2009). Selenium increases seed production in Brassica. *Plant and Soil*, 318(1–2), 73–80. <https://doi.org/10.1007/s11104-008-9818-7>
- Madaan, K., Kumar, S., Poonia, N., Lather, V., & Pandita, D. (2014). Dendrimers in drug delivery and targeting: Drug-dendrimer interactions and toxicity issues. *Journal of Pharmacy and Bioallied Sciences*, 6(3), 139–150. <https://doi.org/10.4103/0975-7406.130965>
- Maini, R. N., Elliott, M. J., Brennan, F. M., & FELDMANN Kennedy, M. (1995). Beneficial effects of tumour necrosis factor-alpha (TNF-a) blockade in rheumatoid arthritis (RA). In *Clin Exp Immunol* (Vol. 101).
- Maiyo, F., & Singh, M. (2017). Selenium nanoparticles: Potential in cancer gene and drug delivery. *Nanomedicine*, 12(9), 1075–1089. <https://doi.org/10.2217/nmm-2017-0024>
- Malhotra, S., Jha, N., & Desai, K. (2014). a Superficial Synthesis of Selenium Nanospheres Using Wet Chemical Approach. *International Journal of Nanotechnology and Application*, 3(4), 2277–4777.
- Malhotra, S., Welling, M. N., Mantri, S. B., & Desai, K. (2016). In vitro and in vivo antioxidant, cytotoxic, and anti-chronic inflammatory arthritic effect of selenium nanoparticles. *Journal of Biomedical Materials Research - Part B Applied Biomaterials*, 104(5), 993–1003. <https://doi.org/10.1002/jbm.b.33448>
- Manam, V. K., Nakkella, A. K., & Gujarathi, J. R. (n.d.). *Frontiers in nanotechnology*.
- Maqbool, I., & Noreen, S. (2019). A Review of Novel Techniques for Nanoparticles Preparation. *Global Drug Design & Development Review*, IV(I), 41–50. [https://doi.org/10.31703/gdddr.2019\(iv-i\).05](https://doi.org/10.31703/gdddr.2019(iv-i).05)
- MARKLUND, S., & MARKLUND, G. (1974). Involvement of the Superoxide Anion Radical in the Autoxidation of Pyrogallol and a Convenient Assay for Superoxide Dismutase. *European Journal of Biochemistry*, 47(3), 469–474. <https://doi.org/10.1111/j.1432-1033.1974.tb03714.x>
- Martínez, F. G., Moreno-Martin, G., Pescuma, M., Madrid-Albarrán, Y., & Mozzi, F. (2020). Biotransformation of Selenium by Lactic Acid Bacteria: Formation of Seleno-Nanoparticles and Seleno-Amino Acids. *Frontiers in Bioengineering and Biotechnology*, 8(June), 1–17. <https://doi.org/10.3389/fbioe.2020.00506>
- Masungi, C., Borremans, C., Willems, B., Mensch, J., Van Dijck, A., Augustijns, P., Brewster, M. E., & Noppe, M. (2004). Usefulness of a novel Caco-2 cell perfusion system. I. In vitro prediction of the absorption potential of passively diffused compounds. *Journal of Pharmaceutical Sciences*, 93(10), 2507–2521. <https://doi.org/10.1002/jps.20149>

- Matsui, I. (2005). Journal Review Nanoparticles for Electronic Device Applications: A Brief Review. In *Journal of Chemical Engineering of Japan* (Vol. 38, Issue 8).
- Maynard, A. D. (2007). Nanotechnology: The next big thing, or much ado about nothing? In *Annals of Occupational Hygiene* (Vol. 51, Issue 1, pp. 1–12).
<https://doi.org/10.1093/annhyg/mel071>
- Mazumdar, S., Chitkara, D., & Mittal, A. (2021). Exploration and insights into the cellular internalization and intracellular fate of amphiphilic polymeric nanocarriers. In *Acta Pharmaceutica Sinica B* (Vol. 11, Issue 4, pp. 903–924). Chinese Academy of Medical Sciences. <https://doi.org/10.1016/j.apsb.2021.02.019>
- Megraj, K., Raju, K., Balaraman, R., & Meenakshisundaram, K. (2011). Biological activities of some Indian medicinal plants. In *Journal of Advanced Pharmacy Education & Research* (Vol. 1, Issue 1).
- Mekail, A., & Sharafaddin, Z. A. (2009). a Study of the Activity of Catalase and Glutathione S-Transferase in Weanling and Adult Rats Intoxicated With Diazinon, Carbaryl and Lambda-cyhalothrin. *J. Duhok Univ.*, 12(Special Issue), 138–145.
- Mekuye, B., & Abera, B. (2023). Nanomaterials: An overview of synthesis, classification, characterization, and applications. *Nano Select*.
<https://doi.org/10.1002/nano.202300038>
- Mellinas, C., Jiménez, A., & del Carmen Garrigós, M. (2019). Microwave-assisted green synthesis and antioxidant activity of selenium nanoparticles using theobroma cacao l. bean shell extract. *Molecules*, 24(22). <https://doi.org/10.3390/molecules24224048>
- Menon, S., Agarwal, H., & Shanmugam, V. K. (2021). Catalytic degradation of industrial dyes using biosynthesized selenium nanoparticles and evaluating its antimicrobial activities. *Sustainable Environment Research*, 31(1).
<https://doi.org/10.1186/s42834-020-00072-6>
- Menon, S., Agarwal, H., Venkat Kumar, S., & Rajeshkumar, S. (2019). Biomimetic synthesis of selenium nanoparticles and its biomedical applications. In *Green Synthesis, Characterization and Applications of Nanoparticles*. Elsevier Inc.
<https://doi.org/10.1016/b978-0-08-102579-6.00008-3>
- Menon, S., KS, S. D., Santhiya, R., Rajeshkumar, S., & S, V. K. (2018). Selenium nanoparticles: A potent chemotherapeutic agent and an elucidation of its mechanism. In *Colloids and Surfaces B: Biointerfaces* (Vol. 170, pp. 280–292). Elsevier B.V. <https://doi.org/10.1016/j.colsurfb.2018.06.006>
- Menon, S., Shrudhi, S. D., Agarwal, H., & Shanmugam, V. K. (2019). Efficacy of Biogenic Selenium Nanoparticles from an Extract of Ginger towards Evaluation on Anti-Microbial and Anti-Oxidant Activities. *Colloids and Interface Science Communications*, 29(November 2018), 1–8.
<https://doi.org/10.1016/j.colcom.2018.12.004>
- Mohanraj, V. J., & Chen, Y. (2006). Nanoparticles-A Review. In *Tropical Journal of Pharmaceutical Research* (Vol. 5, Issue 1). <http://www.tjpr.freehosting.net>

- Mondal, K., & Srivastava, S. K. (2010). A new chemical approach to the low-temperature growth of single crystalline trigonal selenium scrolled nanotubes and nanowires. *Journal of Nanoscience and Nanotechnology*, *10*(1), 555–560. <https://doi.org/10.1166/jnn.2010.1726>
- Mugesh, G., Du Mont, W. W., & Sies, H. (2001). Chemistry of biologically important synthetic organoselenium compounds. *Chemical Reviews*, *101*(7), 2125–2179. <https://doi.org/10.1021/cr000426w>
- Muthu, S., Raju, V., Babu, V., Amsaveni, G., & Karthik, G. (2019). A rapid synthesis and antibacterial property of selenium nanoparticles using egg white lysozyme as a stabilizing agent. *SN Applied Sciences*. <https://doi.org/10.1007/s42452-019-1509-x>
- Naahidi, S., Jafari, M., Edalat, F., Raymond, K., Khademhosseini, A., & Chen, P. (2013). Biocompatibility of engineered nanoparticles for drug delivery. *Journal of Controlled Release*, *166*(2), 182–194. <https://doi.org/10.1016/j.jconrel.2012.12.013>
- Nam, N. H., & Luong, N. H. (2019). Nanoparticles: Synthesis and applications. In *Materials for Biomedical Engineering: Inorganic Micro- and Nanostructures* (pp. 211–240). Elsevier. <https://doi.org/10.1016/B978-0-08-102814-8.00008-1>
- Nandi, A., & Chatterjee, I. B. (1988). Assay of superoxide dismutase activity in animal tissues. *Journal of Biosciences*, *13*(3), 305–315. <https://doi.org/10.1007/BF02712155>
- National Research Council. (2000). Dietary Reference Intakes for vitamin C, vitamin E, selenium, and carotenoids. In *Medicine*. <https://doi.org/10.1111/j.1753-4887.1997.tb01621.x>
- Niewold, T. B., Harrison, M. J., & Paget, S. A. (2007). Anti-CCP antibody testing as a diagnostic and prognostic tool in rheumatoid arthritis. *Qjm*, *100*(4), 193–201. <https://doi.org/10.1093/qjmed/hcm015>
- Nimi, N., Paul, W., & Sharma, C. P. (2011). Blood protein adsorption and compatibility studies of gold nanoparticles. *Gold Bulletin*, *44*(1), 15–20. <https://doi.org/10.1007/s13404-010-0001-6>
- Oktyabrsky, O. N., & Smirnova, G. V. (2007). Redox regulation of cellular functions. In *Biochemistry (Moscow)* (Vol. 72, Issue 2, pp. 132–145). Maik Nauka-Interperiodica Publishing. <https://doi.org/10.1134/S0006297907020022>
- Orr, C. K., Najm, A., Young, F., McGarry, T., Biniecka, M., Fearon, U., & Veale, D. J. (2018). The utility and limitations of CRP, ESR and DAS28-CRP in appraising disease activity in rheumatoid arthritis. *Frontiers in Medicine*, *5*(JUN). <https://doi.org/10.3389/fmed.2018.00185>
- Overview of Gout.* (n.d.).
- Palomar, Q., Xu, X. X., Selegård, R., Aili, D., & Zhang, Z. (2020). Peptide decorated gold nanoparticle/carbon nanotube electrochemical sensor for ultrasensitive

- detection of matrix metalloproteinase-7. *Sensors and Actuators, B: Chemical*, 325. <https://doi.org/10.1016/j.snb.2020.128789>
- Palumbo, P., Picchini, U., Beck, B., Van Gelder, J., Delbar, N., & DeGaetano, A. (2008). A general approach to the apparent permeability index. *Journal of Pharmacokinetics and Pharmacodynamics*, 35(2), 235–248. <https://doi.org/10.1007/s10928-008-9086-4>
- Panahi-Kalamuei, M., Mousavi-Kamazani, M., Salavati-Niasari, M., & Hosseinpour-Mashkani, S. M. (2015). A simple sonochemical approach for synthesis of selenium nanostructures and investigation of its light harvesting application. *Ultrasonics Sonochemistry*, 23, 246–256. <https://doi.org/10.1016/j.ultsonch.2014.09.006>
- Panahi-Kalamuei, M., Salavati-Niasari, M., & Hosseinpour-Mashkani, S. M. (2014). Facile microwave synthesis, characterization, and solar cell application of selenium nanoparticles. *Journal of Alloys and Compounds*, 617, 627–632. <https://doi.org/10.1016/j.jallcom.2014.07.174>
- Pandiarajan, S., Umadevi, M., Briget Mary, M., Rajaram, R. K., & Ramakrishnan, V. (2004). Infrared and Raman spectroscopic studies of L-methioniniun nitrate. *Journal of Raman Spectroscopy*, 35(11), 907–913. <https://doi.org/10.1002/jrs.1224>
- Paola Rosanna, D., & Salvatore, C. (2012). Reactive Oxygen Species, Inflammation, and Lung Diseases. *Current Pharmaceutical Design*, 18(26), 3889–3900. <https://doi.org/10.2174/138161212802083716>
- Papadopoulou, A., Green, R. J., & Frazier, R. A. (2005). Interaction of flavonoids with bovine serum albumin: A fluorescence quenching study. *Journal of Agricultural and Food Chemistry*, 53(1), 158–163. <https://doi.org/10.1021/jf048693g>
- Patel, A. S., Sahoo, H., & Mohanty, T. (2016). Understanding the interactions involved in the formation of fluorescent silver nanoclusters. *Journal of Nanoscience and Nanotechnology*, 16(8), 8246–8251. <https://doi.org/10.1166/jnn.2016.11634>
- Patel, K. D., Singh, R. K., & Kim, H. W. (2019). Carbon-based nanomaterials as an emerging platform for theranostics. In *Materials Horizons* (Vol. 6, Issue 3, pp. 434–469). Royal Society of Chemistry. <https://doi.org/10.1039/c8mh00966j>
- Peng, C., Zhang, W., Gao, H., Li, Y., Tong, X., Li, K., Zhu, X., Wang, Y., & Chen, Y. (2017). Behavior and potential impacts of metal-based engineered nanoparticles in aquatic environments. In *Nanomaterials* (Vol. 7, Issue 1). MDPI AG. <https://doi.org/10.3390/nano7010021>
- Peng, D., Zhang, J., Liu, Q., & Taylor, E. W. (2007). Size effect of elemental selenium nanoparticles (Nano-Se) at supranutritional levels on selenium accumulation and glutathione S-transferase activity. *Journal of Inorganic Biochemistry*, 101(10), 1457–1463. <https://doi.org/10.1016/j.jinorgbio.2007.06.021>
- Pérez-Cano, F. J., Massot-Cladera, M., Franch, À., Castellote, C., & Castell, M. (2013). The effects of cocoa on the immune system. In *Frontiers in Pharmacology: Vol. 4 JUN*. <https://doi.org/10.3389/fphar.2013.00071>

- Petty RE, C. JT. (2016). *Textbook of pediatric rheumatology*. (R. M. L. L. Wedderburn. Carol B. Lindsley, Ed.). Philadelphia: Saunders Elsevier; 2011.
- Phull, A. R., Nasir, B., Haq, I. ul, & Kim, S. J. (2018). Oxidative stress, consequences and ROS mediated cellular signaling in rheumatoid arthritis. In *Chemico-Biological Interactions* (Vol. 281, pp. 121–136). Elsevier Ireland Ltd. <https://doi.org/10.1016/j.cbi.2017.12.024>
- Pillay, N. S., Daniels, A., & Singh, M. (2020). Folate-targeted transgenic activity of dendrimer functionalized selenium nanoparticles in vitro. *International Journal of Molecular Sciences*, 21(19), 1–17. <https://doi.org/10.3390/ijms21197177>
- Plano, D., Baquedano, Y., Ibáñez, E., Jiménez, I., Palop, J. A., Spallholz, J. E., & Sanmartín, C. (2010). Antioxidant-prooxidant properties of a new organoselenium compound library. *Molecules*, 15(10), 7292–7312. <https://doi.org/10.3390/molecules15107292>
- Poole, C. P., & Frank Owens, J. J. (2003). *INTRODUCTION TO NANOTECHNOLOGY @z+::iCIENcE zyxwvutsrqponmlkjihgfe*. www.copyright.com.
- Pouri, S., Motamedi, H., Honary, S., & Kazeminezhad, I. (2017a). Biological Synthesis of Selenium Nanoparticles and Evaluation of their Bioavailability. *Brazilian Archives of Biology and Technology*, 60. <https://doi.org/10.1590/1678-4324-2017160452>
- Pouri, S., Motamedi, H., Honary, S., & Kazeminezhad, I. (2017b). Biological Synthesis of Selenium Nanoparticles and Evaluation of their Bioavailability. *Brazilian Archives of Biology and Technology*, 60. <https://doi.org/10.1590/1678-4324-2017160452>
- Pouri, S., Motamedi, H., Honary, S., & Kazeminezhad, I. (2017c). Biological Synthesis of Selenium Nanoparticles and Evaluation of their Bioavailability. *Brazilian Archives of Biology and Technology*, 60. <https://doi.org/10.1590/1678-4324-2017160452>
- Prado-Gotor, R., & Grueso, E. (2011). A kinetic study of the interaction of DNA with gold nanoparticles: Mechanistic aspects of the interaction. *Physical Chemistry Chemical Physics*, 13(4), 1479–1489. <https://doi.org/10.1039/c0cp00901f>
- Praktikum, P., & Quenching, F. (2016). Fluorescence Quenching Studies. *Physikalisch-Chemisches Praktikum*, 1, 1–14. <https://www.chem.uzh.ch/de/study/download/year2/che211.html>
- Prasad, K. S., Patel, H., Patel, T., Patel, K., & Selvaraj, K. (2013). Biosynthesis of Se nanoparticles and its effect on UV-induced DNA damage. *Colloids and Surfaces B: Biointerfaces*, 103, 261–266. <https://doi.org/10.1016/j.colsurfb.2012.10.029>
- Prasad, L. K., O'Mary, H., & Cui, Z. (2015). Nanomedicine delivers promising treatments for rheumatoid arthritis. *Nanomedicine*, 10(13), 2063–2074. <https://doi.org/10.2217/nmm.15.45>

- Prempeh, A. B. A., & Mensah-Attipoe, J. (2008). *IN VIVO INHIBITION OF PROSTAGLANDIN E 2 PRODUCTION BY CRUDE AQUEOUS EXTRACT OF THE ROOT BARK OF ZANTHOXY-LUM XANTHOXYLOIDES* (Vol. 42).
- Professor of Microbiology, A. (2015). International Journal of Biomedical Research Anti-Cyclic Citrullinated Peptide Antibodies: Clinical utility and their role as early prognostic markers in Erosive Rheumatoid Arthritis. *International Journal of Biomedical Research*, 6(06), 6. <https://doi.org/10.7439/ijbr>
- Puszczewicz, M., & Iwaszkiewicz, C. (2011). Role of anti-citrullinated protein antibodies in diagnosis and prognosis of rheumatoid arthritis. *Archives of Medical Science*, 7(2), 189–194. <https://doi.org/10.5114/aoms.2011.22067>
- Qaddoumi, M. G., Ueda, H., Yang, J., Davda, J., Labhassetwar, V., & Lee, V. H. L. (2004). *The Characteristics and Mechanisms of Uptake of PLGA Nanoparticles in Rabbit Conjunctival Epithelial Cell Layers*.
- Quintana, M., Haro-Poniatowski, E., Morales, J., & Batina, N. (n.d.). *Synthesis of selenium nanoparticles by pulsed laser ablation*.
- Rahman, M. M., Islam, M. B., Biswas, M., & Khurshid Alam, A. H. M. (2015). In vitro antioxidant and free radical scavenging activity of different parts of *Tabebuia pallida* growing in Bangladesh. *BMC Research Notes*, 8(1). <https://doi.org/10.1186/s13104-015-1618-6>
- Rajeshkumar, S., Veena, P., & Santhiyaa, R. V. (2018). Synthesis and Characterization of Selenium Nanoparticles Using Natural Resources and Its Applications. In *Nanotechnology in the Life Sciences* (pp. 63–79). Springer Science and Business Media B.V. https://doi.org/10.1007/978-3-319-99570-0_4
- Rajkumar, K., Sandhya, M. V. S., Koganti, S., & Burgula, S. (2020). Selenium nanoparticles synthesized using *Pseudomonas stutzeri* (Mh191156) show antiproliferative and anti-angiogenic activity against cervical cancer cells. *International Journal of Nanomedicine*, 15, 4523–4540. <https://doi.org/10.2147/IJN.S247426>
- Ramamurthy, C. H., Sampath, K. S., Arunkumar, P., Kumar, M. S., Sujatha, V., Premkumar, K., & Thirunavukkarasu, C. (2013). Green synthesis and characterization of selenium nanoparticles and its augmented cytotoxicity with doxorubicin on cancer cells. *Bioprocess and Biosystems Engineering*, 36(8), 1131–1139. <https://doi.org/10.1007/s00449-012-0867-1>
- Ramos, J. F., & Webster, T. J. (2012). Cytotoxicity of selenium nanoparticles in rat dermal fibroblasts. *International Journal of Nanomedicine*, 7, 3907–3914. <https://doi.org/10.2147/IJN.S33767>
- Randika Perera, Y., Hill, R. A., & Fitzkee, N. C. (2019). Protein Interactions with Nanoparticle Surfaces: Highlighting Solution NMR Techniques. In *Israel Journal of Chemistry* (Vol. 59, Issues 11–12, pp. 962–979). Wiley-VCH Verlag. <https://doi.org/10.1002/ijch.201900080>

- Ricciotti, E., A. G., & Fitzgerald. (2011). [Eicosanoid neuroinflammation] Prostaglandins and Inflammation. *Arterioscler Thromb Vasc Biol.*, 31(5), 986–1000. <https://doi.org/10.1161/ATVBAHA.110.207449>. Prostaglandins
- Rocourt, C. R. B., & Cheng, W. H. (2013). Selenium supranutrition: Are the potential benefits of chemoprevention outweighed by the promotion of diabetes and insulin resistance? *Nutrients*, 5(4), 1349–1365. <https://doi.org/10.3390/nu5041349>
- Saallah, S., & Lenggoro, I. W. (2018). Nanoparticles carrying biological molecules: Recent advances and applications. In *KONA Powder and Particle Journal* (Vol. 2018, Issue 35, pp. 89–111). Hosokawa Powder Technology Foundation. <https://doi.org/10.14356/kona.2018015>
- Saalu, L. C., Kpela, T., Benebo, A., & Oyewopo, A. (2010). The Dose-Dependent Testiculoprotective and Testiculotoxic Potentials of Telfairia occidentalis Hook f. Leaves Extract in Rat. Experimental Varicocele Models View project Role of Volatile organic compounds on testicular functions View project. In *Article in International Journal of Applied Research in Natural Products*. <http://www.doaj.org/doaj?func=openurl&issn=19406223&genre=journal>
- Sabourian, P., Yazdani, G., Ashraf, S. S., Frounchi, M., Mashayekhan, S., Kiani, S., & Kakkar, A. (2020). Effect of physico-chemical properties of nanoparticles on their intracellular uptake. In *International Journal of Molecular Sciences* (Vol. 21, Issue 21, pp. 1–20). MDPI AG. <https://doi.org/10.3390/ijms21218019>
- Sæbø, I. P., Bjørås, M., Franzyk, H., Helgesen, E., & Booth, J. A. (2023). Optimization of the Hemolysis Assay for the Assessment of Cytotoxicity. *International Journal of Molecular Sciences*, 24(3). <https://doi.org/10.3390/ijms24032914>
- Sakata, D., Yao, C., & Narumiya, S. (2010). Prostaglandin E2, an immunoactivator. In *Journal of Pharmacological Sciences* (Vol. 112, Issue 1, pp. 1–5). Japanese Pharmacological Society. <https://doi.org/10.1254/jphs.09R03CP>
- Salatin, S., & Yari Khosroushahi, A. (2017). Overviews on the cellular uptake mechanism of polysaccharide colloidal nanoparticles. In *Journal of Cellular and Molecular Medicine* (Vol. 21, Issue 9, pp. 1668–1686). Blackwell Publishing Inc. <https://doi.org/10.1111/jcmm.13110>
- Samineni, R., Chimakurthy, J., & Konidala, S. (2022). Emerging Role of Biopharmaceutical Classification and Biopharmaceutical Drug Disposition System in Dosage form Development: A Systematic Review. In *Turkish Journal of Pharmaceutical Sciences* (Vol. 19, Issue 6, pp. 706–713). Turkish Pharmacists Association. <https://doi.org/10.4274/tjps.galenos.2021.73554>
- Sanam Dolatia, Sanam Sadreddinic, Davoud Rostamzadeha, M. A., & Farhad Jadidi-Niaraghe, M. Y. (2016). RA. *Biomedicine & Pharmacotherapy*, 80, 30–41.
- Sandhiya, S., & Chandra Pradhan, S. (2009). Novel applications of nanotechnology in medicine. In *Article in The Indian Journal of Medical Research*. <http://ncl.cancer.gov/>

- Sano, R., Shinozaki, Y., & Ohta, T. (2020). Sodium–glucose cotransporters: Functional properties and pharmaceutical potential. In *Journal of Diabetes Investigation* (Vol. 11, Issue 4, pp. 770–782). Blackwell Publishing. <https://doi.org/10.1111/jdi.13255>
- Saptarshi, S. R., Duschl, A., & Lopata, A. L. (2013). Interaction of nanoparticles with proteins: Relation to bio-reactivity of the nanoparticle. *Journal of Nanobiotechnology*, 11(1), 1. <https://doi.org/10.1186/1477-3155-11-26>
- Scheller, E. L., & Krebsbach, P. H. (2009). Gene therapy: Design and prospects for craniofacial regeneration. In *Journal of Dental Research* (Vol. 88, Issue 7, pp. 585–596). <https://doi.org/10.1177/0022034509337480>
- Schrand, A. M., Rahman, M. F., Hussain, S. M., Schlager, J. J., Smith, D. A., & Syed, A. F. (2010). Metal-based nanoparticles and their toxicity assessment. In *Wiley Interdisciplinary Reviews: Nanomedicine and Nanobiotechnology* (Vol. 2, Issue 5, pp. 544–568). <https://doi.org/10.1002/wnan.103>
- Schrauzer, G. N. (2000). Selenomethionine: A Review of Its Nutritional Significance, Metabolism and Toxicity. *The Journal of Nutrition*, 130(7), 1653–1656. <https://doi.org/10.1093/jn/130.7.1653>
- Selenium - Health Professional Fact Sheet*. (n.d.).
- Selenium Elemental Selenium*. (n.d.).
- Selenium-HealthProfessional.pdf*. (n.d.).
- Selmi, C., & Gershwin, M. E. (2014). Diagnosis and classification of reactive arthritis. In *Autoimmunity Reviews* (Vol. 13, Issues 4–5, pp. 546–549). Elsevier. <https://doi.org/10.1016/j.autrev.2014.01.005>
- Serfass, R. E., & Ganther, H. E. (1976). Effects of dietary selenium and tocopherol on glutathione peroxidase and superoxide dismutase activities in rat phagocytes. *Life Sciences*, 19(8), 1139–1144. [https://doi.org/10.1016/0024-3205\(76\)90248-4](https://doi.org/10.1016/0024-3205(76)90248-4)
- Shah, M., Agrawal, Y. K., Garala, K., & Ramkishan, A. A. (n.d.). *Solid Lipid Nanoparticles of a Water Soluble Drug, Ciprofloxacin Hydrochloride*. www.ijpsonline.com
- Shahabadi, N., Zendehecheshm, S., & Khademi, F. (2021). Selenium nanoparticles: Synthesis, in-vitro cytotoxicity, antioxidant activity and interaction studies with ct-DNA and HSA, HHb and Cyt c serum proteins. *Biotechnology Reports*, 30. <https://doi.org/10.1016/j.btre.2021.e00615>
- Shameli, K., Ahmad, M. bin, Yunus, W. Z. W., Ibrahim, N. A., & Darroudi, M. (2010). Synthesis and characterization of silver/talc nanocomposites using the wet chemical reduction method. *International Journal of Nanomedicine*, 5(1), 743–751. <https://doi.org/10.2147/IJN.S13227>
- Shameli, K., Bin Ahmad, M., Zargar, M., Yunus, W. M. Z. W., Ibrahim, N. A., Shabanzadeh, P., & Moghaddam, M. G. (2011). Synthesis and characterization of silver/montmorillonite/chitosan bionanocomposites by chemical reduction method

- and their antibacterial activity. *International Journal of Nanomedicine*, 6, 271–284.
<https://doi.org/10.2147/ijn.s16043>
- Shen, X., Li, C., Zhao, H., Li, S., Chen, J., Kobayashi, Y., & Shen, W. (2011). Inhibitory effects of a traditional Chinese herbal formula TBL-II on type II collagen-induced arthritis in mice. *Journal of Ethnopharmacology*, 134(2), 399–405.
<https://doi.org/10.1016/j.jep.2010.12.033>
- Shinde, V. (2022). *In vitro cytotoxicity, macromolecular interaction and antioxidant potential of dual coated selenium nanoparticles*. November 2021, 1–12.
<https://doi.org/10.1002/jbm.b.35008>
- Shipp, D. W., Sinjab, F., & Notingher, I. (2017). *Spectroscopy, Raman; (180.5655) Raman microscopy; (300.6230) Spectroscopy, coherent anti-Stokes Raman scattering; (170.3880) Medical and biological imaging*.
<https://doi.org/10.1364/aop.XX.XXXXXX>
- Shmerling, R. H., & Delbanco, T. L. (n.d.). *The Rheumatoid Factor: An Analysis of Clinical Utility*.
- Silva, G. B., Reis, B. Z., Maria, S., & Cozzolino, F. (2016). *Pathology and Clinical Research Micronutrients Deficiencies in Rheumatoid Arthritis Patients*.
- Singh, P., Kim, Y. J., Wang, C., Mathiyalagan, R., & Yang, D. C. (2016a). Microbial synthesis of Flower-shaped gold nanoparticles. *Artificial Cells, Nanomedicine and Biotechnology*, 44(6), 1469–1474. <https://doi.org/10.3109/21691401.2015.1041640>
- Singh, P., Kim, Y. J., Wang, C., Mathiyalagan, R., & Yang, D. C. (2016b). Weissella oryzae DC6-facilitated green synthesis of silver nanoparticles and their antimicrobial potential. *Artificial Cells, Nanomedicine and Biotechnology*, 44(6), 1569–1575. <https://doi.org/10.3109/21691401.2015.1064937>
- Singh, P., Kim, Y. J., Zhang, D., & Yang, D. C. (2016a). Biological Synthesis of Nanoparticles from Plants and Microorganisms. In *Trends in Biotechnology* (Vol. 34, Issue 7, pp. 588–599). Elsevier Ltd.
<https://doi.org/10.1016/j.tibtech.2016.02.006>
- Singh, P., Kim, Y. J., Zhang, D., & Yang, D. C. (2016b). Biological Synthesis of Nanoparticles from Plants and Microorganisms. In *Trends in Biotechnology* (Vol. 34, Issue 7, pp. 588–599). Elsevier Ltd.
<https://doi.org/10.1016/j.tibtech.2016.02.006>
- Slocik, J. M., Govorov, A. O., & Naik, R. R. (2011). Plasmonic circular dichroism of peptide-functionalized gold nanoparticles. *Nano Letters*, 11(2), 701–705.
<https://doi.org/10.1021/nl1038242>
- Speakman, S. A. (1902). Introduction to X-Ray Powder Diffraction Data Analysis. *Materials Science*, 20.
<https://www.researchgate.net/file.PostFileLoader.html?id=58d22df3dc332d06c7245969&assetKey=AS%3A474618730422273%401490169331513>

- Stadtman, T. C. (1996). Selenocysteine. *Annual Review of Biochemistry*, 65(1), 83–100. <https://doi.org/10.1146/annurev.bi.65.070196.000503>
- Stobiecka, M., & Hepel, M. (2011). Double-shell gold nanoparticle-based DNA-carriers with poly-l-lysine binding surface. *Biomaterials*, 32(12), 3312–3321. <https://doi.org/10.1016/j.biomaterials.2010.12.064>
- Swanson, J. A. (2008). Shaping cups into phagosomes and macropinosomes. In *Nature Reviews Molecular Cell Biology* (Vol. 9, Issue 8, pp. 639–649). <https://doi.org/10.1038/nrm2447>
- Sylvain Chemtob. (2004). Basic Pharmacologic Principles. In S. H. A. Richard A. Polin, William W. Fox (Ed.), *Fetal and Neonatal Physiology (Third Edition)* (Vol. 1, pp. 179–190). <http://ci.nii.ac.jp/naid/110007387245/>
- Tambe, A., Mokashi, P., & Pandita, N. (2019). Ex-vivo intestinal absorption study of boswellic acid, cyclodextrin complexes and poloxamer solid dispersions using everted gut sac technique. *Journal of Pharmaceutical and Biomedical Analysis*, 167, 66–73. <https://doi.org/10.1016/j.jpba.2018.12.018>
- Tamer, T. M. (2013). Hyaluronan and synovial joint: Function, distribution and healing. In *Interdisciplinary Toxicology* (Vol. 6, Issue 3, pp. 111–125). <https://doi.org/10.2478/intox-2013-0019>
- TAURINE: Uses, Side Effects, Interactions and Warnings - WebMD*. (2009).
- Thomas, T. P., Huang, B., Choi, S. K., Silpe, J. E., Kotlyar, A., Desai, A. M., Zong, H., Gam, J., Joice, M., & Baker, J. R. (2012). Polyvalent dendrimer-methotrexate as a folate receptor-targeted cancer therapeutic. *Molecular Pharmaceutics*, 9(9), 2669–2676. <https://doi.org/10.1021/mp3002232>
- Tinggi, U. (2008a). Selenium: Its role as antioxidant in human health. *Environmental Health and Preventive Medicine*, 13(2), 102–108. <https://doi.org/10.1007/s12199-007-0019-4>
- Tinggi, U. (2008b). Selenium: Its role as antioxidant in human health. *Environmental Health and Preventive Medicine*, 13(2), 102–108. <https://doi.org/10.1007/s12199-007-0019-4>
- Topală, T., Bodoki, A., Oprean, L., & Oprean, R. (2014). Bovine serum albumin interactions with metal complexes. *Clujul Medical*, 87(4), 5. <https://doi.org/10.15386/cjmed-357>
- Tugarova, A. V., Mamchenkova, P. V., Dyatlova, Y. A., & Kamnev, A. A. (2018). FTIR and Raman spectroscopic studies of selenium nanoparticles synthesised by the bacterium *Azospirillum thiophilum*. *Spectrochimica Acta - Part A: Molecular and Biomolecular Spectroscopy*, 192, 458–463. <https://doi.org/10.1016/j.saa.2017.11.050>
- Ughreja, R., & Parikh, R. H. (2019). Optimization of Ethyl Cellulose Microspheres Containing Satranidazole Using 32 Factorial Design. *International Journal of*

- Pharmaceutical Sciences and Nanotechnology*, 12(1), 4371–4380.
<https://doi.org/10.37285/ijpsn.2019.12.1.3>
- Ursini, F., & Pipicelli, G. (2009). Nutritional supplementation for osteoarthritis. *Alternative and Complementary Therapies*, 15(4), 173–177.
<https://doi.org/10.1089/act.2009.15404>
- Vahdati, M., & Tohidi Moghadam, T. (2020a). Synthesis and Characterization of Selenium Nanoparticles-Lysozyme Nanohybrid System with Synergistic Antibacterial Properties. *Scientific Reports*, 10(1). <https://doi.org/10.1038/s41598-019-57333-7>
- Vahdati, M., & Tohidi Moghadam, T. (2020b). Synthesis and Characterization of Selenium Nanoparticles-Lysozyme Nanohybrid System with Synergistic Antibacterial Properties. *Scientific Reports*, 10(1). <https://doi.org/10.1038/s41598-019-57333-7>
- Valko, M., Rhodes, C. J., Moncol, J., Izakovic, M., & Mazur, M. (2006). Free radicals, metals and antioxidants in oxidative stress-induced cancer. In *Chemico-Biological Interactions* (Vol. 160, Issue 1, pp. 1–40). Elsevier Ireland Ltd.
<https://doi.org/10.1016/j.cbi.2005.12.009>
- Van Breemen, R. B., & Li, Y. (2005). Caco-2 cell permeability assays to measure drug absorption. *Expert Opinion on Drug Metabolism and Toxicology*, 1(2), 175–185.
<https://doi.org/10.1517/17425255.1.2.175>
- Varlan, A., & Hillebrand, M. (2010). Bovine and Human Serum Albumin interactions with 3-carboxyphenoxathiin studied by fluorescence and circular dichroism spectroscopy. *Molecules*, 15(6), 3905–3919.
<https://doi.org/10.3390/molecules15063905>
- Vaughns, C. (2007). *Stern-Volmer Quenching of Conjugated Polymers: A Study of Fluorophore Concentration*. 1–22.
https://smartech.gatech.edu/bitstream/handle/1853/19941/vaughns_christopher_f_200712_ro.pdf
- Vigderman, L., Khanal, B. P., & Zubarev, E. R. (2012). Functional gold nanorods: Synthesis, self-assembly, and sensing applications. In *Advanced Materials* (Vol. 24, Issue 36, pp. 4811–4841). <https://doi.org/10.1002/adma.201201690>
- Vonderheide, A. P., Wrobel, K., Kannamkumarath, S. S., B'Hymer, C., Montes-Bayón, M., De León, C. P., & Caruso, J. A. (2002). Characterization of selenium species in Brazil nuts by HPLC-ICP-MS and ES-MS. *Journal of Agricultural and Food Chemistry*, 50(20), 5722–5728. <https://doi.org/10.1021/jf0256541>
- Wahab, R., Kim, Y. S., Hwang, I. H., & Shin, H. S. (2009). A non-aqueous synthesis, characterization of zinc oxide nanoparticles and their interaction with DNA. *Synthetic Metals*, 159(23–24), 2443–2452.
<https://doi.org/10.1016/j.synthmet.2009.08.006>

- Walker, J. M. (1974). *Characterization of Nanoparticles Intended for Drug Delivery (Methods in Molecular Biology, Volume 697)*. www.springer.com/series/7651
- Wang, C., Kim, Y. J., Singh, P., Mathiyalagan, R., Jin, Y., & Yang, D. C. (2016). Green synthesis of silver nanoparticles by *Bacillus methylotrophicus*, and their antimicrobial activity. *Artificial Cells, Nanomedicine and Biotechnology*, *44*(4), 1127–1132. <https://doi.org/10.3109/21691401.2015.1011805>
- Wang, L., Zhao, D., Di, L., Xu, T., Lin, X., Yang, B., Zhou, X., Yang, X., & Liu, Y. (2011). The analgesic and anti-rheumatic effects of *Thladiantha dubia* fruit crude polysaccharide fraction in mice and rats. *Journal of Ethnopharmacology*, *137*(3), 1381–1387. <https://doi.org/10.1016/j.jep.2011.08.004>
- Wang, X., Zhang, D., Pan, X., Lee, D. J., Al-Misned, F. A., Mortuza, M. G., & Gadd, G. M. (2017). Aerobic and anaerobic biosynthesis of nano-selenium for remediation of mercury contaminated soil. *Chemosphere*, *170*, 266–273. <https://doi.org/10.1016/j.chemosphere.2016.12.020>
- Wang, Y. (2009). Differential effects of sodium selenite and nano-se on growth performance, tissue se distribution, and glutathione peroxidase activity of avian broiler. *Biological Trace Element Research*, *128*(2), 184–190. <https://doi.org/10.1007/s12011-008-8264-y>
- Wang, Y., Mo, Y., & Zhou, L. (2011). Synthesis of CdSe quantum dots using selenium dioxide as selenium source and its interaction with pepsin. *Spectrochimica Acta - Part A: Molecular and Biomolecular Spectroscopy*, *79*(5), 1311–1315. <https://doi.org/10.1016/j.saa.2011.04.061>
- Wang, Y., Sun, W., & Li, H. (2015). Microwave-assisted synthesis of graphene nanocomposites: recent developments on lithium-ion batteries. *Reports in Electrochemistry*, *1*. <https://doi.org/10.2147/rie.s65118>
- Wang, Z., Hu, T., Liang, R., & Wei, M. (2020). Application of Zero-Dimensional Nanomaterials in Biosensing. In *Frontiers in Chemistry* (Vol. 8). Frontiers Media S.A. <https://doi.org/10.3389/fchem.2020.00320>
- Webb, D. R. (2018). Animal models of rheumatoid arthritis. *The Microbiome in Rheumatic Diseases and Infection*, *1*(4), 63–72. https://doi.org/10.1007/978-3-319-79026-8_6
- Wieland, H. A., Michaelis, M., Kirschbaum, B. J., & Rudolphi, K. A. (2005). Osteoarthritis - An untreatable disease? In *Nature Reviews Drug Discovery* (Vol. 4, Issue 4, pp. 331–344). <https://doi.org/10.1038/nrd1693>
- Wolfram, J., Yang, Y., Shen, J., Moten, A., Chen, C., Shen, H., Ferrari, M., & Zhao, Y. (2014). The nano-plasma interface: Implications of the protein corona. *Colloids and Surfaces B: Biointerfaces*, *124*, 17–24. <https://doi.org/10.1016/j.colsurfb.2014.02.035>

- Wright, V. (1986). Treatment of severe rheumatoid arthritis. *British Medical Journal (Clinical Research Ed.)*, 292(6518), 431–432. <https://doi.org/10.1136/bmj.292.6518.431>
- Wu, H., Huang, L., Rose, A., & Grassian, V. H. (2020). Impact of surface adsorbed biologically and environmentally relevant coatings on TiO₂nanoparticle reactivity. *Environmental Science: Nano*, 7(12), 3783–3793. <https://doi.org/10.1039/d0en00706d>
- Xiong, Y., Yang, S., Tian, Y., Michelson, A., Xiang, S., Xin, H., & Gang, O. (2020). Three-Dimensional Patterning of Nanoparticles by Molecular Stamping. *ACS Nano*, 14(6), 6823–6833. <https://doi.org/10.1021/acsnano.0c00607>
- Yan, L., Wang, Y., Xu, X., Zeng, C., Hou, J., Lin, M., Xu, J., Sun, F., Huang, X., Dai, L., Lu, F., & Liu, Y. (2012). Can graphene oxide cause damage to eyesight? *Chemical Research in Toxicology*, 25(6), 1265–1270. <https://doi.org/10.1021/tx300129f>
- Yazici, Y., & Regens, A. L. (2011). Promising new treatments for rheumatoid arthritis: The kinase inhibitors. *Bulletin of the NYU Hospital for Joint Diseases*, 69(3), 233–237.
- Yee, S. W. (1997). In vitro permeability across caco 2 cells can predict in vivo absorption in man. In *Pharmaceutical Research*.
- Yu, B., Zhang, Y., Zheng, W., Fan, C., & Chen, T. (2012). Positive surface charge enhances selective cellular uptake and anticancer efficacy of selenium nanoparticles. *Inorganic Chemistry*, 51(16), 8956–8963. <https://doi.org/10.1021/ic301050v>
- Zahidah, A. F., Faizah, O., Nur Aqilah, K., & Anna Taty, K. (2012). Curcumin as an anti-arthritic agent in collagen-induced arthritic Sprague-Dawley rats. *Sains Malaysiana*, 41(5), 591–595.
- Zeng, H., Cao, J. J., & Combs, G. F. (2013). Selenium in bone health: Roles in antioxidant protection and cell proliferation. In *Nutrients* (Vol. 5, Issue 1, pp. 97–110). MDPI AG. <https://doi.org/10.3390/nu5010097>
- Zhai, X., Zhang, C., Zhao, G., Stoll, S., Ren, F., & Leng, X. (2017). Antioxidant capacities of the selenium nanoparticles stabilized by chitosan. *Journal of Nanobiotechnology*, 15(1), 1–12. <https://doi.org/10.1186/s12951-016-0243-4>
- Zhang, C., Zhai, X., Zhao, G., Ren, F., & Leng, X. (2015a). Synthesis, characterization, and controlled release of selenium nanoparticles stabilized by chitosan of different molecular weights. *Carbohydrate Polymers*, 134, 158–166. <https://doi.org/10.1016/j.carbpol.2015.07.065>
- Zhang, C., Zhai, X., Zhao, G., Ren, F., & Leng, X. (2015b). Synthesis, characterization, and controlled release of selenium nanoparticles stabilized by chitosan of different molecular weights. *Carbohydrate Polymers*, 134, 158–166. <https://doi.org/10.1016/j.carbpol.2015.07.065>

-
- Zhang, J. S., Gao, X. Y., Zhang, L. De, & Bao, Y. P. (2001). Biological effects of a nano red elemental selenium. *BioFactors*, *15*(1), 27–38. <https://doi.org/10.1002/biof.5520150103>
- Zhang, J., Wang, X., & Xu, T. T. (2008). Elemental selenium at nano size (Nano-Se) as a potential chemopreventive agent with reduced risk of selenium toxicity: Comparison with se-methylselenocysteine in mice. *Toxicological Sciences*, *101*(1), 22–31. <https://doi.org/10.1093/toxsci/kfm221>
- Zhang, J., Zhou, X., Yu, Q., Yang, L., Sun, D., Zhou, Y., & Liu, J. (2014). Epigallocatechin-3-gallate (EGCG)-stabilized selenium nanoparticles coated with Tet-1 peptide to reduce amyloid- β aggregation and cytotoxicity. *ACS Applied Materials and Interfaces*, *6*(11), 8475–8487. <https://doi.org/10.1021/am501341u>
- Zhdanov, V. P., & Cho, N. J. (2016). Kinetics of the formation of a protein corona around nanoparticles. *Mathematical Biosciences*, *282*, 82–90. <https://doi.org/10.1016/j.mbs.2016.09.018>
- Zheng, J. S., Zheng, S. Y., Zhang, Y. B., Yu, B., Zheng, W., Yang, F., & Chen, T. (2011). Sialic acid surface decoration enhances cellular uptake and apoptosis-inducing activity of selenium nanoparticles. *Colloids and Surfaces B: Biointerfaces*, *83*(1), 183–187. <https://doi.org/10.1016/j.colsurfb.2010.11.023>
- Zhou, X., Zhao, X., Tang, L., Zhang, Y., Ruan, H., Pi, H., Qiu, J., & Wu, J. (2007). Immunomodulatory activity of the rhizomes of *Impatiens pritzellii* var. *hupehensis* on collagen-induced arthritis mice. *Journal of Ethnopharmacology*, *109*(3), 505–509. <https://doi.org/10.1016/j.jep.2006.08.026>

Synopsis

**SYNOPSIS OF THE THESIS SUBMITTED TO THE UNIVERSITY OF NMIMS
(DEEMED-TO-BE UNIVERSITY) FOR THE DEGREE OF DOCTOR OF
PHILOSOPHY (BIOLOGICAL SCIENCES)**

Name of the Candidate	Ms. Vrundali Shinde
Doctoral committee	Dr. Sudeshna Chandra Dr. Mala Menon
Name and Designation of Mentor	Dr. Krutika Desai (Principal, Mithibai College)
Title of the thesis	Selenium-methionine nanoparticles and its application in chronic inflammatory arthritis
Place of Research	Sunandan Divatia School of Science, SVKM's NMIMS (Deemed-to-be University), Vile Parle (W), Mumbai.
Number and Date of Registration	75102140006, 1 st October 2016
Date of Submission of Synopsis	31 st July, 2022
Signature of Candidate	
Signature of Mentor	

Table of Contents	Page no.
Introduction and Literature Review	4
Rationale, Aim, and Objectives	9
Part A: Synthesis, coating, and characterization of selenium nanoparticles	12
Part B: <i>In vitro</i> toxicity and macromolecular interaction studies	15
Part C: Blood compatibility and permeability	19
Part D: <i>In vivo</i> model development and efficacy studies	22
Bibliography	26

INTRODUCTION AND LITERATURE REVIEW

Nanoparticles

Nanotechnology is an emerging field in science, it includes the synthesis, development and utilization of nanoparticles for multiple applications like medicine, cosmetics, oxide batteries and many more [1]. Nanoparticles have benefits over nanoscale size ranging from 1-100 nm, larger surface area, manipulation of surface charge, and various routes of administration. Few limitations would be particle-particle aggregation, the more significant the surface area greater the cellular interactions and constraints in drug loading [2][3]. Nanoparticles of various metals like gold, silver, iron, titanium, zinc, etc. are in use.

Selenium and its antioxidant property

Selenium is an essential element found in chicken, fish, nuts, eggs, etc. The deficiency and toxicity of this element depend on its dietary intake. Selenium has many health benefits. (Figure 1) Various factors can affect the amount of selenium and its function in the body, factors as alcohol, smoking, age, genetic factors, gender, and disease. Elemental selenium status in the body can be easily measured using biomarkers in the plasma. Biomarkers used are selenoproteins P and glutathione peroxidase, as they depend on dose changes in selenium uptake. According to WHO, the optimal concentration of selenium in the plasma in healthy adults should be 39.5–197.4 ng/ml [4]. Researchers are mainly attracted to selenium due to its important role in antioxidant selenoproteins. The important role of Se is that it is present at the active site of these antioxidant enzymes, Antioxidant enzymes such as glutathione peroxidase (GPx), thioredoxin reductase (TrxR), and iodothyronine deiodinases (IDD). It protects against excess reactive oxygen species (ROS) and reactive nitrogen species (NOS) which initiate oxidative stress. Selenium deficiency can lead to inflammation of tissues [5].

Selenium intake could prevent secondary pathological conditions in traumatic brain injury animal models hence, it may be used as novel drug therapy for brain trauma [6]. Selenium also shows a protective effect against arsenic trioxide-induced cytotoxicity, DNA damage, and apoptosis.[7] selenium has great potential for its anti-cancer effect [8]. latest studies show the anti- chronic inflammatory arthritic effect of selenium nanoparticles [9]. This makes selenium a potent element for application in chronic inflammatory arthritis.

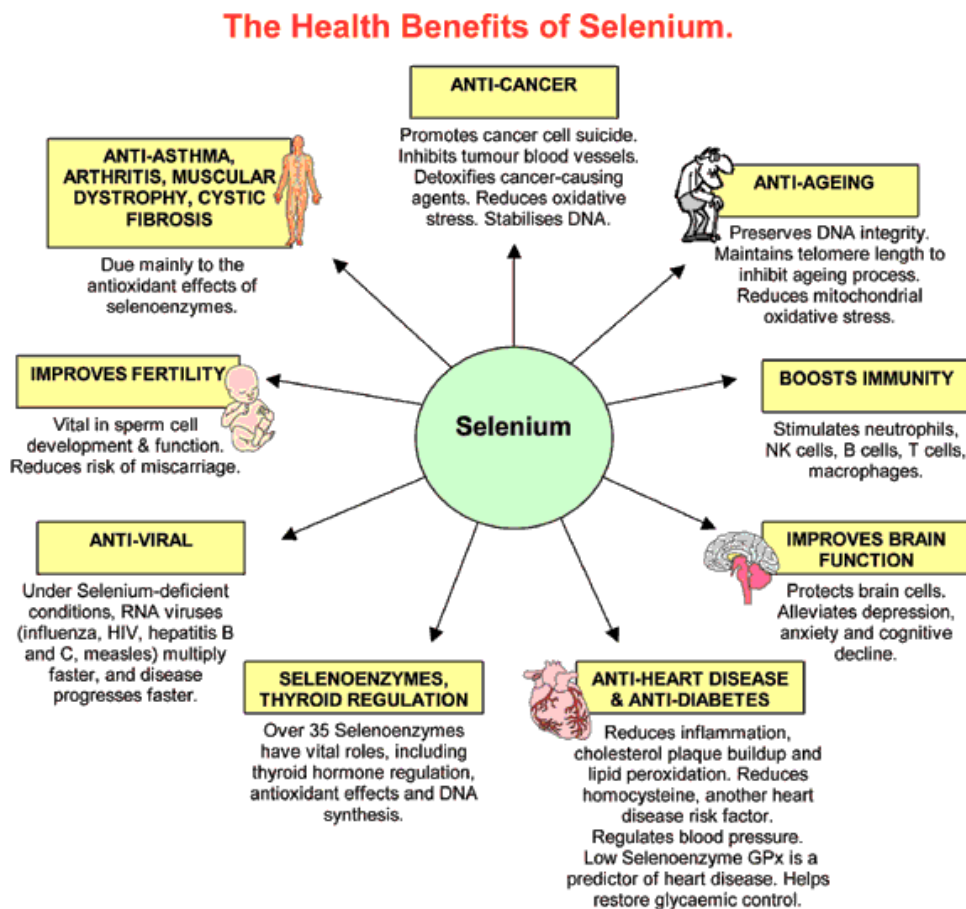


Figure 1: illustration of health benefits of selenium[10]

Methionine and its role in the synthesis of glutathione

Methionine is an essential amino acid, which does not get synthesized in the body it needs to be obtained from the diet. It is involved in DNA methylation and glutathione biosynthesis. Methionine deficiency leads to oxidative damage, as it plays an important role in the synthesis of glutathione. Methionine deficiency also leads to hepatic injury development in a rat model. Research shows that an increase in methionine supplementation in diet can lead to increase production of mitochondrial ROS and mitochondrial DNA oxidative damage in rat liver mitochondria causing hepatotoxicity and also damage in rat heart mitochondria.[12] As methionine deficiency leads to oxidative damage and even an increase in methionine causes oxidative damage to heart and liver mitochondria, if the appropriate amount of methionine is provided through diet or provided as a drug it could reduce ROS, which would even decrease inflammation. When polymorphonuclear neutrophils (PMNs) generate a high amount of ROS, it causes endothelial dysfunction at the site of inflammation. The main role of the

vascular endothelium is to act as a passage for macromolecules and inflammatory cells from blood to tissue. The enhanced generation of ROS by PMNs in inflammatory conditions leads to the opening of the inter-endothelial junction and this stimulates the migration of inflammatory cells across the vascular endothelium. The migrated inflammatory cells help in the clearance of pathogens and also lead to tissue injury.[13][14] As ROS are key signalling molecules in the progression of inflammation and tissue injury.

Folic acid

Folic acid belongs to the vitamin B complex. It is vital for red blood cells and many other cells in the body. Folate receptor (FR)- β has been identified as a promising target for antimacrophage and anti-inflammatory therapies[15]. (FR)- β allows internalization of folate coupled cargo hence, can be beneficial for targeting [16]. (FR)- β is a differentiation marker observed in the myelomonocytic lineage during the period of neutrophil maturation. This receptor is amplified in activated monocytes and macrophages. It is expressed in functional form in chronic myelogenous leukemia, acute myelogenous leukemia, and activated macrophages related to rheumatoid arthritis and chronic inflammatory diseases [17]. Folate receptor expression on activated (but not quiescent) macrophages in both animal models and human patients with naturally occurring RA has opened the possibility of exploiting folic acid to target attached drugs to this population of pathologic cells [18]. Multifunctional selenium nanoparticles coated with baicalin and targeted with folic acid (B-Se NPs-FA) are known to inhibit cancer cell migration and invasion. HepG2215 cell apoptosis induced by B-Se NPs-FA is due to the down-regulation of ROS and HBxAg protein. Hence, B-Se NPs-FA can be a potential therapy for HBV- infected liver cancer [19].

Rheumatoid arthritis

Rheumatoid arthritis (RA) is an autoimmune disorder, in which adaptive and specific immune reactions are against one's cells leading to a unique chronic inflammatory disorder. RA is a common and severe chronic inflammatory disorder. It affects 0.5-1% population in industrialized countries.[20] RA is an organ-specific but often systemic autoimmune disease. It is most common in women between 40 – 60 years of age. Synovial tissue in RA comprises hyperplasia of synoviocytes and the presence of cellular infiltrates of myeloid and lymphoid cells. Interaction between resident and migratory infiltrates leads to chronic synovitis and eventually, it turns to the destruction of cartilage and bone. The inflamed synovium

inappropriately recruits and shows reduced apoptosis of infiltrating cells, angiogenesis, and the presence of lymphoid structures. Troubled individuals produce autoantibodies called rheumatoid factors. These rheumatoid factors are reactive in the Fc region of IgG. A well-known rheumatoid factor is the IgM antibody, which reacts with IgG and forms an IgG-IgM complex and this gets deposited in the joints. These complex also activates complement reactions leading to type III hypersensitivity and chronic inflammation of the joints.[21]

Pathogenesis of Rheumatoid Arthritis (fig 2) includes activation of T cells and leads to overproduction of inflammatory cytokines, which include TNF- α , IL-1 β , and IL-6 by macrophages. These inflammatory cytokines induce receptor activators of nuclear factor β ligand (RANKL), which has a major role in the regulation of osteoclast genesis. Synovial fibroblasts stimulate angiogenesis by producing vascular endothelial growth factor (VEGF), this maintains the inflammation.[22]

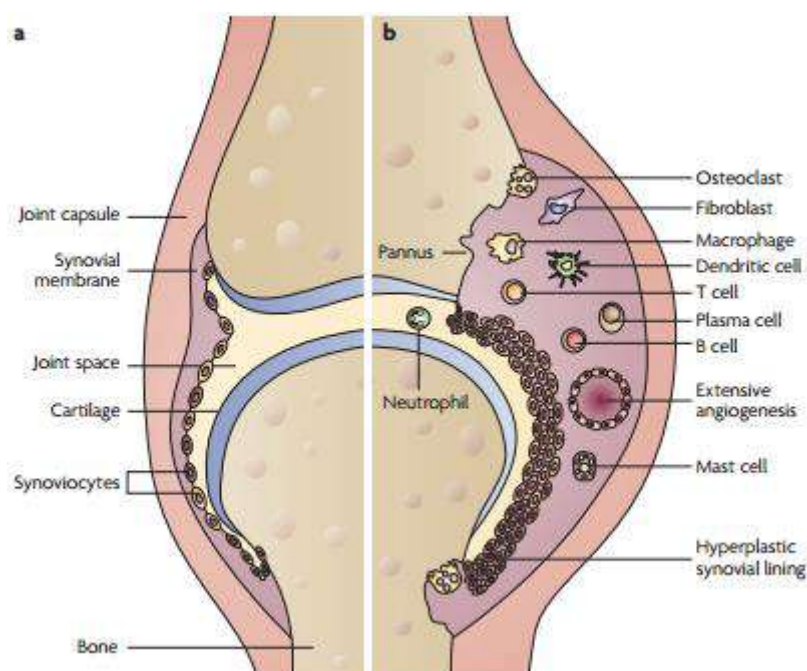


Figure 2: Pathogenesis of Rheumatoid Arthritis – a) healthy joint and b) rheumatoid arthritic joint.[23]

ROS and reactive nitrogen species (RNS) contribute significantly to tissue injury in RA. These ROS and RNS do not directly damage the biological tissues, instead, they get converted

to highly reactive hydroxyl radicals which can react with almost all molecules in a biological system. The resulting chronic inflammation can be controlled with antioxidant therapy. These antioxidant enzymes can inhibit the production of ROS and RNS and could become a significant component of anti-rheumatic prevention and therapy.[24]

RATIONALE, AIM, AND OBJECTIVES

RATIONALE

Selenium an essential trace element is used in this study. It acts as an indirect antioxidant but at a higher dosage (400 μ g/kg b.w./day) causes toxicity [25]. Selenium is available in different forms; organic (Selenomethionine, selenocysteine) and inorganic (selenite, selenate). The inorganic form has reduced bioavailability whereas the organic form has better bioavailability with high toxicity at higher doses. Selenomethionine at 1000 μ g/kg b.w./day shows a No-Observed Adverse Effect Level (NOAEL) and around 90% of it can also be incorporated into proteins [26][27]. Methionine is an essential amino acid required by the body and could increase the bioavailability of selenium nanoparticles once coated with it. Folate is known for its anti-inflammatory properties and its Tolerable upper intake level (UL) for adults is 1000 μ g/day [28][29]. Folate receptor beta is activated on macrophages in conditions like rheumatoid arthritis and chronic inflammatory diseases. Selenium nanoparticles coated with methionine and folic acid, in less concentration may provide better uptake of selenium and help in the management of RA. Hence, selenium-methionine-folate nanoparticles may show better bioavailability and reduction in toxicity as compared to selenium nanoparticles and commercially available drugs.

AIM

Synthesis of selenium-methionine nanoparticles and to study its effects in the treatment of experimentally induced chronic inflammatory arthritis in rats

OBJECTIVES

- g) To carry out the chemical synthesis of selenium-methionine-folic acid nanoparticles (Se-Met-Fa NPs) and their characterization through various analytical techniques.
- h) To check the *in-vitro* and *in vivo* cytotoxicity effects of Se-Met-Fa NPs synthesized using chemical methods.
- i) To check intestinal permeability and bioavailability
- j) Establishment of arthritis model in rats using Freund's Complete Adjuvant.
- k) To investigate the treatment of experimentally induced Rheumatoid Arthritis (RA) in rats using Se-Met-Fa NPs.
- l) To compare Se-Met-Fa NPs with commercially available RA drugs.

PROJECT WORK

Project work is divided into four parts as follows:

Part A: Synthesis, coating, and characterization of selenium nanoparticles

Part B: *In vitro* toxicity, macromolecular interaction studies, and antioxidant assay

Part C: Blood compatibility and Permeability studies

Part D: *In vivo* model development and efficacy studies

Part A: Synthesis, coating, and characterization of selenium nanoparticles

This part includes the synthesis of selenium nanoparticles (Se NPs), its dual coating with methionine and folic acid, and characterization of the same. Selenium-methionine-folic acid nanoparticles (Se-Met-Fa NPs), were synthesized using the wet chemical method with an in-situ coating of methionine and folic acid. Se-Met-Fa NPs were characterized using various microscopic and spectroscopic techniques like UV-Visible spectroscopy, FTIR, X-ray diffraction, ZETA potential, Raman spectroscopy, and Transmission electron microscopy.

Methodology

1. Synthesis and Coating of Selenium-Methionine-Folic Acid Nanoparticles (Se-Met-Fa NPs)

A solution of 100 mM sodium selenite was used as a precursor for the synthesis of Selenium nanoparticles (Se NPs). The precursor was reduced and precipitated using 100 mM ascorbic acid in a ratio of 1: 4. pH of 2 – 2.5 was maintained after the addition of ascorbic acid. The method of synthesis of Se NPs was modified using literature from Sonam et. al., T.A.S. Eldin et. al [30][31]. Dual coating of Se NPs was conducted in situ. Coating materials methionine and folic acid were added respectively; the ratio of precursor: Methionine was 1:5 whereas for precursor: Folic acid was 1: 10. Activation (using 1 N NaOH at pH 9 for 2 hrs incubation) of folic acid before to addition in the reaction mixture was required. The reaction mixture was kept at RT for 24 hours at 1200 rpm on a magnetic stirrer.

2. Characterization of Se-Met-Fa NPs

UV- visible spectroscopy (Perkin Elmer) samples were prepared by making a colloidal solution of 100 µg/ml Se-Met-Fa NPs in 10 ml of D/W with 5 mins of sonication. Samples were measured in the range of 200-700 nm. Samples for FTIR (Jasco FT/IR 4000) were in dry solid form, 1 mg of NPs sample was weighed and a pellet was made using KBr. The range selected for FTIR was from 4000 to 400 cm⁻¹. Zeta potential (Malvern Panalytical) samples were diluted with D/W in a ratio of 1:10. Different sets were prepared according to pH range (2 to 12) and sonicated in two cycles of 5 mins each; these steps were followed before putting the sample in a copper electrode consisting zeta cuvettes. Dried samples weighed 10 mg were used for X-Ray Diffraction, Raman spectroscopy and DSC. ICP-AES technique involved dissolving of nanoparticle samples; aqua regia was utilised to dissolve Se-Met-Fa NPs. TEM

required sample preparation in which samples were diluted with D/W in a ratio of 1: 10, sonicated for 15 mins in two cycles, and later analysed.

Results

Selenium and Selenium-Methionine-Folic acid Nanoparticles were synthesised and dually coated using wet chemical synthesis and the in-situ coating method. UV spectrum observed a prominent peak at 266 nm for Se NPs, whereas peaks observed for Se-Met-Fa NPs are 266, 286, 369 and a slight peak near 200 nm. Compared to peaks of controls of methionine and folic acid it could be seen that the peaks coincide with the Se-Met-Fa NPs spectrum. The absorbance bands observed for FTIR are 3366 cm^{-1} (OH- stretching), 1316 cm^{-1} (OH-bending), 940 cm^{-1} (OH- bending), 1686 cm^{-1} (Amide bond), 2938 cm^{-1} (C-H stretching) and 3415 cm^{-1} (NH- stretching).

Zeta potential measured at each pH from 2 to 12 showed a downward plot from positive to negative charge. ICP-AES determines pure selenium content, Selenium content in Se NPs was 99.7%. Selenium content in Se-Met-Fa NPs was 55%. XRD pattern of Se-Met-Fa NPs was observed with 2θ values: 23.5° , 29.8° , 41.5° , 43.5° , 45.71° , 48.2° , 51.8° , 55.8° , 62° , and 65.2° . these 2θ values correspond to diffraction from (100), (101), (110), (102), (111), (200), (201), (003), (103), and (210) planes respectively. All the 2θ peaks correspond to the trigonal structure of selenium with lattice constants $a = 4.35\text{ \AA}$ and $c = 4.93\text{ \AA}$ and also corresponds with the standard data on JCPDS card no. 06-03620. Scherrer's equation was used to calculate the crystalline size of Se-Met-Fa NPs. The average crystalline size was observed to be 32nm. Raman spectroscopy showed a single peak at $235\text{ Raman shift/cm}^{-1}$, which is of trigonal selenium. TEM image of Se NPs showed spherical morphology and an average size of 50 nm was observed. Se-Met-Fa NPs showed a cloud-like appearance with spherical dots of Se NPs inside it and an average of 52 nm size was observed. The diffraction pattern obtained showed circular rings around both the samples. Thermal stability of Se-Met-Fa NPs was observed using DSC and a melting point of 222° was observed with an exothermic peak obtained at 103° .

Conclusion

Sodium selenite as a precursor and ascorbic acid as a reducing agent in a ratio of 1:4 resulted in the formation of Se NPs with an average size of 50 nm. Dual coatings of methionine and folic acid stabilized the nanoparticles with an average size of 52 nm. UV, FTIR results showed the presence of each biomaterial in the final product of Se-met-Fa NPs. The stability of Se-Met-Fa NPs was studied using Zeta potential and thermal stability using DSC. Overall crystalline nature was confirmed with XRD, TEM diffraction pattern, and Raman spectroscopy.

Part B: *In vitro* toxicity, macromolecular interaction studies, and antioxidant assay

Se-Met-Fa NPs were checked for their *in vitro* cytotoxicity on two different cell lines; NIH-3T3 and Raw 264.7 using two different techniques: MTT assay and AO/EB staining method. Molecular interactions were investigated on BSA protein and plasmid DNA.

Methodology

***In vitro* cell cytotoxicity studies**

1. Cytotoxicity staining

NIH-3T3 primary cell lines were utilised for AO/EB staining. Controls used are as follows: Sodium selenite, Methionine, Folic acid, and cell control. Acridine orange and ethidium bromide were used for staining the cells. Ten thousand cells were seeded in a 35 mm petri dish. DMEM medium with 10% FBS and 1% antibiotics were used for cell growth and maintenance. Incubation parameters include 37° C temperature with 5% CO₂. After 24 hours of incubation, cell media was replaced with 100 µl each of acridine orange and ethidium bromide stains in a 1:1 ratio. Plates were observed under a fluorescence lamp at the FITC filter in dark conditions.

2. MTT assay

Cell cytotoxicity of Se NPs and Se-Met-Fa NPs was studied by MTT (3-(4,5-Dimethylthiazol-2-yl)-2,5-Diphenyltetrazolium Bromide). Two cell lines were considered NIH-3T3 and Raw 264.7. both the cells were cultured in a DMEM medium with 10% FBS and 1% antibiotics. Incubation parameters were 37° C temperature with 5% CO₂. A number of 10,000 cells/well of each cell line were seeded in a 96-well plate. After 24 hours of incubation, the medium was replaced and Se-Met-Fa NPs were added with serum-free media. Different concentrations of nanoparticles were added ranging from (50-100 µg/ml). The next day, after 24 hours of incubation 100 µl of MTT reagent prepared in DPBS of 5 mg/ml concentration was added and incubated for 4 hours. A quantity of 100 µl of DMSO

was added in dark and incubated for 20 mins on a shaker at RT. Readings were taken at 570 and 655 nm on an ELISA reader (Biotek, Epc).

Molecular interaction studies

1. Interaction of Se-Met-Fa NPs with plasmid DNA

Plasmid pBR322 was used for interaction studies with Se-Met-Fa NPs. It was subjected to oxidative stress. Prior to DNA interacting with nanoparticles, the oxidative stress-inducing buffer was prepared. Oxidative stress-inducing buffer known as copper sulfate buffer included 4 μM of CuSO_4 , 130 mM of NaCl, and 5 μM of ascorbic acid. Buffer interacted with NPs in different sets of increasing concentrations of Se-Met-Fa NPs (250, 500, and 750 μl) and incubated at RT for 5 mins. The addition of Plasmid DNA was followed by the addition of 50 μM of H_2O_2 with 30 mins incubation on a shaker with speed level 2 at RT. Samples were then loaded on 1% agarose gel for 1.5 hours at 50 mV.

2. Interaction of Se-Met-Fa NPs with BSA protein

Bovine serum albumin (BSA) protein was interacted with Se-Met-Fa NPs and characterized using UV-Visible spectroscopy, Spectro fluorometer, and Circular dichroism spectrophotometer. Different concentrations (10, 20, 40, 60, 80, and 100 $\mu\text{g/ml}$) of Se-Met-Fa NPs were interacted with 100 μl concentration of BSA and characterized on UV- Visible spectrophotometer for the range of 200-500 nm and also on Spectro fluorometer with an excitation wavelength of 296 nm and emission wavelength of 343 nm. BSA was incubated at RT with the Se NPs and Se-Met-Fa NPs at a ratio of 1: 50 and characterized on CD spectroscopy at a far UV range of 250-190 nm.

Antioxidant assay

Se-Met-Fa NPs were tested for their free radical scavenging ability on the DPPH assay and analysed on an ELISA reader. Concentrations of NPs used were 10, 20, 30, 40, 50 and 100 $\mu\text{g/ml}$. DPPH solution of 0.1 mM concentration was prepared in methanol, from which 1 ml was added to each sample of NPs. Incubation for 1 hour in dark was considered.

Absorbance was measured at 517 nm. %Inhibition of DPPH was calculated using the following formula:

%DPPH inhibition= (Absorbance of control-Absorbance of test)/ Absorbance of control *100.

Results

***In vitro* cytotoxicity**

In AO/EB staining, Sodium selenite shows 100% cell death. Approximately 80% viability was observed of Se-Met-Fa NPs of 100 µg/ml concentration kept for 24 and 48 hours. Around 70% viability was observed for 72 hours with the same sample concentration. MTT assay had similar results, Se NPs showed 50% viability for the concentration of 50 µg/ml and Se-Met-Fa NPs showed 70-80% viability for the same amount of concentration kept for incubation of 24 hours. Se-Met-Fa NPs incubated for 72 hours showed 55-60% viability. Raw cells showed comparable results for Se-Met-Fa NPs of 80% viability for 24 hours and 55% viability for 72 hours.

Molecular interaction studies

Hydrogen peroxide-induced oxidative damage was prevented by both the nanoparticle samples; Se NPs and Se-Met-Fa NPs at the concentration of 250 µg/ml. It was observed that Se-Met-Fa NPs showed improvement in supercoiled DNA of an intensity of 15% which is 5% higher than that of Se NPs at 750 µg/ml concentration.

The absorbance of BSA was observed at 278 nm on UV visible spectroscopy. After BSA interaction with Se-Met-Fa NPs, there was no peak shift observed. There was a gradual increase detected from an increase in concentration (10-100 µg/ml) of nanoparticles. The highest emission wavelength of BSA in the Spectrofluorometric spectrum was 346 nm. The intensity of the spectrum decreased with an increase in the concentration of Se-Met-Fa NPs with no peak shift. The far UV spectra of BSA and BSA interacting with nanoparticle samples were monitored using CD spectroscopy. Two peaks 209 and 222 nm were observed in the spectrum with a change in the intensity of peaks concerning the samples. Alpha helix of BSA for each sample was calculated with the help of the Mean

residue ellipticity value. The decrease in the α -helicity of BSA in the presence of Se-Met-Fa NPs was 4.4%.

Antioxidant assay

Antioxidant activity of Se-Met-Fa NPs was checked using a DPPH assay. Scavenging activity of Se-Met-Fa NPs was observed at 10 $\mu\text{g/ml}$ concentration, 41% of DPPH was reduced in this concentration. Approximately 100% reduction of DPPH was observed at 60 $\mu\text{g/ml}$ concentration.

Conclusion

Nanoparticles were analysed for cytotoxicity on both the cell lines (NIH-3T3 and Raw 267.4)

and at 100 $\mu\text{g/ml}$ concentration of nanoparticles cells were proved to be stable and safe for 48

hours. Se-Met-Fa NPs interacted with BSA protein was studied using UV-Visible spectroscopy, spectrofluorometer, and CD spectroscopy. The ground state complex formation of BSA with nanoparticles was observed in UV-Visible spectroscopy, there was no peak shift with a gradual increase in the intensity of peak concerning the increase in the concentration of nanoparticles. The fluorescence emission study provided data on BSA interacting with Se-Met-Fa NPs and proved the binding of BSA with nanoparticles due to static quenching. CD spectroscopy depicts weak unfolding in peptide strands of BSA due to interaction with nanoparticles. Plasmid DNA interacted with Se-Met-Fa NPs and provided information that these nanoparticles are protective against highly reactive OH radicals induced by metal-mediated buffers. The antioxidant nature of nanoparticles was studied with the help of a DPPH assay.

Part 3: Blood compatibility and Permeability

Blood compatibility of Se-Met-Fa NPs was assessed using a blood haemolysis assay. The quantity of 5 ml of Human blood was collected in EDT- coated vacutainers. Prior approval for human blood was taken from the institutional ethics committee, ethics approval number: NMIMS/IEC/016/2020. Healthy volunteers (n=6) were chosen for giving blood. The Intestinal permeability of Se-Met-Fa NPs was investigated using the novel Permeapad® plate technique. Permeapad® plate mimics intestinal membrane and conditions with being fast, reliable, and cost-effective.

Methodology

Blood haemolysis assay

EDTA stabilized human blood of 5 ml quantity was collected from 6 healthy volunteers. A blood haemolysis assay was performed as a safety measure for Se-Met-Fa NPs prior to *in vivo* studies. The collected 5 ml blood was centrifuged at 1200 rpm for 5 mins. Later, the pellet of red blood cells was washed with PBS buffer twice. After washing, RBCs were diluted with PBS in a ratio of 1:4. Nanoparticles of concentrations 50, 100, and 200 µg/ml were suspended in PBS buffer. RBC suspension of 0.2 ml was added to 0.8 ml PBS solution. Water + RBCs was used as the positive control, whereas PBS + RBCs was used as the negative control. Samples were incubated for 2 hours at 37° C with intermittent shaking every 15 mins. Later, samples were centrifuged at 1200 rpm for 5 mins and observed for haemolysis. Samples of quantity 100 µl were measured for their absorbance at 570 and 655 nm. Haemolysis was calculated using the %haemolysis formula.

Permeability assay

Permeapad® plate (Electro lab) is a 96-well microtiter plate, pre-coated with cellulose membrane which mimics the intestine. This plate is made up of two chambers divided by a membrane, the upper (donor) chamber and a lower (receiver) chamber. The total area of 0.15 cm² is available for permeation.

Nanoparticle samples of 100 µg/ml concentration were diluted with PBS buffer of different pH values (2, 4, 6, 7, 8, and 10). The reaction was run in three sets. Time points considered were 2, 4, and 24 hours. Modification of incorporating pH range from 2 to 10 was adapted. Samples

were collected from the receiver end with the help of a syringe. After sample collection, the spectrum was checked at lambda max 265 nm on an ELISA reader.

Results

Blood haemolysis assay

RBC haemolysis indicates incompatibility with blood and no haemolysis indicates compatibility with blood. Positive control showed blood haemolysis with the highest OD of 1.3 at 570 nm and was considered 100% haemolysis. Coated and non-coated nanoparticles along with negative control showed OD of less than 0.3.

Permeability assay

The apparent permeability of Se NPs and Se-Met-Fa NPs was calculated. No fluctuation was observed in both the nanoparticle samples incubated for 2 and 4 hours of 2 to 8 ph. Samples incubated for 24 hours shows variability with an increase of apparent permeability at pH 10. Comparing data of Se NPs and Se-Met-Fa NPs it was observed that Se-Met-Fa NPs have increased Papp value up to 1.5×10^{-6} cm/s at pH 10 incubated for 24 hours. Similarly, a 1.2×10^{-6} cm/s increase in Papp value was observed for samples incubated for 4 hours, and samples incubated for 2 hours showed no difference.

Barrier integrity was studied using different time points and it was observed that an increase in incubation time has increased Papp values. Samples of Se NPs, incubated at 2 and 4 hours had a 4.5×10^{-6} cm/s difference. Comparing 2- and 24-hours gives a difference of approximately 16×10^{-6} cm/s. Samples of Se-Met-Fa NPs, 2- and 4-hours samples had approximately 4.5×10^{-6} cm/s. Samples incubated at 4- and 24-hours had 5×10^{-6} cm/s difference and for 2- and 24-hours difference had been 22.5×10^{-6} cm/s. The sample incubation time of 24 hours showed the highest Papp values. Control groups were considered to be 100%. The highest permeability of 70% was observed in Se-Met-Fa NPs at pH 10 and pH 2-8, permeability was observed from 50-70%. Permeability for Se NPs for pH range 2 to 10, 35-45% permeability was observed.

Conclusion

The given data have mapped the biological effects of Se-Met-Fa NPs on blood and their permeability on the mimicked intestinal barrier-Permeapad® plate. Less than 5% of blood haemolysis was observed, indicating it to be blood compatible. Apparent permeability of coated Se NPs being higher than 10×10^{-6} cm/s confirms its high permeability efflux through the

intestinal membrane. A novel technique being utilized in this current study gives ease in studying the permeation of nanoparticles with being more cost-effective than other techniques.

Part 4: *In Vivo* Model Development and Efficacy Studies

Methodology

Grouping of animals

In vivo model development for efficacy studies, Male Wistar Rats of 180-200g weight were purchased from Bharat Serum and vaccines Pvt. Ltd. Pune. Ethical clearance from CPCSEA (CPCSEA/IAEC/P-11/2019). Before initiation of the study animals were acclimatized to the laboratory conditions. These animals were housed for 14 days under standard conditions of temperature ($23\pm 1^{\circ}\text{C}$) and 12 hours of light and dark cycles before the start of the experiment and given food and water *ad libitum* till the end of the study.

The animals were randomly grouped as follows with 6 animals/ group.

Group I: Normal without any disease.

Group II: Arthritic control which was induced with 0.1 mL of CFA.

Group III: Carboxymethylcellulose (CMC- Vehicle control)

Group IV: Standard drug Prednisolone (10 mg/kg b.w.).

Group V: Se-Met-Fa nanoparticles (250 $\mu\text{g}/\text{kg b.w.}$).

Group VI: Se-Met-Fa nanoparticles (500 $\mu\text{g}/\text{kg b.w.}$).

Group VII: Se-Met-Fa nanoparticles (750 $\mu\text{g}/\text{kg b.w.}$).

Anti-arthritic study

The different concentrations of Se-Met-Fa NPs (250, 500, and 750 $\mu\text{g}/\text{kg}$ body weight) were compared with the standard drug Prednisolone (10 mg/kg b.w., Wysolone, Pfizer Ltd.), Carboxymethylcellulose (CMC) used as Vehicle control for Se-Met-Fa NPs and a group of Normal control was maintained which was not treated with any drug. Wistar rats were segregated into 7 groups with 6 animals each. All groups except Normal Control and Vehicle Control were induced with chronic inflammation using 0.1ml Complete Freund's adjuvant in the left hind paw region. Complete Freund's Adjuvant (CFA) was purchased from Sigma-Aldrich. The animal models were given the standard drug and different concentrations of nanoparticles for 21 days. Induction of chronic inflammation was considered as zero-day. Animal weights and inflammation in the paw region were monitored every week up till the 21st

day. Paw inflammation was periodically checked on the digital vernier calliper. After 21 days, the animals were ethically sacrificed and different organs such as spleen, kidney, and liver were dissected. Blood was collected from each animal by heart puncture technique and centrifuged for separation of serum within 1 hour of blood removal. The paw region was dissected for histopathological analysis and Radiography (X-Ray). Paw samples were outsourced to OVI diagnostics, Dadar, Mumbai.

Inflammatory marker testing

Blood samples were centrifuged at 3000 rpm for 10 mins. The supernatant (serum) was stored at -20°C. Before inflammatory marker testing serum was thawed and utilized. Serum samples were then used for testing C-Reactive Protein (OVI diagnostics, Dadar, Mumbai.), Prostaglandin E2 was tested using BIOTECH Desk Kit, and TNF- α was tested using Ray biotech kit.

Antioxidant enzyme assay

The organs dissected were the spleen, kidney, and liver; these organs were tested for the enzyme levels of Superoxide Dismutase, Catalase, and Glutathione Peroxidase. The enzyme Superoxide Dismutase was studied using a modified protocol from Marklund and Marklund's method [32]. Catalase and Glutathione Peroxidase enzymes were studied using the protocol mentioned by Malhotra S. et al [9].

Results

Chronic Inflammatory arthritis was experimentally induced using Complete Freund's Adjuvant in Wistar rats. The results for animal weight and paw inflammation were statistically analysed using two-way ANOVA. All animals except Normal control and Vehicle control showed inflammation in the paw region, which was observed for 21 days of study using a digital vernier calliper. The results determining inflammatory marker studies and antioxidant enzyme studies were statistically analysed using one-way ANOVA. Inflammation in the paw region was observed from day 1 to day 21 for all the groups. The arthritic group of rats showed a steady increase up to day 7 and later constantly inflamed paw up till the 21st day. The diseased groups showed a significant decrease in paw inflammation when treated with Se-Met-Fa NPs (250, 500, and 750 $\mu\text{g/ml}$) from day 7th onwards. Animal weight was significantly increasing for all the groups except the rats in the arthritic group. The prognosis of chronic inflammatory arthritis was checked using C-Reactive protein (CRP), Prostaglandin E2, and TNF- α . It was

observed that CRP levels had increased drastically for the Arthritic group up to 1.5 mg/dl and other treated groups showed regained levels of CRP similar to the normal group. The treatment group of Se-Met-Fa NPs of 750 µg/ml displayed equivalent results to the normal group. The standard drug prednisolone showed similar results as compared to the treatment group of 250 µg/ml concentration. The 500 µg/ml concentration group shows one-fold better results as compared to the prednisolone group. Similar results were observed for the Prostaglandin E2 marker, where prostaglandin E2 levels were reduced for all treated groups. The standard drug prednisolone showed similar improvement as compared to the 750 µg/ml concentration group. TNF-alpha marker shows drastic improvement for all treatment groups including the lowest concentration group of 250 µg/ml Se-Met-Fa NPs. The arthritic control group depicted the highest concentration of TNF-alpha around 6 pg/ml as compared to all other treatment groups. The histopathology of the paw region for the arthritic group clearly shows degeneration in the inner region of tissues, necrotic changes in tissues, congestion, and deposits of adipose tissues. The overall grade for pathological change for the arthritic group was 4th grade which represents a severity higher than 75%. Compared to the arthritic group all other treatment groups showed 1 or 2 grades, which represents mild severity up to 25%. Radiographic images of the paw region indicated mild swelling, degeneration around the ankle joint, and articular changes for arthritic control. The treatment group of Se 250, Se 500, and Prednisolone showed minimal swelling as compared to other treatment groups. Se 750 group showed the least deformities with nearly no changes and had regained paw shape and size to the normal control group. All other histopathological images of the spleen, kidney, and liver, were observed for toxicity and it appeared that except for the arthritic group all other treatment groups were normal with no to minimal lesions. The arthritic group showed mild lesions which indicated 11-25% pathological changes. The antioxidant enzyme status of organs like the spleen, kidney, and liver were studied using SOD, CAT, and GPx. The SOD, CAT, and GPx levels in the organs of animals treated with Se 250, Se 500, and Se 750 showed improvement and had almost restored to normal levels.

Conclusion

Disease progression was weakly checked using a digital Vernier calliper. It was observed that except for the arthritic group, all other groups showed improvement and reduction in paw size and also improved health. The major difference was observed in groups Se 500, Se 750, and standard drug prednisolone. It was observed that Se 250, Se 500, and Se 750 showed no toxicity

in any organs under histopathological studies. The inflammatory marker studies indicative of the prognosis of chronic inflammation showed higher levels of SOD, CAT, and GPx in the arthritic group and significant improvement in all treatment groups. The concentration of 250 µg/ml considered as least concentration of Se-Met-Fa NPs, also showed a significant difference as compared to the arthritic group. The antioxidant enzyme assays depicted the positive response of animals towards the treatment of Se-Met-Fa NPs. This also focused on reducing the stress levels inside the body, up to protein level, and regaining the altered levels to the normal control values. Histopathology of the paw region showed improved inner tissue structure with minimal to very low lesions for treated groups as compared to the arthritic control group which had destroyed inner tissue lining. The radiography technique indicated the presence of deformities in the ankle joint with minor swelling around the ankle region for the arthritic group of animals. Improved results of no deformities with minimal swelling were observed for treatment groups. This elaborate study including enzyme levels, alteration in antioxidant and inflammatory markers, histopathology, and radiography of the paw region, with the constant observation of animals, gave a complete understanding of how Se-Met-Fa NPs of 500 or 750 µg/ml concentration showed no toxicity with improvement in diseased animals.

BIBLIOGRAPHY

- [1] S. Hasan, "A Review on Nanoparticles : Their Synthesis and Types," *Res. J. Recent Sci. Res. J. Recent. Sci. Uttar Pradesh (Lucknow Campus)*, vol. 4, no. February, pp. 1–3, 2014.
- [2] S. L. Pal, U. Jana, P. K. Manna, G. P. Mohanta, and R. Manavalan, "Nanoparticle: An overview of preparation and characterization," *J. Appl. Pharm. Sci.*, vol. 1, no. 6, pp. 228–234, 2011, doi: 10.7897/2230-8407.04408.
- [3] "No Title." .
- [4] C. R. B. Rocourt and W. H. Cheng, "Selenium supranutrition: Are the potential benefits of chemoprevention outweighed by the promotion of diabetes and insulin resistance?," *Nutrients*, vol. 5, no. 4, pp. 1349–1365, 2013, doi: 10.3390/nu5041349.
- [5] U. Tinggi, "Selenium: Its role as antioxidant in human health," *Environ. Health Prev. Med.*, vol. 13, no. 2, pp. 102–108, 2008, doi: 10.1007/s12199-007-0019-4.
- [6] J. E. Yeo and S. K. Kang, "Selenium effectively inhibits ROS-mediated apoptotic neural precursor cell death in vitro and in vivo in traumatic brain injury," *Biochim. Biophys. Acta - Mol. Basis Dis.*, vol. 1772, no. 11–12, pp. 1199–1210, 2007, doi: 10.1016/j.bbadis.2007.09.004.
- [7] V. Selvaraj, M. Yeager-Armstead, and E. Murray, "Protective and antioxidant role of selenium on arsenic trioxide-induced oxidative stress and genotoxicity in the fish hepatoma cell line PLHC-1," *Environ. Toxicol. Chem.*, vol. 31, no. 12, pp. 2861–2869, 2012, doi: 10.1002/etc.2022.
- [8] V. G. P. Aristi P. Fernandes, "fernandes2014," *Biochim. Biophys. Acta - Gen. Subj.*, vol. 1850, no. 8, pp. 1642–1660, 2015.
- [9] S. Malhotra, M. N. Welling, S. B. Mantri, and K. Desai, "In vitro and in vivo antioxidant, cytotoxic, and anti-chronic inflammatory arthritic effect of selenium nanoparticles," *J. Biomed. Mater. Res. - Part B Appl. Biomater.*, vol. 104, no. 5, pp. 993–1003, 2016, doi: 10.1002/jbm.b.33448.
- [10] "selenium benefits." .
- [11] H. S. Oz, T. S. Chen, and M. Neuman, "Methionine deficiency and hepatic injury in a dietary steatohepatitis model," *Dig. Dis. Sci.*, vol. 53, no. 3, pp. 767–776, 2008, doi: 10.1007/s10620-007-9900-7.
- [12] J. Gomez *et al.*, "Effect of methionine dietary supplementation on mitochondrial oxygen radical generation and oxidative DNA damage in rat liver and heart," *J. Bioenerg. Biomembr.*, vol. 41, no. 3, pp. 309–321, 2009, doi: 10.1007/s10863-009-9229-3.
- [13] M. Mittal, M. R. Siddiqui, K. Tran, S. P. Reddy, and A. B. Malik, "Reactive oxygen species in inflammation and tissue injury," *Antioxidants Redox Signal.*, vol. 20, no. 7, pp. 1126–1167, 2014, doi: 10.1089/ars.2012.5149.
- [14] D. Paola Rosanna and C. Salvatore, "Reactive Oxygen Species, Inflammation, and Lung Diseases," *Curr. Pharm. Des.*, vol. 18, no. 26, pp. 3889–3900, 2012, doi: 10.2174/138161212802083716.

-
- [15] E. Nogueira, A. C. Gomes, A. Preto, and A. Cavaco-Paulo, "Folate-targeted nanoparticles for rheumatoid arthritis therapy," *Nanomedicine Nanotechnology, Biol. Med.*, vol. 12, no. 4, pp. 1113–1126, 2016, doi: 10.1016/j.nano.2015.12.365.
- [16] E. Nogueira, A. C. Gomes, A. Preto, and A. Cavaco-Paulo, "Folate-targeted nanoparticles for rheumatoid arthritis therapy," *Nanomedicine Nanotechnology, Biol. Med.*, vol. 12, no. 4, pp. 1113–1126, 2016, doi: 10.1016/j.nano.2015.12.365.
- [17] X. Zhao, H. Li, and R. J. Lee, "Targeted drug delivery via folate receptors," *Expert Opin. Drug Deliv.*, vol. 5, no. 3, pp. 309–319, 2008, doi: 10.1517/17425247.5.3.309.
- [18] C. M. Paulos, M. J. Turk, G. J. Breur, and P. S. Low, "Folate receptor-mediated targeting of therapeutic and imaging agents to activated macrophages in rheumatoid arthritis," *Adv. Drug Deliv. Rev.*, vol. 56, no. 8, pp. 1205–1217, 2004, doi: 10.1016/j.addr.2004.01.012.
- [19] X. Fang *et al.*, "Targeting selenium nanoparticles combined with baicalin to treat HBV-infected liver cancer," *RSC Adv.*, vol. 7, no. 14, pp. 8178–8185, 2017, doi: 10.1039/C6RA28229F.
- [20] T. Kelkka, *Reactive Oxygen Species*. 2013.
- [21] C. Vaman Rao (cept. of zoology/ St. Xavier's college. Mumbai), "Immunology," in *Immunology*, Second edi., Narosa publishing house, 2008, pp. 541–544.
- [22] M. A. Sanam Dolatia, Sanam Sadreddinic, Davoud Rostamzadeha and M. Y. Farhad Jadidi-Niaraghe, "RA," *Biomed. Pharmacother.*, vol. 80, pp. 30–41, 2016.
- [23] L. S. O. F. and S. R. P. Opeyemi S. Ademowo, *Genes and Autoimmunity - Intracellular Signaling and Microbiome Contribution*. InTech, 2013.
- [24] K. Bauerová and A. Bezek, "Role of reactive oxygen and nitrogen species in etiopathogenesis of rheumatoid arthritis.," *Gen. Physiol. Biophys.*, vol. 18 Spec No, pp. 15–20, Oct. 1999.
- [25] National Research Council, *Dietary Reference Intakes for vitamin C, vitamin E, selenium, and carotenoids*. 2000.
- [26] EFSA, "L-selenomethionine as a source of selenium added for nutritional purposes Scientific Opinion of the Panel on Food Additives and Nutrient Sources added to Food Adopted on 14 May 2009," *EFSA J.*, no. 1082, pp. 1–38, 2009.
- [27] A. Baines, M. Taylor-Parker, A. C. Goulet, C. Renaud, E. W. Gerner, and M. A. Nelson, "Selenomethionine inhibits growth and suppresses cyclooxygenase-2 (COX-2) protein expression in human colon cancer cell lines," *Cancer Biol. Ther.*, vol. 1, no. 4, pp. 370–374, 2002, doi: 10.4161/cbt.1.4.9.
- [28] "TAURINE: Uses, Side Effects, Interactions and Warnings - WebMD." 2009.
- [29] C. E. Butterworth and T. Tamura, "Folic acid safety and toxicity: a brief review.," *Am. J. Clin. Nutr.*, vol. 50, no. 2, pp. 353–8, Aug. 1989.
- [30] S. Malhotra, N. Jha, and K. Desai, "a Superficial Synthesis of Selenium Nanospheres Using Wet Chemical Approach," *Int. J. Nanotechnol. Appl.*, vol. 3, no. 4, pp. 2277–4777, 2014.

- [31] T. A. S. Eldin, “Nutritional Evaluation of Selenium-methionine Nanocomposite as a Novel Dietary Supplement for Laying Hens,” *J. Anim. Heal. Prod.*, vol. 3, no. 3, pp. 64–72, 2015, doi: 10.14737/journal.jahp/2015/3.3.64.72.
- [32] A. Nandi and I. B. Chatterjee, “Assay of superoxide dismutase activity in animal tissues,” *J. Biosci.*, vol. 13, no. 3, pp. 305–315, 1988, doi: 10.1007/BF02712155.

Appendix-I

Statistical Analysis

Protein-NP Interaction- (Stern-Volmer plot)

Q	F0/F
10	1.148
20	1.211
40	1.379
60	1.581
80	1.785
100	2.002

Slope	0.009574 ± 0.0003106
Y-intercept when X=0.0	1.023 ± 0.01885
X-intercept when Y=0.0	-106.8
1/slope	104.4
95% Confidence Intervals	
Slope	0.008712 to 0.01044
Y-intercept when X=0.0	0.9707 to 1.075
X-intercept when Y=0.0	-122.8 to -93.47
Goodness of Fit	
r ²	0.9958
Sy.x	0.02422
Is slope significantly non-zero?	
F	950.3
DFn, DFd	1.000, 4.000
P value	< 0.0001
Deviation from zero?	Significant
Data	
Number of X values	6
Maximum number of Y replicates	1
Total number of values	6
Number of missing values	0

MTT Assay (NIH 3T3 cell line)

Concentration	50	75	100
cell control	100	100	100
	100	100	100
	100	100	100
Bare selenium NPs 24hours	56.90104	41.79688	34.11458
	44.53125	36.19792	35.80729
	34.76563	27.99479	32.94271
Bare selenium NPs 48hours	47.00626	31.27793	36.46112
	37.89098	31.45666	26.98838
	33.51207	19.66041	25.73726
Bare selenium NPs 72hours	24.70669	29.53761	12.28433
	26.77709	26.36301	14.07868
	17.66736	24.01656	12.97447
Selenium-met-Folate NPs 24hrs	101.3072	104.1322	96.05264
	108.1699	92.2865	65.78947
	100	91.73553	72.36842
Selenium-met-Folate NPs 48hrs	101.3774	105.7018	72.72727
	100.4683	89.03509	82.64463
	90.35812	69.29825	69.69697
Selenium-met-Folate NPs 72hrs	75.4386	105.5556	60.78431
	110.7719	62.0915	58.82353
	93.42105	57.84314	60.78431

Two-way ANOVA

Source of Variation	% of total variation	P value
Interaction	2.33	0.2696
Column Factor	87.18	P<0.0001
Row Factor	4.09	P<0.0001

Source of Variation	P value summary	Significant?

Interaction	ns	No
Column Factor	***	Yes
Row Factor	***	Yes

Source of Variation	Df	Sum-of-squares	Mean square	F
Interaction	12	1513	126.1	1.273
Column Factor	6	56660	9443	95.35
Row Factor	2	2658	1329	13.42
Residual	42	4160	99.04	

Bonferroni Posthoc test

Cell control vs Bare selenium NPs 24hours				
Row Factor	cell control	Bare selenium NPs 24hours	Difference	95% CI of diff.
50	100	45.4	-54.6	-80.43 to -28.77
75	100	35.33	-64.67	-90.50 to -38.84
100	100	34.29	-65.71	-91.54 to -39.88
Row Factor	Difference	t	P value	Summary
50	-54.6	6.72	P<0.001	***
75	-64.67	7.959	P<0.001	***
100	-65.71	8.087	P<0.001	***
Cell control vs Bare selenium NPs 48hours				
Row Factor	cell control	Bare selenium NPs 48hours	Difference	95% CI of diff.
50	100	39.47	-60.53	-86.36 to -34.70
75	100	27.47	-72.54	-98.36 to -46.71
100	100	29.73	-70.27	-96.10 to -44.44
Row Factor	Difference	t	P value	Summary

50	-60.53	7.449	P<0.001	***
75	-72.54	8.927	P<0.001	***
100	-70.27	8.648	P<0.001	***
Cell control vs Bare selenium NPs 72hours				
Row Factor	cell control	Bare selenium NPs 72hours	Difference	95% CI of diff.
50	100	23.05	-76.95	-102.8 to -51.12
75	100	26.64	-73.36	-99.19 to -47.53
100	100	13.11	-86.89	-112.7 to -61.06
Row Factor	Difference	t	P value	Summary
50	-76.95	9.47	P<0.001	***
75	-73.36	9.028	P<0.001	***
100	-86.89	10.69	P<0.001	***

Cell control vs Selenium-met-Folate NPs 24hrs			
Row Factor	cell control	Selenium-met-Folate NPs 24hrs	Difference
50	100	103.2	3.159
75	100	96.05	-3.949
100	100	78.07	-21.93
Row Factor	Difference	t	P value
50	3.159	0.3888	P > 0.05
75	-3.949	0.4859	P > 0.05
100	-21.93	2.699	P < 0.05
Cell control vs Selenium-met-Folate NPs 48hrs			
Row Factor	cell control	Selenium-met-Folate NPs 48hrs	Difference
50	100	97.4	-2.599
75	100	88.01	-11.99

100	100	75.02	-24.98
Row Factor	Difference	t	P value
50	-2.599	0.3198	P > 0.05
75	-11.99	1.475	P > 0.05
100	-24.98	3.074	P < 0.05
Cell control vs Selenium-met-Folate NPs 72hrs			
Row Factor	cell control	Selenium-met-Folate NPs 72hrs	Difference
50	100	93.21	-6.789
75	100	75.16	-24.84
100	100	60.13	-39.87
Row Factor	Difference	t	P value
50	-6.789	0.8356	P > 0.05
75	-24.84	3.057	P < 0.05
100	-39.87	4.907	P<0.001

MTT Assay (Raw 264.7 cell line)

Concentration	50	75	100
Cell control	100	100	100
	100	100	100
	100	100	100
SeNPs24hrs	28.83129	39.88176	18.82674
	37.78991	27.78536	20.64575
	33.65166	31.51432	15.0523
SeNPs 48hrs	18.38124	16.23802	11.01866
	22.31467	20.17146	14.75038
	21.50782	17.82652	16.46495
SeNPs 72hrs	16.03459	17.56675	13.37985
	24.09009	18.20388	15.98908
	20.28216	17.08131	11.99939
SeMetFa NPs 24hrs	97.82119	95.37491	86.32607
	94.29001	93.83922	93.38843
	104.5079	83.02029	90.60857
SeMetFa NPs 48hrs	90.47292	85.90359	79.18666
	86.36052	83.0249	64.29061
	66.57528	67.809	79.68929
SeMetFa NPs 72hrs	63.91407	68.40862	62.69521
	74.57911	59.19098	48.14505
	69.17041	46.54529	54.16317

Two-way ANOVA

Source of Variation	% of total variation	P value
Interaction	0.58	0.4704
Column Factor	96.35	P<0.0001
Row Factor	1.02	0.0002

Source of Variation	P value summary	Significant?
Interaction	ns	No
Column Factor	***	Yes
Row Factor	***	Yes

Source of Variation	Df	Sum-of-squares	Mean square	F
Interaction	12	411.9	34.33	0.9944
Column Factor	6	68270	11380	329.6
Row Factor	2	721.5	360.8	10.45
Residual	42	1450	34.52	

Bonferroni Posthoc test

Cell control vs SeNPs24hrs				
Row Factor	cell control	SeNPs24hrs	Difference	95% CI of diff.
50	100	33.42	-66.58	-81.82 to -51.33
75	100	33.06	-66.94	-82.19 to -51.69
100	100	18.17	-81.83	-97.07 to -66.58
Row Factor	Difference	t	P value	Summary
50	-66.58	13.88	P<0.001	***
75	-66.94	13.95	P<0.001	***
100	-81.83	17.06	P<0.001	***
Cell control vs SeNPs 48hrs				

Row Factor	cell control	SeNPs 48hrs	Difference	95% CI of diff.
50	100	20.73	-79.27	-94.51 to -64.02
75	100	18.08	-81.92	-97.17 to -66.67
100	100	14.08	-85.92	-101.2 to -70.67
Row Factor	Difference	t	P value	Summary
50	-79.27	16.52	P<0.001	***
75	-81.92	17.08	P<0.001	***
100	-85.92	17.91	P<0.001	***
Cell control vs SeNPs 72hrs				
Row Factor	cell control	SeNPs 72hrs	Difference	95% CI of diff.
50	100	20.14	-79.86	-95.11 to -64.62
75	100	17.62	-82.38	-97.63 to -67.14
100	100	13.79	-86.21	-101.5 to -70.96
Row Factor	Difference	t	P value	Summary
50	-79.86	16.65	P<0.001	***
75	-82.38	17.17	P<0.001	***
100	-86.21	17.97	P<0.001	***

Cell control vs SeMFNPs 24hrs				
Row Factor	cell control	SeMFNPs 24hrs	Difference	95% CI of diff.

50	100	98.87	-1.127	-16.37 to 14.12
75	100	90.74	-9.255	-24.50 to 5.992
100	100	90.11	-9.892	-25.14 to 5.355
Row Factor	Difference	t	P value	Summary
50	-1.127	0.2349	P > 0.05	ns
75	-9.255	1.929	P > 0.05	ns
100	-9.892	2.062	P > 0.05	ns
Cell control vs SeMFNPs 48hrs				
Row Factor	cell control	SeMFNPs 48hrs	Difference	95% CI of diff.
50	100	81.14	-18.86	-34.11 to - 3.616
75	100	78.91	-21.09	-36.34 to - 5.840
100	100	74.39	-25.61	-40.86 to - 10.36
Row Factor	Difference	t	P value	Summary
50	-18.86	3.932	P<0.001	***
75	-21.09	4.396	P<0.001	***
100	-25.61	5.339	P<0.001	***
Cell control vs SeMFNPs 72hrs				
Row Factor	cell control	SeMFNPs 72hrs	Difference	95% CI of diff.
50	100	69.22	-30.78	-46.03 to - 15.53
75	100	58.05	-41.95	-57.20 to - 26.70
100	100	55	-45	-60.25 to - 29.75

Row Factor	Difference	t	P value	Summary
50	-30.78	6.416	P<0.001	***
75	-41.95	8.745	P<0.001	***
100	-45	9.38	P<0.001	***

Blood Compatibility

One-way analysis of variance	
P value	0.0233
P value summary	*
Are means signif. different? (P < 0.05)	Yes
Number of groups	6
F	3.976
R squared	0.6236

ANOVA Table	SS	df	MS
Treatment (between columns)	0.03755	5	0.00751
Residual (within columns)	0.02267	12	0.00189
Total	0.06022	17	

Tukey's Multiple Comparison Test	Mean Diff.	q	Significant? P < 0.05?	Summary	95% CI of diff
Se NP 50ug vs Se NP 100ug	-0.0773	3.082	No	ns	-0.1966 to 0.04187
Se NP 50ug vs Se NP 200ug	-0.1031	4.11	No	ns	-0.2223 to 0.01609
Se NP 50ug vs SeMetFa NP 50ug	0.03383	1.348	No	ns	-0.08539 to 0.1530
Se NP 50ug vs SeMetFa NP 100ug	-0.0277	1.105	No	ns	-0.1469 to 0.09148
Se NP 50ug vs SeMetFa NP 200ug	-0.044	1.754	No	ns	-0.1632 to 0.07521
Se NP 100ug vs Se NP 200ug	-0.0258	1.027	No	ns	-0.1450 to 0.09343
Se NP 100ug vs SeMetFa NP 50ug	0.1112	4.43	No	ns	-0.008048 to 0.2304

Se NP 100ug vs SeMetFa NP 100ug	0.04961	1.977	No	ns	-0.06961 to 0.1688
Se NP 100ug vs SeMetFa NP 200ug	0.03333	1.328	No	ns	-0.08588 to 0.1525
Se NP 200ug vs SeMetFa NP 50ug	0.1369	5.458	Yes	*	0.01773 to 0.2562
Se NP 200ug vs SeMetFa NP 100ug	0.07539	3.004	No	ns	-0.04383 to 0.1946
Se NP 200ug vs SeMetFa NP 200ug	0.05911	2.356	No	ns	-0.06010 to 0.1783
SeMetFa NP 50ug vs SeMetFa NP 100ug	-0.0616	2.453	No	ns	-0.1808 to 0.05765
SeMetFa NP 50ug vs SeMetFa NP 200ug	-0.0778	3.102	No	ns	-0.1970 to 0.04138
SeMetFa NP 100ug vs SeMetFa NP 200ug	-0.0163	0.6485	No	ns	-0.1355 to 0.1029

Permeability Studies

Two-way ANOVA

Source of Variation	% of total variation	P value
Interaction	1.1	0.0065
Column Factor	96.45	P<0.0001
Row Factor	1.16	0.0002

Source of Variation	P value summary	Significant?
Interaction	**	Yes
Column Factor	***	Yes
Row Factor	***	Yes

Source of Variation	Df	Sum-of-squares	Mean square	F
Interaction	10	397	39.7	3.066
Column Factor	2	34840	17420	1345
Row Factor	5	418.9	83.79	6.471
Residual	36	466.2	12.95	

Bonferroni Posthoc test

Control vs Se NPs				
Row Factor	Control	Se NPs	Difference	95% CI of diff.
2	100	37.61	-62.39	-71.38 to -53.40
4	100	38.7	-61.3	-70.29 to -52.31
6	100	36.96	-63.04	-72.03 to -54.05
7	100	40	-60	-68.99 to -51.01

8	100	41.3	-58.7	-67.69 to - 49.71
10	100	44.13	-55.87	-64.86 to - 46.88
Row Factor	Difference	t	P value	Summary
2	-62.39	21.24	P<0.001	***
4	-61.3	20.87	P<0.001	***
6	-63.04	21.46	P<0.001	***
7	-60	20.42	P<0.001	***
8	-58.7	19.98	P<0.001	***
10	-55.87	19.02	P<0.001	***
Control vs SeMetFa NPs				
Row Factor	Control	SeMetFa NPs	Difference	95% CI of diff.
2	100	51.3	-48.7	-57.69 to - 39.71
4	100	57.61	-42.39	-51.38 to - 33.40
6	100	51.96	-48.04	-57.03 to - 39.05
7	100	55	-45	-53.99 to - 36.01
8	100	52.61	-47.39	-56.38 to - 38.40
10	100	69.57	-30.43	-39.43 to - 21.44
Row Factor	Difference	t	P value	Summary
2	-48.7	16.57	P<0.001	***
4	-42.39	14.43	P<0.001	***
6	-48.04	16.35	P<0.001	***

7	-45	15.32	P<0.001	***
8	-47.39	16.13	P<0.001	***
10	-30.43	10.36	P<0.001	***

Animal Weight

	Before Induction	Day 1	Day 7	Day 14	Day 21
AC	234	232	288	286	312
	221	202	238	220	254
	210	218	252	233	282
	240	224	276	246	296
	192	183	218	196	256
	226	206	261	234	290
Normal control	208	220	245	250	265
	220	222	244	254	265
	214	230	244	256	271
	220	232	256	264	279
	207	211	233	243	260
	208	239	265	275	285
CMC	195	213	244	265	280
	181	216	253	286	293
	197	224	263	298	314
	180	174	210	232	243
	211	225	261	271	287
	192	219	266	295	315
prednisolone	210	204	216	199	263
	192	194	217	206	265
	180	180	206	189	255
	191	176	184	173	217
	199	198	226	213	280
	196	224	237	216	280
se250ug	221	212	240	249	265
	205	190	211	226	265
	224	217	232	288	271
	200	200	207	205	279
	256	255	276	246	260

	241	256	260	260	285
se500ug	233	230	254	265	272
	243	233	238	265	241
	246	253	257	271	289
	265	280	306	279	326
	273	284	292	260	307
	236	247	266	285	280
se750ug	206	242	275	291	302
	243	296	318	331	335
	209	243	257	256	280
	205	196	226	245	265
	236	218	254	268	280
	207	206	240	256	289

Paw Volume
Two-way ANOVA

Source of Variation	% of total variation	P value
Interaction	20.3	P<0.0001
Column Factor	46.24	P<0.0001
Row Factor	29.31	P<0.0001

Source of Variation	P value summary	Significant?
Interaction	***	Yes
Column Factor	***	Yes
Row Factor	***	Yes

Source of Variation	Df	Sum-of-squares	Mean square	F
Interaction	24	83.95	3.498	14.27
Column Factor	6	191.2	31.87	130
Row Factor	4	121.2	30.3	123.6
Residual	70	17.16	0.2451	

Bonferroni Posthoc test

AC vs NC				
Row Factor	AC	NC	Difference	95% CI of diff.
Row 1	4.977	4.393	-0.5833	-1.906 to 0.7389
Row 2	8.89	4.46	-4.43	-5.752 to -3.108
Row 3	9.003	4.207	-4.797	-6.119 to -3.474

Row 4	9.043	4.327	-4.717	-6.039 to - 3.394
Row 5	9.003	4.203	-4.8	-6.122 to - 3.478
Row Factor	Difference	t	P value	Summary
Row 1	-0.5833	1.443	P > 0.05	ns
Row 2	-4.43	10.96	P<0.001	***
Row 3	-4.797	11.87	P<0.001	***
Row 4	-4.717	11.67	P<0.001	***
Row 5	-4.8	11.87	P<0.001	***
AC vs CMC				
Row Factor	AC	CMC	Difference	95% CI of diff.
Row 1	4.977	4.607	-0.37	-1.692 to 0.9522
Row 2	8.89	4.587	-4.303	-5.626 to - 2.981
Row 3	9.003	4.347	-4.657	-5.979 to - 3.334
Row 4	9.043	4.283	-4.76	-6.082 to - 3.438
Row 5	9.003	4.243	-4.76	-6.082 to - 3.438
Row Factor	Difference	t	P value	Summary
Row 1	-0.37	0.9152	P > 0.05	ns
Row 2	-4.303	10.64	P<0.001	***
Row 3	-4.657	11.52	P<0.001	***
Row 4	-4.76	11.77	P<0.001	***
Row 5	-4.76	11.77	P<0.001	***
AC vs prednisolone				

Row Factor	AC	prednisolone	Difference	95% CI of diff.
Row 1	4.977	5.42	0.4433	-0.8789 to 1.766
Row 2	8.89	9.65	0.76	-0.5622 to 2.082
Row 3	9.003	7.233	-1.77	-3.092 to - 0.4478
Row 4	9.043	6.683	-2.36	-3.682 to - 1.038
Row 5	9.003	6.473	-2.53	-3.852 to - 1.208
Row Factor	Difference	t	P value	Summary
Row 1	0.4433	1.097	P > 0.05	ns
Row 2	0.76	1.88	P > 0.05	ns
Row 3	-1.77	4.378	P<0.001	***
Row 4	-2.36	5.838	P<0.001	***
Row 5	-2.53	6.258	P<0.001	***
AC vs se250ug				
Row Factor	AC	se250ug	Difference	95% CI of diff.
Row 1	4.977	4.163	-0.8133	-2.136 to 0.5089
Row 2	8.89	9.187	0.2967	-1.026 to 1.619
Row 3	9.003	7.517	-1.487	-2.809 to - 0.1645
Row 4	9.043	8.107	-0.9367	-2.259 to 0.3855
Row 5	9.003	7.02	-1.983	-3.306 to - 0.6611
Row Factor	Difference	t	P value	Summary
Row 1	-0.8133	2.012	P > 0.05	ns

Row 2	0.2967	0.7338	P > 0.05	ns
Row 3	-1.487	3.677	P < 0.01	**
Row 4	-0.9367	2.317	P > 0.05	ns
Row 5	-1.983	4.906	P < 0.001	***
AC vs se500ug				
Row Factor	AC	se500ug	Difference	95% CI of diff.
Row 1	4.977	4.41	-0.5667	-1.889 to 0.7555
Row 2	8.89	9.007	0.1167	-1.206 to 1.439
Row 3	9.003	8.01	-0.9933	-2.316 to 0.3289
Row 4	9.043	6.455	-2.589	-3.911 to - 1.266
Row 5	9.003	6.303	-2.7	-4.022 to - 1.378
Row Factor	Difference	t	P value	Summary
Row 1	-0.5667	1.402	P > 0.05	ns
Row 2	0.1167	0.2886	P > 0.05	ns
Row 3	-0.9933	2.457	P > 0.05	ns
Row 4	-2.589	6.403	P < 0.001	***
Row 5	-2.7	6.679	P < 0.001	***
AC vs se750ug				
Row Factor	AC	se750ug	Difference	95% CI of diff.
Row 1	4.977	4.293	-0.6833	-2.006 to 0.6389
Row 2	8.89	10.04	1.145	-0.1769 to 2.468
Row 3	9.003	5.677	-3.327	-4.649 to - 2.004

Row 4	9.043	6.04	-3.003	-4.326 to - 1.681
Row 5	9.003	5.603	-3.4	-4.722 to - 2.078
Row Factor	Difference	t	P value	Summary
Row 1	-0.6833	1.69	$P > 0.05$	ns
Row 2	1.145	2.833	$P < 0.05$	*
Row 3	-3.327	8.229	$P < 0.001$	***
Row 4	-3.003	7.429	$P < 0.001$	***
Row 5	-3.4	8.41	$P < 0.001$	***

Catalase Liver

ANOVA Table	SS	df	MS
Treatment (between columns)	7636	6	1273
Residual (within columns)	1020	14	72.84
Total	8656	20	

Dunnett's Multiple Comparison Test	Mean Diff.	q	Significant? P < 0.05?	Summary	95% CI of diff
Arthritic control vs Normal control	-59.72	8.569	Yes	***	-80.01 to -39.42
Arthritic control vs CMC	-53.35	7.656	Yes	***	-73.65 to -33.06
Arthritic control vs Prednisolone	-21.99	3.156	Yes	*	-42.29 to -1.696
Arthritic control vs Se250	-17.78	2.551	No	ns	-38.08 to 2.517
Arthritic control vs Se500	-28.68	4.115	Yes	**	-48.97 to -8.380
Arthritic control vs Se750	-31.79	4.561	Yes	**	-52.08 to -11.49

Dunnett's Multiple Comparison Test	Mean Diff.	q	Significant? P < 0.05?	Summary	95% CI of diff
Normal control vs Arthritic control	59.72	8.569	Yes	***	39.42 to 80.01
Normal control vs CMC	6.364	0.9132	No	ns	-13.93 to 26.66
Normal control vs Prednisolone	37.73	5.414	Yes	***	17.43 to 58.02
Normal control vs Se250	41.94	6.018	Yes	***	21.64 to 62.23

Normal control vs Se500	31.04	4.454	Yes	**	10.75 to 51.34
Normal control vs Se750	27.93	4.008	Yes	**	7.636 to 48.23

Catalase Kidney

ANOVA Table	SS	df	MS
Treatment (between columns)	2670	6	445
Residual (within columns)	275.6	14	19.68
Total	2946	20	

Dunnett's Multiple Comparison Test	Mean Diff.	q	Significant? P < 0.05?	Summary	95% CI of diff
Arthritic control vs Normal control	-34.45	9.511	Yes	***	-45.01 to -23.90
Arthritic control vs CMC	-36.4	10.05	Yes	***	-46.95 to -25.85
Arthritic control vs Prednisolone	-24.06	6.642	Yes	***	-34.61 to -13.51
Arthritic control vs Se250	-18.87	5.209	Yes	***	-29.42 to -8.319
Arthritic control vs Se500	-24.56	6.781	Yes	***	-35.11 to -14.01
Arthritic control vs Se750	-28.95	7.992	Yes	***	-39.50 to -18.40

ANOVA Table	SS	df	MS
Treatment (between columns)	2670	6	445
Residual (within columns)	275.6	14	19.68
Total	2946	20	

Dunnett's Multiple Comparison Test	Mean Diff.	q	Significant? P < 0.05?	Summary	95% CI of diff
Normal control vs Arthritic control	34.45	9.511	Yes	***	23.90 to 45.01

Normal control vs CMC	-1.943	0.5364	No	ns	-12.49 to 8.608
Normal control vs Prednisolone	10.39	2.869	No	ns	-0.1564 to 20.95
Normal control vs Se250	15.58	4.302	Yes	**	5.034 to 26.14
Normal control vs Se500	9.89	2.73	No	ns	-0.6607 to 20.44
Normal control vs Se750	5.503	1.519	No	ns	-5.048 to 16.05

Catalase Spleen

ANOVA Table	SS	df	MS
Treatment (between columns)	5317	6	886.2
Residual (within columns)	434.1	14	31.01
Total	5751	20	

Dunnett's Multiple Comparison Test	Mean Diff.	q	Significant? P < 0.05?	Summary	95% CI of diff
Arthritic control vs Normal control	-43.24	9.511	Yes	***	-56.48 to -30.00
Arthritic control vs CMC	-39.97	8.79	Yes	***	-53.21 to -26.72
Arthritic control vs Prednisolone	-12.63	2.778	No	ns	-25.87 to 0.6116
Arthritic control vs Se250	-20.26	4.457	Yes	**	-33.51 to -7.023
Arthritic control vs Se500	-25.78	5.67	Yes	***	-39.02 to -12.54
Arthritic control vs Se750	-45.93	10.1	Yes	***	-59.17 to -32.69

ANOVA Table	SS	df	MS
Treatment (between columns)	5317	6	886.2
Residual (within columns)	434.1	14	31.01
Total	5751	20	

Dunnett's Multiple Comparison Test	Mean Diff.	q	Significant? P < 0.05?	Summary	95% CI of diff
Normal control vs Arthritic control	43.24	9.511	Yes	***	30.00 to 56.48
Normal control vs CMC	3.278	0.7209	No	ns	-9.964 to 16.52

Normal control vs Prednisolone	30.61	6.733	Yes	***	17.37 to 43.85
Normal control vs Se250	22.98	5.054	Yes	***	9.736 to 36.22
Normal control vs Se500	17.46	3.841	Yes	**	4.223 to 30.71
Normal control vs Se750	-2.685	0.5905	No	ns	-15.93 to 10.56

GPx Liver

ANOVA Table	SS	df	MS
Treatment (between columns)	84780	6	14130
Residual (within columns)	9449	14	674.9
Total	94230	20	

Dunnett's Multiple Comparison Test	Mean Diff.	q	Significant? P < 0.05?	Summary	95% CI of diff
Arthritic control vs Normal control	-200.8	9.466	Yes	***	-262.6 to -139.0
Arthritic control vs CMC	-198.7	9.367	Yes	***	-260.5 to -136.9
Arthritic control vs Prednisolone	-104.3	4.915	Yes	**	-166.0 to -42.48
Arthritic control vs Se250	-102	4.81	Yes	**	-163.8 to -40.25
Arthritic control vs Se500	-122.8	5.79	Yes	***	-184.6 to -61.03
Arthritic control vs Se750	-147.4	6.947	Yes	***	-209.1 to -85.58

ANOVA Table	SS	df	MS
Treatment (between columns)	84780	6	14130
Residual (within columns)	9449	14	674.9
Total	94230	20	

Dunnett's Multiple Comparison Test	Mean Diff.	q	Significant? P < 0.05?	Summary	95% CI of diff
Normal control vs Arthritic control	200.8	9.466	Yes	***	139.0 to 262.6

Normal control vs CMC	2.089	0.0985	No	ns	-59.69 to 63.87
Normal control vs Prednisolone	96.52	4.551	Yes	**	34.74 to 158.3
Normal control vs Se250	98.75	4.655	Yes	**	36.97 to 160.5
Normal control vs Se500	77.97	3.676	Yes	*	16.19 to 139.8
Normal control vs Se750	53.42	2.518	No	ns	-8.360 to 115.2

Gpx Kidney

ANOVA Table	SS	df	MS
Treatment (between columns)	45210	6	7535
Residual (within columns)	5220	14	372.9
Total	50430	20	

Dunnett's Multiple Comparison Test	Mean Diff.	q	Significant? P < 0.05?	Summary	95% CI of diff
Arthritic control vs Normal control	-141.4	8.969	Yes	***	-187.3 to -95.48
Arthritic control vs CMC	-130.6	8.282	Yes	***	-176.5 to -84.65
Arthritic control vs Prednisolone	-116.4	7.38	Yes	***	-162.3 to -70.44
Arthritic control vs Se250	-101.6	6.443	Yes	***	-147.5 to -55.67
Arthritic control vs Se500	-128.9	8.179	Yes	***	-174.9 to -83.03
Arthritic control vs Se750	-143.2	9.081	Yes	***	-189.1 to -97.25

ANOVA Table	SS	df	MS
Treatment (between columns)	45210	6	7535
Residual (within columns)	5220	14	372.9
Total	50430	20	

Dunnett's Multiple Comparison Test	Mean Diff.	q	Significant? P < 0.05?	Summary	95% CI of diff
Normal control vs Arthritic control	141.4	8.969	Yes	***	95.48 to 187.3

Normal control vs CMC	10.83	0.6868	No	ns	-35.09 to 56.75
Normal control vs Prednisolone	25.04	1.588	No	ns	-20.88 to 70.96
Normal control vs Se250	39.82	2.525	No	ns	-6.102 to 85.74
Normal control vs Se500	12.45	0.7898	No	ns	-33.47 to 58.37
Normal control vs Se750	-1.767	0.1121	No	ns	-47.69 to 44.15

Gpx Spleen

ANOVA Table	SS	df	MS
Treatment (between columns)	194400	6	32400
Residual (within columns)	6360	14	454.3
Total	200800	20	

Dunnett's Multiple Comparison Test	Mean Diff.	q	Significant? P < 0.05?	Summary	95% CI of diff
Arthritic control vs Normal control	-291.1	16.73	Yes	***	-341.7 to -240.4
Arthritic control vs CMC	-306.5	17.61	Yes	***	-357.2 to -255.8
Arthritic control vs Prednisolone	-193.6	11.13	Yes	***	-244.3 to -143.0
Arthritic control vs Se250	-198.7	11.42	Yes	***	-249.4 to -148.0
Arthritic control vs Se500	-237.9	13.67	Yes	***	-288.6 to -187.2
Arthritic control vs Se750	-271.3	15.59	Yes	***	-322.0 to -220.6

ANOVA Table	SS	df	MS
Treatment (between columns)	194400	6	32400
Residual (within columns)	6360	14	454.3
Total	200800	20	

Dunnett's Multiple Comparison Test	Mean Diff.	q	Significant? P < 0.05?	Summary	95% CI of diff
Normal control vs Arthritic control	291.1	16.73	Yes	***	240.4 to 341.7

Normal control vs CMC	-15.45	0.8881	No	ns	-66.14 to 35.23
Normal control vs Prednisolone	97.42	5.598	Yes	***	46.73 to 148.1
Normal control vs Se250	92.36	5.307	Yes	***	41.68 to 143.0
Normal control vs Se500	53.13	3.053	Yes	*	2.447 to 103.8
Normal control vs Se750	19.72	1.133	No	ns	-30.96 to 70.40

SOD Liver

ANOVA Table	SS	df	MS
Treatment (between columns)	91.97	6	15.33
Residual (within columns)	32.36	14	2.312
Total	124.3	20	

Dunnett's Multiple Comparison Test	Mean Diff.	q	Significant? P < 0.05?	Summary	95% CI of diff
Arthritic Control vs Normal Control	-5.942	4.787	Yes	**	-9.558 to -2.327
Arthritic Control vs CMC	-5.865	4.724	Yes	**	-9.480 to -2.249
Arthritic Control vs Prednisolone	-3.76	3.029	Yes	*	-7.376 to -0.1447
Arthritic Control vs Se250	-1.56	1.257	No	ns	-5.176 to 2.055
Arthritic Control vs Se500	-2.521	2.031	No	ns	-6.137 to 1.095
Arthritic Control vs Se750	-4.936	3.976	Yes	**	-8.552 to -1.320

ANOVA Table	SS	df	MS
Treatment (between columns)	91.97	6	15.33
Residual (within columns)	32.36	14	2.312
Total	124.3	20	

Dunnett's Multiple Comparison Test	Mean Diff.	q	Significant? P < 0.05?	Summary	95% CI of diff
Normal Control vs Arthritic Control	5.942	4.787	Yes	**	2.327 to 9.558
Normal Control vs CMC	0.07767	0.06256	No	ns	-3.538 to 3.693

Normal Control vs Prednisolone	2.182	1.758	No	ns	-1.434 to 5.798
Normal Control vs Se250	4.382	3.53	Yes	*	0.7664 to 7.998
Normal Control vs Se500	3.421	2.756	No	ns	-0.1943 to 7.037
Normal Control vs Se750	1.006	0.8106	No	ns	-2.609 to 4.622

SOD Kidney

ANOVA Table	SS	df	MS
Treatment (between columns)	22.15	6	3.692
Residual (within columns)	11.18	14	0.7983
Total	33.33	20	

Dunnett's Multiple Comparison Test	Mean Diff.	q	Significant? P < 0.05?	Summary	95% CI of diff
Arthritic Control vs Normal Control	-3.4	4.66	Yes	**	-5.524 to -1.275
Arthritic Control vs CMC	-2.938	4.027	Yes	**	-5.063 to -0.8132
Arthritic Control vs Prednisolone	-2.328	3.191	Yes	*	-4.453 to -0.2032
Arthritic Control vs Se250	-1.646	2.257	No	ns	-3.771 to 0.4784
Arthritic Control vs Se500	-2.029	2.781	No	ns	-4.153 to 0.09609
Arthritic Control vs Se750	-2.678	3.671	Yes	*	-4.803 to -0.5536

ANOVA Table	SS	df	MS
Treatment (between columns)	22.15	6	3.692
Residual (within columns)	11.18	14	0.7983
Total	33.33	20	

Dunnett's Multiple Comparison Test	Mean Diff.	q	Significant? P < 0.05?	Summary	95% CI of diff
Normal Control vs Arthritic Control	3.4	4.66	Yes	**	1.275 to 5.524

Normal Control vs CMC	0.4617	0.6328	No	ns	-1.663 to 2.586
Normal Control vs Prednisolone	1.072	1.469	No	ns	-1.053 to 3.196
Normal Control vs Se250	1.753	2.403	No	ns	-0.3714 to 3.878
Normal Control vs Se500	1.371	1.879	No	ns	-0.7538 to 3.496
Normal Control vs Se750	0.7213	0.9888	No	ns	-1.403 to 2.846

SOD Spleen

ANOVA Table	SS	df	MS
Treatment (between columns)	13.46	6	2.244
Residual (within columns)	5.798	14	0.4141
Total	19.26	20	

Dunnett's Multiple Comparison Test	Mean Diff.	q	Significant? P < 0.05?	Summary	95% CI of diff
Arthritic Control vs Normal control	-2.581	4.912	Yes	**	-4.112 to -1.051
Arthritic Control vs CMC	-2.533	4.821	Yes	**	-4.063 to -1.003
Arthritic Control vs Prednisolone	-1.625	3.093	Yes	*	-3.156 to -0.09486
Arthritic Control vs Se250	-1.748	3.328	Yes	*	-3.279 to -0.2181
Arthritic Control vs Se500	-1.645	3.13	Yes	*	-3.175 to -0.1145
Arthritic Control vs Se750	-2.058	3.917	Yes	**	-3.589 to -0.5280

ANOVA Table	SS	df	MS
Treatment (between columns)	13.46	6	2.244
Residual (within columns)	5.798	14	0.4141
Total	19.26	20	

Dunnett's Multiple Comparison Test	Mean Diff.	q	Significant? P < 0.05?	Summary	95% CI of diff
Normal control vs Arthritic Control	2.581	4.912	Yes	**	1.051 to 4.112

Normal control vs CMC	0.04823	0.0918	No	ns	-1.482 to 1.579
Normal control vs Prednisolone	0.956	1.819	No	ns	-0.5744 to 2.486
Normal control vs Se250	0.8328	1.585	No	ns	-0.6976 to 2.363
Normal control vs Se500	0.9363	1.782	No	ns	-0.5940 to 2.467
Normal control vs Se750	0.5229	0.9951	No	ns	-1.007 to 2.053

C-Reactive Protein

One-way analysis of variance	
P value	P<0.0001
P value summary	***
Are means signif. different? (P < 0.05)	Yes
Number of groups	7
F	18.6
R squared	0.7613

Bartlett's test for equal variances	
Bartlett's statistic (corrected)	6.668
P value	0.3527
P value summary	ns
Do the variances differ signif. (P < 0.05)	No

ANOVA Table	SS	df	MS
Treatment (between columns)	5.565	6	0.9275
Residual (within columns)	1.745	35	0.04986
Total	7.31	41	

Dunnett's Multiple Comparison Test	Mean Diff.	q	Significant? P < 0.05?	Summary	95% CI of diff
Normal Control vs Arthritic Control	-1.133	8.791	Yes	***	-1.481 to -0.7852
Normal Control vs CMC	-0.0467	0.362	No	ns	-0.3948 to 0.3014
Normal Control vs Predisolone	-0.03167	2.456	No	ns	-0.6648 to 0.03143

Normal Control vs SeMetFaNPs 250microg	-0.35	2.715	Yes	*	-0.6981 to - 0.001904
Normal Control vs SeMetFaNPs 500microg	- 0.1833	1.422	No	ns	-0.5314 to 0.1648
Normal Control vs SeMetFaNPs 750microg	-0.05	0.3878	No	ns	-0.3981 to 0.2981

One-way analysis of variance	
P value	P<0.0001
P value summary	***
Are means signif. different? (P < 0.05)	Yes
Number of groups	7
F	18.6
R squared	0.7613

Bartlett's test for equal variances	
Bartlett's statistic (corrected)	6.668
P value	0.3527
P value summary	ns
Do the variances differ signif. (P < 0.05)	No

ANOVA Table	SS	df	MS
Treatment (between columns)	5.565	6	0.9275
Residual (within columns)	1.745	35	0.04986
Total	7.31	41	

Dunnett's Multiple Comparison Test	Mean Diff.	q	Significant? P < 0.05?	Summary	95% CI of diff
---	------------	---	---------------------------	---------	----------------

Predisolone vs Arthritic Control	-0.8167	6.335	Yes	***	-1.165 to -0.4686
Predisolone vs Normal Control	0.3167	2.456	No	ns	-0.03143 to 0.6648
Predisolone vs CMC	0.27	2.094	No	ns	-0.07810 to 0.6181
Predisolone vs SeMetFaNPs 250microg	-0.03333	0.2586	No	ns	-0.3814 to 0.3148
Predisolone vs SeMetFaNPs 500microg	0.1333	1.034	No	ns	-0.2148 to 0.4814
Predisolone vs SeMetFaNPs 750microg	0.2667	2.068	No	ns	-0.08143 to 0.6148

Prostaglandin E2

ANOVA Table	SS	df	MS
Treatment (between columns)	877400	6	146200
Residual (within columns)	72800	14	5200
Total	950200	20	

Dunnett's Multiple Comparison Test	Mean Diff.	q	Significant? P < 0.05?	Summary	95% CI of diff
AC vs NC	649.6	11.03	Yes	***	478.2 to 821.1
AC vs CMC	580.3	9.856	Yes	***	408.8 to 751.8
AC vs Prednisolone	352.9	5.993	Yes	***	181.4 to 524.3
AC vs se250	215.9	3.666	Yes	*	44.38 to 387.3
AC vs se500	264.5	4.492	Yes	**	93.01 to 436.0
AC vs se750	392.9	6.672	Yes	***	221.4 to 564.3

ANOVA Table	SS	df	MS
Treatment (between columns)	877400	6	146200
Residual (within columns)	72800	14	5200
Total	950200	20	

Dunnett's Multiple Comparison Test	Mean Diff.	q	Significant? P < 0.05?	Summary	95% CI of diff
NC vs AC	-649.6	11.03	Yes	***	-821.1 to -478.2
NC vs CMC	-69.37	1.178	No	ns	-240.9 to 102.1

NC vs Prednisolone	-296.8	5.041	Yes	***	-468.3 to - 125.3
NC vs se250	-433.8	7.368	Yes	***	-605.3 to - 262.3
NC vs se500	-385.2	6.542	Yes	***	-556.6 to - 213.7
NC vs se750	-256.8	4.361	Yes	**	-428.3 to - 85.30

Tumor Necrosis Factor- α

ANOVA Table	SS	df	MS
Treatment (between columns)	49.67	6	8.278
Residual (within columns)	0.9776	14	0.06983
Total	50.65	20	

Dunnett's Multiple Comparison Test	Mean Diff.	q	Significant? P < 0.05?	Summary	95% CI of diff
AC vs NC	4.554	21.11	Yes	***	3.926 to 5.182
AC vs CMC	4.557	21.12	Yes	***	3.929 to 5.185
AC vs Prednisolone	4.155	19.26	Yes	***	3.527 to 4.784
AC vs Se250	4.135	19.17	Yes	***	3.507 to 4.764
AC vs Se500	4.425	20.51	Yes	***	3.797 to 5.054
AC vs Se750	4.403	20.41	Yes	***	3.775 to 5.032

ANOVA Table	SS	df	MS
Treatment (between columns)	49.67	6	8.278
Residual (within columns)	0.9776	14	0.06983
Total	50.65	20	

Dunnett's Multiple Comparison Test	Mean Diff.	q	Significant? P < 0.05?	Summary	95% CI of diff
NC vs AC	-4.554	21.11	Yes	***	-5.182 to -3.926

NC vs CMC	0.00302	0.014	No	ns	-0.6254 to 0.6314
NC vs Prednisolone	-0.3986	1.848	No	ns	-1.027 to 0.2297
NC vs Se250	-0.4187	1.941	No	ns	-1.047 to 0.2097
NC vs Se500	-0.1289	0.5973	No	ns	-0.7573 to 0.4995
NC vs Se750	-0.1508	0.6991	No	ns	-0.7792 to 0.4776

Appendix-II

Reagent Preparations

100 mM Sodium selenite:

0.3459 g of sodium selenite was dissolved in 20 ml of MilliQ water.

50 mM Ascorbic Acid:

0.88065 g of ascorbic acid was dissolved in 100 ml of MilliQ water.

100 mM Methionine:

1.4921 g of methionine in 100 ml of MilliQ water.

1 mM Folic acid:

0.08828 g of folic acid in 200 ml of MilliQ water.

10% Fetal Bovine Serum containing media:

4ml of FBS is mixed with 36 ml of DMEM media to make up the total volume upto 40 ml.

1% Penstrep (antibiotic):

0.5 ml of Penstrep was mixed with 45.5 ml of DMEM media.

5 mg/ml MTT reagent:

5 mg of MTT powder was dissolved in 1ml of DPBS solution to make the stock solution. 1:10 dilution was prepared of this stock solution and 20 μ l of this diluted MTT solution was then added to each well.

 μ M Copper sulphate:

A stock solution of 1000 μ M of CuSO_4 was prepared by dissolving 25 mg of CuSO_4 in 100 ml of MilliQ water. 0.04 μ l of this stock solution was then used in 10 μ l mixture in order to achieve the final concentration of 4 μ M Copper sulphate.

 μ M Ascorbic acid:

A stock solution of 1000 μ M of ascorbic acid was prepared by dissolving 17 mg of ascorbic acid in 100 ml of MilliQ water. 0.05 μ l of this stock solution

was then used in 10 μ l mixture in order to achieve the final concentration of 5 μ M ascorbic acid.

130 mM NaCl:

A stock solution of 1000 mM of NaCl was prepared by dissolving 5.84 g of NaCl in 100 ml of MilliQ water. 1.3 μ l of this stock solution was then used in 10 μ l mixture in order to achieve the final concentration of 5 μ M ascorbic acid.

50 μ M H₂O₂:

A stock solution of 50 mM of H₂O₂ was prepared by mixing 5.67 μ l of H₂O₂ in 1 ml of MilliQ water. 10 μ l of this stock solution was then further diluted in 1ml of MilliQ water to form a concentration of 500 μ M. 1 μ l of this diluted H₂O₂ solution was then used in 10 μ l mixture in order to achieve the final concentration of 50 μ M H₂O₂.

50 mM EDTA:

A stock solution of 500 mM of NaCl was prepared by dissolving 9.3 g of EDTA in 50 ml of MilliQ water (pH adjusted to 8). 1 μ l of this stock solution was then used in 10 μ l mixture in order to achieve the final concentration of 50 mM EDTA.

1mg/ml BSA:

10 mg of Bovine Serum Albumin was dissolved in 10 ml of MilliQ water.

10% Formalin:

10 ml of formalin was diluted with 90 ml of MilliQ water.

0.1 M Phosphate buffer (pH 7.4):

16.04 ml of 1M K₂HPO₄ and 3.96 ml of 1M KH₂PO₄ was mixed and volume was made upto 200 ml using MilliQ water.

50 mM Tris EDTA buffer:

605.7 mg of Tris Base and 37 mg of EDTA was dissolved in 100 ml of MilliQ

water. pH was adjusted to 8.2 using HCl.

0.1 mM Pyrogallol:

Stock of 0.1 M pyrogallol (0.12611 g) was prepared in 10 mM HCl. 10 μ l of the stock solution was added to the mixture.

19.6 mM H₂O₂:

0.22 ml of H₂O₂ was diluted with 99.78 ml of 10mM phosphate buffer (pH 7.4).

10 mM Sodium azide:

6.5 mg of sodium azide was dissolved in 10 ml of 200 mM phosphate buffer (pH 7.6).

1mM Reduced Glutathione:

0.01535 g of reduced glutathione was dissolved in 50 ml of 0.1 N HCl.

2 mM H₂O₂:

2.24 μ l of H₂O₂ was diluted in 10 ml of 200 mM phosphate buffer (pH 7.6).

1mM Ellman's reagent:

19.8 mg of Ellman's reagent was dissolved in 50 ml of 200 mM Phosphate buffer (pH 7.6).

5% TCA:

5ml of Trichloroacetic acid was diluted with 45 ml of 200 mM Phosphate buffer (pH 7.6).

Appendix-III

Ethics Approvals

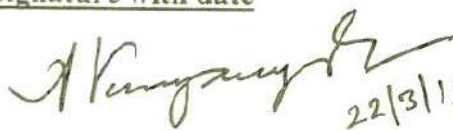
Animal Ethics ApprovalCertificate

This is certified that the project title "Anti-arthritis activity of selenium-methionine and selenium-methionine-folate nanoparticles" has been approved by the IAEC.
(CPCSEA/IAEC/P-11/2019)

Name of Chairman/ Member Secretary IAEC:
Dr. Addepalli V.

Name of CPCSEA nominee:
Dr. Rahul Thorat

Signature with date


22/3/19

Chairman/ Member Secretary of IAEC:



CPCSEA nominee:

Blood Ethics Approval



**SUNANDAN DIVATIA
SCHOOL OF SCIENCE**

SVKM's INSTITUTIONAL ETHICS COMMITTEE (IEC)

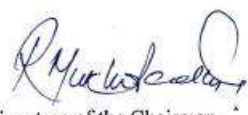
9th March 2020

To
Principal Investigator
SVKM's Mithibai College,
Mumbai

Sub: Project proposal No: NMIMS/IEC/016/2020

The Committee has reviewed and approved the proposal entitled "Synthesis of selenium-methionine nanoparticles and its application in chronic inflammatory arthritis" in its meeting held on 18th February 2020 for a period of three years. The progress report and final report of the proposal should be submitted to the Committee.


Signature of the Member-Secretary
(Dr. Brijesh Sukumaran)


Signature of the Chairman
(Dr. Rabindranath Mukhopadhyaya)

Copy forwarded to protocol applicant: ✓
Copy in File

SVKM'S
Narsee Monjee Institute of Management Studies
Deemed to be UNIVERSITY
V. L. Mehta Road, Vile Parle (West), Mumbai - 400 056, India.
Tel: (91-22) 42355555
Email: enquiry@nmims.edu | Web: www.nmims.edu



Appendix-IV

Certificates

Appendix-V

Conferences and Publications

Conferences

- National Post-Doctoral Symposium 2022, IISER TRIVANDRUM (KERALA)- Selected for talk for title “Therapeutic Potential of Selenium nanoparticles aimed at inflammatory diseases”.
- International Conference on Health Sciences 2022, SRILANKA Oral presentation titled: “Therapeutic Potential of Selenium nanoparticles aimed at inflammatory diseases”. – Sessions Best presentation award.
- AMSAB 2019, MUMBAI (International conference) Poster presentation titled: Synthesis of Selenium-methionine Nanoparticles and its Application in Chronic Inflammatory Arthritis.
- BESCON 2018, IIT MUMBAI Poster Presentation titled: “Functionalized Selenium Nanoparticles Using Amino Acid and Its Anti-Cytotoxic Effect”.

Publications

- Shinde V, Desai K. *In vitro* cytotoxicity, macromolecular interaction, and antioxidant potential of dual coated selenium nanoparticles. J Biomed Mater Res. 2022;1-12. doi:10.1002/jbm.b.35008.
- Selenium Nanoparticles and it's *In Vivo* efficacy against Chronic RA. (Under Review)